2019

Antifouling Coatings Developed from Functionalised Silica Nanoparticles

Brianna Rose Knowles
University of Wollongong

UNIVERSITY
OF WOLLONGONG
AUSTRALIA

Antifouling Coatings Developed from Functionalised Silica Nanoparticles

Brianna Rose Knowles

This thesis is presented as required for the conferral of the degree:

Doctor of Philosophy

Supervisor:
Dr. Paul Molino, Assoc. Prof. Michael Higgins, Dr. Pawel Wagner

The University of Wollongong
Australian Institute for Innovative Materials

May, 2019

This research has been conducted with the support of an Australian Government Research Training Program Scholarship.

Declaration

I, *Brianna Rose Knowles*, declare that this thesis is submitted in fulfilment of the requirements for the conferral of the degree *Doctor of Philosophy*, from the University of Wollongong, is wholly my own work unless otherwise referenced or acknowledged. This document has not been submitted for qualifications at any other academic institution.

Brianna Rose Knowles

May 8, 2019

Abstract

Biological fouling of surfaces, occurring through the attachment and accumulation of microorganisms, is an extensive problem affecting the marine, biomedical, building, and food processing industries. Commercial coatings that are applied to surfaces to reduce or prevent biological fouling frequently rely on the incorporation of toxic antimicrobial chemicals, where their release from the surface is uncontrolled and can have undesirable secondary effects. New approaches to prevent fouling focus on the development of surfaces or coatings with tailored physicochemical properties which inhibit the interaction and attachment of fouling species. Despite advances in the use of nanomaterials for antifouling applications, many emerging coating technologies are complex, expensive, and unable to be scaled-up for industrial applications. In this thesis, functionalised silica nanoparticles (SiNP) are explored as an emerging platform material for the development of hydrophilic antifouling coatings. SiNPs are common additives to surface coatings as they are cheap, highly processable, and able to be simply functionalised through silane coupling chemistry. In this work, particles were functionalised with zwitterionic and cationic quaternary ammonium chemistries to investigate the effect of chemistry on the nanoparticle coating hydrophilicity and antifouling behaviour.

In Chapter 2, two methods of preparing hydrophilic low-fouling surface coatings were explored through reaction of SiNP suspensions and pre-deposited SiNP films with zwitterionic sulfobetaine (SB). SiNP suspensions were functionalised with SB across three pH conditions and deposited as thin films via a simple spin-coating process to generate hydrophilic antifouling coatings. In addition, coatings of predeposited SiNP were surface functionalised via exposure to zwitterionic solutions. Quartz crystal microgravimetry with dissipation monitoring (QCM-D) was employed as a high throughput technique for monitoring and optimising reaction to the SiNP surfaces. Functionalisation of nanoparticle films was rapid and could be achieved over a wide pH range and at low zwitterion concentrations. All functionalised particle surfaces presented a high degree of wettability and resulted in large reductions in adsorption of bovine serum albumin (BSA) protein. Particle coatings also showed a reduction in adhesion of fungal spores (*Epicoccum nigrum*) and bacteria (*Escherichia coli*) by up to 87% and 96%, respectively.

In a similar manner, Chapter 3 investigates zwitterionic carboxybetaine (CB) as an alternative low-fouling chemistry for the functionalisation of SiNP dispersions and SiNP coatings. This work demonstrated three methods of coating preparation via direct tethering of CB to pre-deposited particle films, a two-step surface functionalisation process, and deposition of CB functionalised particle dispersions. Functionalisation pH was found to drastically influence the mechanism of CB attachment and affect the protein resistant properties of the resultant coatings. Depending on the method of coating preparation, protein binding to functionalised particle coatings was reduced by up to 94% compared to unfunctionalised SiNP control surfaces. As a result, all three methods offer simple and scalable fabrication routes for the generation of hydrophilic, zwitterionic interfaces with improved inhibition to protein fouling.

In Chapter 4, the effect of nanoscaled coating topography on the antifouling behaviour of particle coatings was examined through the preparation of coatings from different size SiNPs functionalised with zwitterionic chemistries. Zwitterionic SB was reacted to SiNPs ranging in size from 7 to 75 nm. Particle stability and grafting density were confirmed using dynamic light scattering and thermogravimetric analysis. Thin coatings of nanoparticles were prepared by spin-coating aqueous particle dispersions. The resulting coatings were characterised using scanning electron microscopy, atomic force microscopy, and contact angle goniometry. SB functionalised particle coatings displayed increased hydrophilicity compared to unmodified particle coating controls while increasing particle size correlated with increased coating roughness and increased surface area. Coatings of zwitterated particles demonstrated a high degree of nonspecific protein resistance, as measured by QCM-D. Adsorption of BSA and hydrophobin proteins were reduced by up to 91 and 94%, respectively. Adhesion of bacteria (*E. coli*) to zwitterion modified particle coatings were also significantly reduced over both short and long-term assays. Maximum reductions of 97% and 94% were achieved over 2 and 24 h assay periods, respectively. For unmodified particle coatings, protein adsorption and bacterial adhesion were generally reduced with increasing particle size. Adhesion of fungal spores (*E. nigrum*) to SB modified SiNP coatings was also reduced, however no clear trends in relation to particle size were demonstrated.

Finally, Chapter 5 presents an investigation into the antifouling and antimicrobial behaviours of quaternary ammonium silanes (QAS) grafted from coatings of SiNPs; independently and in combination with zwitterionic (SB) chemistries. The binding of QAS to SiNP coatings was monitored using QCM-D under varied pH and solution concentrations. Adsorption of BSA protein was reduced on QAS modified SiNP coatings prepared under alkaline conditions due to the proposed generation of a pseudozwitterionic interface, where the underlying SiNP surface presents an anionic

charge at high pH. Significant reductions were achieved even at low concentrations (0.5 mM) and short modification times. Additionally, SiNP coatings modified with a combination of QAS and SB chemistries were investigated. Surface modifications were performed sequentially, varying silane concentration and order of addition, and monitored using QCM-D. Dual-functionalised surfaces presented enhanced resistance to protein adsorption compared to QAS modified surfaces alone, even at low functionalisation concentrations. The antiadhesive and antibacterial properties of functionalised surfaces were investigated by challenging the surfaces against *E. coli*. All dual-functionalised coatings showed equal or reduced bacterial adhesion compared to QAS and SB functionalisations alone, while high concentrations of combined chemistries reduced adhesion of bacteria by up to 95%. None of the prepared coatings elicited a dramatic bactericidal effect, either due to the presence of zwitterionic SB or due to the pseudozwitterionic effect of cationic QAC in close proximity to the negative surface charge of the silica nanoparticles.

The work presented in this thesis offers a significant contribution to the development and fabrication of simple and scalable antifouling coatings for widespread applications. In addition to establishing SiNPs as a platform material for coating fabrication, this thesis details how particle size and conditions of particle modification with hydrophilic chemistries can be used to tune the properties of SiNP coatings, offering tailoring of physicochemical properties for targeted antifouling applications.

Acknowledgments

Firstly, I would like to thank my supervisors, Dr. Paul Molino, Assoc. Prof. Michael Higgins, and Dr. Pawel Wagner, for their support, advice, and encouragement throughout my PhD. I would also like to thank the Australian Steel Manufacturing Research Hub, external collaborators, my industry advisor Dr. Shane Maclaughlin, and my BlueScope colleagues for the opportunity to be a part of this project and for the help, advice, and support this collective group has offered during my studies.

I would like to thank the members of my research group for their help, comradery, and support. I am particularly grateful for the many occasions you gave up your time to listen to and provide feedback on presentations. A special thank you to Ms. Dan Yang, who has joined me on the Hub journey and whose enthusiasm and support has never waivered.

To my friends, thank you for your patience and your encouragement throughout the more difficult and frustrating times. Your support has not gone unnoticed. To my "bromates", studying chemistry would not have been the same without you. You made the hard times easier and the easy times unforgettable.

To my family, particularly my parents, you have backed me from day one and always helped me to believe in myself. I would not be where I am today without your unwavering love and support. Thank you.

Finally, to my husband Brett. I can't believe where we both are today and I am incredibly proud of our achievements. You have been there to support me, inspire me, and push me to be a better version of myself. I only hope that I can repay the favour as you complete your PhD.

Preface

Publications

Publications associated with chapters of this thesis:

Chapter 2

B. R. Knowles, P. Wagner, S. Maclaughlin, M. J. Higgins, and P. J. Molino, "Silica Nanoparticles Functionalized with Zwitterionic Sulfobetaine Siloxane for Application as Versatile Antifouling Coating System", *ACS Appl. Mater. Interfaces*, 2017, **9**,18584–18594, doi:10.1021/acsami.7b04840.

Chapter 3

B. R. Knowles, P. Wagner, S. Maclaughlin, M. J. Higgins, and P. J. Molino, "Carboxybetaine Functionalized Nanosilicas as Protein-Resistant Surface Coatings", Submitted to *Colloids and Surfaces B: Biointerfaces* (under review).

Chapter 4

B. R. Knowles, D. Yang, P. Wagner, S. Maclaughlin, M. J. Higgins, and P. J. Molino, "Zwitterion Functionalized Silica Nanoparticle Coatings: The Effect of Particle Size on Protein, Bacteria, and Fungal Spore Adhesion", *Langmuir*, 2018, doi:10.1021/acs.langmuir.8b01550.

Chapter 5

B. R. Knowles, P. Wagner, S. Maclaughlin, M. J. Higgins, and P. J. Molino, "Modified Silica Nanoparticle Coatings: Dual Antifouling Effects of Self-Assembled Quaternary Ammonium and Zwitterionic Silanes" (in preparation).

Candidates contributions to other publications:

B. R. Knowles, B. Zhang, M. J. Higgins, and P. J. Molino, "Surface Modification of Silica Nanoparticles for the Development of Fouling Resistant Coatings", *China Coatings Journal*, 2017, 37–47.

P. J. Molino, D. Yang, M. Penna, K. Miyazawa, B. R. Knowles, S. Maclaughlin, T. Fukuma, I. Yarovsky and M. J. Higgins, "Hydration Layer Structure of Biofouling Resistant Nanoparticles", *ACS Nano*, 2018, doi:10.1021/acsnano.8b06856.

Conference Presentations

Oral and poster presentations where the candidate was the primary and presenting author:

Australian Colloid and Interface Society Conference, **2017**, "Antifouling Coatings Developed from Functionalised Silica Nanoparticles"

American Chemical Society National Meeting, **2017**, "Self-Assembly of Zwitterionic Sulfobetaine Siloxane onto Silica Nanoparticles for Application as a Versatile Antifouling Coating System"

Materials Research Society Spring Meeting, **2017**, "Self-Assembly of Zwitterionic Sulfobetaine Siloxane onto Silica Nanoparticles for Application as a Versatile Antifouling Coating System"

International Conference of Nanoscience and Nanotechnolgy, **2018**, "Silica Nanoparticle Antifouling Coatings: Does Size Matter?"

Conference of the Combined Australian Materials Societies, **2018**, "Hydrophilic Antifouling Surface Coatings"

Author Statement and Acknowledgements

The work presented herein is the original work of the candidate. Experiments were conducted with the guidance of Dr. Paul Molino. Revisions to written work were contributed by Dr. Paul Molino, Assoc. Prof. Michael Higgins, Dr. Pawel Wagner, and Dr. Shane Maclaughlin.

The following contributions from collaborative authors are hereby acknowledged. Ms. Dan Yang and Dr. Paul Molino assisted in the characterisation of surfaces by Atomic Force Microscopy. Dr. Tony Romeo assisted in the sample preparation and imaging of particle coatings using Scanning Electron Microscopy.

Contents

List of Abbreviations

AFM	Atomic Force Microscopy
AS	Aminosilane
ATRP	Atom Transfer Radical Polymerisation
BSA	Bovine Serum Albumin
CA	Contact Angle
CB	Carboxybetaine
CBAA	Carboxybetaine acrylamide
CBMA	Carboxybetaine methacrylate
CI	Confidence Interval
CTAB	Cetyltrimethylammonium bromide
DLS	Dynamic Light Scattering
EOC	Essential Oil Components
EPS	Extracellular Polymeric Substances
EtOH	Ethanol
FR	Fouling-Release
FTIR	Fourier Transform InfraRed
HCl	Hydrochloric acid
LB	Luria-Bertani
MEG	Mono(ethylene glycol)
MeOH	Methanol
METAC	Methacryloyloxyethyltrimethylammonium chloride
NaOH	Sodium hydroxide
NMR	Nuclear Magnetic Resonance
OEG	Oligo(ethylene glycol)
OEGMA	Oligo(ethylene glycol) methacrylate
PBS	Phosphate Buffered Saline
PC	Phosphorylcholine
PDMS	Polydimethylsiloxane
PEG	Poly(ethylene glycol)
PEI	Poly(ethylenimine)

PL	β-propiolactone
QAC	Quaternary Ammonium Compound
QAS	Quaternary Ammonium Silane
QCM	Quartz Crystal Microbalance
RMS	Root-Mean-Square
RPM	Revolutions per minute
SAM	Self-Assembled Monolayer
SB	Sulfobetaine
SBMA	Sulfobetaine methacrylate
SD	Standard Deviation
SEM	Scanning Electron Microscope
SiNP	Silica Nanoparticle
SPMA	Sulfopropyl methacrylate
TBT	Tributyltin
TGA	Thermogravimetric Analysis
ZP	Zeta Potential

List of Figures

List of Tables

Chapter 1

Introduction

1.1 Biofouling

Biological fouling or 'biofouling' is a dynamic and complex process involving the undesirable attachment and build-up of microorganisms on surfaces. Microorganisms are ubiquitous, being found in almost all environmental settings, and therefore have the potential to impact a wide range of industries. Artificial surfaces submerged in an aqueous or marine environment are quickly inundated by fouling species, compromising the form and function of these surfaces. This is associated with huge financial penalties across the shipping, offshore oil, and aquaculture industries.[1] In medicine, bacterial contamination of implantable devices as well as surgical tools and hospital surfaces increase the risk of patient infection and the spread of nosocomial diseases.[2] Within the food industry, biological contamination during food processing and packaging can result in food spoilage, transmission of pathogenic microorganisms, and ultimately endanger consumers' health.[3] Additionally, bacterial and fungal colonisation of terrestrial or 'unsaturated' surfaces, including concrete and polymeric coatings, can result in their biodeterioration and biodegradation.

Biofouling of surfaces is a multi-stage process that is heavily influenced by the environmental conditions to which the surfaces are exposed. Initial sections of this review detail the processes involved in marine biofouling, the formation of bacterial biofilms and their relevance within the field of medicine, and the fouling of terrestrial surfaces. Later sections describe past and present coating technologies designed to inhibit biofouling processes, progressing from rudimentary release-based coatings, to sophisticated responsive coatings, contact killing surfaces, and surfaces with tailored physicochemical properties for improved biological fouling resistance.

1.1.1 Marine Biofouling

Within the marine environment, vessels and submerged structures are constantly inundated by aquatic species attempting to adhere and colonise these artificial surfaces.[4] Organisms such as bacteria, algae, and barnacles accumulate on submerged surfaces, compromising function and integrity.[5] The build-up of algal slimes onto ship hulls increases hydrodynamic drag resulting in loss of maneuverability, increased fuel consumption, and greater greenhouse gas emissions.[1, 6, 7] The primary cost associated with fouling is overwhelmingly due to increased fuel consumption, however, significant financial penalties are also attributed to hull coating and cleaning costs.[8] Additionally, fouled hulls can facilitate the translocation of invasive or non-native species to new environments.[5, 9] Marine biofouling is generally described in terms of the adsorption and adhesion processes that occur during the formation of a biofilm (Figure 1.1). Fouling of marine substrata begins with the rapid adsorption of dissolved organic material onto the submerged surface.[9] This layer of organic material forms what is known as a conditioning film, and is comprised of glycoproteins, humic acids, proteins, aromatic amino acids, carbohydrates, and uronic acids.[10–12] The conditioning process is governed by physical forces such as electrostatic interactions, Brownian motion and van der Waals forces.[13]

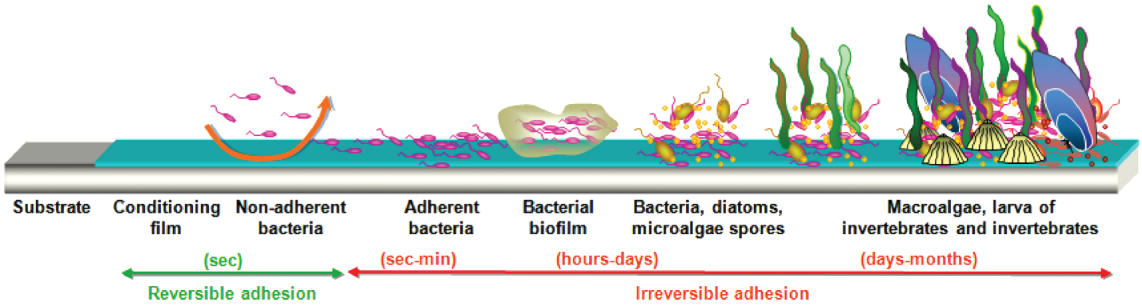

Figure 1.1: Schematic of the marine biofouling process. An organic conditioning layer adheres within seconds of immersion. Microorganisms rapidly attach to the conditioning film and adhere irreversibly via cellular appendages and exopolymers. Mature biofilms develop and facilitate attachment of larger marine organisms. Reproduced from [10].

Conditioning films have been found to develop within seconds of immersion and lay the foundation for primary surface colonisation by bacteria, diatoms (microalgae), and other unicellular microorganisms.[7, 12] Fouling species firstly adsorb to the surface, again through physical processes,[9] and then adhere irreversibly through secretion of extracellular polymeric substances (EPS) that envelope and anchor the colonising microorganism to the substrate.[4] The next stage of biofilm formation involves the organisation of cells into matrix-enclosed microcolonies that facilitate the transportation of nutrients and waste through an interconnected network of

water channels.[14] Subsequent stages involve settlement and growth of larger marine invertebrates and microalgae, and finally, biofilm maturation and dispersal.[15] Whilst the marine biofouling model is often described as a successional process involving a number of discrete stages, in reality, fouling is a highly dynamic process with biofilm formation depending heavily on the species present, substratum properties, season, and geographic location.[7]

1.1.2 Bacterial Biofilms

The prevention of bacterial biofilm development is a major challenge within the health and biomedical industries. Bacterial and fungal contamination of surfaces such as countertops, surgical tools and medical devices contribute to the spread of potentially deadly hospital-acquired (nosocomial) infections.[2, 16] A US study showed that of 1.7 million hospital-acquired infections, approximately 99,000 of these were associated with patient death.[17] The risk of infection associated with implanted medical devices remains a leading cause of device failure and the need for surgical removal,[18, 19] while the emergence of antibiotic resistant microorganisms has prompted further investigation into infection resistant materials and coatings.[20] In addition to the risk posed by the spread of medical pathogens, there is growing concern within the food industry to prevent the spread of food-borne infectious diseases. There is increasing demand for coatings that exhibit antimicrobial properties for the processing and packaging of foods. Such coatings could reduce premature food spoilage, extend food shelf-life, and prevent the spread of food-borne infectious diseases.[3, 21, 22]

While biofilm formation in the marine environment often develops from multiple microbial species adhering to surfaces, singular bacterial species may be responsible for colonisation of unsaturated (non-aqueous) surfaces, including the contamination of medical devices and biomedical implants.[23] Bacterial biofilm formation is again considered to follow a successional fouling model consisting of multiple stages (Figure 1.2). Bacterial cells interact with abiotic surfaces though physicochemical, van der Waals, hydrophobic, ionic and polar interactions.[24] The presence of a pre-formed conditioning film consisting of biomolecules (proteins, glycoproteins, plasma components etc.) has also been shown to mediate bacterial attachment to surfaces.[25] Once a particular threshold of bacteria is present, cells will signal that this site is suitable for colonisation.[26] This form of communication, known as quorum sensing, assists regulation of bacterial physiological activities in response to fluctuations in cell-population density.[27] As cell populations increase, bacteria assemble into cellular aggregates or 'microcolonies', which become more firmly adhered to the substrate through secretion of EPS. EPS makes up the bulk structure of the biofilm and consists of polysaccharides, proteins, nucleic acids, and phospholipids.[14] As

the biofilm matures, the EPS develops an interconnected network of water channels that facilitate the transport of oxygen and nutrients to cells growing deep within the biofilm.[28] Bacteria protected within the biofilm (EPS matrix) present increased tolerance to biological, chemical or physical stresses,[29] and are drastically more resistant to antibiotics and biocides than unattached planktonic cells.[18, 30] The final stage of the biofilm cycle is the detachment and dispersal of cells from the biofilm itself, providing the bacteria with an opportunity to colonise other favourable surfaces.[14]

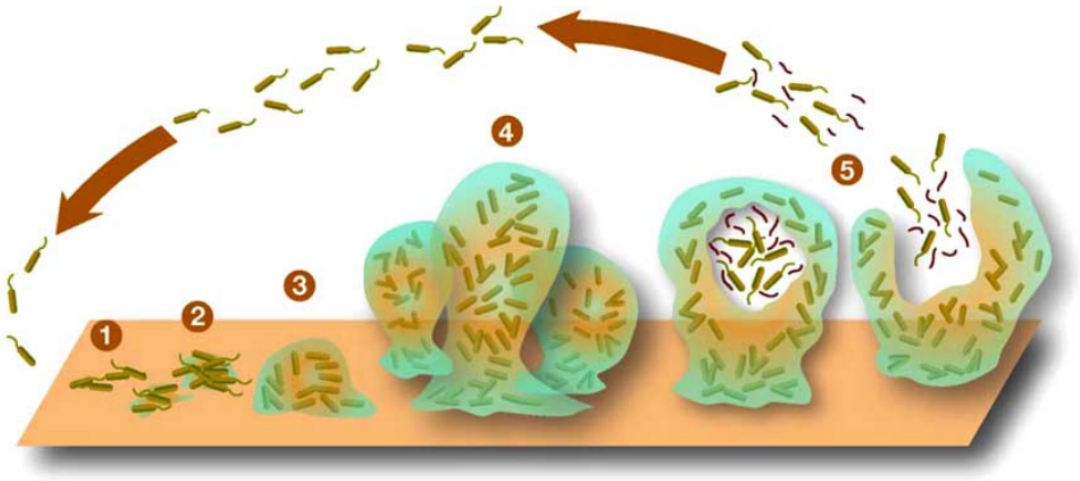

Figure 1.2: Schematic of the bacterial biofilm cycle illustrating the following distinct stages: individual cells interact with and populate the surface (1), irreversible attachment through EPS production (2), biofilm architecture develops (3) and matures (4), cells are released and dispersed from the biofilm (5). Image © Creative Commons Library.

1.1.3 Terrestrial Fouling

The focus of microbial contamination of surfaces is often their impacts on human health; however, there are broader implications in terms of the compromised functionality and appearance of surfaces that have been colonised by microorganisms. Microbial growth on surfaces in low water environments is termed unsaturated or terrestrial fouling.[29] Terrestrial fouling may arise from a range of organisms, including bacteria, fungi, algae, and protozoa,[31] and can result in the degradation of the underlying substrate.[32] Fungal growth in particular is a major biodeteriogen, reposonsible for degradation of paintings,[33, 34] wooden artefacts[35] and cultural heritage.[36, 37] Additionally, fungi and algae are the primary colonisers of human-built structures, responsible for the 'greening' of surfaces by photosynthetic cyanobacteria or algae, and the 'blackening' of surfaces by inhabiting fungi.[38] The growth of these microbial colonisers can also result in biodeteriorative processes, via

physical and biochemical mechanisms, such as the penetration of cracks, the expansion and contraction of biomass, and the secretion of degrading chemical metabolites (Figure 1.3).[39]

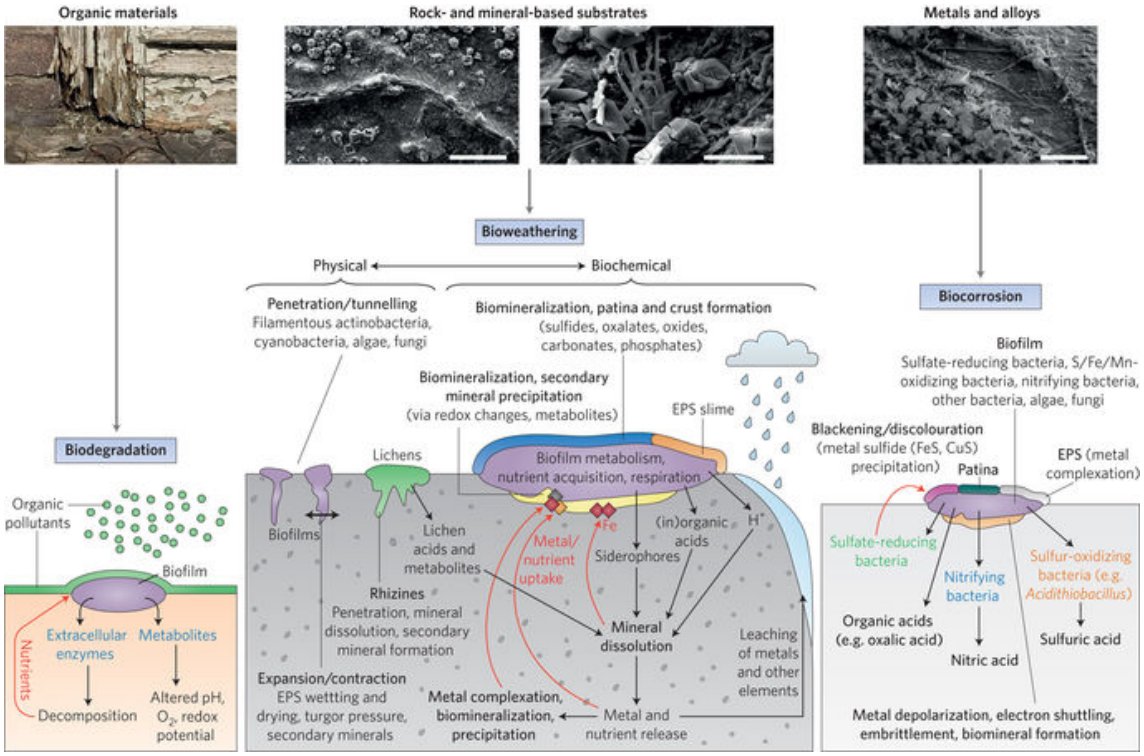

Figure 1.3: Examples of biodegradation, bioweathering, and biocorrosion of terrestrial surfaces brought about by microorganisms. Reproduced from [39].

Discoloration of exterior building materials by biological fouling is an increasingly recognised problem in the growing field of environmentally friendly architecture and the development of energy efficient buildings. Fouling of materials designed to maximise thermal efficiency reduces their capacity to reflect thermal energy, resulting in increased costs associated with the maintenance of internal building temperature.[40, 41]

The process of fungal colonisation is initiated by airborne spores settling and attaching to appropriate host surfaces. Upon contact, spores may attach through purely physical interactions or chemically through the secretion of adhesive proteins.[42] Following adhesion, spores begin to germinate with the generation of a 'germ tube' that elongates in contact with the surface.[43] If conditions are favourable, the germ tube will differentiate into appressorium, which can penetrate into the substrate to which it is bound.[42] Alternatively, germ tubes develop into vegetative hyphae that grow through apical extension and colonise the surface via establishing elaborate interconnected networks known as mycelium.[44, 45] A highly branched mycelial structure increases the colonies ability to spread over a substrate, enabling sensing of the local environment and facilitating nutrient uptake and transport.[44,

45] In this way, fungal species are well adapted to adhering to a range of different substrates, and thus present a significant challenge in preventing their attachment and colonisation of terrestrial surfaces.

1.2 Biocidal Coating Development

To date, fouling resistant coating developments have primarily focused on biocidal coating technologies which exhibit an antimicrobial effect through the slow release of toxic compounds over time. Such strategies may rely on the release of toxic metal ions, antibiotics or organic antimicrobial agents, to inhibit microbial fouling through species specific or sometimes broad-spectrum mechanisms. The effectiveness of different biocidal coatings is discussed below.

1.2.1 Early Strategies

Techniques used to prevent marine fouling date back to as early as the 3rd century B.C., where lead and possibly copper sheathing were used to protect ship hulls.[9, 13, 46] Ancient cultures were also credited with coating hulls in wax, pitch, tar, and asphaltum to improve water-tightness and to protect against ship worms.[10, 46] The first antimicrobial paints emerged around the mid-19th Century and contained copper, arsenic, or mercury oxide.[13, 47] Commercial coatings that have been developed since have typically been divided into three categories based on their release mechanism: insoluble matrix (contact leaching coatings), soluble matrix, and self-polishing coatings (Figure 1.4).[9, 13] Contact leaching coatings were developed by incorporating high amounts of toxicants into paints comprised of high molecular weight insoluble polymer binders.[10] As seawater spreads through pores in the coating, it dissolves the toxic species and enables its release from the coating matrix. However, as the surface toxicants are depleted, the rate of release gradually decreases over time as seawater is forced to penetrate further into the coating to facilitate release.

Due to the rapid depletion in efficiency of water insoluble paint matrices, water soluble matrix paints were developed to extend biocide release by utilising seawater soluble binders (e.g. rosin).[48] Upon immersion in seawater, the biocide and soluble binder are dissolved and released simultaneously from the coating.[10] While soluble matrix paint formulations have improved efficiencies compared to contact leaching coatings, they also suffer from uncontrolled dissolution rates making coating lifetime difficult to predict.[47]

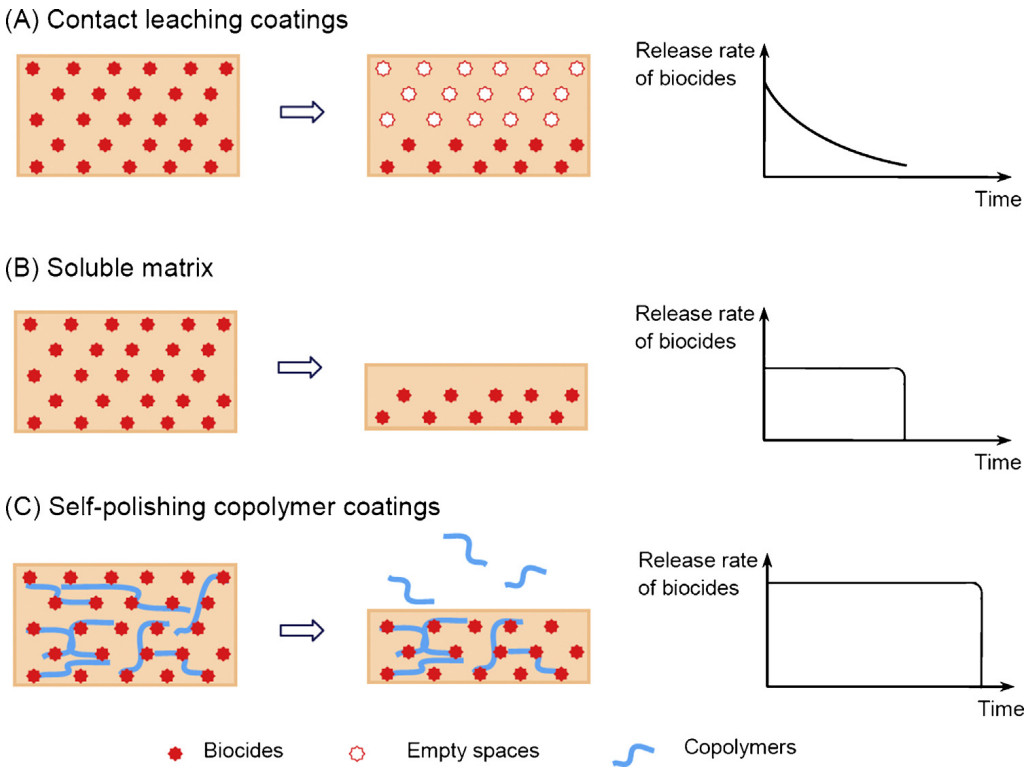

Figure 1.4: Biocide release from: contact leaching coatings (A), soluble matrix coatings (B), and self-polishing copolymer coatings (C). Reproduced from [6].

The emergence of self-polishing paints in the 1960s revolutionised the antifouling coating industry. Self-polishing paints containing organotin compounds were found to be highly effective at preventing biofouling accumulation with an increased degree of control over biocide release and coating erosion.[49] A coating matrix composed of tributyltin (TBT) and acrylic or methacrylate copolymers are gradually hydrolysed by seawater, providing a slow and controlled release of the toxic TBT species and leaves behind a polished coating surface with reduced drag.[6, 13] However, self-polishing organotin systems have since been shown to have detrimental environmental effects on non-target organisms including the development of imposex in sea snails,[50] stunted growth in mussels,[51] and shell-defects and reduced reproductive capability in oysters.[52] As a result, the use of TBT in antifouling paints was banned by the International Maritime Organisation in 2008.[53] Tin-free antifouling systems employed today typically contain copper compounds and organic boosters,[49] however, uncertainties regarding the toxicity and bioaccumulation of these compounds has led to their increased scrutiny and environmental regulation.[9]

1.2.2 Biocidal Coatings

There are large numbers of biocidal coatings, functioning through the release of toxic species or chemical agents, which have been shown to be effective at killing or

deterring growth of fouling microorganisms. The applications of such coatings vary widely from food packaging, to crop protection, and implantable medical devices.

1.2.2.1 Organic Biocides

The ban of TBT has led to the search for alternative biocides for marine vessel protection. Copper and zinc have again been increasingly used in the formulations of controlled depletion coatings and self-polishing coatings.[9] Metallic inclusions have also been coupled with organic booster biocides to improve the scope of fouling protection through synergistic effects. While increased copper concentrations in the aquatic environment have not been considered to have significant effects on marine ecosystems due to high degrees of speciation (reduced bioavailability),[54] toxicity to non-target organisms is still a large concern and has increasingly led to their restriction in the use of marine antifouling coatings.[55, 56]

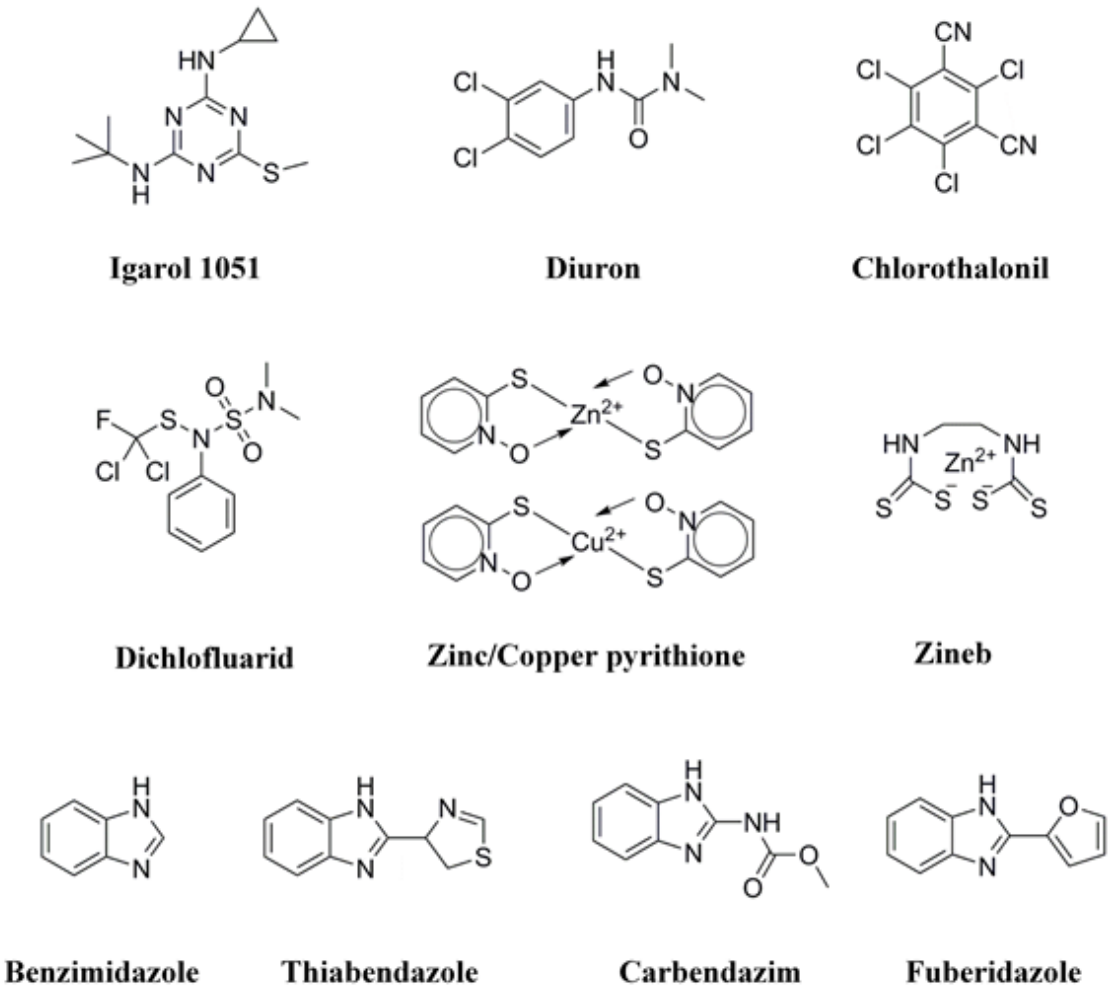

Figure 1.5: Chemical structures of common biocides.

Common booster biocides added to antifouling paints include Irgarol 1051, diuron, chlorothalonil, dichlofluanid, copper and zinc pyrithione, and zineb (Figure 1.5).[54,

57] Irgarol 1051 and diuron were previously among the most popular biocide booster additives to coatings but have since been found to accumulate in recreational waterways at high concentrations.[58] These biocides are not readily biodegradable, persisting in the water column and causing damage to non-target marine organisms through inhibition of natural photosynthetic pathways.[59]

The use of organic biocides is not limited to marine coatings, such compounds also have agricultural uses in the form of pesticides, herbicides, and fungicides.[54] Benzimidazole based compounds including thiabendazole, carbendazim, and fuberidazole (Figure 1.5) have been applied as fungicidal agents to control fungal diseases affecting field crops and for the prevention of crop spoilage during transport and storage.[60, 61] Whilst generally effective, the fungicidal action of benzimidazoles can be hindered by their low water solubility. The use of cyclodextrins to form inclusion complexes has provided a method of encapsulating benzimidazole compounds to improve their solubility, stability and bioavailability.[62, 63]

In recent years there has been a growing demand for the use of natural antimicrobials to protect and preserve foodstuffs due to health and safety concerns over synthetic chemical preservatives. The use of inherently antimicrobial substances produced by plants to control fungal growth have been considered as an alternative to synthetic pesticides and food preservatives. Essential oil components (EOC) are natural bioactive compounds that possess antimicrobial, antiparasitic and insecticidal properties.[64] Despite the well documented antifungal properties of EOCs, their application as antimicrobial agents is hindered by their high volatility and hydrophobicity. Encapsulation of EOCs with β-cyclodextrin or loading of EOCs into mesoporous silica scaffolds has been shown to reduce volatility of EOCs allowing for sustained antifungal activity.[65] Further studies are required to investigate EOCs as broad-spectrum biocides and to develop suitable methods of application.

1.2.2.2 Antibiotics

The prevalence of post-surgical bacterial infections has driven investigation of coatings that can either kill or prevent attachment of bacteria to the surface of implantable devices. Coatings that contain or release antibiotics at the sight of implantation have been developed to prevent bacterial infection.[48] Catheters are medical devices with some of the largest volumes of use and consequently their protection from microbial contamination is required to reduce infection.[66] Kohnen et al. were able to impregnate ventricular silicone catheters with a combination of rifampin and sparfloxacin antibiotics to produce a long lasting device with a broad antimicrobial spectrum (Figure 1.6).[67] While the device suffered from a decrease in release rate after an initial burst release of the antibiotic, it was found to still prevent colonisation of the catheter surface from Gram-positive *Staphylococcus epidermidis* for at least

one year.

Antibiotics have also been grafted directly from bulk polymers to produce antimicrobial coatings. The attachment of penicillin to poly(tetrafluoroethylene) (PTFE), a general antiadhesive polymer with a low surface energy, was described by Aumsuwan et al.[68, 69] Modified PTFE surfaces exhibited high antimicrobial activity toward Gram-positive *Staphylococcus aureus* bacteria. The effectiveness of these materials was partially attributed to the presence of a poly(ethylene glycol) (PEG) spacer. The PEG spacer was found to facilitate the mobility of the immobilised penicillin molecules, preventing the proliferation of microbes. This study was extended to examine attachment of the antibiotic ampicillin to PTFE and a strong antimicrobial effect was observed across a range of Gram-positive and Gram-negative bacteria.[70]

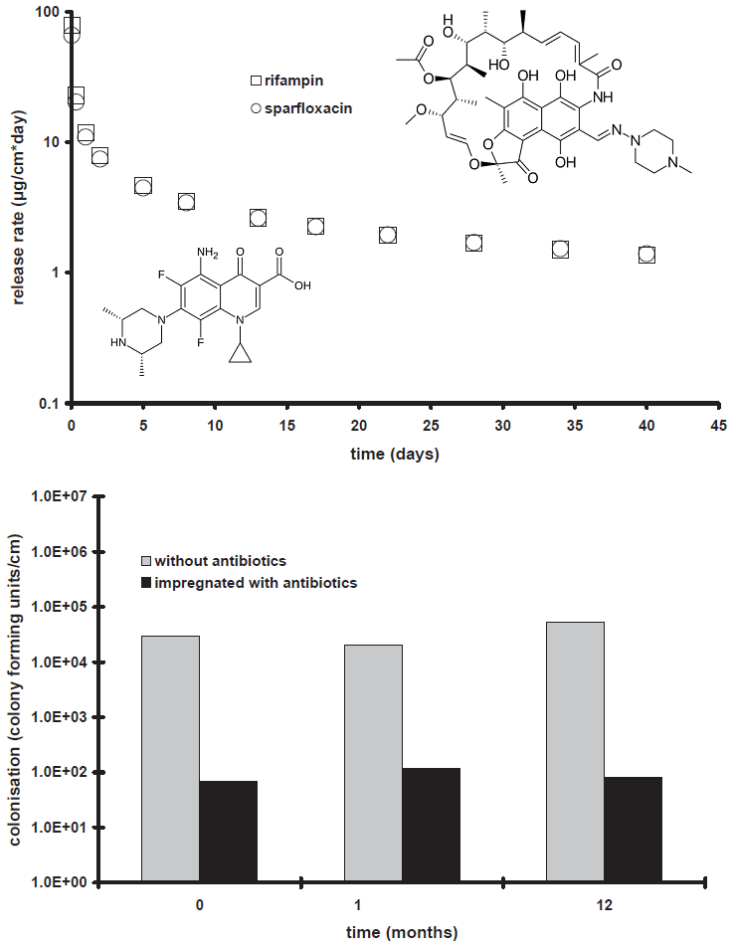

Figure 1.6: Antibiotic release from a catheter impregnated with rifampin and sparfloxacin (top), and catheter colonisation by *S. epidermidis* (bottom). Reproduced from [67].

Sophisticated methods of antibiotic release have been developed to account for the widely differing timescales of device infection. Biodegradable polyelectrolyte multilayers incorporating the antibiotic gentamicin have been fabricated to allow precisely tunable dosages of antibiotics to be released as the coating gradually

degrades.[71] The dosage of encapsulated antibiotic could be precisely controlled by the number of deposited layers, while the release rate could be controlled by varying the film architecture and polymer chemistry. Antibiotic gentamicin has also been loaded into chitosan hydrogels to produce a biocompatible coating with combined antibacterial and osteogenic activities.[72] Adjusting levels of the hydrogel cross-linker (genipin) was reported to tune the release of the gentamicin antibiotic species.

Despite the novel techniques emerging in the field of antibiotic containing and releasing biomedical coatings, there are still two main issues that will largely affect their in-field performance. The first is the depletion of the antibiotic species over time resulting in reduced efficiency (particularly for late onset infections), and the second, and potentially more alarming, is the emergence of antibiotic resistance amongst bacterial strains.[20, 73] As a result, alternative antimicrobial coatings are increasingly sought after to reduce the proliferation of antibiotic resistant bacteria.

1.2.2.3 Metal Release

Metals, such as Na, Mg, K, Ca, Mn, Cu, Zn and Fe, play a vital role in cell functioning and are essential for normal physiological cellular processes.[74] However, an excess of these essential metals can be lethal to cells and their concentrations must be constantly regulated. A number of non-essential metals, including silver, tellurium and mercury, have also been shown to exhibit intrinsically antimicrobial properties, with strong biocidal activity exhibited at exceptionally low concentrations.[66, 75] The use of bulk metals for antimicrobial applications is generally not feasible and alternate methods of incorporating metals into coatings and onto surfaces are currently being explored.

Metal Ions As mentioned previously, metal sheathing of ships and metal inclusions to paints have been used for many years within the marine industry to prevent or reduce the build-up of biological fouling. Metal ions leached from these surfaces are available for uptake by marine organisms, often resulting in their death. Copper (Cu^{2+}) ions have known toxicity to a range of marine species including tube worms, barnacles and a number of different algae.[54] Additional to marine applications, copper has been utilised for centuries for the sterilisation of water and treatment of wounds.[76] In recent years, the use of copper in the health care industry has gained renewed attention due to the rapid killing of bacteria, viruses, and yeasts that come into contact with metallic copper surfaces.[77] The contact killing effect exhibited by metallic copper is due to the release of copper ions from the metal surface. An early study by Beswick et al. found that the valence of copper affects its antimicrobial activity, with Cu^{+} ions exhibiting a stronger bactericidal effect than Cu^{2+} ions.[78]

This study was supported by Mathews et al., who demonstrated that Cu^{2+} ions on iron surfaces would be reduced to Cu^{+}, producing an enhanced antimicrobial effect.[79]

While the exact mechanism of contact killing copper surfaces has not yet been fully elucidated, a number of mechanisms have been tentatively proposed (Figure 1.7). Copper ions have been demonstrated to generate reactive oxygen species (hydroxyl radicals), causing oxidation of proteins and lipids, and resulting in cellular damage.[80] Copper alloys and copper (I) complexes have also been shown to actively degrade bacterial DNA, causing widespread cell death.[81] Studies indicate that DNA is rapidly destroyed, preventing the transfer of genetic material and reducing the likelihood of genetic resistance developing.[82]

These reports contrast with recent findings by Santo et al. who demonstrated that bacterial cells suffer extensive membrane damage and loss of cell integrity within minutes of exposure to copper surfaces.[83, 84] These findings suggest that membrane damage may be the primary mechanism behind cellular death and that DNA damage or damage by reactive oxidative species is a secondary event. Similar findings were reported by Ma et al.,[85] who demonstrated that Cu^{2+} and ZnO species adsorbed to the surface of clay particles changed the cellular morphology of pathogenic *Escherichia coli* and *Salmonella typhimurium* bacteria, destroying the bacterial wall and resulting in an efflux of intracellular nutrients.

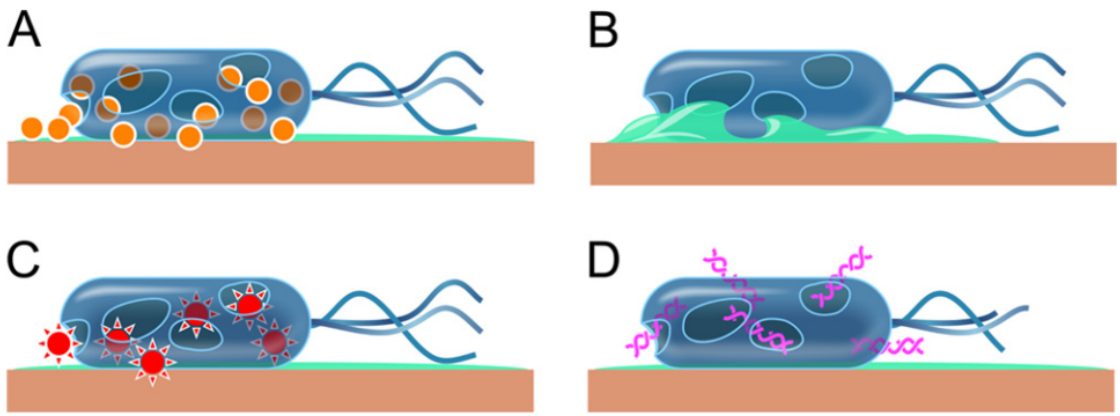

Figure 1.7: Tentatively proposed mechanisms of contact killing on copper surfaces: cell damage caused by dissolved copper (A), cell membrane rupture leading to loss of cytoplasmic content (B), cell damage from generation of reactive oxygen species (C), and DNA degradation (D). Reproduced from [77].

Silver is another intrinsically antimicrobial metal that has been used for many years in the treatment of burns, application of wound dressings, and in the coating of medical devices and catheters to prevent infection.[18, 48, 86] Silver exhibits broad spectrum antimicrobial activity, with demonstrated toxicity to bacteria, fungi, and some viruses.[87] Silver containing surfaces have attracted particular attention

due to their strong bactericidal effect against prokaryotic cells, while exhibiting a far less pronounced effect in eukaryotes.[88] Nanoscopically smooth thin films of silver prepared by magnetron sputtering are reported to exhibit bactericidal activity towards both Gram-positive and Gram-negative bacteria.[89] A less pronounced effect was observed against Gram-positive bacteria due to increased thickness of the peptidoglycan cell wall; a finding consistent with previous reports.[86]

Similar to copper, the exact mechanism of action of silver is not yet fully understood but is generally thought to be associated with the ionic form and not the elemental metal.[66] Silver ions have previously been claimed to form complexes with a range of biological molecules including RNA, DNA, and amino acids with P, S, N and O donors.[90] Gordon et al. have since reported that silver relies primarily on its interactions with sulfhydryl (thiol) groups in amino acids for its antimicrobial activity.[91] Binding of Ag^+ to thiol groups was demonstrated to inhibit enzymatic activity of proteins and promote the liberation of iron from iron-sulfur protein clusters with subsequent generation of hydroxyl radicals via Fenton-type reactions.[74, 91] Treatment of bacterial cells with Ag^+ has also been shown to transform DNA molecules into a condensed form, impeding its ability to replicate and ultimately leading to cell death.[92]

Metal Nanoparticles Metal and metal oxide particles in the size range of 1–100 nm have been heavily investigated in recent years for their unique antimicrobial properties. Metal nanoparticles exhibit increased chemical activity compared to their bulk counterparts owing to their large surface area to volume ratios.[93] They are also highly processable and have potential uses across a multitude of applications ranging from agriculture to textiles, food packaging, and healthcare.[74, 76, 94] The antimicrobial activity of silver nanoparticles is largely attributed to the generation of silver ions at their surface, an effect which is enhanced by their large specific surface area. Smaller sized silver nanoparticles present a larger surface area to volume ratio and hence exhibit enhanced antimicrobial activity through increased release of Ag^+ ions.[86] Some studies have indicated that the toxicity of silver nanoparticles relies on particles penetrating bacterial membranes; increasing their permeability and resulting in structural changes and membrane degradation.[93, 95] However, later studies have argued that generation of silver ions must be the primary mechanism contributing to cellular death as antimicrobial activity is not observed under anaerobic conditions (silver ion generation requires the presence of both water and oxygen) Figure 1.8).[96–98]

Silver nanoparticles are considered promising materials for the development of antimicrobial coatings. Coatings for implantable medical devices have been developed by impregnating silicone with silver nanoparticles to impart a high degree of

antimicrobial activity.[99] However, washing of the impregnated silicone was shown to decrease the antimicrobial activity of the polymer indicating removal of surface deposited silver nanoparticles. Interestingly, the antimicrobial effect was not abolished completely, suggesting that some silver nanoparticles buried deeper within the polymer matrix were still able to be released and provide some antimicrobial affect.

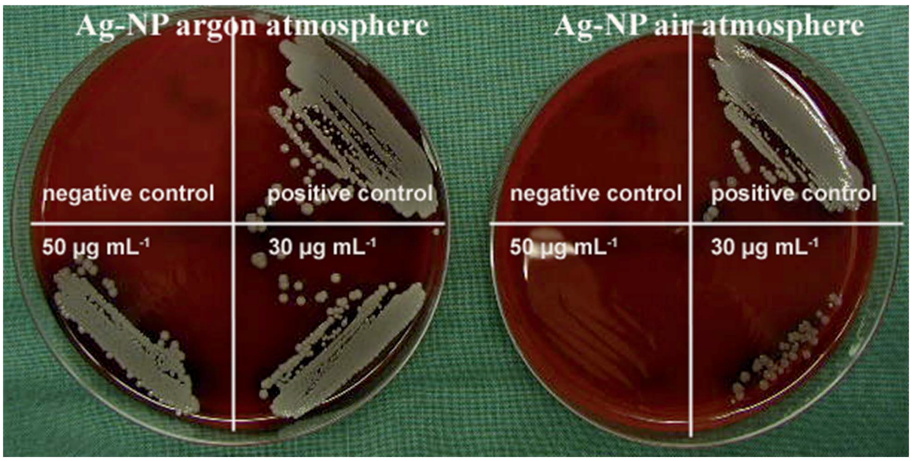

Figure 1.8: Colonies of *S. aureus* on blood agar plates under argon and air atmosphere. Silver nanoparticles at concentrations of 30 and 50 μgmL^{-1} were far less toxic to bacteria under argon conditions than those stored under air. Reproduced from [98].

Sophisticated nanocomposite materials have been designed for widespread application and to try and increase coatings antimicrobial lifetime. Hydrophobic silver nanoparticle polymer composites have demonstrated long-term bactericidal activity, eliminating bacteria even after storage in water for 100 days.[96] This result was attributed to the hydrophobic polymer limiting diffusion of water, and thus hindering the generation and release of silver ions. Similarly, the release of silver ions from polymer nanocomposites can be tuned through the application of a hydrophobic polymer overcoat, providing controlled rates of silver ion release from the polymer matrix.[100] Silver nanoparticles loaded into paints have also demonstrated antifungal activity, outperforming commercial fungicides when prepared at concentrations of 2–3% (10–15 ppm).[101] However, extensive use of silver has led to the emergence of bacterial strains with silver resistance.[102, 103]

Copper nanoparticles are being investigated as a replacement for traditional copper sulfate disinfectants for control of fungal crop diseases. Copper nanoparticles offer enhanced antimicrobial activity compared to copper salt due to their large surface area to volume ratio. They have demonstrated promising antifungal activity against a range of plant pathogenic fungi, outperforming a commercially available fungicide (bavistin).[104] Polymer-copper nanocomposites capable of releasing quantifiable amounts of copper, have also demonstrated biostatic activity against eukaryotic microorganisms.[105] Metal dissolution of Cu^{2+} species was observed from copper

nanoparticles embedded in polyvinylmethylketone (PVMK), polyvinylchloride (PVC) and polyvinylidene fluoride (PVDF) matrices, with a strong correlation observed between nanoparticle loading, Cu^{2+} release, and antimicrobial effect. A follow up study by Cioffi et al. demonstrated the effectiveness of polymer-copper nanocomposites against a range of bacteria, mould, and yeast.[88] Despite the promising antimicrobial properties of metal nanoparticles, their use in biomedical applications are limited due to interactions with proteins which lead to particle increases in size and agglomeration. Nanoparticle aggregation is also a problem during coating preparation and application, usually resulting in decreased specific surface area and a lowering of antimicrobial activity in the resultant coatings.[106]

Metal nanoparticles have been investigated as antifungal additives for indoor paints.[107] The incorporation of silver, copper, and zinc oxide nanoparticles into acrylic paints did not drastically alter the colour or gloss of the paints (except at the highest silver concentrations) and imparted a degree of bio-resistance across the three particles studied. Inhibition of fungal growth was most improved on the silver inclusive coating, where decreasing the silver particle size generated a more pronounced antifungal effect. Only minimal reductions in fungal growth were achieved by the copper and zinc oxide nanoparticles. Nano-metals have been added to other conventional building materials in an effort to improve biological resistance. Addition of silver, copper, and zinc nanoparticles to eight different building materials produced some reductions in fungal growth but failed to provide complete protection against fungal fouling.[108] More work is needed in this area to ensure coating function and appearance is not drastically altered by inclusion of metal nanoparticles and antimicrobial activity is retained after coatings are subjected to prolonged exposure.

1.2.2.4 Photocatalytic

Materials that present photocatalytic properties have been employed in applications requiring the removal of organic contaminants and in the disinfection of surfaces, air, and water.[109] Photocatalytic nanomaterials, particularly TiO_2, have been increasingly investigated for their ability to inactivate a wide variety of microorganisms under photoillumination. TiO_2 can be activated by photon energies that fall within the solar spectrum, meaning exposure to sunlight can promote an electron from the valence band to the conduction band, and in the process leave behind a positively charged hole in the valence band.[109] The electron and hole may recombine or may react with molecular oxygen and water to give reactive oxygen species (ROS) such as superoxide, hydroxyl and hydroperoxyl radicals, and hydrogen peroxide. ROS are capable of destroying cellular membranes, causing damage to DNA and proteins, and disrupting electron transfer processes.[110] As a result, photocatalysts are effective at killing a wide range of microorganisms including bacteria,[111, 112] viruses,[113]

and fungi.[114, 115]

The addition of TiO_2 to commerical facade paints have resulted in improved antifungal efficiencies,[116] while TiO_2 coatings of polypropylene films for food packaging show large reductions in *E. coli* bacteria after irradiation with UVA light.[117] Similarly, TiO_2 treated wood has demonstrated antifungal activity when irradiated with UVA light,[115] however, fungal regrowth was observed when the light source was removed. This indicates that TiO_2 could successfully suppress fungal growth under irradiation but was not sufficient for total disinfection of the underlying wood.

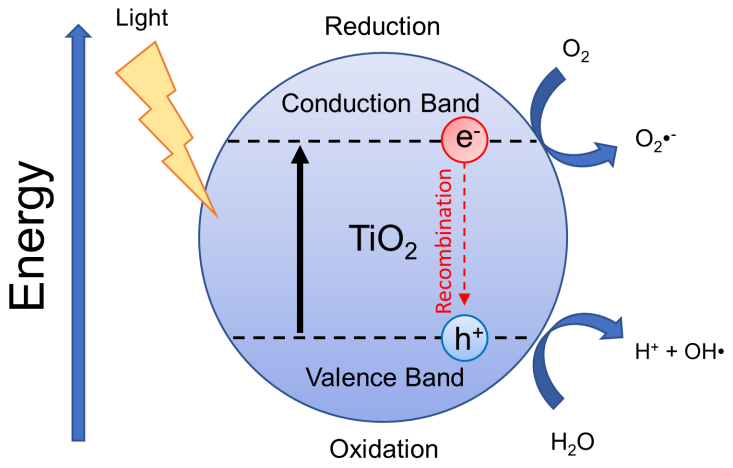

Figure 1.9: Schematic of TiO_2 irradiation, electron hole separation, and generation of reactive oxygen species.

Applications of TiO_2 based coatings may be limited due to the need to expose coatings to UV light (only a small proportion of total solar energy) in order to generate an antimicrobial effect. Additionally, TiO_2 suffers from rapid electron/hole recombination and low photocatalytic efficiencies.[118] In an effort to overcome these issues, TiO_2 has been paired with photosensitive materials that present a plasmon resonance response. Plasmonic photocatalysts, such as noble metal (Ag, Au, and Pt) nanoparticles, exhibit strong absorption in the UV-vis range due to surface plasmon resonance; the collective oscillation of surface electrons upon interaction with electromagnetic radiation.[119] Additionally, antibacterial activity is enhanced through promotion of more efficient electron/hole separation and prevention of charge recombination.[120]

While numerous studies have demonstrated the effectiveness of TiO_2 based materials as promising antimicrobial agents, they are unable to be incorporated into traditional organic coatings as ROS generation will degrade the coating matrix.[48] Further work in the area of photocatalytic antimicrobials is ongoing, with a focus on developing stable coatings for long-term applications.

1.2.2.5 Polymeric Antimicrobials

An alternative strategy to release-based mechanisms of imparting antimicrobial activity is through covalent attachment of antimicrobial agents to surfaces. Cationic antimicrobials such as quaternary ammonium compounds, guanidine polymers or phosphonium salts, either embedded in coatings or immobilised on surfaces, have demonstrated broad-spectrum antimicrobial activity through a contact killing mechanism.[121–123] Unlike the release-based mechanisms described earlier, cationic coatings possess a long-lasting antimicrobial effect and do not result in unwanted secondary contamination of the environment.[122, 124] Arguably the most widely explored polymeric antimicrobial coatings are composed of or contain quaternary ammonium compounds (QAC). The antimicrobial activity of QACs were initially attributed to penetration of bacterial or fungal cell membranes by sufficiently long and flexible cationic polymer chains.[125] This form of membrane disruption would result in cell lysis and eventually lead to cell death. However, this mode of action does not explain the antimicrobial activity exhibited by low molecular weight QACs with insufficient length to fully penetrate the cellular membrane.

An alternative hypothesis proposed by Kugler et al., involved loss of membrane integrity due to ion exchange occurring between structurally critical mobile cations within the cellular membrane and the cationic surface.[126] In order for this exchange to occur, the number of available cationic sites must exceed a charge-density threshold. While this threshold is known to vary between microbial species, it has been reported that surfaces with cationic density greater than 10^{15} quaternary amine units/cm^2 will result in an antimicrobial surface. A study by Murata et al. demonstrated that both QAC polymer chain length and chain density play a role in the antimicrobial activity presented by functionalised surfaces.[127] They observed that short chain length, high density QAC brushes exhibited bactericidal effects that were not associated with cell penetration. While lower grafting densities of QACs required increased chain length to exhibit effective bactericidal activity. Interestingly, surfaces that presented charge densities in excess of 3×10^{15} charges/cm^2 were found to kill bacteria regardless of initiator density and chain length (Figure 1.10).

The antimicrobial mechanism of two common biocides, one QAC and one tertiary amine, used in commercial contact lens cleaning solutions were investigated against a range of ocular bacteria and fungi.[128] This study found that the quaternary ammonium species showed pre-dominantly antibacterial activity, through induced K^+ leakage, while the amine species showed activity against all the studied organisms but exhibited stronger antifungal and antiprotozoal activity.

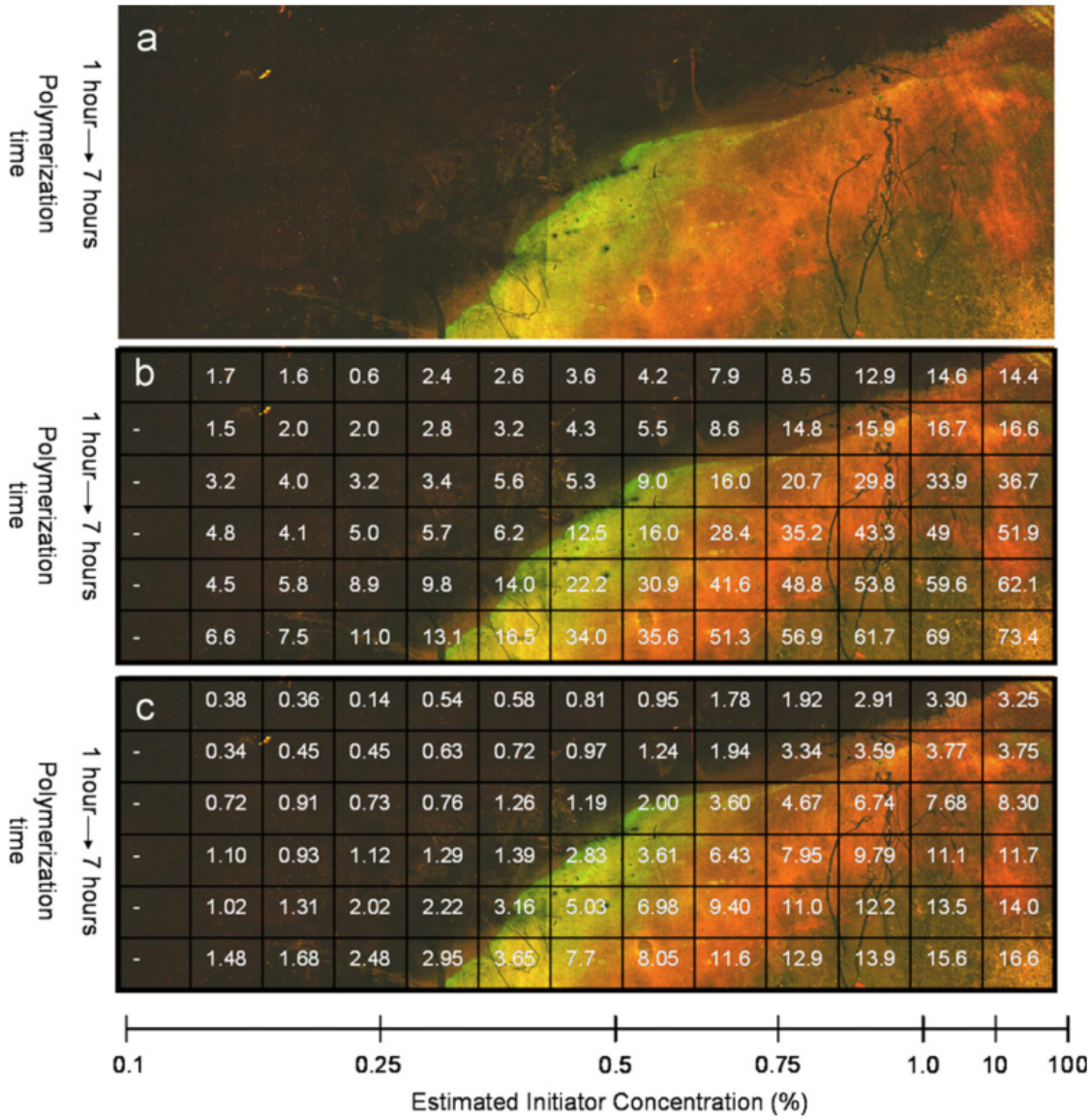

Figure 1.10: Quaternary ammonium functionalised glass slide with varied polymerisation time and initiator concentrations: live/dead staining of *E. coli* on the slide (a), superimposed with the polymer layer thickness (b), and charge density presented by the surface (positive charges/cm^2 $\times$ 10^{15}) (c). Reproduced from [127].

Ahlstrom et al. investigated the effect of hydrocarbon chain length on the fungicidal effect of a series of amphiphilic quaternary ammonium surfactants.[129] Antimicrobial action was found to be strongly related to binding affinity. The longest chain studied, cetyltrimethylammonium bromide (CTAB), was found to have the highest degree of binding and the strongest fungicidal affect at concentrations below the critical micelle concentration (CMC). This result was attributed (in part) to the CTABs higher degree of hydrophobicity and thus increased tendency to interact and bind with hydrophobic structures at the cell surface.

Similarly, Vieira and Carmona-Ribeiro investigated the mechanism of action of two

antimicrobial QAC surfactants, dioctadecyldimethylammonium bromide (DOD-AB) and CTAB against the fungus, *Candida albicans*.[130] They found that DODAB required lower concentrations than CTAB to kill 50% of *C. albicans* cells and again this was attributed to the larger hydrophobicity of the DODAB molecule. In contrast to other published work, this study demonstrated that cell lysis did not occur for either chemistry and that cell death occurred at submicellular concentrations when cell electrophoretic mobility shifted from positive to negative.

This area of work is not restricted to only QAC type surfactants; great success has also been shown by cationic polymeric materials. Low molecular weight water-soluble chitosan,[131] and quaternised polyethyleneimine (PEI) derivatives[16] have also demonstrated promising antimicrobial action through the rupture of cellular membranes. However, the biocompatibility of quaternary ammonium polymers remains an issue, as their antimicrobial properties are often also accompanied with haemolytic behaviour.[132] Additionally, QAC functionalised surfaces can become fouled by the accumulation of dead microbes, which then block surface functional groups resulting in loss of antimicrobial activity.[48]

1.3 Antifouling Coating Development

Increased awareness of the potential environmental impacts posed by antimicrobial coatings has stimulated the development of alternative coatings that do not rely on the incorporation or release of toxic components. Antifouling coatings that focus on inhibiting initial surface interactions and prevention of microbial adhesion are an attractive substitute to traditional contact killing coatings. This approach relies on tailoring surface chemical and physical properties to limit adhesion strength of biocontaminents and minimise overall surface colonisation.

1.3.1 Physicochemical Strategies

Interactions between microbial species and surfaces are primarily influenced by the intrinsic physicochemical properties of the substrate. Strategies involving alteration of surface physicochemical properties through chemical functionalisation and polymerisation, or through tuning of surface roughness and wettability, have been employed to develop novel non-fouling surfaces. Substratum surface energy plays an important role in determining the extent to which an organism can interact with and attach to a given surface.[133] There exists a relationship between the critical surface free energy and the relative amount of bioadhesion that is likely to occur. This relationship is described by the Baier curve (Figure 1.11) and illustrates the minimum in relative adhesion is most likely achieved at a critical surface tension in

the range of 22–24 mN/m.[134]

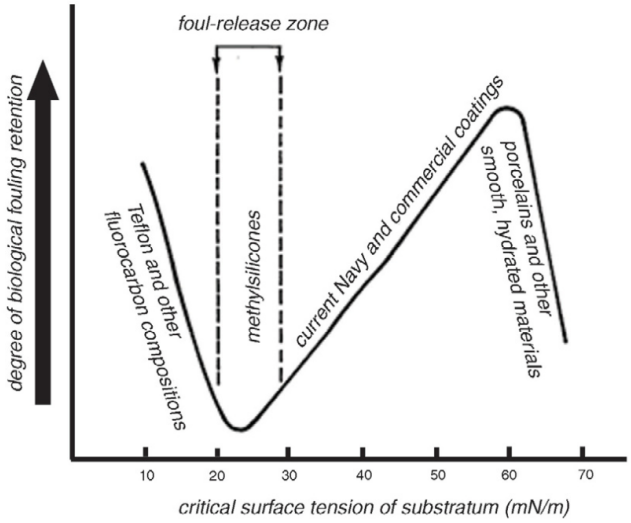

Figure 1.11: Baier curve of minimal adhesion in relation to critical surface energy. Reproduced from [134].

In addition to surface energy, surface wettability is also known to influence interactions with fouling species. Wettability, measured by the contact angle made by a sessile droplet on the surface of a substratum, relates the interfacial energies of the solid-liquid (γ_{SL}), solid-vapour (γ_{SV}) and liquid-vapour (γ_{LV}) interfaces[135] via Young's equation:

$$\cos\theta = \frac{(\gamma_{SV} - \gamma_{SL})}{\gamma_{LV}}$$

While this relationship holds true for chemically homogenous and atomically smooth surfaces, roughness has been demonstrated to either promote wettability ($\theta < 90°$) or reduce wettability ($\theta > 90°$), depending on the chemical nature of the substratum.[135] An early study by Wenzel reported a correlation between surface wetting and topography, proposing that a roughened surface will have magnified wetting characteristics.[136] In order to account for differences between the geometric surface area and the actual surface area of the substratum, a new expression was devised that included a 'roughness factor' (r):

$$\cos\theta^* = r\cos\theta$$

where θ is the angle described by Young's equation and r is the ratio of actual surface area to geometric surface area. The work of Wenzel was extended by Cassie and Baxter to including the wetting behaviour of porous surfaces. The model proposed by Cassie-Baxter describes the two wetting regimes observed on porous surfaces: air entrapment and wicking.[137] Air entrapment between topographical

surface structures increases surface hydrophobicity, with water droplets forced to rest partially on the surface and partially on pockets of trapped air. In the case of hydrophilic surfaces, water is drawn down into topographical cavities in a process called wicking. Water droplets on the substrate now rest on a combination of the contactable surface and the liquid trapped in the pores of the material.[12] The following equations are used to describe the Cassie-Baxter wetting model:

for air entrapment,

$$\cos\theta = -1 + \phi_s(\cos\theta + 1)$$

and for wicking,

$$\cos\theta = 1 + \phi_s(\cos\theta - 1)$$

where ϕ_s is the fraction of the surface in contact with the liquid.

These findings show the dramatic effect that topography has on the surface energy and wettability of a substratum, and indicate the potential for manipulation of topography to generate enhanced wetting characteristics.

1.3.1.1 Foul-Release Coatings

Since banning the use of many self-polishing coatings to protect commercial ship-hulls, the most prevalent coating replacement has come in the form of 'fouling-release' (FR) coatings. These FR coatings have been developed from materials that possess a critical surface tension within the foul-release zone described by Baier.[134] Low surface energy FR coatings do not prevent organism settlement but instead minimise adhesion strength of fouling species. Weakly adhered species are dislodged from the coated surface through hydrodynamic shear forces generated by a ships motion through water or can be removed by gentle mechanical cleaning.[56]

Typically, FR coatings are composed of silicone or fluorine based elastomers.[138] Such coatings present a hydrophobic interface with low surface energy, low elastic modulus and exhibit excellent fouling-release properties. Poly(dimethylsiloxane) (PDMS) based coatings present FR properties as a result of their chemical structure; combining a flexible Si-O-Si backbone with low surface energy side groups, allowing for high polymer mobility to facilitate surface migration.[47] Studies have demonstrated that PDMS coatings reduce adhesion strength of fouling species such as mussels[139] and barnacles,[140] however, they are inefficient against primary colonisers such as bacteria and diatoms which are responsible for the development of microbial slimes and facilitate attachment of larger macrofoulers.[141–143] Additionally, FR coatings can be difficult to apply to surfaces, they are typically mechanically weak

or easily damaged, and they are unsuited for applications where shear forces are not present.[144]

1.3.1.2 Bioinspired Topographies

For many years, scientists have drawn inspiration from the environment to try and replicate self-cleaning surfaces that are present in nature. Current developments in antifouling coating design have focused on the generation of biomimetic surfaces that possess self-cleaning properties or are capable of resisting colonisation. Inhibition of microbial fouling has been linked to the presence of micro- and nano-topographical features. The presence of appropriately scaled topographies has been shown to reduce cellular attachment by limiting the contactable surface area available for the fouling organism to adhere.[66, 145]

The Lotus leaf (*Nelumbo nucifeara*) is a classic example of a self-cleaning surface. It presents a rough surface comprised of convex epidermal microstructures with small hair-like protrusions emanating from the leaf surface and combines this with the secretion of a waxy-type substance that increases surface hydrophobicity.[135, 146] This results in air-entrapment and extremely high contact angles. Water beads on the leaf surface and will roll across the surface, collecting contaminants. A number of studies have been carried out to try and replicate the self-cleaning effect displayed by the lotus leaf. Lotus leaf substructures have been recreated through a nanocasting technique, where the surface of the lotus leaf is used to generate a negative template.[145, 147, 148] Coatings of polyurethane, poly(vinylchloride) (PVC) and PDMS prepared using this technique were found to be extremely hydrophobic, presenting high water contact angles and potential self-cleaning properties (Figure 1.12).

In addition to self-cleaning surfaces, other natural surfaces demonstrate the ability to prevent surface colonisation by fouling species. Appropriately scaled surface topography can effectively deter organism attachment, however, the height and spacing of topographic features has been shown to influence the degree of organism interaction and attachment. To examine the effect of topographical feature size, Scardino et al. prepared three hydrophobic coatings with varied physical architecture and investigated adhesion of five marine fouling species.[149] While all three surface coatings were superhydrophobic (contact angles $> 155°$), large variations in the degree of microbial attachment were seen between the different coating architectures. This result indicated that settlement responses were indeed strongly influenced by micro- and nanoscale topographic effects. Furthermore, many other artificial surfaces have been prepared that mimic the topographic features of antifouling surfaces present in nature. Carman et al. generated topographical patterns that were inspired by the naturally antifouling surface of shark skin (Sharklet AF^{TM}).[150] Patterns of

pillars and ridges prepared from low surface energy PDMS elastomer were shown to significantly reduce settlement of *Ulva* zoospores due to the feature dimensions being smaller than the spore body, and thus reducing the contactable surface area. Furthermore, this work demonstrated that by increasing the spacing between the ridges that the density of settled spores also increased, approaching that of the settling observed on smooth PDMS surfaces.

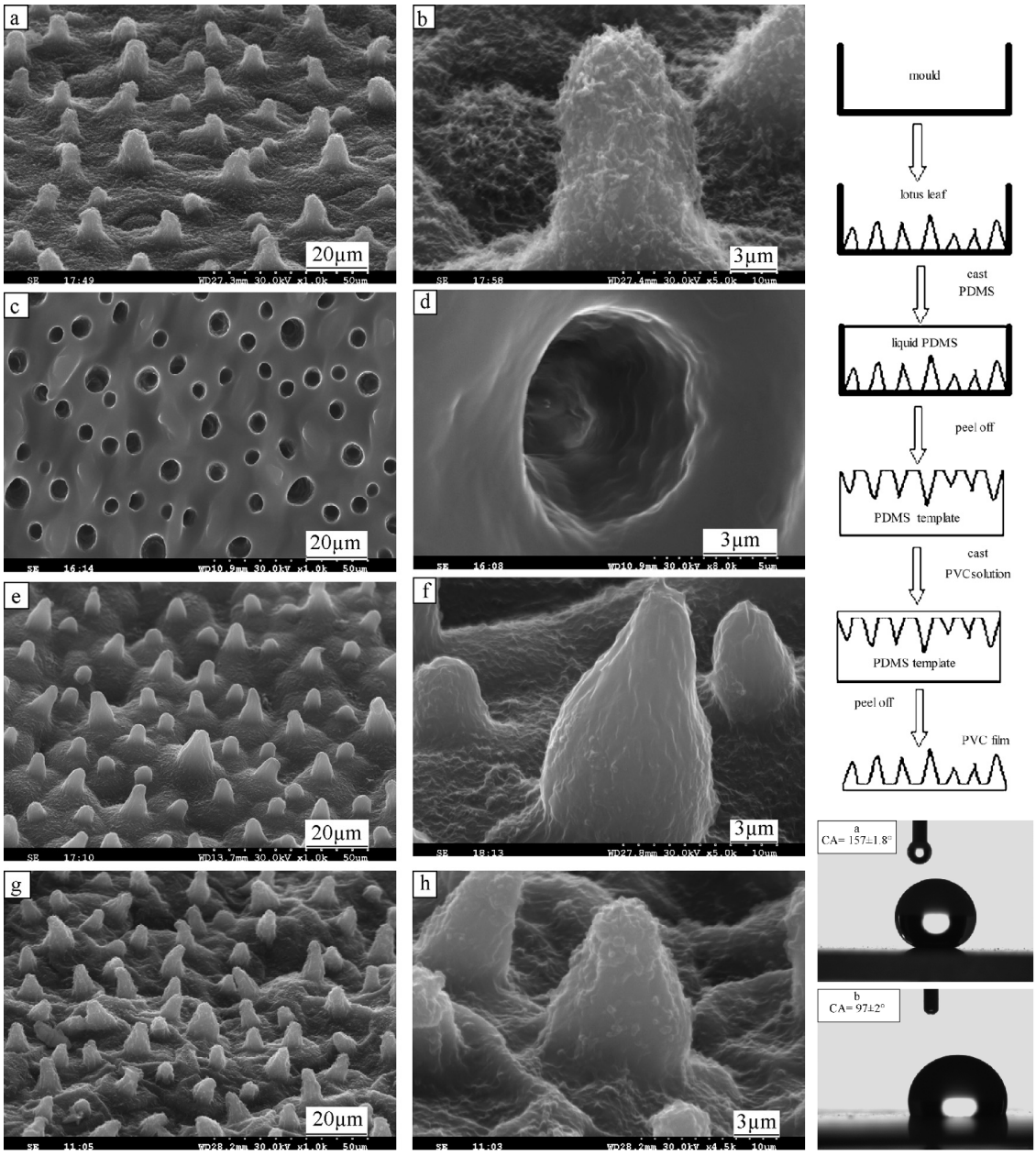

Figure 1.12: Left: SEM images of a fresh lotus leaf (a,b), a PDMS negative template of the lotus leaf (c,d), the positive template super-hydrophobic PVC film (e,f), and a dried natural lotus leaf (g,h). Right: Schematic diagram of the PVC film preparation process (top), and water droplets on lotus-leaf mimic PVC film (a) and smooth PVC film (b) (bottom). Reproduced from [147].

Cao et al. prepared a surface mimicking the morphology of the skin of a pilot whale

using polyelectrolyte self-assembly.[151] The structuring of this surface decreased interactions with spores of the green alga *Ulva*, with minimal settlement observed for structures on the same scale as the topographical features present on the skin of the pilot whale. The results from these studies indicate that both the scaling of topographic features and the size of the fouling organism play a role in determining the degree of microbial fouling. This means it would be necessary to prepare multi-scaled topographies to repel multiple organisms simultaneously. With that in mind, Schumacher et al. designed coatings in PDMS with multiple length scales to inhibit fouling from two marine species: barnacle cyprids of *Balanus amphirite* and algal zoospores of *Ulva linza* (Figure 1.13).[152] By superimposing smaller *Ulva*-specific topographies onto larger barnacle repellent features, coatings provided effective multi-species fouling resistance. However, for complex fouling environments, it would be impossible to scale topographies to prevent attachment of all available microorganisms.

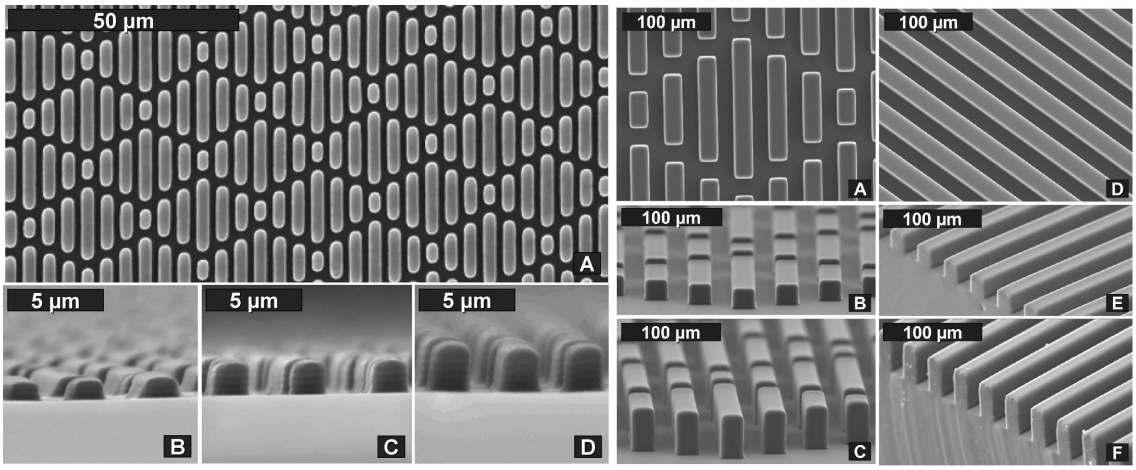

Figure 1.13: Left: Top-down (A) and cross-sectional (B–D) SEM images of *Ulva*-specific Sharklet AF^{TM} prepared in PDMS. Right: Top-down (A,D) and cross-sectional (B,C,E,F) SEM images of barnacle specific topographies engineered in PDMS. Reproduced from [152].

1.3.2 Hydrophilic Coatings

In recent years, hydrophilic coatings have been increasingly investigated for their ability to inhibit biofouling. Hydrophilic polymers physisorbed or covalently bound to surfaces have been demonstrated to significantly reduce protein adsorption and bacterial adhesion. Interactions between fouling species and hydrophilic surfaces are prevented by the presence of an interfacial water layer. This layer of structured water molecules at the air-surface interface forms a physical and energetic barrier preventing nonspecific protein adsorption and cell adhesion.[153, 154] Adsorption of fouling species to the surface is energetically unfavourable due to disruption of the

hydration layer and dehydration of the surface hydrophilic groups, leading to strong repulsive forces acting on the approaching biomolecule.[155, 156]

Water may be bound to surfaces via hydrogen bonding or through ionic solvation. The degree of surface hydration is determined by the physicochemical properties of the material, including: surface chemistry, film thickness, packing density, and chain flexibility.[153] Polymer chain length and mobility also play a role in preventing nonspecific protein adsorption. Short polymer chains inhibit fouling interactions purely through the organisation of a tightly bound water layer at the interface, while long chain hydrophilic polymers combine the effect of a hydration layer with a steric repulsion effect (Figure 1.14). Compression of longer chains causes a decrease in conformational energy and subsequent rejection of any incoming fouling species i.e. proteins and bacteria.[19, 56]

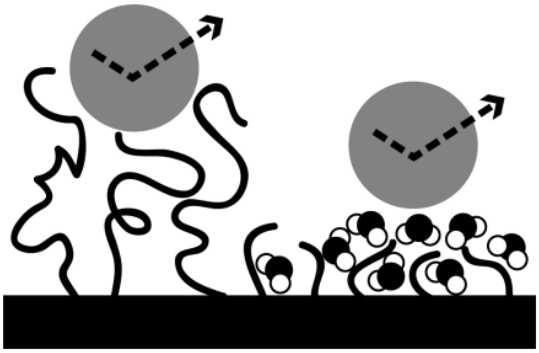

Figure 1.14: Inhibition of protein fouling by surfaces grafted with hydrophilic polymers due to steric repulsions presented by long polymer chains (left) and the presence of a tightly bound hydration layer surrounding short polymer chains (right). Reproduced from [157].

Over the years, a number of methods of attaching hydrophilic polymers to surfaces have been devised. Details of surface modification, via functionalisation and polymerisation approaches, and commonly investigated hydrophilic polymers for antifouling applications, are outlined below.

1.3.2.1 Surface Functionalisation

The preparation of hydrophilic coatings requires covalent attachment of hydrophilic polymers onto a substrate. While hydrophilic coatings can be prepared via physisorption of polymers onto surfaces, covalent attachment is generally preferred in order to generate stable and robust polymer interfaces. Functionalisation of surfaces with hydrophilic polymers can typically be achieved through either "grafting-from" or "grafting-to" methods (Figure 1.15). "Grafting-to" involves the attachment of pre-formed polymers to a surface through reaction with complementary surface chemistries. This technique results in the spontaneous organisation of polymer

chains into well-ordered arrays, generating what are known as "self-assembled monolayers" or SAMs.[158] "Grafting-to" reactions can be performed onto a variety of substrates with examples including gold-thiol coupling and reactions of chlorosilanes and methoxysilanes onto glass and silica,[157] with cross-linking of silanes known to increase stability within coatings of SAMs. Ordering within SAM assemblies is highly dependent upon interactions between the substrate and adsorbate, and the type and strength of intermolecular interactions between assembling molecules.[158] Whilst generally effective at preparing organised polymer coatings, this method can result in lower than desirable grafting densities as a result of steric crowding.[159]

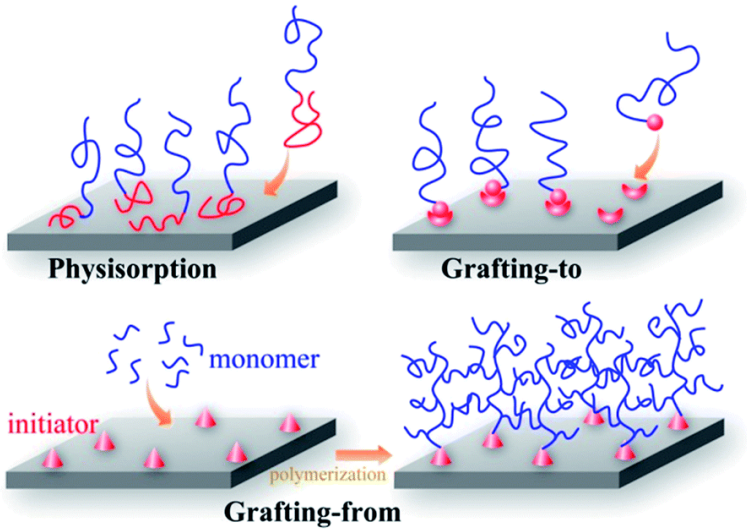

Figure 1.15: Different methods of immobilising hydrophilic polymers onto solid surfaces i.e. physisorption, "grafting-to" and "grafting-from" methods. Reproduced from [160].

The "grafting-from" method typically involves radical polymerisation, where polymer growth propagates from an initiator molecule covalently bound to the reaction surface. This technique generally achieves higher grafting densities and denser polymer brushes than those prepared via the "grafting-to" method. Recent advances in controlled polymerisation reactions has resulted in increased control over polymer length and grafting density, making possible the preparation of highly controlled and reproducible hydrophilic polymer coatings. Probably the most widely used "grafting-from" technique is atom transfer radical polymerisation (ATRP). ATRP is a controlled polymerisation process that has been used to prepare uniform polymer brushes with high grafting density, well-defined architecture, and precisely controlled molecular weight. ATRP reactions require a monomer, initiator, and catalyst (composed of a transition metal complexed by suitable ligand(s)).[161] Initiators are typically alkyl halides (R-X), where the R-group is similar in structure to the monomer. Vinyl momomers, including styrenes, acrylates, and methacrylates, are commonly utilised in ATRP reactions but acrylonitriles, and (meth)acrylamides

have also been investigated. As shown in Figure 1.16, ATRP reactions are dependent upon the equilibrium between propagating radicals and dormant species, namely the initiator alkyl halide/macromolecular halide species.[162] The dormant species will periodically react with transition metal complexes, causing metal oxidation and abstraction of the halogen atom. This in turn, generates an organic radical that can propagate with vinyl monomers (K_p), return back to a dormant organic halide species through abstraction of the halogen, or terminate polymerisation through reaction with another radical.[163] For ATRP reactions, the steady-state concentration of radicals is small, and thus termination reactions are limited. This makes ATRP a useful tool for the production of precisely controlled block and graft copolymers, as well as a valuable technique for the functionalisation of surfaces where reaction initiator molecules are immobilised on a substrate.

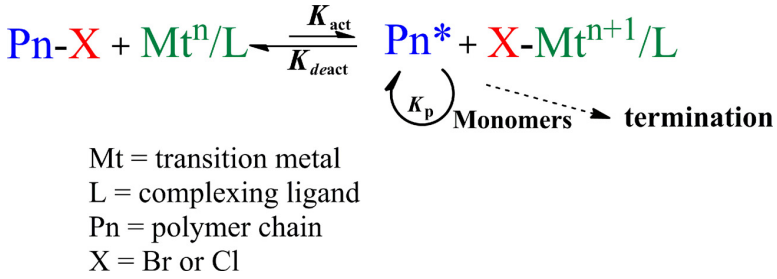

Figure 1.16: Transition metal catalysed ATRP. Reproduced from [162].

Utilising "grafting-from" and "grafting-to" functionalisation techniques, surfaces have been modified to present hydrophilic monomers and polymers for antifouling applications. The two main classes of hydrophilic polymers that have been investigated for their low-fouling properties are non-ionic hydrophilic polymers (primarily poly(ethylene glycol)) and zwitterionic hydrophilic polymers.

1.3.2.2 Poly(ethylene glycol)

For many years, poly(ethylene glycol) (PEG) has been considered the gold standard for preparing hydrophilic coatings with antifouling characteristics. The protein repellent properties of PEG are well documented. Early studies by Prime and Whitesides investigated SAMs of oligo(ethylene oxide) (OEG) on gold, revealing resistance to non-specific adsorption of four different proteins.[164] They found that monolayers containing high mole fractions of OEG groups showed good protein resistance, regardless of chain length. Later studies have shown increasing the grafting density of PEG, both covalently bound and physisorbed to surfaces, also results in decreased protein adsorption.[165]

Early theoretical studies of PEG by De Gennes and co-workers identified steric repulsion as the key mechanism inhibiting protein adsorption.[166] Compression of

polymer chains were shown to result in unfavourable entropy loss leading to protein repellency. This effect was proposed to be enhanced with increasing chain length and higher surface grafting densities. This theory was later improved by Szleifer, who used single-chain mean-field theory to demonstrate that protein resistance was independent of the molecular weight of the grafted chain, and instead relied on grafted surface coverage.[167] This model explains why high levels of protein resistance have been observed for self-assembled monolayers of low molecular weight OEG.[168, 169] In the aforementioned modelling studies, adsorbed water was treated as continuous medium and conformational changes of both the adsorbing protein and polymer chains were not accounted for. More detailed molecular simulations were carried out by Zheng et al. that included explicit solvent water molecules and optimal protein orientation on SAM surfaces.[170] This study found that improved resistance to protein binding was observed for SAM surfaces generated from mixed OEG and CH_3-SAMs between the ratios of 0.5–0.8. At these ratios, SAMs displayed the highest degree of hydration (hydrogen bonding) and also higher flexibility than surfaces of densely packed pure OEG-SAMs or dilute mixed OEG-SAMs. They concluded that OEG-SAMs containing a large number of hydrogen bonds with water have improved non-fouling properties or that a higher degree of flexibility of hydrated chains is responsible for protein repellency.

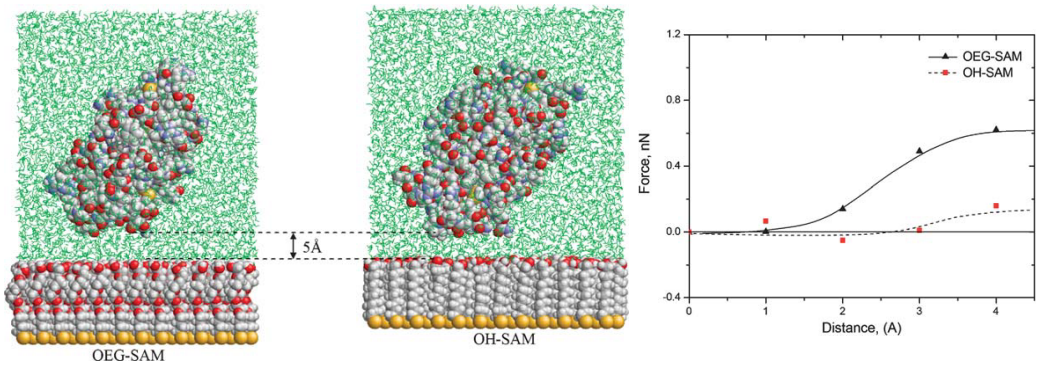

Figure 1.17: Molecular simulation of lysozyme protein interacting with OEG-SAM (left) and OH-SAM surface (middle). Solvent water molecules are shown explicitly (green wire frame). Comparison hydration forces on lysozome as a function of the distance normal to OEG-SAM and OH-SAM surfaces (right). Reproduced from [171].

A follow-up study compared protein interaction forces with surfaces composed of OEG-SAM, OH-SAM, and CH_3-SAMs.[154] Their simulations demonstrated that the repulsive forces acting on proteins decreased in the order of OEG-SAMs > OH-SAMs > CH_3-SAMs. The repulsive forces observed were shown to be generated from interfacial hydration water not from the SAM surface itself, with the force becoming more repulsive with increasing hydrogen bonding between the water molecules and the SAM surfaces. Further work was carried out by the same group comparing the

interfacial hydration of OEG-SAM and OH-SAM surfaces to elucidate the origin of repulsive forces acting on proteins (Figure 1.17).[171] They found that water molecules had a stronger association with the OEG-SAM surface (with a longer residence time) and confirmed that the strong repulsive forces acting on the protein arose from the hydration layers above the OEG-SAM surface; an effect that was not observed for the OH-SAM surface.

The presence of an internal ether oxygen has been the subject of many investigations to try and elucidate its effect on promoting antifouling behaviour. Computer simulations have been carried out to investigate the relationship between surface hydration, surface kosmotropicity (molecular level water-structuring) and antifouling behaviour. Studies found that both internal and interfacial hydrophilicity/kosmotropicity must be displayed in order for superior antifouling behaviour to be achieved. Sheikh et al. carried out a systematic investigation, comparing surface hydration of mono(ethylene glycol) (MEG) grafted SiO_2 surfaces to other structurally related organosilane adlayers.[172] The radial distribution function was used to describe the probability of water molecule organisation at certain distances from the silane adlayers. They found that the fully alkylated OTS adlayer was unable to organise water, while all other adlayers possessed the ability to coordinate interfacial water to various extents (Figure 1.18). Furthermore, O-OTS, MEG-OMe, and MEG-OH adlayers were shown to absorb and organise water about their internal ether oxygens, displaying both interfacial and internal water coordination. Disturbance of water embedded in the organosilane adlayers by adsorbing proteins was found to carry an increased thermodynamic penalty. This was thought to explain the improved protein resistance exhibited by surfaces with both internal and interfacial hydrophilicity and kosmotropicity.

Supporting the findings of molecular simulation models, self-assembled monolayers of simple mono(ethylene glycol) (MEG) based organic films on quartz have demonstrated that the presence of a single internal oxygen atom can have a profound effect on the surfaces antifouling behaviour.[173] Follow-up studies using gold substrate modified with MEGylated thiol molecules have revealed clear reductions in protein adsorption and reliance on surface hydration to impart antifouling behaviour.[174] Similarly, glass surfaces modified with silinated PEG produced reductions in fibrinogen adsorption by more than 95% compared to control surfaces.[168] In addition to preventing nonspecific protein binding, PEG surfaces also show resistance to other fouling species. Cao et al. have demonstrated that micro- and nano-structured surfaces grafted with PEG polymers were able to significantly reduce the settlement of *Ulva* zoospores compared to the same surface morphologies grafted with other hydrophilic and hydrophobic chemistries.[151]

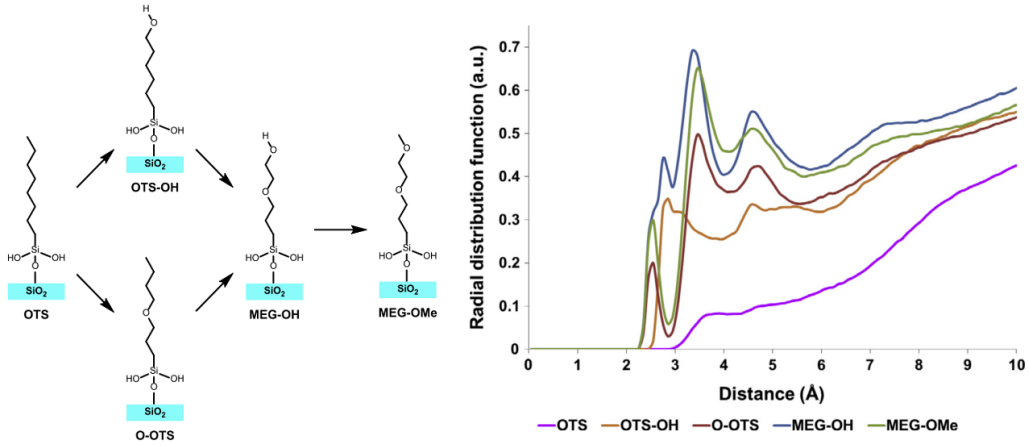

Figure 1.18: Organosilane adlayers used by Sheikh et al. for molecular dynamic computer simulations (left), and radial distribution of water for the examined organosilane adlayers (right). Reproduced from [172].

Concentrated PEG polymer brushes have also been grafted from surfaces via ATRP to produce antifouling surfaces. This method produces a thicker polymer brush and increased control over polymer length. Surfaces produced using this method have a high hydration capacity and demonstrate almost complete inhibition of protein adsorption, with a demonstrated size-exclusion effect.[175] ATRP prepared polymer surfaces grafted with oligo(ethylene glycol) methacrylate (OEGMA) show vast improvements in resistance to adsorption of 100% human plasma compared to OEG SAM surfaces.[176, 177] Additionally, fouling of PVDF membranes that are employed in micro-, ultra-, and nanofiltration, can be significantly reduced through grafting of hydrophilic poly(ethylene glycol) methacrylate (PEGMA) brushes via ATRP.[178]

Recently, interest has grown in the preparation of nanoparticle materials that show biofouling resistance for biomedical applications including drug encapsulation, medical diagnosis, and analysis measurements inside biological systems. PEG coated silica nanoparticles have been developed that show enhanced colloidal stability, good biocompatibility, and reduced nonspecific protein binding, making them suitable for biomedical application.[179] Functionalisation with PEG reduces particle surface charge (negatively charged silica particles are stabilised by mutual repulsion between particles) but introduces steric stabilisation that provides particle stability over a broader pH range.[180] Additionally, PEG functionalised silica nanoparticles provide improved resistance to protein adsorption, and reduced phagocytosis and hemolysis compared to ungrafted silica nanoparticles.[181] Silica nanoparticles grafted with PEG have also been used to develop mechanically robust nonadhesive coatings that demonstrate inhibition of protein adsorption and bacterial adhesion.[182] The prepared coatings presented comparable hardness to conventional anti-scratch coatings and could be useful in the design of biocompatible surfaces for both biomedical and

everyday coating applications.

While PEG has shown much promise as a standard non-fouling material that can be grafted from a range of surfaces, it is susceptible to oxidation in the presence of transition metal ions, making it unsuitable for applications requiring long-term stability. For this reason, more intrinsically stable hydrophilic polymers are being investigated for their potential application in broad-spectrum antifouling coating design.

1.3.2.3 Zwitterions

Zwitterions have been increasingly investigated in recent years due to their unique antifouling behaviour. Zwitterions belong to an interesting group of materials that contain both cationic and anionic functionality but are overall electrically neutral. Zwitterions can be further classified into the following subgroups: monomeric and polymeric betaines (carrying alternate charges on the same monomer unit), and polyampholytes and mixed charge complexes (carrying alternate charges on separate monomer units) (Figure 1.19).[183]

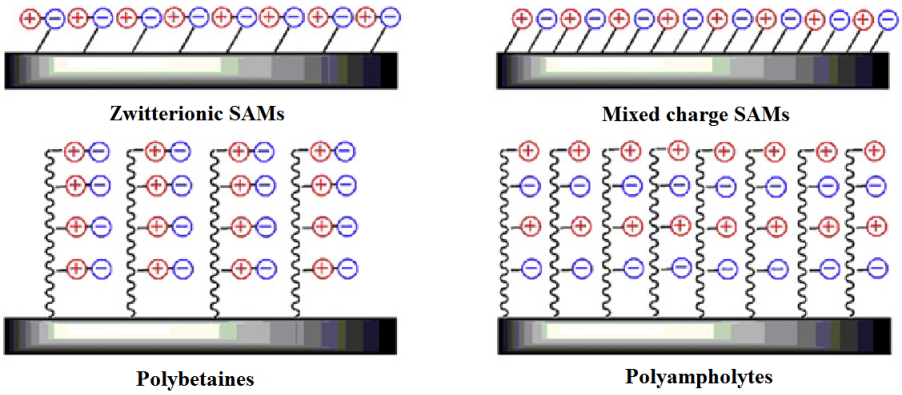

Figure 1.19: Schematic illustrating self-assembled monolayers (SAMs) of short chain zwitterions and mixed charge systems, and polymer brushes prepared from polybetaines and polyampholytes. Reproduced from [153].

The antifouling behaviour of zwitterionic materials arises from its ability to promote the formation of a surface hydration layer through solvation of charged terminal groups.[153, 184] Unlike PEG, which binds water solely through hydrogen bonding, zwitterionic polymers bind water even more strongly through electrostatically induced hydration.[185, 186] The high degree of ionic solvation presented by zwitterions means displacement of highly ordered and tightly bound water molecules by biomolecules is energetically unfavourable. Zwitterionic materials encompass a diverse range of polymer species, supporting large variations in their chemical structure. Polymeric zwitterions may present any combination of ionic groups (e.g. phosphate, carboxylate, or sulfonate anionic groups and quaternary ammonium, phosphonium, or imidazolium

cationic groups), and offer flexibility in terms of the spatial arrangement of charged species.[187] This degree of compositional diversity allows for greater freedom of molecular design and tailoring of zwitterionic materials to give unique chemical properties.

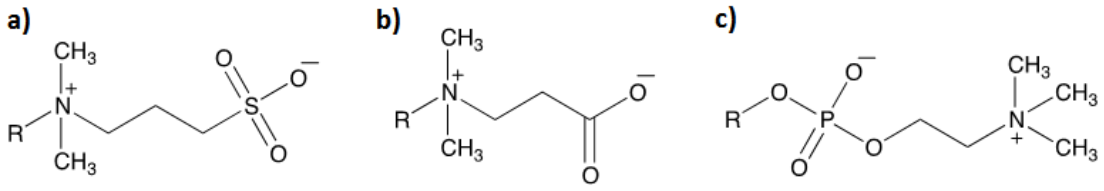

Figure 1.20: Zwitterionic betaines presenting cationic and anionic functionality on the same monomer unit: sulfobetaine (a), carboxybetaine (b), and phosphorylcholine (c).

Regardless of their chemical composition, zwitterions fulfil the chemical criteria described by Whitesides et al. for protein resistance: they are hydrophilic (polar), containing hydrogen bond acceptors, no hydrogen bond donors and are overall electrically neutral.[188–191] Additionally, zwitterions display excellent biocompatibility due to their biomimetic properties, with a number of zwitterionic analogs present in nature. For example, phospholipids found in the outer layer of eukaryotic cell membranes present zwitterionic phosphorylcholine (PC) chemistries responsible for anti-thrombogenic activity.[192] It has been demonstrated that the anti-thrombogenic properties of PC betaines translate to general antifouling behaviour.[193]

SAMs prepared from thiolated PC onto gold substrates have demonstrated enhanced resistance to protein binding and platelet adherence,[186, 194] indicating their potential to impart antifouling properties to surfaces. Similarly, self-assembly of a silinated PC coupling agent onto a silicon substrate resulted in increased hydrophilicity, improved anticoagulation properties, and reduced platelet adhesion.[195] Feng et al. prepared longer polymeric PC brushes on silicon wafers using ATRP.[196] Keeping the grafting density constant, they were able to demonstrate that adsorption of fibrinogen and lysozyme proteins could be decreased with increasing chain length.

The interactions of PC-SAMs with the model protein lysozyme have been modelled using molecular simulations (Figure 1.21).[197] This work showed that PC-SAMs display a stronger repulsive force on proteins than those generated from simulations of EOG-SAMs. The origin of protein repulsion was also demonstrated to be significantly different between the two SAM surfaces. Firstly, hydration layer residence times are longer and reorientation of water molecules is much slower for PC-SAMs than those observed for OEG-SAMs, indicating that water molecules are more tightly bound to the PC-SAM surface. Secondly, the dipole distribution of water molecules near the PC-SAM surface have larger reorientation dynamics that more closely mimic those

observed for bulk water molecules, indicating water is bound by ionic solvation. These findings support the conclusion that repulsive forces observed at the protein-surface interface are generated from the hydration layer present at the SAM surface. While PC containing polymers have been used to prepare effective antifouling interfaces, they are difficult to synthesise and purify, and the phosphoester group is susceptible to hydrolysis.[198, 199]

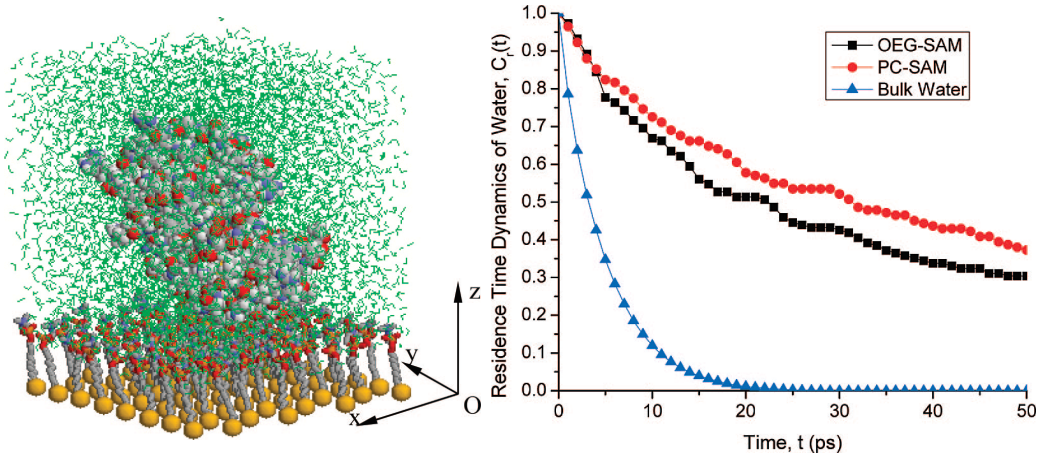

Figure 1.21: Molecular simulation of lysozyme protein interacting with PC-SAM surface (left). Solvent water molecules are shown explicitly (green wire frame). Comparison residence times of water molecules near PC-SAM and OEG-SAM surfaces (right). Reproduced from [197].

Other polybetaines that have been investigated in recent years include carboxybetaines (CB) and sulfobetaines (SB), which are chemically similar to naturally occurring glycine and taurine betaines, respectively.[200] Short chain monomer assembly of these types of zwitterions onto surfaces have been demonstrated to significantly reduce nonspecific protein adsorption. Additionally, mixed charge materials, presenting a 1:1 ratio of cationic and anionic subgroups have also proven to be highly resistant to nonspecific protein adsorption.[189] Thin films of self-assembled zwitterionic CB prepared onto glass substrates by vapour and solution deposition have shown significant improvements in resistance to protein adsorption and blood cell adhesion,[201] while glass functionalised with silinated SB has presented antiadhesive properties, reducing adhesion of *E. coli* and *S. aureus* bacteria by more than 99%.[202]

Simple silane coupling has been employed to produce zwitterion grafted cellulose membranes, which typically suffer from bioaccumulation.[203] Functionalising membranes with CB and SB silanes improved resistance to protein adhesion, platelet adhesion and cell attachment, without compromising the membranes biocompatibility. Interestingly, SB modified membranes showed improved resistance to bovine serum albumin and bovine fibrinogen over the CB modified membranes. Additionally, SB functionalised PDMS has shown exceptional bioinertness, resisting adsorption of

protein, bacteria, and lipids over long exposure periods (Figure 1.22).[204]

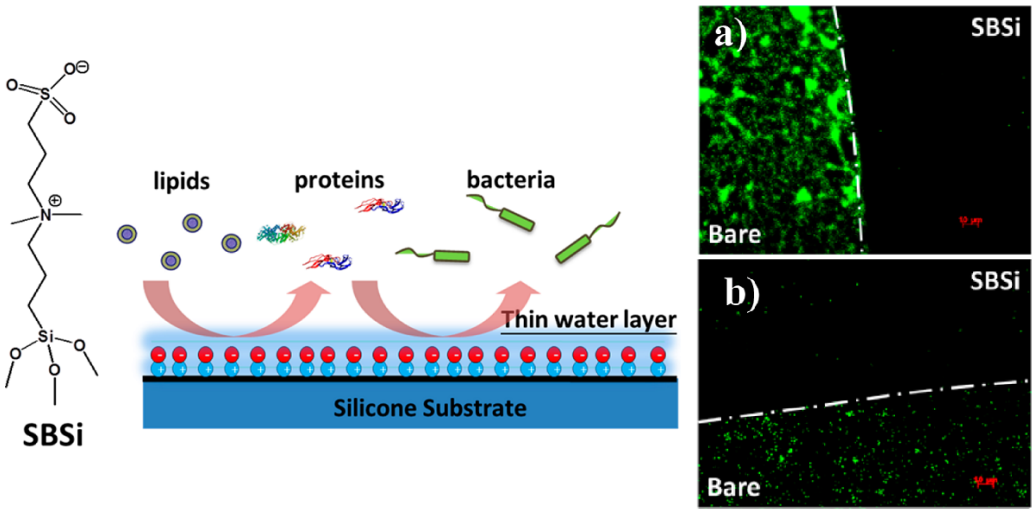

Figure 1.22: PDMS membrane functionalised with SBSi zwitterion: fluorescence images of *P. aeruginosa* (a) and *S. epidermidis* (b) on partially modified PDMS. Reproduced from [204].

While both SB and CB materials have demonstrated excellent antifouling properties, each of these chemistries show distinct hydration, ionic interactions, and self-associations which impact on their applications as antifouling materials.[205] A molecular simulation study carried out by Shao et al. studied the hydration capacity and dynamics of SB and CB zwitterionic moieties.[206] Similar behaviour of water molecules was observed around the positively charged quaternary ammonium site for both zwitterions, while larger differences were observed between anionic groups. The negatively charged sulfonate group of SB was found to coordinate a larger number of water molecules about its SO_3^- group, while water molecules interacting with the CO_2^- group of CB had longer residence times, sharper spatial distribution, and more preferential dipole orientation. The high hydration capacity of both zwitterionic materials is understood to be responsible for their exceptional antifouling performance. A follow-up study conducted by the same group investigated the hydration free energy of 12 zwitterionic moieties and their self-association and protein interactions (Figure 1.23).[207] They found that all investigated zwitterions possessed hydration free energies lower than ethylene glycol, indicating strong hydration capacity and associated fouling resistance. Interestingly, increasing the charge density of charged groups did not lead to lower hydration free energies. This result was attributed to the observation that charged groups with high charge densities can reduce the charge densities of adjacent groups. Variation of cationic groups was not found to affect the coordination number of water molecules about the anionic species but did influence water residence time, as the cationic group can affect the charge densities of the anionic groups. Despite the excellent hydration capacity of the studied zwitterionic

moieties, this alone was not enough to prevent self-associations and protein interactions. Zwitterionic moieties possessing quaternary ammonium groups formed a low number of self-associations and were proven to resist nonspecific protein adsorption, regardless of their anionic counterparts. Increasing the number of hydrogen atoms attached to the nitrogen was found to promote self-association between zwitterionic moieties and thus reduce their ability to resist protein adsorption.

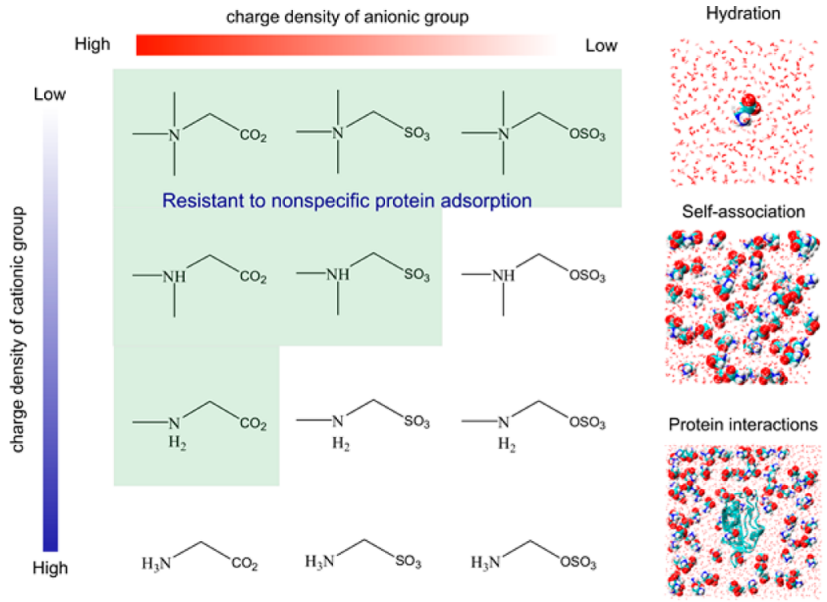

Figure 1.23: Molecular structures of 12 zwitterionic moieties studied for their hydration properties and protein resistance. Reproduced from [207].

While CB and SB zwitterions display similar degrees of hydrophilicity and fouling resistance, CB is unique in that its zwitterionic properties are pH dependent. Under low pH conditions it becomes protonated and exists as a cationic surfactant.[208] In this way, CB is able to switch between a cationic antimicrobial form and a hydrophilic antifouling form. Additionally, carbon spacer length between charged groups has a pronounced effect on the antifouling behaviour of CB, with spacer lengths of 1 to 2 carbons shown to be highly effective at generating protein resistant surfaces.[209] Spacer lengths longer than 2 carbon units are less effective at reducing nonspecific protein adsorption as a result of increased hydrophobicity.

When comparing the effect of grafting method on the preparation of zwitterionic surfaces, it should be noted that while SAMs of short chain monomers can effectively resist nonspecific protein adsorption and bacterial adhesion, that they are sometimes ineffective at preventing fouling from more complex media. For example, SAMs of mixed charge SB and CB prepared onto gold surfaces show good resistance to adsorption of human serum, however, only polymeric sulfobetaine methacrylate (SBMA) and carboxybetaine methacrylate (CBMA) zwitterions grafted via ATRP were able to protect surfaces from adsorption of human plasma, containing complex

mixtures of proteins.[176] Similarly, the ability of zwitterionic SAMs to prevent nonspecific protein adsorption does not necessarily translate into bacterial adhesion resistance. In a study by Cheng et al., both a mixed charge zwitterionic SAM ($SO_3^-/N^+(CH_3)_3$) and a SBMA grafted surface were highly resistant to protein adsorption and short-term adhesion of *S. epidermidis* and *P. aeruginosa* bacteria.[210] However, only the SBMA modified surface was able to effectively reduce bacterial adhesion over longer-term studies.

The grafting of SBMA and CBMA to initiator-covered surfaces using ATRP, has produced surfaces with exceptional fouling resistance. Glass functionalised with pSBMA and pCBMA have shown reductions in adsorption of human fibrinogen protein and bovine aortic endothelial cells comparable to surfaces grafted with PEG.[211] Additionally, CBMA grafted glass surfaces have shown suppression of biofilm formation after long-term exposure to *P. aeruginosa* and *P. putida* bacteria.[212] The mechanism behind the antifouling behaviour of polymeric zwitterions is undoubtedly of interest, particularly in relation to polymeric ethylene glycol based systems. Sum frequency generation (SFG) has been used to investigate and compare protein perturbation of the hydration layer at pSMBA and pOEGMA interfaces.[213] Highly ordered and densely grafted pSBMA surfaces saw almost no change in SFG signal before and after contacting bovine serum albumin, fibrinogen, and lysozyme proteins, indicating that the hydration layer surrounding the zwitterionic polymers was undisturbed. However, for pOEGMA grafted surfaces, the water signal changed dramatically upon contacting the protein solutions. This result indicated that water molecules adjacent to the pOEGMA surface were disrupted by the presence of protein solutions. Water signal of pOEGMA could be recovered after rinsing and placing in water again. This indicates a reversible interaction with OEG chains and thus why OEG still exhibits negligible protein adsorption. SFG has also been used to investigate the difference in hydration properties between zwitterionic SB and CB species.[214] While ordering of water molecules surrounding SB polymers is unaffected by pH, interfacial ordering of water with CB is decreased with decreasing pH, as zwitterionic functionality is lost as the carboxylate group becomes protonated.

1.3.3 Targeted Applications

A large number of studies have demonstrated the ease with which low-fouling zwitterionic surfaces can be prepared through functionalisation of ideal substrates presenting complementary functional groups. Greater effort is now being devoted to the immobilisation of zwitterionic monomers and polymers onto a wider range of surfaces for real-world applications.[215] Additionally, some approaches to fouling prevention are combining multiple techniques to promote enhanced fouling resistance.

The widespread use of stainless steel in food preparatory and health care environments has prompted investigation of coatings to prevent microbial fouling. Polymeric PC coatings onto stainless steel have been shown to significantly reduce adhesion of multiple bacterial strains (including *S. aureus*, *S. epidermidis*, and *P. aeruginosa*) and prevent formation of biofilms.[216] Similarly, polymeric SB coatings grafted from stainless steel prevented protein adsorption, blood cell adhesion and platelet activation, and imparted improved antibacterial properties (Figure 1.24).[217]

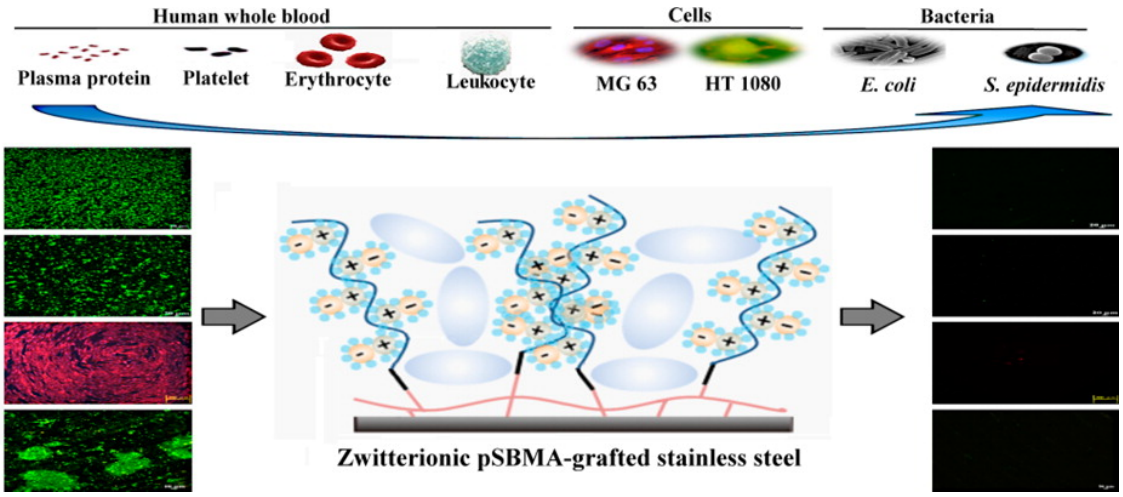

Figure 1.24: Polymeric zwitterion grafted from stainless steel providing resistance to fouling from a wide range of organisms. Reproduced from [217].

Marine coatings with amphiphilic character are being investigated for their potential non-toxic, antifouling, and foul-release properties. Polyurethane coatings containing zwitterionic-PDMS copolymers have been formulated, where the zwitterionic component was expected to impart low-fouling properties, and the PDMS component would elicit a fouling-release response.[218, 219] Previous studies have demonstrated that polyurethane siloxane systems undergo self-stratification, with the low surface energy siloxane segregating to the surface and the polyurethane forming the bulk coating material.[220] It is expected that any groups covalently bound to the low surface energy polymer (i.e. zwitterions) would also segregate to the coating surface; thus both low-fouling and foul-release properties would be presented at the coating interface.

Similarly, synergistic strategies have been developed for resisting algal settlement through the combined effect of surface chemistry and surface topography.[221] Polymer brushes of OEGMA and sulfopropyl methacrylate (SPMA) chemistries were grafted from micropatterned PDMS (prepared through exposure to oxygen plasma under stretching) via surface-initiated ATRP. Both surface topography and surface chemistry were found to influence adhesion of marine organisms, with significant reductions observed for the settlement of *Chorella* and *Ulva* zoospores (Figure

1.25). However, the effectiveness of surface topography in preventing zoospore settlement was found to be dependent upon organism size; an observation supported by previously proposed attachment point theories.[222]

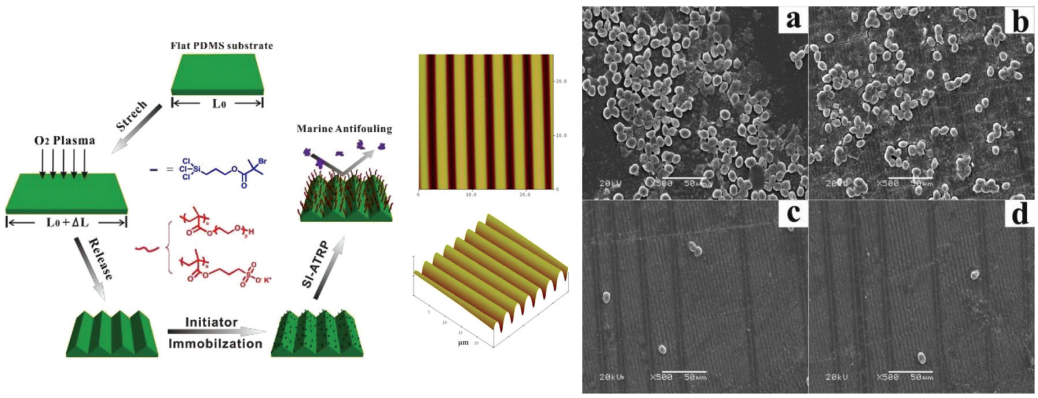

Figure 1.25: Preparation of OEGMA and SPMA functionalised micropatterned PDMS (left). Interactions of *Chorella* zoospores with: (a) PDMS; (b) wrinkled PDMS; (c) wrinkled OEGMA-PDMS; (d) wrinkled SPMA-PDMS. Reproduced from [221].

The simultaneous presentation of low-fouling and self-cleaning chemistries has also been explored in the area of wastewater treatment. PVDF membranes have been prepared with amphiphilic block copolymers of hydrophilic zwitterionic and low surface energy fluorinated chemistries for the treatment of wastewater.[199] Where PVDF control membranes exhibited poor antifouling and self-cleaning properties, amphiphilic copolymer membranes effectively suppressed fouling from water/oil emulsions and optimal copolymer compositions suffered minimal flux-decline even after separation of protein solutions and yeast cell suspensions.

Cellulose polymers and membranes employed for biomedical applications often suffer from poor biocompatibility, particularly for applications in blood purification therapies. Zwitterionic SB and PC brushes have been grafted from cellulose membranes via ATRP to improve blood compatibility and reduce protein and platelet adhesion.[223–225] Similar results were achieved by reaction of zwitterionic alkoxysilanes to cellulose membranes, via simple coupling reactions.[203] CB and SB modification of membranes only slightly decreased membrane permeation flux, thus minimally affecting membrane productivity and efficiency.

Surface properties of biological materials can be tailored to suit particular pH environments and physiological conditions through polymeric modification. Tuning of surface charge has been achieved through combined functionalisation of zwitterionic SBMA and cationic methacryloyloxyethyltrimethyl ammonium chloride (METAC) polymer brushes to SiO_2 surfaces (Figure 1.26).[226] Varying the ratio of SBMA to METAC allowed the surface charge (zeta potential) to be tuned to zero at physiological pH, with minimal disturbance of other surface physicochemical properties.

Additionally, surfaces with zero surface charge showed improved suppression of protein binding and bacterial adhesion.

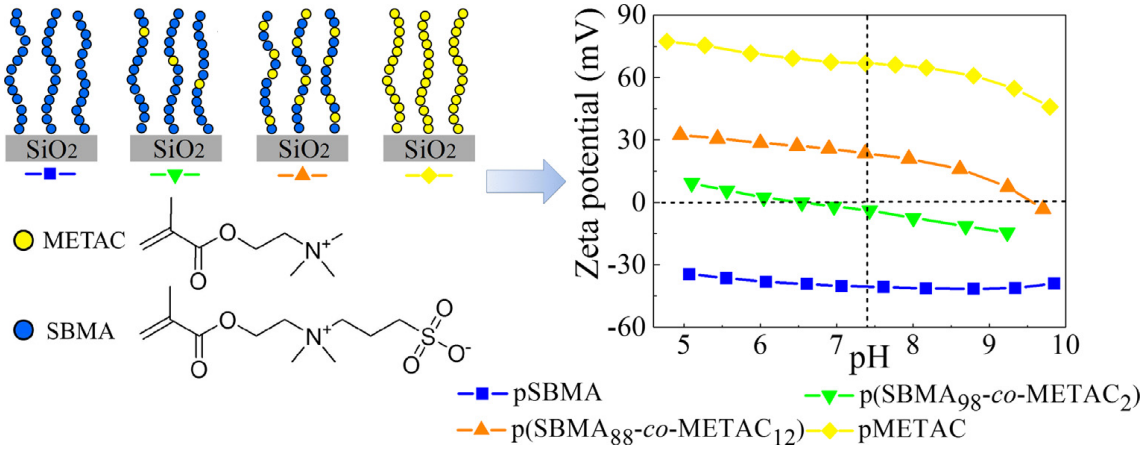

Figure 1.26: Combined functionalisation of cationic METAC and zwitterionic SBMA to prepare surfaces presenting different surface charge. Reproduced from [226].

With the increasing use of nanoparticles in medicine as tools for medical therapeutics, diagnostics, and drug delivery, there has been a growing need to address the issue of nanoparticle aggregation on exposure to physiological conditions.[227] Modification of nanoparticles with hydrophilic and zwitterionic polymers has been demonstrated to improve nanoparticle biocompatibility and colloidal stability in complex media. Yang et al. functionalised gold nanoparticles with a range of chemistries including PEG and zwitterionic poly(carboxybetaine acrylamide) (pCBAA) and evaluated their stability in a range of media.[228] It was found that bare gold nanoparticles and those functionalised with OEG and PEG suffered an increase in hydrodynamic size on exposure to lysozyme protein and NaCl salt solution, while the diameter of pCBAA modified particles remained unchanged. Similarly, when challenged with undiluted (100%) human blood serum, only the pCBAA functionalised nanoparticles were resistant to aggregation, demonstrating their exceptional stability in complex media. A later study by the same group showed that self-assembled CB-thiols with a UV cross-linkable diacetylene group reacted onto gold nanoparticles were stable at low pH and high temperature, and are highly resistant to protein adsorption, even from undiluted human blood serum.[229] In addition to gold nanoparticles, silica nanoparticles have also been coated with pCBAA to impart improved stability and resistance to aggregation upon exposure to both negative and positive protein solutions.[230]

Estephan et al. compared the protein resistance and stability of SiO_2 surfaces and silica nanoparticles functionalised with silinated SB and PEG. Both SB and PEG functionalised planar SiO_2 surfaces were effectively able to resist protein adsorption, however, only the zwitterated silica nanoparticles were found to be stable at both

high temperature and salt concentration.[231] Similarly, assemblies of short chain CB and SB silanes on silica nanoparticles drastically improve particle stability, imparting resistance to aggregation under exposure to protein and high salt conditions.[232, 233] Thicker shells of zwitterionic polymers have also been grafted from silica nanoparticles via ATRP for enhanced particle stability and resistance to aggregation in complex biological media.[230, 234, 235] These particles are thought to be suited for future applications in drug delivery and diagnostics.

Whilst effective at preparing well-defined polymeric coatings, ATRP requires the use of metal catalysts that have been associated with potentially hazardous environmental impacts.[236] Additionally, ATRP methods are difficult to scale-up and require further investigation before they could be implemented for preparing industrial coatings.[124]

1.3.4 Responsive Coating Development

Despite the general effectiveness of cationic and non-fouling surfaces, there are some fundamental limitations to both of these approaches. Non-fouling coatings that do suffer from any form of microbial attachment have no mechanism to release the attached species, while antimicrobial cationic systems suffer from accumulation of dead cells that shield surface functional groups.[187] New coatings are now being developed from responsive materials that combine antimicrobial and non-fouling properties or that possess the ability to "react" to their surrounding environment to be better equipped to prevent surface fouling. Kill-release materials respond to changes in external conditions i.e pH, temperature, salt solution etc., switching from biocidal type surfaces to low-fouling surfaces, prompting the release of dead microbes.

Zhang et al. prepared cationic polycarboxybetaine esters that, upon hydrolysis, were converted to non-fouling zwitterionic polymers.[237] This work compared the effect of spacer length between the quaternary ammonium and ester groups on the polymers antimicrobial activity. They observed that increased antimicrobial (bactericidal) activity was observed with increased spacer length and that all esters became non-fouling upon hydrolysis. Similarly, a CB ester grafted onto a gold substrate via ATRP demonstrated reduced protein adsorption and release of 98% of dead bacterial cells after hydrolysis to zwitterionic form. [238] However, the antimicrobial activity of these polymers could not be restored after hydrolysis, limiting them to a single use.

New approaches are looking at surfaces that can reversibly switch functions between attacking and defending against bacteria. Cao et al. grafted zwitterionic CB with additional OH functionality to gold substrates via ATRP.[239] Immersing the substrate in trifluoroacetic acid promoted the conversion of zwitterionic CB into

a CB-ring, resulting in loss of zwitterionic character and the generation of a cationic surface. The CB-ring surface presented bactericidal activity, effectively killing 99.9% of bacteria in contact with the surface in one hour. The zwitterionic CB form showed no bactericidal activity but was able to release ~90% of the bacteria. This"smart" coating was able to be repeatedly cycled between cationic and zwitterionic forms and still retain both its bactericidal and antiadhesive characteristics under the respective conditions (Figure 1.27).

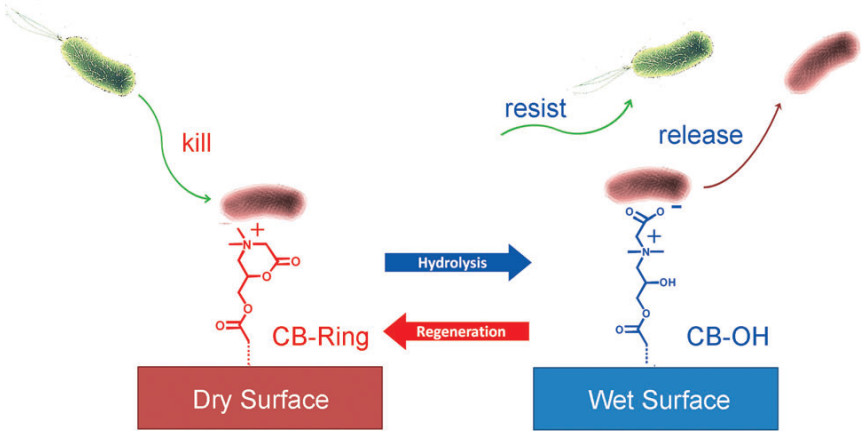

Figure 1.27: Zwitterionic CB-OH can be switched to a cationic CB-ring structure by immersion in acidic media. CB-OH can be regenerated by hydrolysis of the CB-ring in neutral or basic conditions. Reproduced from [239].

Responsive hydrogels have been prepared from zwitterionic vinyl acetate monomers that are capable of cyclisation to form cationic ring structures.[240] Ring formation is promoted under acidic conditions and under neutral or basic conditions these materials return to their zwitterionic form. Hydrogels presenting the cationic ring form killed $>$ 99.9% of *E. coli* attached to surfaces, while switching to the zwitterionic form not only released dead cells but also resisted further bacterial adhesion. Additionally, the mechanical properties of these materials were superior to standard zwitterionic hydrogels, due to the presence of hydroxyl groups capable of participating in hydrogen-bonding, thus broadening the potential applications of these materials.

In addition to pH triggered fouling release, release of fouling species has also been achieved through mechanical deformation of a substrate. Poly(vinylmethylsiloxane) elastomers modified with zwitterionic polymers could resist fouling by bacteria and barnacle cyprids over short-term exposures, while biofilms that accumulated over prolonged exposure could be detached through mechanical deformation of the elastomer substrate.[241] However, the fouling resistance of mechanically strained films was reduced compared to pristine films, indicating that repeated cycles of biofilm detachment affected the stability and performance of zwitterionic polymers.

1.4 Functionalised Silica Nanoparticles

In addition to the inclusion of metallic nanoparticles into coatings for the generation of antimicrobial effects via dissolution of toxic metal cations, a range of inorganic nanoparticles have been functionalised with chemistries to provide enhanced stability and improved resistance to microbial fouling. In particular, functionalised silica nanoparticles (SiNPs) have been widely utilised in the fields of medicine and biotechnology, where they have found applications in diagnostics, drug delivery, and gene transfection.[242, 243] Without functionalisation, particles cannot be utilised due to poor biocompatibility. The native negative charge of SiNPs renders them an immediate target for protein interaction and high salt concentration can shield surface groups and result in particle destabilisation leading to particle aggregation and precipitation.

Aside from biomedical applications, silica nanoparticles has also been used as additives to surface coatings as binders and fillers, where they have shown enhanced resistance to abrasion, increased solvent resistance, and flame-retardant properties.[244, 245] SiNPs are commercially produced, inexpensive materials that are highly processable, dispersible in a number of solvents, and stable across a wide pH range.[246] They have a high surface area and present reactive surface groups, making them available for functionalisation reactions with a wide range of chemistries. Additionally, they can be added to existing coatings or prepared as free-standing films on their own. For this reason, silica nanoparticles were selected as a platform material for the preparation of hydrophilic low-fouling coatings presented in this thesis. By combining the robust and scalable application of SiNPs in coatings with the enhanced levels of fouling resistance demonstrated by functionalised SiNP dispersions, this work presents a new method of preparing low-fouling surface coatings for widespread antifouling applications. This section will be devoted to exploring SiNP and silane reaction chemistry in more detail.

1.4.1 SiNP Synthesis

In the same way that SiO_2 and polymeric organosilicons (e.g. PDMS) can be easily functionalised, SiNPs offer a reactive silanol surface in addition to a large surface area. A number of synthetic methods can be utilised to produce silica nanoparticles including reverse micro-emulsion, flame synthesis, and sol-gel process.[247] The sol-gel technique is a widely used approach to synthesise SiNPs as it offers a high degree of control over the resultant particle properties. Most commonly, this method proceeds via the controlled hydrolysis and condensation of silica alkoxides, such as tetraethylorthosilicate (TEOS), in the presence of ammonia as a catalyst, as described

by Stöber.[248] Particle size was found to be determined by the concentration of water and ammonia present in the reaction, while alkoxide concentration was found to have no significant influence on particles size.

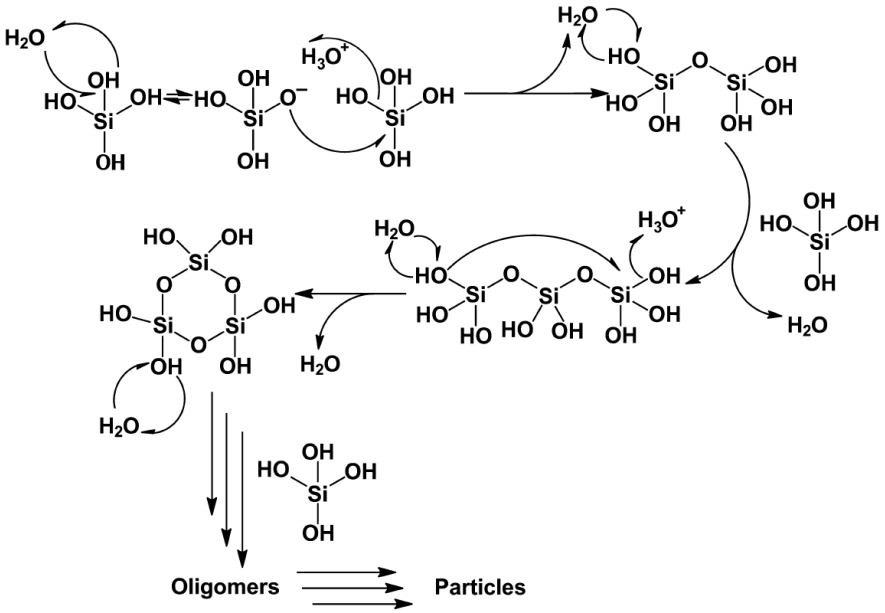

Figure 1.28: Condensation reactions of silicic acid molecules to produce linear and cyclic oligomeric structures. Reproduced from [249].

The reaction of TEOS that leads to SiNP growth typically proceeds by the initial hydrolysis of TEOS, producing orthosilicic acid ($Si(OH)_4$) and ethanol (EtOH). Silanol groups can then undergo either water or alcohol condensation reactions with silanol and ethoxy groups of fully or partially hydrolysed silane species, forming the siloxane linkages (Si-O-Si) that make up the silica particle structure.[247] The silanol groups of silicic acid are mildly acidic (pK_a of 9.8) and a small proportion will be deprotonated at neutral pH.[249] Ionised molecules will readily react with neutral silicic acid monomers to produce oligomers, which serve as nuclei for silica nanoparticle formation (Figure 1.28).

Preparation of SiNPs via base-catalysed mechanisms causes partial deprotonation of polysilicic acid molecules, leading to particles presenting a negatively charged surface.[250] This results in stable suspensions of colloidal silica, where gelation is inhibited by electrostatic repulsion between charged particles. Only when the pH of SiNP suspensions approaches the isoelectric point of silica (∼2)[251] would interparticle repulsion be reduced enough to allow particle aggregation to occur.

1.4.2 SiNP Properties

The physical and chemical properties of synthetic SiNPs are known to vary with particle size. A study conducted by Rahman et al. revealed (as with most nano-

materials) decreasing particle size dramatically increases the specific surface area presented by SiNPs, particularly when particle size is reduced below 50 nm.[252] Additionally, decreasing particle size has the related effect of increasing the concentration of silanol groups per gram of silica (Figure 1.29). In contrast to this, the number of silanol groups per unit area ($OH.nm^{-2}$) was reported to decrease with decreasing particle size. It was hypothesised that the silanol group formation could become incomplete or retarded as particle size was reduced. This finding deviates from the Kiselev-Zhuralev value of 4.6 $OH.nm^{-2}$ that is widely cited in the literature as the physiochemical constant for fully hydroxylated amorphous silicas.[253].

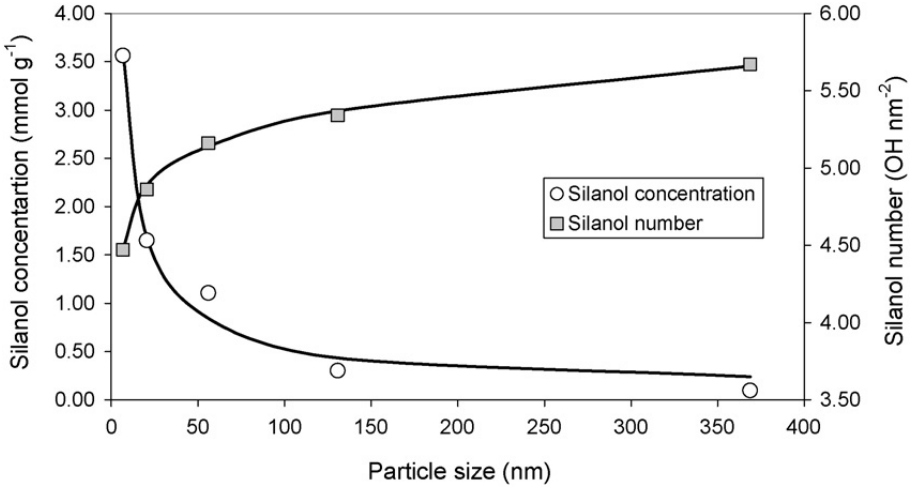

Figure 1.29: Concentration of silanol groups per gram and per nm^2, relative to silica nanoparticle size. Reproduced from [252].

In addition to the number of OH groups present at the surface of nanosilicas, the type of silanol group should also be considered. Similar to planar silica surfaces, surface OH groups may be present in the form of isolated silanols, geminal silanols, or vicinal (H-bonded) silanols (Figure 1.30). For particles in a fully hydroxylated state (4.6 $OH.nm^{-2}$), it is reported that geminal OH groups make up the smallest portion of the surface chemistry (0.6 $OH.nm^{-2}$), vicinal OH groups make up the largest portion of OH groups (2.8 $OH.nm^{-2}$), and isolated OH groups make up the rest (1.20 $OH.nm^{-2}$).[254] Surface siloxanes are not expected to be present unless particles are significantly dehydrated from heat treatment.

The size of SiNPs has also been shown to influence the types of silanol groups presented at the particle interface, as well as their mode of bonding/interaction with water. At diameters > 30 nm, surface groups are more likely to be present in the from of hydrogen-bonded silanols, while small particles (diameter < 10 nm) have reduced numbers of hydrogen bonded silanols and increased surface density of isolated silanol groups.[255] As a result, larger SiNPs present stronger hydration forces between particles. Evidently, the types of silanol groups present on the surface

of SiNPs will depend on their method of production and will dramatically affect particle reactivity and hydration capacity. Additionally, the aging of silicates can ultimately affect the structure and properties of siloxane networks over time.[256]

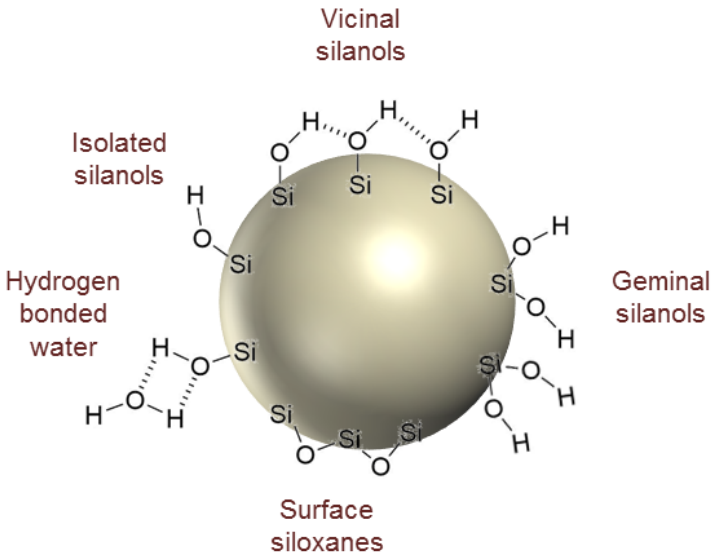

Figure 1.30: Examples of isolated silanols, geminal silanols, vicinal silanols, surface siloxanes, and hydrogen bonded water on the surface of a SiNP.

1.4.3 SiNP Coupling Reactions

Having considered the synthesis and properties of silica nanoparticles, of equal importance is an understanding of the silane coupling reactions that can be used to functionalise the surface of silica particles. Silanisation of SiO_2 substrates, occurring through the covalent binding and self-assembly of silane molecules, has to been used to add chemical functionality to surfaces for a wide number of applications. Similar to silica nanoparticle formation itself, reactions of silanes to surfaces are dependent upon hydrolysis and condensation processes.

Alkyltrialkoxysilanes (derived from chlorosilanes) are most commonly used for the silanisation of surfaces. Alkoxysilane hydrolysis occurs via both base and acid-catalysed mechanisms to produce silanetriols.[257] Hydrolysis proceeds in a step-wise manner, where the formation of alkyldialkoxysilanes is the slowest and subsequent hydrolysis to give silanediols and silanetriols occurs more rapidly.[258] Acid and base-catalysed hydrolysis are proposed to occur via different reaction mechanisms. Under basic conditions, hydroxyl ions attack the silicon atom in an S_N2-type mechanism, forming a pentacoordinate intermediate before displacing an alkoxy group ($^-$OR) with inversion of chemistry. Pohl and Osterholtz [258] propose the formation of a five coordinated intermediate in which the silicon acquires a formal negative charge. Electron withdrawing substituents help to stabilise the developing negative charge

on silicon and lower the energy of the transition state.[259]

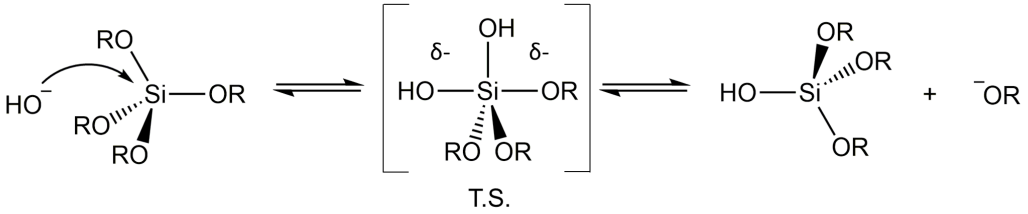

Figure 1.31: Base-catalysed mechanism of silane hydrolysis.

Under acidic conditions, an alkoxide group is first protonated by a hydronium ion, withdrawing electron density from silicon and making it more susceptible to nucleophilic attack from water.[260] Attack from a water molecule, again proceeding via an S_N2-type mechanism, forms a pentacoordinate intermediate before displacing the alkoxy group. Addition of a water molecule reduces the partial positive charge on the protonated alkoxide, making alcohol a better leaving group.[260]

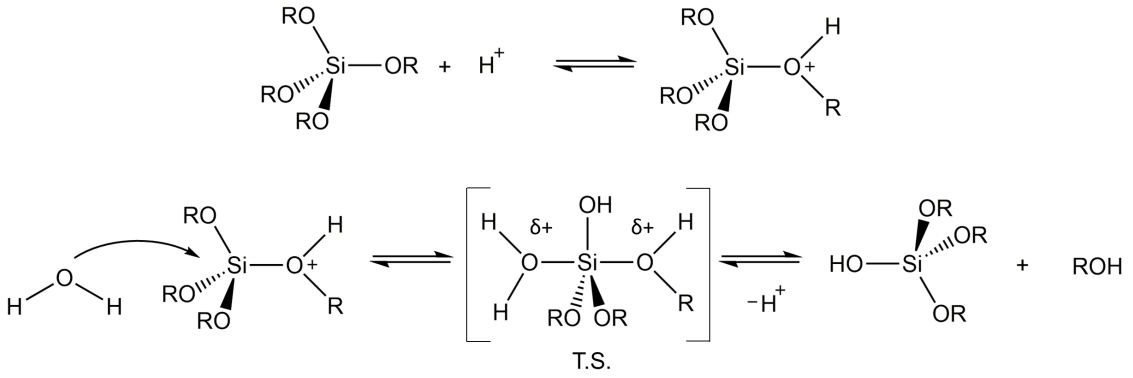

Figure 1.32: Acid-catalysed mechanism of silane hydrolysis.

As both acid and base-catalysed reaction mechanisms propose the formation of pentacoordinate intermediates or transition states, the rate of alkoxy group hydrolysis is affected by the steric bulk of substituents, where decreased steric crowding should result in an increase in hydrolysis rate: $CH_3O > C_2H_5O > t$-C_4H_9O.[257, 258] Additionally, substituent inductive effects will affect the rate of hydrolysis, where: increasing the degree of alkyl (electron providing) substitution increases hydrolysis rates under acidic conditions, and increasing the degree of alkoxy (electron withdrawing) substitution increases hydrolysis rates in basic conditions, due to increased stabilisation of positively and negatively charged transition states, respectively.[260]

While alkoxysilane hydrolysis can be promoted under either acidic or basic pH, hydrolysis rates reach a minimum under neutral pH conditions. Early reports

by Pohl and Osterholtz,[258] and McNeil et al.,[261] studied the hydrolysis rates of γ-glycidoxypropyltrialkoxysilane and tris-(2-methoxyethoxy)phenylsilane, where reaction rate profiles revealed that minimum rates of hydrolysis occurred around pH 7 (Figure 1.33).

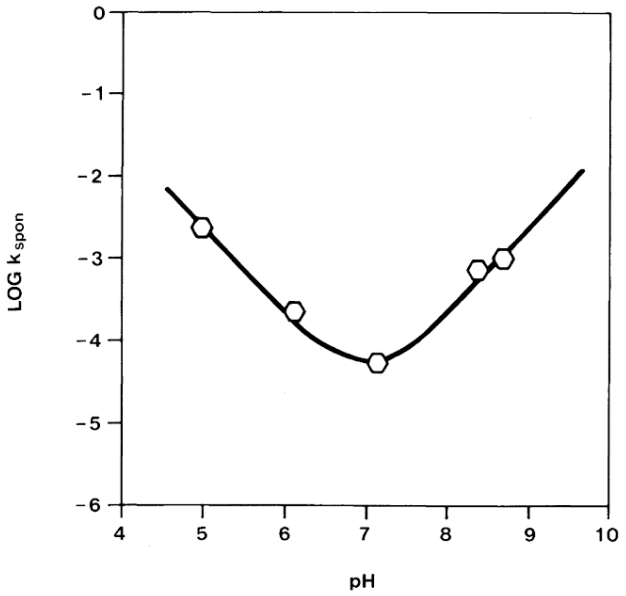

Figure 1.33: pH dependent hydrolysis rate profile of γ-glycidoxypropyltrialkoxysilane. The line is calculated from second-order rate constants. Reproduced from [258].

The pH dependent nature of alkoxysilane hydrolysis extends to the subsequent condensation reactions of the resultant silanetriols. The hydrolysis and self-condensation reactions of alkoxysilanes have been monitored using ^{1}H, ^{13}C, and ^{29}Si NMR, where evolution of free alcohol was used to determine the hydrolysis rates of silane coupling reagents (^{1}H and ^{13}C), and ^{29}Si was used to quantify self-condensation reactions.[262–264] Salon et al. carried out an in depth study of alkoxysilane hydrolysis and self-condensation reactions, investigating the effect of pH, silane concentration and reaction temperature.[262] They selected four alkoxysilane (R'-Si(-OR)$_3$) coupling agents with different organic side groups, namely: 3-aminopropyl triethoxy silane (APES), 3-mercaptopropyl trimethoxy silane (MRPMS), 3-methacryloxypropyl trimethoxy silane (MPMS), and octyl triethoxy silane (OES).

Their work showed that under neutral conditions, hydrolysis rates were very slow (less than 10% hydrolysed) for all silanes, except APES. APES was hydrolysed quickly under neutral conditions (80% after 2 h reaction time) and also rapidly formed self-condensation products, predominately T^3 units which indicates the formation of three-dimensional siloxane networks. Reaction under alkaline conditions was found to promote hydrolysis of the other three silanes, albeit at slower rates than APES, and also resulted in rapid self-condensation reactions, even before silane hydrolysis

was complete. Again, ^{29}Si spectra indicated high proportions of T^3 units present, with intermediate dimer (T^1) and trimer (T^2) units being difficult to detect. In comparison, acidic conditions were found to promote the rapid hydrolysis of all silanes but also appeared to stabilise silanol groups; with self-condensation reactions appearing to be limited to dimer T^1 and trimer T^2 unit formation.

Further work from the same group revealed that choice of solvent, in combination with the nature of the organic group, will also affect alkoxysilane hydrolysis and self-condensation events.[263] Reactions carried out in H_2O/EtOH solutions under acidic conditions, revealed that increasing water content favoured hydrolysis of amino-bearing silanes and limited their self-condensation reactions. However, for other functionalised silanes, high water content enhanced hydrolysis and promoted self-condensation events.

The results of these studies indicate that careful consideration should be given to the choice of reaction conditions when conducting silane coupling reactions, whether that be to planar surfaces or to silica particles, so as to maximise the degree of functionalisation. While the self-assembly of silanes onto planar studies has been well studied, early reports of silane SAM formation were conducted in pure organic solvents or organics with trace amounts of water.[265–269] Ideally, silanisation could instead by carried out in water under controlled pH conditions to avoid the use of bulk organic solvents. This is particularly relevant when considering reaction to silica particles, where silica particles are prepared and stably stored as aqueous dispersions.

A number of examples of functionalised nanosilicas have already been discussed earlier in this review as potential drug-carriers and medical therapeutics. In these examples, hydrophilic polymers have been used to functionalise the silica surfaces to increase particle stability in complex media and to improve their ability to resist adsorption of proteins. In a similar way, this thesis aims to explore the use of functionalised silica nanoparticles in the preparation of protein resistant and antifouling surface coatings. Despite the widespread inclusion of SiNPs into paints as fillers and binders, and the use of functionalised nanosilicas in biomedical applications, very limited work has been conducted around utilising SiNPs as the base material for antifouling applications

In this work, silica nanoparticles are employed as a vehicle to deliver and present hydrophilic chemistries at interfaces to improve their fouling resistant properties. The ease of silica nanoparticle functionalisation and the processability of nanoparticle dispersions, makes them an ideal platform material for antifouling coating generation and application. Where nanosilicas are utilised as coating materials, thin layers can be deposited as stand-alone coatings (where particles can be functionalised either before or after their deposition onto surfaces) or particles can be added into existing coating formulations to improve fouling resistance. The versatility of nanosilicas,

in terms of their size and their stability across a broad range of pH, in addition to the wide range of alkoxysilane chemistries available for particle modification, allow for the careful tuning of particle surface chemistry and, ultimately, the interfacial properties of deposited coatings.

1.5 Chapter Conclusions

This Chapter has detailed the biofouling process and provided an overview of the development of antifouling technologies to date. The mechanisms of biological fouling prevention, including biocidal and antifouling approaches, have been reviewed in detail and their relative efficiencies compared. It has been established that coatings containing or releasing biocidal compounds present high levels of antimicrobial activity initially but may present toxicity to non-target organisms, in addition to suffering from short in-field lifetimes due to uncontrolled biocide release. A number of emerging antifouling technologies have also been identified, where optimisation of surface physicochemical properties leads to reduced interactions with fouling species. Despite improvements in the preparation and efficacies of fouling resistant surfaces, methods of producing such surfaces are often complex and the carefully controlled laboratory conditions under which these surfaces are prepared cannot be easily scaled-up to offer robust industrial solutions for biological fouling prevention. The field of hydrophilic antifouling chemistries is a growing area that offers a passive solution to the prevention of biological interaction and attachment to surfaces. However, there remains a demand for the simple preparation and application of hydrophilic antifouling coatings, in which chemistries can be attached to a broader range of surfaces. Taking inspiration from existing coating technologies could provide a path forward for the development of robust and scalable coatings for widespread antifouling applications.

1.6 Aims

This thesis aimed to further the development of antifouling coatings through the use of hydrophilic nanomaterials. Silica nanoparticles were employed as a vehicle for the delivery and presentation of hydrophilic chemistries onto surfaces, for their protection from biological fouling. This work sought to further our understanding of zwitterionic and quaternary ammonium modified silica nanoparticle coatings towards the development of platform antifouling materials for widespread applications. The focus of this thesis can be broken down into three broad aims.

The first was to investigate and optimise the attachment of zwitterionic sulfobetaine and carboxybetaine silanes to SiNP dispersions and SiO_2/SiNP coatings. Additionally, quartz crystal microgravimetry with dissipation monitoring would be developed as a tool to investigate the effect of pH and silane concentration on particle coating functionalisation, with the end goal of producing hydrophilic surfaces with enhanced resistance to fouling by proteins, bacteria, and fungal spore adhesion.

Second, this thesis aimed to investigate the effect of surface nanotopography on the antifouling properties of deposited nanosilicas. Specifically, this study sought to examine the fouling resistance of thin coatings of zwitterion modified SiNPs of different sizes and compare this to the fouling resistance of unmodified SiNP coatings.

The third and final aim was to introduce a dual antimicrobial-antifouling effect through the simultaneous presentation of zwitterionic and quaternary ammonium silane chemistries at the SiNP coating interface. The effect of quaternary ammonium functionalised SiNPs was firstly to be examined on its own, and then in combination with zwitterionic sulfobetaine. The preparation of surfaces would be controlled through sequential exposure to silane solutions, varying the order of addition and the solution concentration. The overall objective was to compare the protein resistance and antimicrobial properties of dual-chemistry SiNP systems to SiNPs modified with quaternary ammonium and zwitterionic chemistries separately.

Chapter 2

Silica Nanoparticles Functionalised with Zwitterionic Sulfobetaine for Antifouling Coating Applications

This Chapter has been adapted from the article "Silica Nanoparticles Functionalized with Zwitterionic Sulfobetaine Siloxane for Application as Versatile Antifouling Coating System", *ACS Appl. Mater. Interfaces*, 2017, **9**,18584–18594, doi:10.1021/acsami.7b04840.

As detailed in Chapter 1, there is a gap between antifouling functionalisation technologies and their ability to be easily and simply applied to surfaces for widespread applications. This Chapter introduces silica nanoparticles coupled with short chain, zwitterionic sulfobetaine as a platform material for the simple preparation of hydrophilic antifouling surface coatings.

2.1 Introduction

Antifouling coatings that can prevent the interaction and attachment of microorganisms to surfaces are highly sought after for a multitude of applications. In recent years, significant effort has been directed into the design of environmentally benign fouling resistant surfaces that function through tailoring of the physicochemical and nanotopographical properties of surfaces and coatings.[66, 150, 151] Hydrophilic chemistries have emerged as promising fouling resistant materials that prevent microbial interactions and subsequent attachment through surface water structuring. Coatings developed from hydrophilic polymers possess a hydration layer at the coating interface. This hydration layer presents a physical and energetic barrier, preventing protein adsorption and microbial attachment onto the surface.[153, 200]

Zwitterionic polymers are among a number of hydrophilic materials being investigated for their antifouling properties.[185, 201] Zwitterionic polymers bear an equal number of cationic and anionic chemistries that promote the formation of a surface hydration layer through solvation of charged terminal groups.[153, 184] Grafting of zwitterionic carboxybetaine and sulfobetaine polymers from gold,[177, 210, 270] silicon,[271, 272] and glass,[202, 212, 273] have produced hydrophilic surfaces with good chemical stability and exceptional fouling resistance.

Despite the excellent antifouling properties exhibited by zwitterionic polymers, grafting such chemistries to a wider range of surfaces remains a challenge. The ability to immobilise zwitterionic chemistries onto surfaces is currently limited by the surface composition and availability of reactive functional groups at the substrata surface. Thus, advances are needed in antifouling coating design to facilitate the incorporation of low-fouling chemistries into existing coating technologies or support grafting from inert surfaces. Recently, nanomaterials have begun to be explored as potential microbial and fouling inhibitors, owing to their unique physical and chemical properties.[74, 247] The ability of some nanomaterials to be functionalised with a range of polymer chemistries has allowed the tuning of surface properties, with fine control over the presentation of chemistries at the material interface.[274] Nanosilicas functionalised with hydrophilic and zwitterionic chemistries have been investigated as drug nanocarriers due to their high stability and good biocompatibility[232, 233, 246, 275, 276] but are yet to be explored in the development of fouling resistant surfaces and coatings.

Silica nanoparticles (SiNP) have already found a place within the coatings industry, with their addition to paints shown to provide increased abrasion resistance[244] and flame retardant properties.[245] Additionally, they are low cost and provide an easily functionalisable silanol surface. Reactions of SiNPs with silane species occur rapidly in an aqueous solution and across a wide pH range, making this an attractive option for producing versatile low-fouling coating materials through functionalisation with hydrophilic chemistries. This approach allows for organisation of molecules on the particle surface with fine control as well as the option of incorporating those chemistries into existing coating technologies to present highly organised nanostructures at coating interfaces.

Herein, I have examined the attachment of a zwitterionic sulfobetaine (SB) monomers to SiNPs for application as a versatile antifouling coating system. The chosen SB siloxane species has been used previously to functionalise glass,[202, 277] and poly(dimethyl siloxane)[204] to produce surfaces with exceptional wettability, self-cleaning, and antifog properties, as well as demonstrating a high degree of protein and bacterial resistance. Surfaces functionalised with SB have been shown to be non-toxic,[202] and robust enough to withstand harsh environmental conditions[277]

and thus suitable to be applied as a broad-spectrum antifouling agent.

The SiNPs employed in this study were commercially available Ludox® HS-40 colloidal silica particles. Ludox® HS-40 is supplied as an aqueous dispersion of silica particles of low size and narrow particle size distribution. These particles are negatively charged, stabilised by a sodium counterion, and are stable across a wide range of conditions (e.g. varied pH, temperature, salt, and particle concentration). The stability and uniformity of these commercial particles made them an ideal choice to be employed as the primary SiNPs investigated in this Chapter and in following Chapters.

First, I examined the reaction of SB to SiO_2 sensors and SiNP modified sensors using a quartz crystal microbalance with dissipation monitoring (QCM-D). QCM-D has previously been employed across various research disciplines to monitor polymer growth, adsorption kinetics, and to measure interfacial interactions with proteins.[278, 279] In this work, QCM-D was engaged as a tool through which to optimise the reaction conditions of SB to the SiO_2 and SiNP surfaces. Surface functionalisation was monitored quantitatively within QCM-D to determine the effect of zwitterion concentration and solution pH on monomer self-assembly. Second, I prepared solution functionalised nanoparticles and examined particle stability and zwitterion grafting density as a function of the reaction pH. Films of functionalised particles were prepared by spin-coating and their fouling resistant behaviour characterised by challenging them against protein, bacteria, and fungal spores.

2.2 Experimental

2.2.1 Materials

Ludox® HS-40 colloidal silica (12 nm diameter), phosphate buffered saline (PBS, P5368), (*N,N*-dimethylaminopropyl)trimethoxysilane (539287), 1,3-propane sultone (P50706), bovine serum albumin (BSA, A3059), poly(ethylenimine) solution (PEI, P3143), and acetone (270725) were purchased from Sigma-Aldrich. Acetone was dried with 3 Å molecular sieves and distilled before use. All other reagents purchased from commercial suppliers were used without further purification. Water used in experiments and to prepare aqueous solutions was purified using a Millipore water purification system, with a minimum resistivity of 18.2 MΩ.cm at 25 ℃.

2.2.2 Synthesis of Zwitterionic SB

The synthesis of zwitterionic SB (3-{[dimethyl(3-trimethoxysilyl)propyl]ammonio}-propane-1-sulfonate) was adapted from Litt et al.[280] (*N,N*-dimethylaminopropyl)-

trimethoxysilane (2.08 g, 0.01 mol) was added to 1,3-propane sultone (1.22 g, 0.01 mol) in anhydrous acetone (10 mL) under Ar. The reaction was stirred vigorously under Ar for 6 h. The formed precipitate was filtered off and washed several times with anhydrous acetone. The resultant white solid was dried at 70 ℃ under vacuum overnight and stored under Ar.
Yield 78%; ^{1}H NMR (400 MHz, D_2O) δ 0.69 (t, 2H), 1.90 (quin, 2H), 2.23 (quin, 2H), 3.00 (t, 2H), 3.11 (s, 6H), 3.36 (s, 9H), 3.37 (t, 2H), 3.42 (t, 2H); ^{13}C NMR (400 MHz, D_2O) δ 10.9, 18.7, 20.9, 50.0, 51.6, 53.3, 64.9, 68.8.
IR (cm^{-1}): 3271, 2930, 1485, 1414, 1176, 1091, 1033, 914, 783.

2.2.3 Reaction of SB to SiNPs

Reaction of SB to SiNPs was carried out following the procedure described by Estephan et al.[232] The appropriate amount of SB monomer for reaction with SiNPs was calculated on the basis of the surface area reported by the manufacturer and 4.9 silanol groups per nm^2 of silica surface.[253] SB, dissolved in minimal H_2O, was added to a 10 wt% nanoparticle suspension heated to 60 ℃ (± 5 ℃) dropwise with vigorous stirring. The pH of particle dispersions was adjusted to 3.5, 7.0, and 9.5 using dilute HCl and NaOH. The reaction mixture was stirred under reflux for 2 h. The particle dispersions were placed into a dialysis membrane with 12 K molecular weight cutoff and dialysed against pure water for 5 days, with water changed every 12 h to remove unreacted SB monomers. Particles were dried via freeze-drying for further characterisation.

2.2.4 Nanoparticle Characterisation

2.2.4.1 Fourier Transform Infrared Spectroscopy

Fourier transform infrared (FTIR) spectra were acquired on a Shimadzu Prestige-21 FTIR spectrophotometer with a PIKE MIRacle ATR attachment.

2.2.4.2 Nuclear Magnetic Resonance Spectroscopy

^{1}H and ^{13}C NMR (400 MHz) spectra were obtained on a Bruker AVANCE III HD NMR Spectrometer at 25 ℃ using D_2O as a solvent.

2.2.4.3 Dynamic Light Scattering/Zeta Potential

Z-Average particle size (hydrodynamic particle diameter) measured by dynamic light scattering (DLS) and zeta potential (ZP) measurements were performed on a Malvern Zetasizer Nano-ZS at 25 ℃ (colloidal silica refractive index: 1.40, absorption:

0.010, measurement angle: 173°). ZP measurements were performed on 0.25 wt% aqueous particle dispersions, pH adjusted with HCl and NaOH. DLS measurements were carried out on 0.25 wt% particle solutions dispersed in 10 mM NaCl.

2.2.4.4 Thermogravimetric Analysis

The quantity of zwitterion bound to the particle surface was determined using thermogravimetric analysis (TGA, Q500). Dried nanoparticles were heated from room temperature to 800 ℃ at a heating rate of 10 ℃/min under a nitrogen atmosphere. The mass of polymer bound to the particle surface was calculated from the weight loss measured between 150 and 800 ℃. The mass retained at 800 ℃ after polymer decomposition was assumed to be the mass of bare SiNPs.

2.2.5 Preparation of SiNP Coatings

Silica nanoparticle solutions were prepared as 4 wt% dispersions in water for spin-coating onto gold QCM-D sensors. Two types of coatings were prepared. First, dispersions of unreacted particles were prepared for fabrication of nanoparticle coatings that would undergo functionalisation within the QCM. The other coatings were prepared from dispersions of SB functionalised SiNPs (pH 3.5, pH 7.0, and pH 9.5) for assessment of their antifouling properties. The silica nanoparticle dispersions were spin-coated onto A-T cut QCM-D sensors with a 10 mm diameter gold electrode (Q-Sense AB Västra, Frölunda, Sweden) and a fundamental resonance frequency of 5 MHz. Prior to coating, the gold sensor surface of each crystal was cleaned with piranha solution (7:3 v/v mixture of H_2SO_4 (98%) and H_2O_2 (33%)) for 3 min, rinsed with deionised water, and dried in a stream of nitrogen gas. Cleaned QCM-D sensors were then incubated in 0.5% poly(ethylenimine) (PEI) solution to form an adhesive layer on the electrode surface. The PEI was thoroughly rinsed from the sensors after 10 min with deionised water and sensors were dried in a stream of nitrogen gas. The QCM sensors were mounted onto glass slides and nanoparticle films were prepared by depositing 20 μL of each of the prepared nanoparticle dispersions onto the gold electrode of the sensor and spin-coated at 5000 rpm for 30 s. The coatings were cured for 1 h at 120 ℃ and thereafter thoroughly rinsed with deionised water and dried in a stream of nitrogen gas. SiNP coatings prepared onto gold QCM sensors were thin, uniform, and could be distinguished from uncoated gold sensors by visual inspection (Figure A.1).

2.2.6 Particle Coating Characterisation

2.2.6.1 Contact Angle Goniometry

The mean static contact angles made by 2 μL sessile water droplets on the surface of each of the particle coatings were measured with a Dataphysics Contact Angle System (OCA 15EC) in conjunction with SCA20 software. A minimum of three measurements were obtained for triplicate samples of each particle coating.

2.2.6.2 Scanning Electron Microscopy

Imaging of the particle coatings was performed using a field emission scanning electron microscope (SEM, JEOL JSM-7500FA) in secondary electron imaging mode. Images were obtained without further modification of the particle coating surface.

2.2.6.3 Atomic Force Microscopy

The surface morphology of SiNP coatings was examined using a Parks System atomic force microscope (AFM) operated in tapping mode, with a Mikromash NSC15 cantilever (spring constant $\sim$37 N/m). Image scans of 5 μm $\times$ 5 μm were obtained at a scan rate of 1 Hz in air. The surface area and coating roughness were calculated using Gwyddion v. 2.4.8 software.

2.2.7 Quartz Crystal Microbalance

SB adsorption onto SiO_2 sensors and SiNP coated gold sensors and protein adsorption experiments onto the SB functionalised SiO_2 and SiNP coatings were carried out using a Q-Sense E4 QCM-D (Q-Sense AB Västra, Frölunda, Sweden) coupled with an ISMATEC IPC High Precision Multichannel Dispenser (IDEX, Wertheim, Germany) in a flow-through setup. The use of the QCM allows for correlation between a change in the quartz crystal's fundamental oscillation frequency and calculation of a mass adsorbed to a surface (for review, see Marx[281]). Q-Sense QTools analysis software v3.0.10.286 (Biolin Sci, AB) was used to apply the Voigt model to calculate the mass of SB and protein adsorbed onto the sensor surface. The following input parameters provided the best fit for the layer density (1150 kg/m^3), fluid density (1020 kg/m^3), layer viscosity ($10^{-6} \leq 10^{-2}$ kg/ms), layer shear modulus ($10^4 \leq 10^8$ Pa) and mass ($1.15 \leq 1.155$ ng/cm^2). The 3^{rd}, 5^{th}, and 7^{th} overtones were used for modelling calculations.

2.2.7.1 Functionalisation of SiO_2 and SiNP Substrates

Adsorption of SB onto SiO_2 QCM sensors and SiNP coated gold QCM sensors were monitored within the QCM. SiO_2 sensors were cleaned with piranha solution (7:3 v/v mixture of H_2SO_4 (98%) and H_2O_2 (33%)) to generate the surface silanol groups available for reaction. SiNP coated sensors were used without any further surface treatment. Aqueous solutions of SB monomer (1.0 and 10 mM) were prepared immediately prior to experiments and pH adjusted as necessary. Solutions were introduced into the QCM chamber at a flow rate of 60 μL/min and surfaces were exposed for a period of 30 min. Sensors were then rinsed with deionised water at the same flow rate for a further 30 min or until the QCM measurement parameters stabilised. All experiments were run in triplicate.

2.2.7.2 Protein Adsorption Measurements

QCM sensors coated with the various SiNP films were placed into standard Q-Sense flow modules (QFM 401) and equilibrated in PBS for a minimum of 1 h at a constant temperature of 22.00 ± 0.02 ℃. BSA dissolved in PBS at a concentration of 1 mg/mL was introduced into the flow chamber at a constant flow rate of 60 μL/min for 30 min. Sensors were subsequently rinsed with PBS for a further 30 min at the same flow rate or until QCM measurement parameters stabilised. All experiments were run in triplicate.

2.2.8 Bacterial Adhesion Study

2.2.8.1 Cell Culture

Bacterial solutions were prepared from a precultured JM109 strain of *Escherichia coli* and inoculated overnight in 5 mL of sterile Luria-Bertani (LB) medium at 37 ℃ in a Bioline incubator shaker 8500 (Edwards Instrument Co., Narellan, Australia). Inoculated culture (0.3 mL) was added to 10 mL of LB medium and optical density (OD) measurements carried out every 30 min using a Spectronic 200 (Thermo Scientific, Waltham, MA) until the desired turbidity was achieved (OD_{600} 0.6–1.0). The number of colony forming units (CFUs) in the bacterial suspension was determined by plating out dilutions of the suspension and was found to be 3.5×10^6 CFU/mL.

2.2.8.2 Bacterial Adhesion Study

Coverslips with coatings of surface functionalised and solution functionalised particles were first sterilised by briefly immersing them in EtOH (2 s) and then placed into individual wells of sterile 12-well culture plates. PBS (2 mL) with bacterial cells

were added to each well, and culture plates were incubated at 37 ℃ for either 2 or 24 h time periods. Coverslips were then removed from incubation and placed into fresh sterile 12-well culture plates. Coverslips were rinsed with 0.7% NaCl solution to remove loosely adhered bacteria. This process was repeated three times for each sample. Adhered bacteria were chemically fixed by depositing 0.5 mL of 3.7% paraformaldehyde in PBS solution onto the surface of each sample. After 30 min the samples were again rinsed with 0.7% NaCl solution.

2.2.8.3 Bacterial Staining and Imaging

Samples were stained with a 20 μg/mL Hoechst 33342, trihydrochloride, trihydrate working solution (Invetrogen - Life Technologies (Thermo Scientific)). Hoechst working solution (1 mL) was deposited onto each of the coated QCM sensors and left for 15 min. Stained bacteria were imaged using a Zeiss AxioImager A1M, with an open HBO 100 mercury lamp and an Axiocam MRm camera (Carl Zeiss, Oberkochen, Germany). Images were obtained at 50× magnification, with percent area coverage determined using ImageJ® software (v.1.50b).

2.2.9 Fungal Spore Adhesion Study

2.2.9.1 Adhesion Assay

The antifouling properties of the SB functionalised nanoparticle coatings were evaluated against *Epicoccum nigrum* (ATCC 42773). *E. nigrum* spores were collected from a precultured agar plate (Potato dextrose agar (BD 213400)) and dispersed in 7 mL of sterile water. The spore suspension was shaken vigorously and placed on an orbital shaker for 2 h. The suspension was then centrifuged for 5 min at 1500 rpm. The supernatant was removed and spores were resuspended in 7 mL sterile water. The spore suspension was then filtered through a 40 μm hollander weave mesh to ensure good spore separation and diluted ∼10-fold.

Spin-coated nanoparticle coatings were placed into a sterile Greiner 12-well cell culture plate and covered with 1 mL of sterile deionised water. An aliquot of the spore suspension was then deposited onto the coatings to give a concentration of 6 × 10^3 spores per cm^2 and samples were incubated at 30 ℃ for 24 h. The samples were removed from the incubator after 24 h and each coverslip was immersed in sterile water (3×) with gentle agitation, then washed (3×) with sterile water. Spores were fixed with 2.5% (v/v) glutaraldehyde solution.

2.2.9.2 Cell Imaging

Fixed spores were imaged at 5× magnification using a Zeiss Axiovert inverted microscope. Areas imaged were chosen randomly and spores counted using ImageJ® software (v.1.50b). Four images were obtained for each sample surface and each surface was sampled in triplicate with the total average reported.

2.2.10 Statistical Analysis

Numerical results were expressed as means ± 95% CI. Results were analysed using one-way analysis of variance (ANOVA) with Tukey post hoc test. Probabilities of $p < 0.05$ were considered to be significantly different. All statistical analyses were performed using IBM SPSS Statistics 21 software.

2.3 Results and Discussion

2.3.1 Functionalisation of SiO_2 and SiNP Surfaces

Zwitterionic SB was prepared via a nucleophilic ring-opening reaction of 1,3-propane sultone by aminoalkoxysilane. SB dissolved in water hydrolyses the methoxy substituents producing silanol groups available for condensation reaction with SiO_2 or SiNP surfaces. Previous studies have indicated that hydrolysis of alkoxysilanes proceeds rapidly via both acid and base-catalysed mechanisms but that self-condensation reactions are favoured under basic conditions.[257] Figure 2.1 illustrates the three methods employed to prepare SB functionalised surfaces: grafting directly to SiO_2 QCM sensors (a), grafting to SiNP coated QCM sensors (b), and QCM sensors coated with functionalised nanoparticles (c).

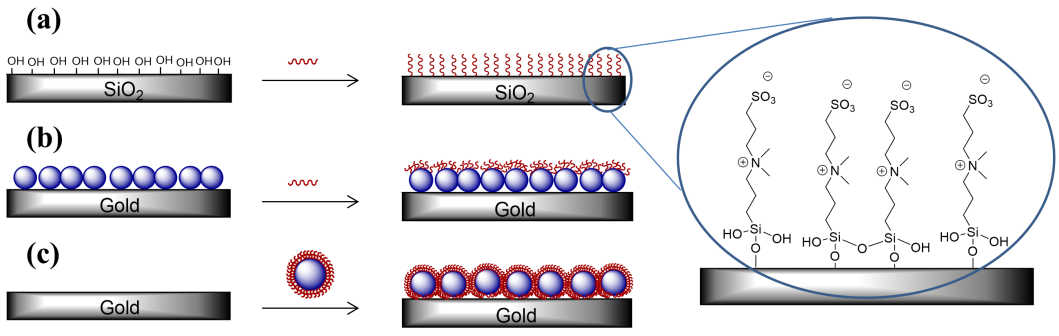

Figure 2.1: Methods of preparing SB modified surfaces: grafting directly to SiO_2 QCM sensors (a), grafting to SiNP coatings on gold QCM sensors (b), and dispersion functionalised SiNPs deposited as coatings onto gold QCM sensors (c).

To optimise the reaction conditions for solution functionalised particles, the reaction

of SB to the SiO_2 and SiNP coated sensors was first monitored using QCM-D (Figure 2.2). Silanisation of these surfaces with SB was carried out within a standard QCM module at 1 and 10 mM solution concentrations under acidic (pH 3.5), neutral (pH 7.0), and basic (pH 9.5) conditions.

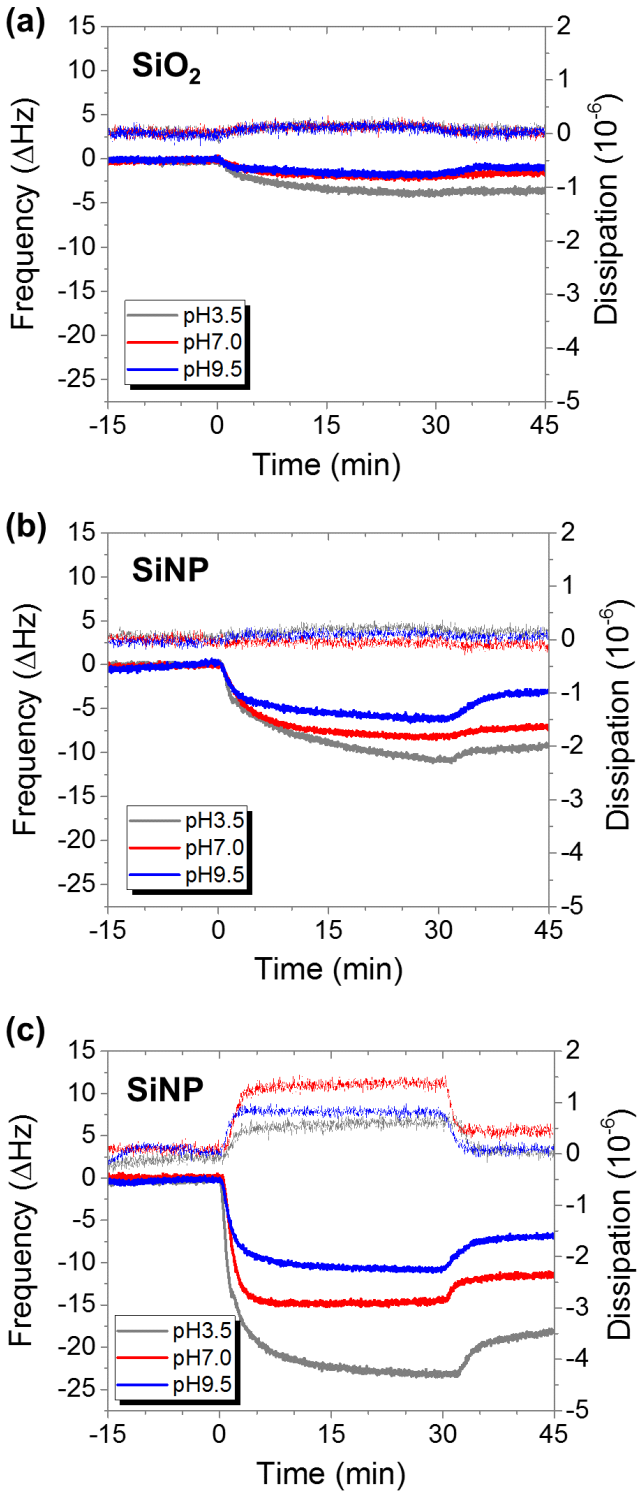

Figure 2.2: SiO_2 sensor f and D responses to 1 mM SB solutions (a), and SiNP coated QCM sensor f and D responses on exposure to 1 mM (b) and 10 mM (c) SB solutions at pH 3.5, 7.0, & 9.5 (data presented is from the 5^{th} overtone).

Surface functionalisation was facilitated through condensation reactions with silanol groups (present at the SiO_2/SiNP surface), promoting the formation of a self-assembled monolayer. Self-assembly was confirmed by characteristic frequency (f) and dissipation (D) parameter shifts indicating increased mass at the sensor surface. Figure 2.2 presents the time dependent f/D responses for SiO_2 and SiNP coated sensors upon exposure to 1 and 10 mM SB solutions with varied pH. Introduction of the SB solutions into the sensor chamber at time 0 generated immediate negative f shifts, indicating rapid monomer attachment. Across all conditions, f shifts were quick to stabilise and rinsing surfaces after 30 min exposure only resulted in a slight increase in the observed frequency, indicating that the majority of the SB monomer was covalently bound to the SiO_2 sensor or SiNP surface.

Exposure of the SiO_2 QCM sensors to the 1 mM SB solution produced the smallest f shift of the examined surfaces (Figure 2.2a). Interestingly, for the same zwitterion concentration, larger negative f shifts were observed for SiNP coated QCM sensors, indicating a larger mass of SB bound to the coating surface (Figure 2.2b). Increasing the SB solution concentration to 10 mM appeared to drive further surface attachment with significantly larger f and D shifts observed (Figure 2.2c). These results indicate that the application of a thin layer of SiNPs provides a method of introducing silanol chemistries to otherwise inert surfaces making them available for functionalisation.

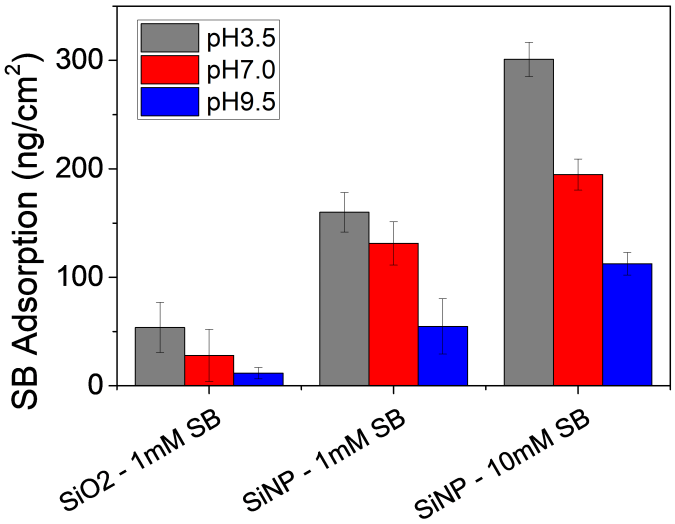

Figure 2.3: Mass of SB attached to SiO_2 and SiNP coatings with varied concentration and pH, modelled from 3^{rd}, 5^{th}, and 7^{th} overtone f and D QCM-D responses. Error bars represent 95% CIs (n=3).

The mass of surface bound zwitterion was estimated by fitting the Voigt-based viscoelastic model to account for any dissipative energy losses that may be experienced by adsorption of the hydrated zwitterionic species. A higher degree of surface functionalisation was demonstrated by the SiNP coated sensors compared to that on

the pristine SiO_2 surface for the same zwitterion solution concentration (1 mM SB) (Figure 2.3). It is thought that this increase in zwitterion binding is the result of the SiNP coatings presenting an increased surface area available for reaction. Additionally, the SiNP coatings may allow for zwitterion penetration into the nanoparticle film, as a result of increased porosity. Increasing the zwitterion concentration to 10 mM saw a subsequent increase in the mass bound to the SiNP coatings, demonstrating that higher zwitterion concentrations promoted increased coupling to the nanoparticle surface.

Modelling revealed that the mass of SB bound to the SiNP coated sensors under acidic conditions was significantly larger than that achieved under neutral and basic conditions for both 1 and 10 mM solution concentrations (one-way ANOVA, $p < 0.05$). Similarly, mass of SB bound to the SiO_2 sensors was significantly different between the acidic and basic pH treatments. It is proposed that the smaller degree of SB attachment observed under basic conditions is the result of oligomer adsorption due to rapid hydrolysis and condensation reactions, which are known to dominate under alkaline pH.[262] Oligomers tethered to the SiO_2 and SiNP surfaces then inhibit the approach of additional oligomer units, thus limiting uniform monolayer assembly and reducing the mass observed at the sensor surface (Figure 2.4).

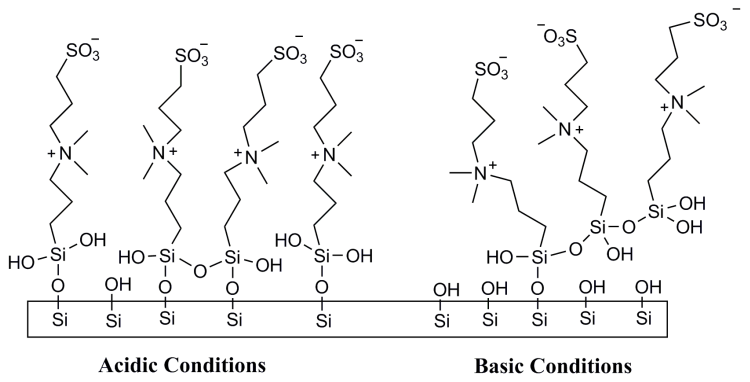

Figure 2.4: Self-assembly of SB monomers under acidic conditions (left) and oligomer attachment under basic conditions (right).

After SB functionalisation, water contact angles of the prepared surfaces were measured (Table A.1). All surfaces were appreciably hydrophilic, including the unfunctionalised SiNP control coating (9.5 ± 0.3°). Functionalisation of SiNP coatings with SB reduced the measured contact angles of the resultant coatings to between 5.4 and 6.1°, regardless of the concentration and pH at which they were prepared. These results indicate that the zwitterionic moiety was able to impart a higher degree of surface wettability to the already hydrophilic SiNP coatings.

2.3.2 SiNP Functionalisation

Functionalised silica nanoparticles (SiNP+SB) were prepared in solution via a simple silanisation process at 60 ℃. The appropriate amount of zwitterion added for reaction was calculated on the basis of the surface area reported by the manufacturer (220 m^2/g) and 4.9 silanol groups per nm^2 of the silica surface (8 $\mu mol/m^2$).[253] Zwitterion dissolved in water was added to 10 wt% SiNP dispersions prepared at pH 3.5, pH 7.0, and pH 9.5 by NaOH or HCl adjustment. The reaction mixtures were stirred at 60 ℃ for 2 h, after which time the resulting particles were dialysed to remove any unreacted zwitterion from the solution. Particles were collected via freeze-drying for FTIR and TGA analysis and redispersed in water for ZP/DLS measurements. The IR spectrum obtained for unmodified SiNP was relatively featureless (Figure A.2), presenting characteristic Si-O-Si stretch as a broad peak centered at 1060 cm^{-1} and another broad peak at 800 cm^{-1} attributed to Si-OH deformation vibrations.[282] For the prepared SB compound, bands were observed at 1033 and 1176 cm^{-1} confirming the symmetric and asymmetric stretching vibrations of SO_3^-. Peaks at 1485 and 1414 cm^{-1} were assigned as the C-H and N-H stretching vibrations of the quaternary ammonium group, respectively.[283] Upon particle functionalisation, broadening of the Si-O-Si band was observed and the predominant peak shifted to 1095 cm^{-1}, as a result of an overlap from asymmetric Si-O-C stretching vibrations, indicating successful zwitterion attachment.

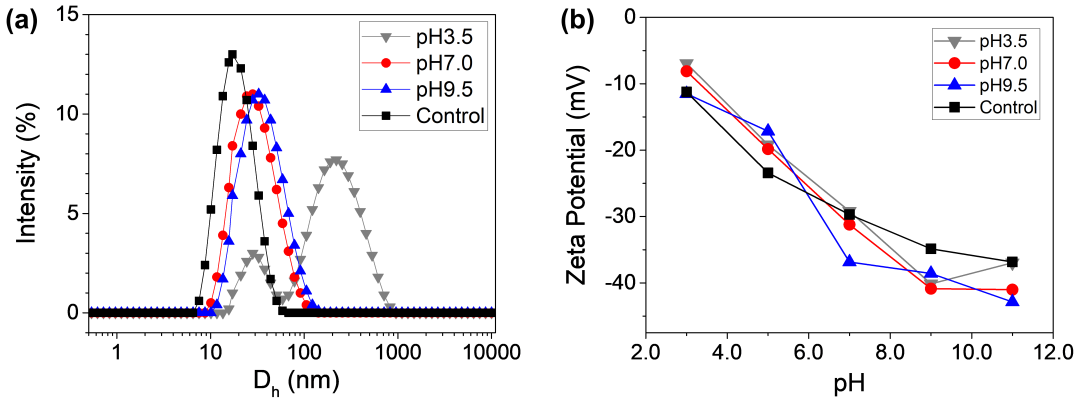

Figure 2.5: DLS size distribution by intensity of SB functionalised SiNPs (a). ZP of SB functionalised SiNPs measured between pH 3.0 and pH 11.0 (b).

The hydrodynamic diameters (D_h) of the SiNPs in water were measured before and after modification with SB (Figure 2.5a). Functionalisation under neutral and basic conditions resulted in an increase in hydrodynamic diameter from 18.2 to 24.9 and 30.1 nm, respectively, indicating successful particle modification (Table A.2). The increases in particle size observed upon functionalisation were larger than the scale of the SB monomer, potentially indicating oligomer adsorption to the particle surface

and a subsequent increase in particle hydration. These results were consistent with the proposed attachment mechanism in Figure 2.4. After functionalisation under acidic conditions, particles could not be easily redispersed and the average diameter measured was unexpectedly high (147.9 nm). It is thought that the acidic conditions caused nanoparticle destabilisation due to reduced surface charge, resulting in irreversible particle aggregation.[284] A similar result was reported by Chu et al.,[285] where functionalisation of silica colloids with (glycidoxypropyl)trimethoxysilane under acidic conditions resulted in the formation of nanoparticle aggregates.

The effect of SB functionalisation on particle surface charge was evaluated by measuring the zeta potential (ZP) in 0.01 M NaCl solution as a function of pH (Figure 2.5b). Unfunctionalised particles produced a large negative ZP at neutral and basic pH. Increasing acidity resulted in an increase in ZP (approaching zero), as the Si-O^- terminus of the SiNP outer surface became protonated. Functionalisation with the SB moiety did not result in a dramatic shift in the ZP response. Particles still exhibited a largely negative ZP after addition of the electrically neutral SB, potentially indicating that a large number of silanol groups on the particle surface remained unreacted. Because of the weakly basic nature of the sulfonate group, protonation would not be expected to occur in the pH range studied.[286] These results were consistent with the ZP observed for SB functionalisation of cellulose membranes.[203]

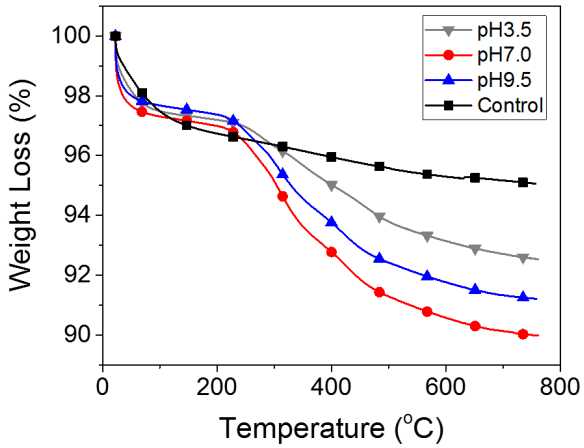

Figure 2.6: TGA weight loss curves of SB functionalised SiNPs prepared at pH 3.5, 7.0, and 9.5, compared to unfunctionalised SiNPs.

The amount of zwitterion bound to the particle surface was determined quantitatively by TGA (Figure 2.6). Initial mass decreases observed below 200 ℃ were attributed to loss of adsorbed water. Mass losses above this temperature were attributed to decomposition of the SB monomer and were used to calculate the degree of particle functionalisation. Fitting with the QCM model, particles reacted at pH 7.0 showed a higher degree of functionalisation than those prepared at pH

9.5. However, although it was expected that the pH 3.5 particles would exhibit the highest degree of functionalisation, they instead produced the lowest degree of attachment. It is thought that due to the aggregate formation indicated by the DLS measurements a smaller surface area would have been available for functionalisation.

For each functionalisation condition, enough zwitterion was added to theoretically functionalise every available silanol site on the particle surface (8 μmol/m^2). However, the grafting densities that were achieved were only 0.8, 1.2, and 1.1 μmol/m^2 for the 3.5, 7.0, and 9.5 pH conditions, respectively (Table A.3). These results were consistent with the findings of Estephan et al.[232] who showed a deviation from stoichiometric surface coverage at zwitterion concentrations above 1 μmol/m^2; however, they fell short of the 1.7 μmol/m^2 surface coverage reported by the same group. Similarly, previous studies have also demonstrated that concentrations well above the theoretical saturation values are required to achieve full coverage of the nanoparticle materials.[274]

2.3.3 Fabrication of Functionalised Particle Coatings

A layer of poly(ethylenimine) was first coated onto the gold QCM sensors to assist particle adhesion. SB functionalised silica nanoparticles (SiNP+SB) were then deposited onto the PEI coated QCM sensors and spin-coated to produce a thin layer (Figure 2.1c). Curing coatings at 120 ℃ was thought to improve particle stability on the sensor surface and promote polycondensation between unreacted silanol groups.

SEM revealed that the spin-coating process produced a uniform coating, with a thickness of the order of just a few particles (Figure 2.7e). Gold substructure of the underlying QCM sensor surface can be clearly seen beneath the particle coating. Although uniform films of particles functionalised at pH 7.9 and 9.5 were obtained, some heterogeneity was observed for coatings prepared from particles functionalised at pH 3.5. This was thought to confirm the presence of particle aggregates formed under acidic conditions, as indicated by DLS measurements (Figure A.4).

Contact angles of SiNP+SB coatings were consistently low across all pH reaction conditions (3.6 $\pm$ 0.3°, 4.8 $\pm$ 0.7°, and 5.3 $\pm$ 0.2° for pH 3.5, 7.0, and 9.5, respectively), indicating high surface energy and superhydrophilic properties. This high degree of surface wettability was attributed to the presence of the SB moiety and its ability to bind water through ionic solvation. AFM was used to probe the morphology of the nanoparticle coatings, as surface roughness is known to affect hydrophilicity and antifouling behaviour. Nanoparticle coatings presented low surface roughness (R_{RMS} = 3.18 $\pm$ 0.22 nm) and the measured surface areas closely matched the scan area (for the 5 $\times$ 5 μm^2 images taken, the average surface area was 25.20 μm^2) (Figure A.3). For this reason, it is unlikely that the roughness of the nanoparticle coatings

would play a role in affecting adhesion of the organisms investigated in this study.

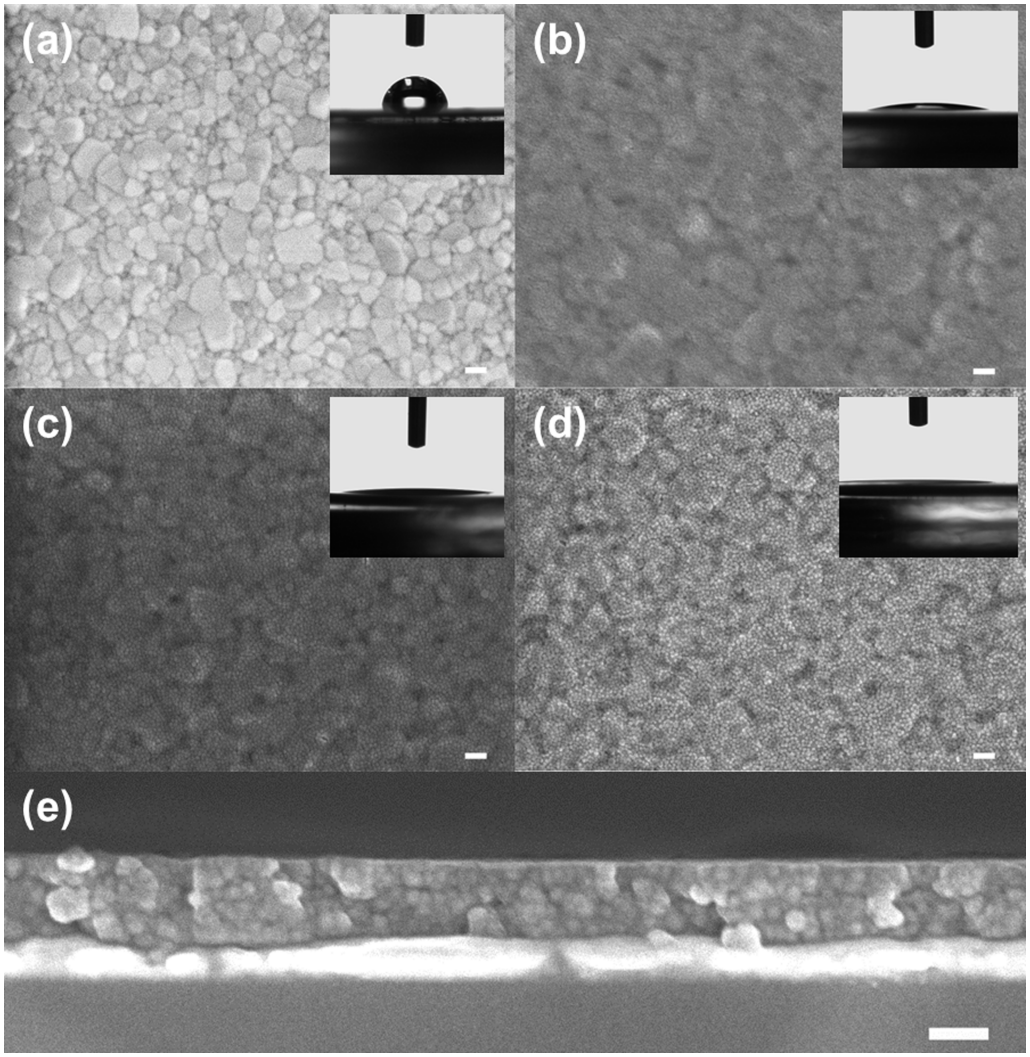

Figure 2.7: Scanning electron microscope images taken at 50 000× magnification: gold QCM sensor (a), SiNP coated QCM sensor (b), SiNP coated QCM sensor functionalised with 10 mM SB solution (pH 9.5) (c), SiNP+SB (pH 9.5) functionalised particles coated onto gold QCM sensor (d), and cross section of SiNP coated QCM sensor (e). All scale bars are 100 nm. The insets are photographs of typical contact angles measured for the presented surfaces.

2.3.4 Protein Adsorption Experiments

The antifouling properties of the SB functionalised SiO_2/SiNP surfaces were examined by measuring adsorption of BSA protein using QCM-D. Nanoparticle coatings were first equilibrated in PBS, wherein QCM sensors were quick to stabilise and no drift in f/D parameters were observed. This indicated that the coatings presented a high degree of stability in salt solution and were not suffering from any particle loss during protein adsorption experiments. Significant reductions in protein adsorption were observed across all functionalised surfaces and across the entire pH range studied compared to those for the unfunctionalised SiNP control coating (one-way ANOVA,

$p < 0.05$). SB self-assembled onto the optimal SiO_2 sensor surface resulted in near-negligible protein adsorption (Figure 2.8), with no statistical difference observed across the pH treatments. For the same 1 mM SB concentration, adsorption of BSA protein onto the SiNP surfaces was still significantly reduced compared to that for the unfunctionalised SiNP coating but was unable to provide the same level of resistance as that demonstrated by the SiO_2 sensors.

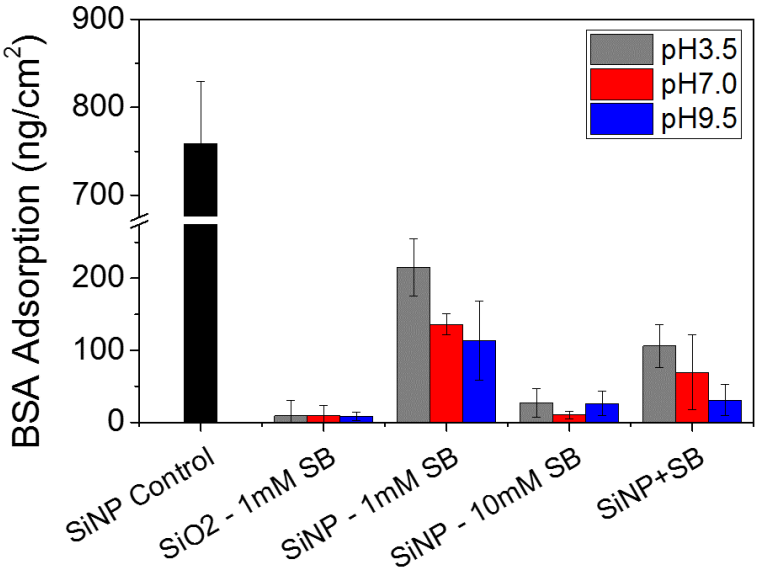

Figure 2.8: BSA adsorption onto SB functionalised SiO_2 sensors and SiNP coatings prepared at various concentrations and pH. Mass of the adsorbed protein was calculated from modelling the 3^{rd}, 5^{th}, and 7^{th} overtone f and D responses within the QCM-D. Error bars represent 95% CIs (n=3).

Although SB adsorption studies indicated that a higher degree of functionalisation could be achieved under acidic conditions, improved protein inhibition was observed for coatings prepared from 1 mM solutions under neutral and alkaline conditions. It is proposed that although a higher degree of organisation (self-assembly) may be achieved under acidic conditions, the oligomer adsorption observed under alkaline conditions actually provides an improved steric barrier in preventing interactions with fouling species. Increasing the SB solution concentration to 10 mM further improved the protein resistance of the SiNP films across the pH range studied, likely due to increased mass of SB bound to the particle surface (as indicated by the earlier QCM-D study). At this increased zwitterion concentration, pH was not found to have a statistically significant effect on protein adsorption. It should be noted that although the SiO_2 sensors were treated with piranha solution prior to functionalisation, the SiNP coatings did not receive any surface treatment before exposure to the SB solutions, indicating the relative ease of SiNP functionalisation and their excellent low-fouling capability.

Coatings prepared from solution functionalised particles (SiNP+SB) were also shown to significantly improve protein resistance, with adsorption reduced by up to 96% for particles prepared under alkaline conditions. Interestingly, SiNP functionalisation within the QCM (10 mM SB) resulted in improved protein resistance compared to solution functionalised particles. The increased availability of SB monomer under higher concentration conditions was thought to drive surface immobilisation, resulting in a higher degree of functionalisation and subsequent improvement in protein inhibition.

2.3.5 Bacterial Adhesion Study

Because of the superior protein resistance displayed by SB functionalised particles prepared under alkaline conditions, surface and solution functionalised SB particle coatings (prepared at pH 9.5) were chosen to perform the microbial adhesion studies, with unfunctionalised nanoparticle coatings acting as a control surface. Bacterial adhesion assays were carried out over 2 and 24 h time periods using *E. coli* to investigate initial bacterial adhesion and long-term fouling resistance (Figure 2.9).

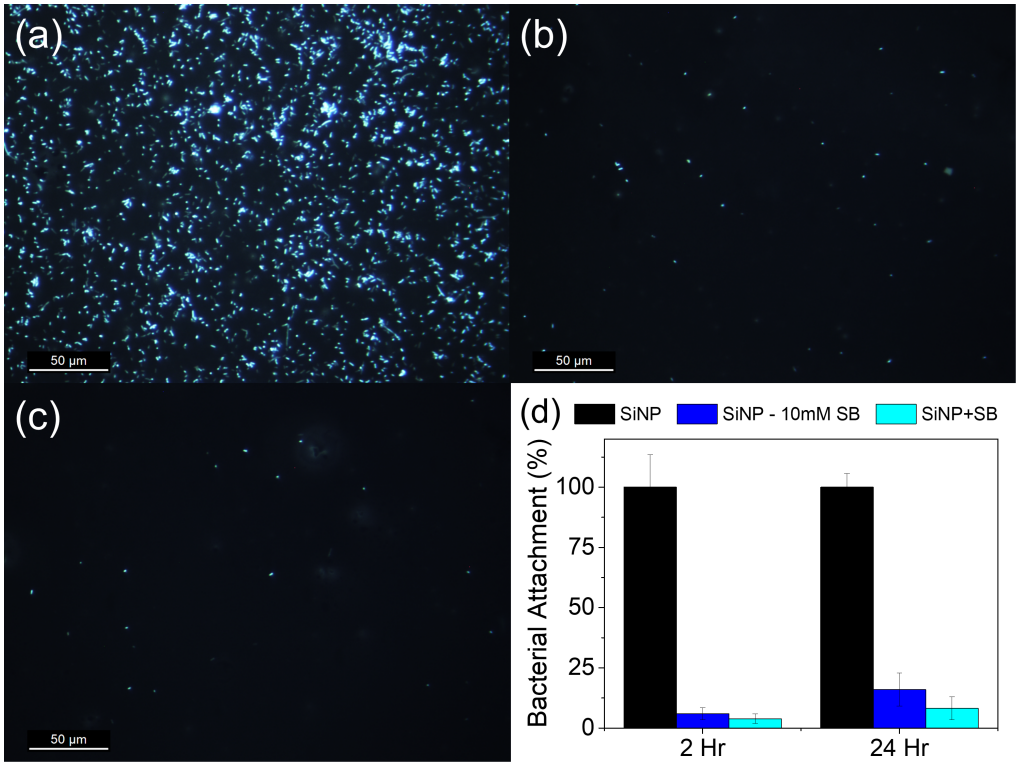

Figure 2.9: Representative images of *E.coli* attachment after 2 h on unfunctionalised SiNP control (a), surface functionalised SiNP - 10 mM SB (pH 9.5) (b), and solution functionalised SiNP+SB (pH 9.5) particle coatings (c). Normalised bacterial attachment (%) of SB functionalised particle coatings compared to that of unfunctionalised SiNP coating controls after 2 and 24 h (d).

Short-term adhesion was tested against high concentrations of *E. coli* (3.5 ×

10^6 CFUs) wherein both surface and solution functionalised nanoparticle coatings demonstrated drastic reductions in bacterial adhesion compared to the control surface (95 and 96% reductions, respectively). For the 24 h study, bacterial attachment was again significantly lower (relative to the unfunctionalised control coating), with the solution functionalised particles slightly outperforming coatings prepared via surface functionalisation. However, no statistical difference was observed between the two coating methods. Traditionally, the antibacterial properties of zwitterionic surface coatings reported in the literature have typically been based on polymeric systems that utilise complex synthesis methods such as atom transfer radical polymerisation to generate hydrophilic, zwitterionic interfaces. In contrast, this work has demonstrated a facile aqueous-based surface modification strategy to generate highly bacterial resistant SiNP based zwitterionic surface coatings that can easily be applied to a range of materials for antifouling applications.

2.3.6 Fungal Spore Adhesion Study

The fungus chosen for this study (*E. nigrum*) is a filamentous fungus that has been recognised as a major biodeteriogen.[287] Nanoparticle coatings were incubated with *E. nigrum* fungal spores for a 24 h period, after which time, surfaces were rinsed and the remaining spores counted. It should be noted that the number of spores deposited onto the coatings remains constant throughout the duration of the study; thus, spores remaining after the rinsing process are those that have adhered strongly to the tested surfaces. The SiNP coated control suffered a high degree of fungal spore attachment with extensive hyphal growth across the coating surface (Figure 2.10a). It was found that surface functionalisation of SiNP films (10 mM SB) resulted in a 50% decrease in the observed number of adhered spores. Solution functionalised particle coatings (SiNP+SB) produced an even larger decrease in spore adhesion, with an 87% reduction compared to the unfunctionalised control. Both coatings showed statistically significant differences to the control surface (one-way ANOVA, $p < 0.05$).

Fungal spores possess a proteinaceous cell wall coating that is involved in surface hydrophobicity and adhesion and acts as a protective surface coating. Hydrophobins, a key protein in this surface coating, have been demonstrated to mediate spore and hyphal-surface interactions, initiating and maintaining adhesion between the fungus and the surface.[288] It is proposed that the ability for the zwitterion functionalised surfaces to resist adhesion of fungal spores is the result of hydration at the polymer interface, which limits adhesion between this proteinaceous adhesive layer and the surface. The improved adhesion resistance exhibited by the solution functionalised particles is thought to be the result of a higher degree of functionalisation at particle

boundaries. Overall, the improved protein, bacterial, and fungal spore resistance imparted by the SB functionalisation, in combination with the ease of particle functionalisation and coating fabrication, highlight the potential for SiNPs to be further developed as low-fouling coatings for widespread applications.

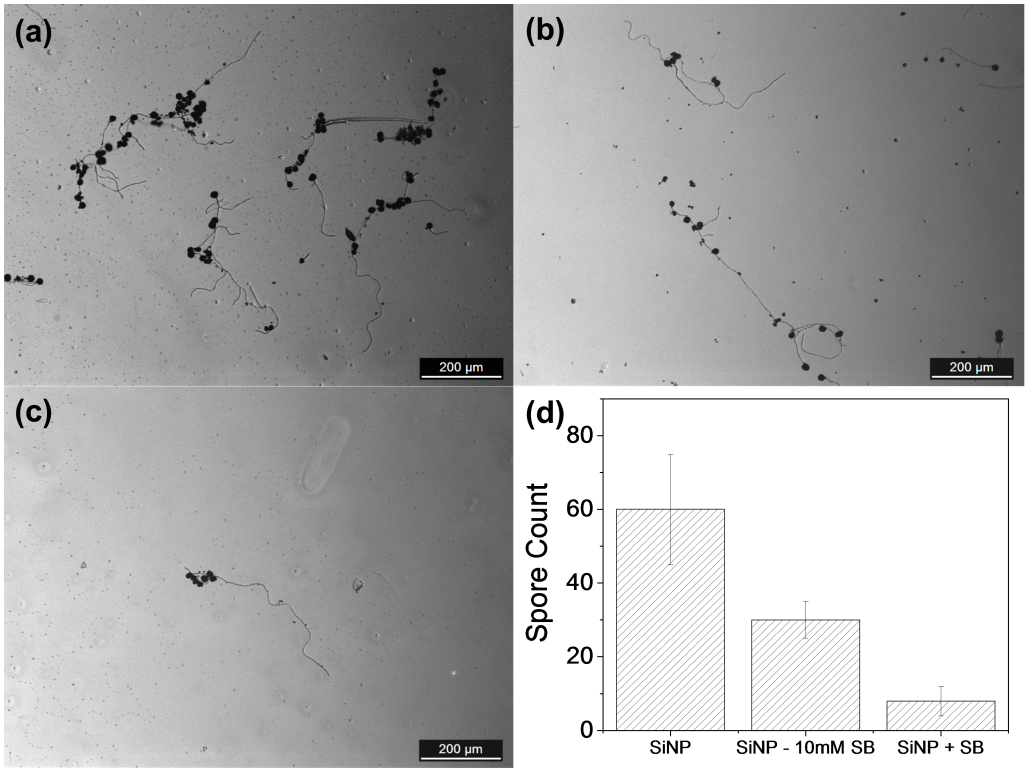

Figure 2.10: Representative optical microscopy images of *E. nigrum* spores remaining on SiNP control (a), SiNP - 10 mM SB (pH 9.5) (b), and SiNP+SB (pH 9.5) (c) coatings, and total adhered spore counts (d) after 24 h adhesion study. Error bars represent 95% CIs (n=3).

2.4 Conclusions

In this study, zwitterionic SB functionalised SiNPs were prepared as hydrophilic surface coatings, with excellent fouling resistant properties against protein, bacteria, and fungal spore adhesion. The modification of nanoparticle dispersions and nanoparticle coatings could be carried out in an aqueous solution across a large pH range, without the need for a catalyst. QCM-D was introduced as a facile and efficient method to optimise the SiO_2 reaction conditions, acting as a model for dispersion based functionalisation of the SiO_2 nanoparticles. Coatings of particles functionalised with SB were highly resistant to the adsorption of protein and adhesion of bacteria and showed significant reductions in fungal spore adhesion and hyphal growth. Surface functionalisation of predeposited SiNPs provided a rapid method of imparting hydrophilic chemistries to surfaces with good antifouling properties, whereas solution functionalised particles could be used to generate robust antifouling coatings that may be suitable for long-term applications. Zwitterion functionalised SiO_2 nanoparticles provide a promising platform for use as antifouling coatings for a suite of different applications and in different coatings and materials technologies. The materials are cheap, highly processable, and chemical processes are easily scalable and do not require organic solvents. This platform system provides opportunities for further investigation of functionalised nanosilicas, as detailed in later Chapters of this thesis.

Chapter 3

Carboxybetaine Functionalised Nanosilicas as Protein-Resistant Surface Coatings

This Chapter has been adapted from the article "Carboxybetaine Functionalized Nanosilicas as Protein-Resistant Surface Coatings", submitted to *Colloids and Surfaces B: Biointerfaces* (under review).

The success of silica nanoparticle functionalisation with zwitterionic sulfobetaine led to further investigation with a silanated carboxybetaine chemistry. This work explored three different methods of preparing carboxybetaine functionalised silica nanoparticle coatings and compared the protein resistant behaviour of these zwitterionic surfaces prepared under different reaction conditions.

3.1 Introduction

The antifouling properties of zwitterionic polymers have been largely attributed to their exceptional hydration capacity. Studies investigating zwitterion hydration using molecular modelling have demonstrated that the residence time, orientation, and number of water molecules associated with zwitterionic chemistries is dependent upon the identity and electrochemical properties of the charged groups present.[197, 206, 289] Theoretical simulations comparing zwitterionic carboxybetaine (CB) and sulfobetaine (SB) have shown that the sulfonate group (SO_3^-) of SB coordinates a larger number of water molecules than the carboxylate group (CO_2^-) of CB, while CB coordinated water molecules have sharper spatial distribution and longer residence times.[206] It is anticipated that these subtle differences in hydration capacity would influence the ability of these materials to prevent biological fouling. Indeed, previous

studies have demonstrated that SB modified cellulose membranes have better protein resistance than CB modified surfaces,[203] while polymeric CB modified surfaces have shown improved resistance to nonspecific protein adsorption from human blood plasma and serum over polymeric SB and self-assembled mixed charge zwitterionic surfaces.[176]

In addition to differences in hydration capacity, the electronegativity of zwitterionic anionic groups will influence their response to media and variation in pH. The sulfonate group of SB is a weak base and will remain negatively charged even at low pH, however, the carboxylate group of CB is a strong conjugate base (carboxyl group is a weak acid with a typical pK_a between 3 and 5) and is susceptible to protonation under low pH conditions.[187] As a result, the zwitterionic character and resultant antifouling properties of CB modified surfaces will be dependent upon the pH conditions of preparation and exposure.

The previous Chapter reported on the preparation of hydrophilic, low-fouling coatings from SB functionalised silica SiNPs, where SiNPs could be functionalised either before or after their deposition onto surfaces for improved fouling resistance. In this Chapter, three methods were employed to generate SiNP coatings presenting zwitterionic CB functionality for enhanced resistance to protein fouling. CB was used to directly modify the surface of SiNP films, where conditions of reaction (i.e. pH, solution concentration) were monitored using QCM-D. SiNP coatings were also modified utilising a two-step process, eliminating the need for preparation of the CB monomer species separately. Additionally, suspensions of SiNPs were functionalised and deposited as thin films for the investigation of their antifouling properties. All of the prepared surfaces were hydrophilic and showed improved resistance to protein binding. This study demonstrated that the self-assembly or polymeric type organisation of CB chemistries onto the SiNP surfaces was pH dependent and ultimately influenced the mechanism of protein repellency. The ease of preparation and effectiveness of these surfaces is compared to the SB modified SiNP surfaces discussed in Chapter 2.

3.2 Experimental

3.2.1 Materials

Ludox® HS-40 colloidal silica (12 nm diameter), phosphate buffered saline (PBS, P5368), (*N,N*-dimethylaminopropyl)trimethoxysilane (539287), acetone (270725), poly(ethylenimine) solution (PEI, P3143), and bovine serum albumin (BSA, A3059) were purchased from Sigma-Aldrich. Acetone was dried with 3 Å molecular sieves and distilled before use. β-propiolactone (H0168) was purchased from Tokyo Chemical

Industry. All other reagents purchased from commercial suppliers were used without further purification. Water used in experiments and to prepare aqueous solutions was purified using a Millipore water purification system with a minimum resistivity of 18.2 MΩ.cm at 25 ℃.

3.2.2 Synthesis of Zwitterionic CB

The synthesis of zwitterionic CB (3-(dimethyl(3-(trimethoxysilyl)propyl)ammonio)-propanoate) was adapted from Hu et al.[233] (*N,N*-dimethylaminopropyl)trimethoxysilane (2.08 g, 0.01 mol) was added dropwise to β-propiolactone (0.72 g, 0.01 mol) in anhydrous acetone (5 mL) under Ar. The reaction was stirred under Ar for 24 h and resulted in the formation of a white precipitate. Unreacted material was removed by rotary evaporator. The resulting material was collected and dried at 70 ℃ under vacuum.
^{1}H NMR (400 MHz, D_2O): δ 0.69 (t, 2H), 1.86 (quin, 2H), 2.63 (m, 2H), 2.85 (m, 2H), 3.06 (s, 6H), 3.31 (s, 9H), 3.53 (t, 2H).
IR (cm^{-1}): 1728, 1585, 1485, 1373, 1195, 1061, 930.

3.2.3 Reaction of CB to SiNPs

The appropriate amount of CB monomer for reaction with SiNPs was calculated on the basis of the surface area reported by the manufacturer and 4.9 silanol groups per nm^2 of silica surface.[253] CB was dissolved in minimal H_2O and pH adjusted to 10 by addition of NaOH. The CB solution was added dropwise to a stirred solution of SiNPs with a final particle concentration of 10 wt%. The reaction mixture was stirred for 6 h. Thereafter, particle solutions were placed into a dialysis membrane with a 12 K molecular weight cutoff and dialysed against distilled water for 5 days. Particles were freeze-dried for further characterisation.

3.2.4 Preparation of SiNP Coatings

Silica nanoparticle solutions were prepared as 4 wt% dispersions in water for spin-coating onto gold QCM-D sensors. Two types of coatings were prepared. First, dispersions of unreacted SiNPs were prepared for fabrication of nanoparticle coatings that would undergo functionalisation within the QCM. Second, coatings were prepared from dispersions of CB functionalised SiNPs for assessment of their antifouling properties. The silica nanoparticle dispersions were spin-coated onto A-T cut quartz crystal microbalance sensors with a 10 mm diameter gold electrode (QCM-D, Q-Sense AB Västra, Frölunda, Sweden) and a fundamental resonance frequency of 5 MHz. Prior to coating, the gold sensor surface of each sensor was cleaned with piranha

solution (7:3 v/v mixture of H_2SO_4 (98%) and H_2O_2 (33%)) for 3 min, rinsed with deionised water and dried in a stream of nitrogen gas. Cleaned QCM-D sensors were then incubated in 0.5% poly(ethylenimine) (PEI) solution for 10 min to form an adhesive layer on the electrode surface. The PEI was thoroughly rinsed from the sensors with deionised water and sensors were dried in a stream of nitrogen gas. The QCM sensors were mounted onto glass slides and nanoparticle films were prepared by depositing 20 μL of each of the prepared nanoparticle dispersions onto the gold electrode of the sensor and spin-coating at 5000 rpm for 30 s. Coatings were cured for 1 h at 120 ℃ and thereafter thoroughly rinsed with deionised water and dried in a stream of nitrogen gas.

3.2.5 Two-Step CB Functionalisation of SiNP Coatings

The procedure for the two-step surface functionalisation of SiNP coatings with CB was adapted from Huang and Chang.[201] SiNP coated sensors were first immersed in a 20 mM solution of (*N,N*-dimethylaminopropyl)trimethoxysilane in EtOH with 2% addition of H_2O for 6 h. Substrates were removed from solution, rinsed with EtOH and dried in a stream of nitrogen gas. Substrates were then cured in an oven at 120 ℃ for 1 h. A 10 mM solution of β-propiolactone in acetonitrile was prepared and the silane modified substrates were incubated in this solution at 4 ℃ for 6 h. Coatings were rinsed with acetonitrile and dried in a stream of nitrogen gas.

3.2.6 Characterisation

3.2.6.1 Fourier Transform Infrared Spectroscopy

Fourier transform infrared (FTIR) spectra were acquired on a Shimadzu Prestige-21 FTIR spectrophotometer with a PIKE MIRacle ATR attachment.

3.2.6.2 Nuclear Magnetic Resonance Spectroscopy

^{1}H NMR (400MHz) spectra were obtained on a Bruker AVANCE III HD NMR Spectrometer at 25 ℃ using D_2O as a solvent.

3.2.6.3 Dynamic Light Scattering/Zeta Potential

Z-Average particle size (hydrodynamic particle diameter) measured by dynamic light scattering (DLS) and zeta potential (ZP) measurements were performed on a Malvern Zetasizer Nano-ZS at 25 ℃ (colloidal silica refractive index: 1.40, absorption: 0.010, measurement angle: 173 °). ZP measurements were performed on 0.5 wt% aqueous particle dispersions, pH adjusted with NaOH and HCl. DLS measurements were carried out on 0.5 wt% particle solutions dispersed in 10 mM NaCl.

3.2.6.4 Thermogravimetric Analysis

The quantity of zwitterion bound to the particle surface was determined using thermogravimetric analysis (TA, Q500). Dried nanoparticles were heated from room temperature to 800 ℃ at a heating rate of 10 ℃/min under a nitrogen atmosphere. The mass of polymer bound to the particle surface was calculated from the weight loss measured between 150 and 800 ℃. The mass retained at 800 ℃ after polymer decomposition was assumed to be the mass of bare SiNPs.

3.2.6.5 Contact Angle Goniometry

The mean static contact angle made by a 2 μL sessile water droplet on the surface of each of the particle coatings were measured with a Dataphysics Contact Angle System (OCA 15EC) in conjunction with SCA20 software. A minimum of three measurements were obtained for triplicate samples of each particle coating.

3.2.6.6 Scanning Electron Microscopy

Imaging of particle coatings was performed using a field emission scanning electron microscope (SEM, JEOL JSM-7500FA). Images were obtained without further modification of the particle coating surface.

3.2.7 Quartz Crystal Microbalance

CB adsorption onto SiNP coated gold sensors and protein adsorption experiments onto the CB functionalised SiNP coatings were carried out using a Q-Sense E4 QCM-D (Q-Sense AB Västra, Frölunda, Sweden) coupled with an ISMATEC IPC High Precision Multichannel Dispenser (IDEX, Wertheim, Germany) in a flow-through setup. Q-Sense QTools analysis software v3.0.10.286 (Biolin Sci, AB) was used to apply the Voigt model to calculate the mass of CB or adsorbed protein onto the modified sensor surface. The following input parameters provided the best fit for the layer density (1150 kg/m^3), fluid density (1020 kg/m^3), layer viscosity ($10^{-6} \leq 10^{-2}$ kg/ms), layer shear modulus ($10^4 \leq 10^8$ Pa) and mass ($1.15 \leq 1.155$ ng/cm^2). The 3^{rd}, 5^{th}, and 7^{th} overtones were used for modelling calculations.

3.2.7.1 CB Adsorption onto SiNP Substrates

Adsorption of CB onto SiNP coated gold QCM sensors were monitored within the QCM-D. SiNP coated sensors were used without any further surface treatment. Aqueous solutions of CB monomer (1.0 and 10 mM) were prepared immediately prior to experiments and pH adjusted as necessary. Solutions were introduced into the QCM chamber at a flow rate of 60 μL/min and surfaces were exposed for a

period of 30 min. Sensors were then rinsed with deionised water at the same flow rate for a further 30 min or until the QCM measurement parameters stabilised. All experiments were run in triplicate.

3.2.7.2 Protein Adsorption

SiNP coated sensors were placed into standard Q-Sense flow modules (QFM 401) and equilibrated in PBS for a minimum of 1 h at a constant temperature of 22.00 ± 0.02 ℃. BSA dissolved in PBS at a concentration of 1 mg/mL was introduced into the flow chamber at a constant flow rate of 60 μL/min for 30 min. Sensors were subsequently rinsed with PBS for a further 30 min at the same flow rate or until QCM measurement parameters stabilised. All experiments were run in triplicate.

3.2.8 Statistical Analysis

Numerical results are expressed as means ± 95% CI. Results were analysed using one-way analysis of variance (ANOVA) with Tukey post hoc test. Probabilities of $p < 0.05$ were considered to be significantly different. All statistical analyses were performed using IBM SPSS Statistics 21 software.

3.3 Results and Discussion

3.3.1 CB functionalisation of SiNP coatings using QCM

The carboxybetaine (CB) species used throughout this study was prepared via a nucleophilic ring-opening reaction of β-propiolactone by an aminosilane, generating a quaternary ammonium cation and carboxylate anion (Figure 3.1). The resulting product was very hygroscopic, consistent with previous reports in the literature.[290, 291]

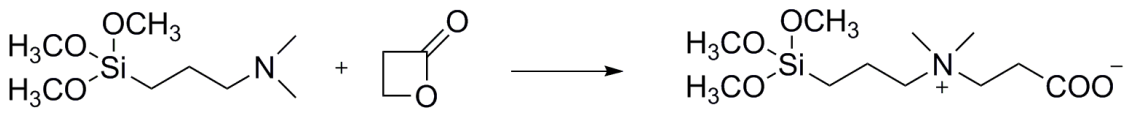

Figure 3.1: Generation of carboxybetaine via ring-opening of β-propiolactone by (*N,N*-dimethylaminopropyl)trimethoxysilane.

Thin films of SiNPs were cast onto gold QCM sensors via spin coating, where they generated a uniform, hydrophilic, and reactive substrate for functionalisation with CB (Figure A.5). Sensors were placed into QCM modules and equilibrated in deionised water until frequency (f) and dissipation (D) parameters stabilised.

Solutions of CB at concentrations of 1 and 10 mM were prepared immediately prior to their introduction into the QCM and pH adjusted to 3.5, 7.0, and 9.5 with addition of dilute NaOH or HCl. Gradual decreases in f were observed on exposure to 1 mM CB solutions, with decreasing pH resulting in larger negative f shifts (Figure 3.2a).

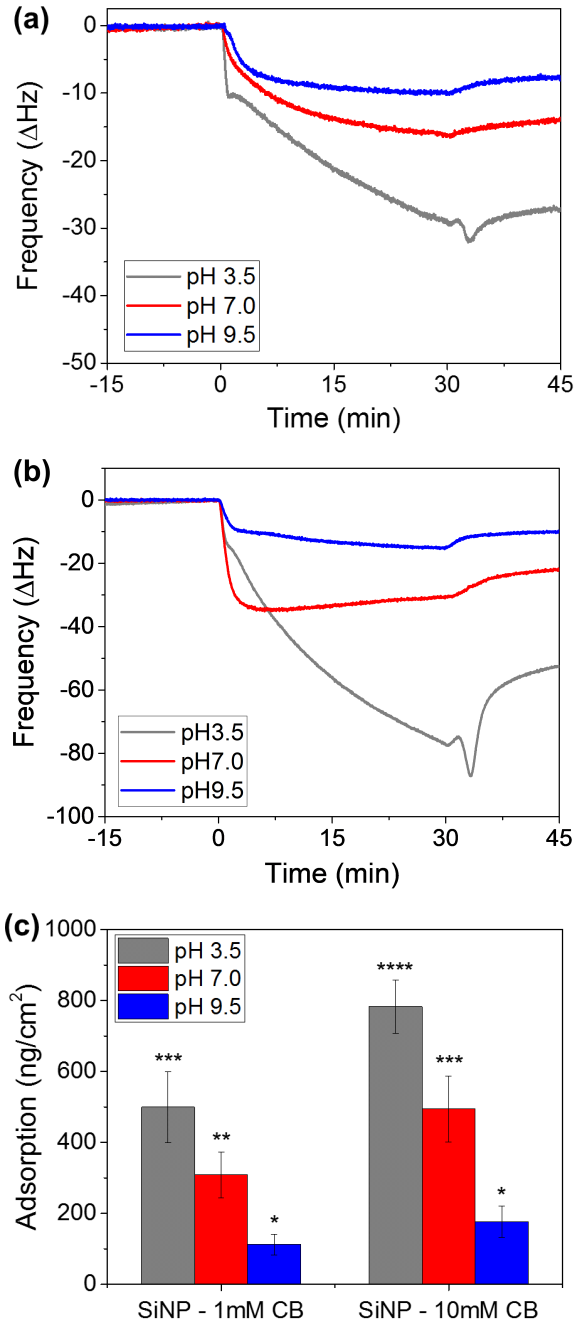

Figure 3.2: Raw QCM f shifts (5^{th} overtone) of SiNP coatings on exposure to 1 mM (a) and 10 mM (b) CB solutions adjusted to pH 3.5, 7.0, and 9.5. Mass of CB adsorbed onto SiNP coatings with varied concentration and pH (c). Mass was calculated from modelling the 3^{rd}, 5^{th}, and 7^{th} overtone f/D responses. Error bars represent 95% CIs (n=3). Asterisks (*) indicate statistically similar subsets.

Increasing the solution concentration to 10 mM dramatically increased the rate of

binding for CB solutions of pH 7.0 and 9.5, where large initial f shifts were observed before the rate of adsorption slowed and plateaued (Figure 3.2b). For acid-catalysed functionalisation of SiNP coatings at both 1 and 10 mM solution concentrations, the rate of CB attachment slowed but did not level off during the 30 min exposure period. Based on this observation, it was thought that the attachment mechanism occurring under low pH conditions may differ significantly from those occurring at neutral and alkaline pH. The magnitude of the f response to CB under acidic conditions could indicate that uncontrolled surface polymerisation reactions are occurring in place of monolayer self-assembly, resulting in large adsorptions at the coating interface. The mass of covalently bound CB was calculated by fitting the Voigt-based viscoelastic model, accounting for dissipative energy losses due to water associated with highly hydrated polymers. As anticipated from the raw QCM f responses, the mass of adsorbed CB increased with decreasing pH and with increasing concentration (Figure 3.2c). For both 1 and 10 mM functionalisation concentrations, the differences in adsorbed CB across the three pH conditions were all found to be significantly different (one-way ANOVA, $p < 0.05$).

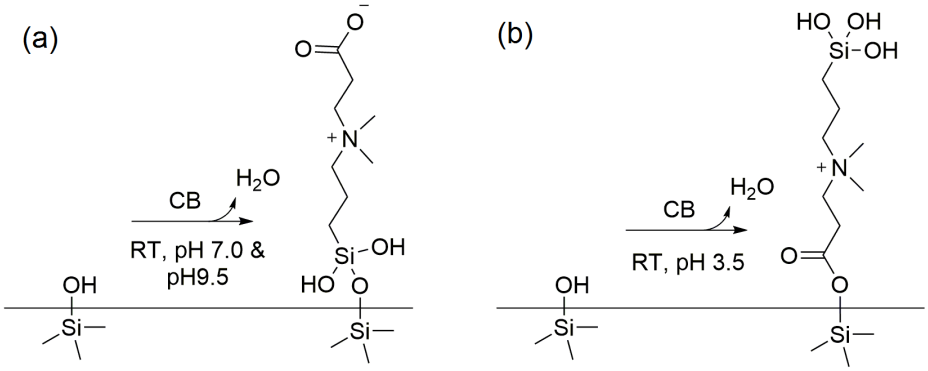

Figure 3.3: Proposed reaction scheme of CB attachment occurring via standard silanol coupling reactions under neutral & basic conditions (a) and CB attachment occurring via reaction of protonated carboxylate groups with free silanol groups on the SiNP surface (b).

Previous reports in the literature have shown that the hydrolysis of alkoxysilanes and the condensation reactions that bind them to surfaces can be facilitated under both high and low pH conditions.[259, 262–264] Most reports agree that hydrolysis and condensation reactions occur rapidly at basic pH, however, high pH conditions can also promote self-condensation in solution, limiting the number of molecules available for surface reaction or causing surface crowding through attachment of oligomers. In this way, the degree of surface functionalisation could be reduced, as was observed for CB mass binding at pH 9.5. While the total mass of CB attachment was significantly less at pH 9.5 than at pH 7.0, the similar f attachment profiles observed in the QCM lead us to believe that CB self-assembly onto the SiNP surface

was occurring via the mechanism proposed in Figure 3.3a.

Acidic conditions have been shown to promote hydrolysis but slow the rate self-condensation reactions,[259] allowing for the organisation of tightly packed and uniform self-assembled monolayers. However, the distinct f attachment profile and large mass adsorption of CB at pH 3.5 indicate that surface reactions under acidic conditions are not forming self-assembled monolayers but instead may be generating a polymeric type network at the sensor surface. It is proposed that at low pH the carboxylate group of CB will become protonated and silane-ester condensation reactions can occur. Similar acid-catalysed ester condensation reactions have been reported by Schmidt et al., where carboxylic acid groups reacted with free silanol groups on a bare silicon oxide surface and unreacted silanol groups of other anchored organosilanes.[292] In this way, functionalisation of the SiNP surface could occur either through standard silanol coupling reaction with the surface or via carboxylic acid reaction with silanol groups on the SiNP surface (Figure 3.3b).

Assuming self-assembly of CB proceeds in this way under acidic conditions, it is anticipated that organisation of an initial monolayer at the SiNP surface would present a random assortment of oppositely orientated CB molecules. This would result in the presentation of two available sites for further reactions. As shown in Figure 3.4, condensation reactions may propagate from either free silanols or from protonated carboxyl groups, leading to uncontrolled polymerisation type reactions and large mass adsorptions at the QCM sensor surface.

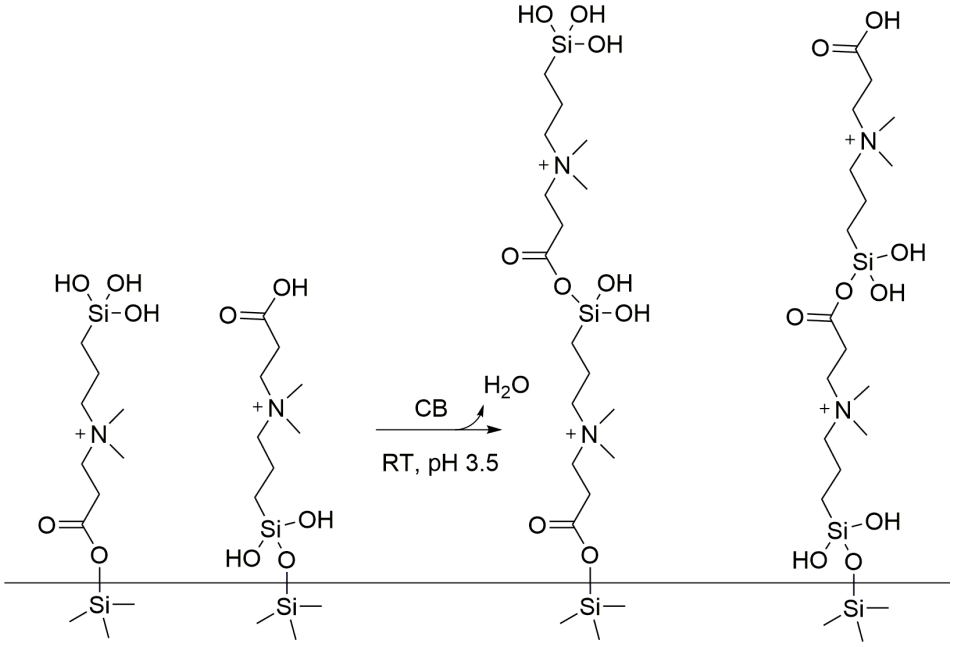

Figure 3.4: Proposed mechanism of uncontrolled polymerisation type reactions propagating from oppositely orientated CB molecules under acidic conditions.

Water contact angles (CA) of the QCM prepared SiNP coatings were measured after functionalisation with CB. Typically SiNP coatings are already very hydrophilic, presenting CA's of ∼10°. Reaction with 10 mM CB at pH 9.5 did not drastically affect the measured contact angle, however, slight increases were observed after reaction with CB at pH 3.5 and 7.0 (Figure A.6). Despite the increased mass binding at pH 3.5 and 7.0, it is thought that the basic nature of the carboxylate group could lead to protonation at these pH conditions, resulting in (partial) loss of zwitterionic character and a subsequent increase in the measured contact angles. This same trend was observed for reaction with CB at 1 mM concentration, however, the increase in CA was not as pronounced (Figure A.7).

3.3.2 Two-Step CB functionalisation of SiNP coatings

An alternate method of generating zwitterionic CB interfaces in the form of a two-step process was also explored. By preparing surfaces in this way, the preparation and storage of the highly hygroscopic CB monomer can be avoided. In this method, SiNP films were first functionalised with the aminosilane (AS) species and then exposed to β-propiolactone (PL) to generate a zwitterionic interface (Figure 3.5d).

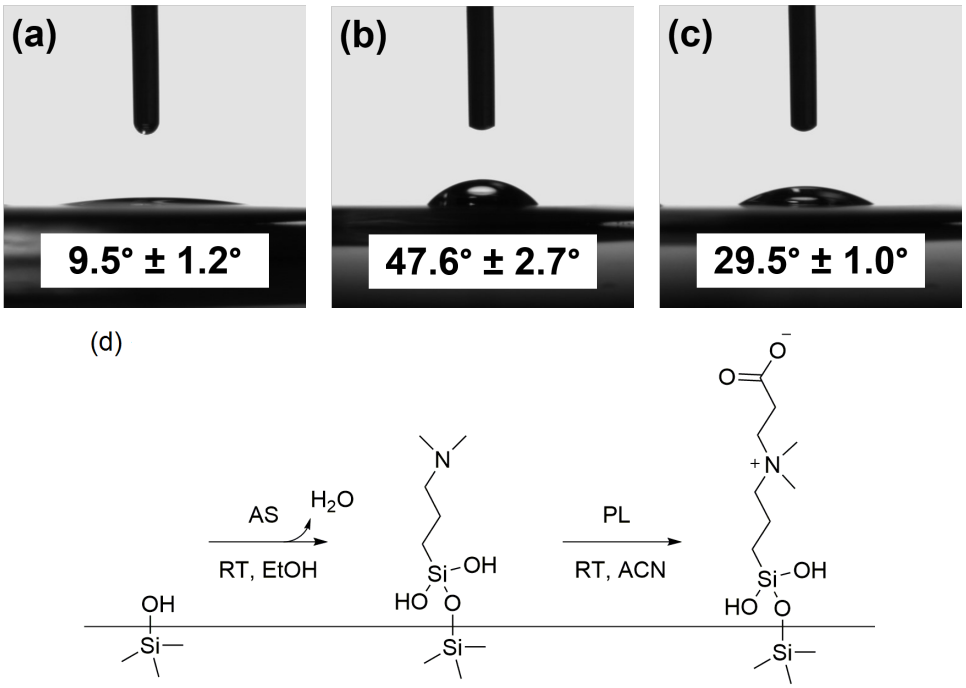

Figure 3.5: Representative images of water contact angles made with the surface of SiNP coatings before functionalisation (a), after reaction with aminosilane (b), and after further reaction with β-propiolactone (c). Insets: Average contact angles measured on the prepared surfaces (± SD). Schematic of two-step surface functionalisation (d).

SiNP coatings were exposed to a solution containing 20 mM (*N,N*-dimethylamino-

propyl)trimethoxysilane in EtOH with 2% addition of H_2O. Previous studies have demonstrated that hydrolysis of amino alkoxysilanes occurs rapidly in EtOH/H_2O mixtures and that increasing temperature enhances the rate of self-condensation reactions.[262, 264] For this reason, substrates were cured briefly after expsoure to AS (120 ℃, 1 h) to enhance stability through promotion of condensation reactions between bound chemistries. After exposing SiNP surfaces to the AS moiety, the measured water contact angle increased from 9.5° to 47.6° indicating successful surface functionalisation (Figure 3.5b). AS-SiNP surfaces were then exposed to a 10 mM solution of β-propiolactone (PL) in acetonitile at 4 ℃, where a nucleophilic ring-opening reaction was anticipated to generate the desired zwitterionic interface. This reaction had to be carried out with the exclusion of water, as PL is highly susceptible to hydrolysis and will generate 3-hydroxypropionic acid. Additionally, PL can polymerise at room temperature and thus the reaction was performed at reduced temperature. Contact angles were measured again after reaction with PL and were found to have decreased to 29.5° (Figure 3.5c). These results were consistent with similar functionalisations presented in the literature,[201] and also comparable to the contact angles measured on the CB modified SiNP surfaces prepared using QCM-D, indicating the successful generation of hydrophilic, zwitterionic functionalised SiNP surfaces.

3.3.3 CB functionalisation of SiNP dispersions

While the two methods of SiNP coating functionalisation presented above offer simple approaches of preparing CB modified surfaces, in some instances it may not be possible to perform a surface based modification after the application of a SiNP film. Under these circumstances it may be advantageous to functionalise nanosilicas prior to their deposition, allowing for single stage coating fabrication. For this reason, the reaction of CB to SiNP dispersions was also investigated and coatings of the functionalised particles prepared for assessment of their protein resistant properties.

Reactions of CB with 10 wt% SiNP dispersions were initially conducted at pH 3.5 and pH 7.0, where pH adjusted solutions of CB were slowly added to particle dispersions. However, addition of CB to SiNPs resulted in rapid and irreversible aggregation of particles. Under these conditions, it is possible that partial protonation of the carboxylate group resulted in loss of zwitterionic character and subsequent attraction of the positively charged quaternary ammonium group to the native negative surface of the silica particles. Additionally, acid-catalysed carboxylic acid and silanol coupling reactions could promote further particle aggregation.

This reaction was retried with the pH of the CB solution and particles adjusted to ∼10 to ensure complete deprotonation of CB and stabilisation of particles. Under

these conditions there was no evidence of particle aggregation upon addition of CB. After reaction, particles were placed in dialysis tubing and dialysed against distilled water to remove any unbound monomer. After several days the particle solution turned cloudy, signaling some degree of particle association. It was observed that the solution pH had fallen to ∼7, however, adjusting the pH to above or below 7 restored the solutions to a clear state, indicating that particle association was a reversible process (Figure 3.6a).

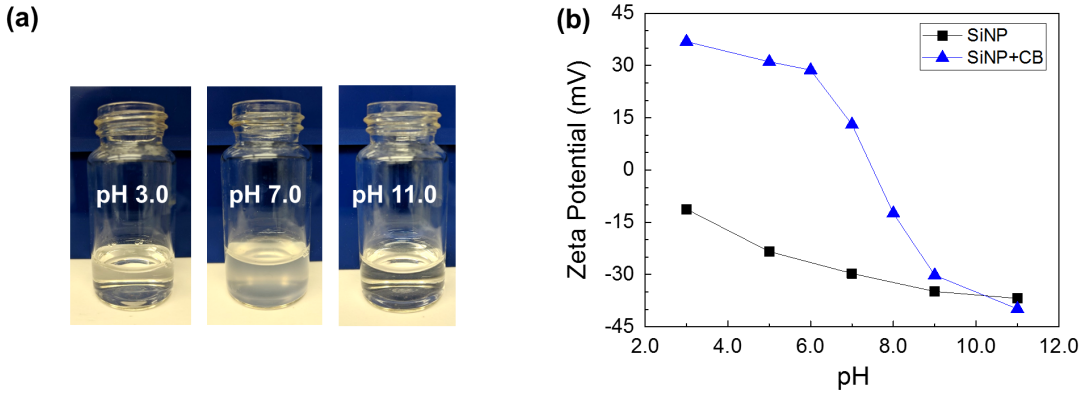

Figure 3.6: Images of CB modified SiNPs at various pH, showing reversible aggregation at neutral pH (a) and ZP measurements of SiNP+CB across pH 3.0 to 11.0 (b).

Zeta potential measurements were conducted on particle dispersions across the pH range of 3.0 to 11.0 (Figure 3.6b). While similar negative ZP values were recorded for both bare SiNP and SiNP+CB at pH $\geq$ 9.0, decreasing pH resulted in a dramatic positive shift in ZP values for SiNP+CB particles. The isoelectric point was estimated to be ∼7.5 and could explain the cloudiness (aggregation behaviour) observed in this pH region. The switch to a positive potential was attributed to carboxylate protonation of CB and the resultant presentation of cationic quaternary ammonium groups.

In addition to ZP measurement, the hydrodynamic diameter of particles was measured before and after functionalisation with CB. As presented in Figure 3.7a, CB functionalisation resulted in an increase in hydrated particle size from 18.3 nm to 39.5 nm. This may be partially attributed to the CB chemistry itself and its associated hydration, although the measured increase in particle size was roughly double that of bare particles and may indicate a degree of particle association.

Particles were collected via freeze-drying for FTIR and TGA analysis. The IR spectrum of functionalised particles (SiNP+CB) was compared to the spectra of unreacted SiNPs and CB (Figure A.8). The CB monomer presented a strong band at 1585 cm^{-1}, characteristic of the asymmetric stretching vibration of carboxylic acid salts (CO_2^-)[282] and the small peak at 1485 cm^{-1} was assigned to methyl

stretching vibrations of the quaternary ammonium group.[203] The IR spectrum of unmodified SiNPs was relatively featureless, presenting characteristic Si-O-Si stretch as a broad peak centered at 1060 cm^{-1} and another broad peak at 800 cm^{-1} attributed to Si-OH deformation vibrations.[282] Functionalisation of particles with CB (SiNP+CB) resulted in a broadening of the Si-O-Si band and shifted the predominant peak to 1095 cm^{-1} due to overlap from Si-O-C stretching vibrations.

Thermogravimetric analysis of SiNP+CB by gradual heating of dried particles brought about the decomposition of the CB moiety at temperatures above 200 ℃ (Figure 3.7b). From the mass loss observed, the CB grafting density was calculated to be 0.92 μmol/m^2 . This value was comparable to the grafting density achieved from SB particle functionalisation (as presented in Chapter 2). The use of small SiNPs and the choice to conduct reactions at basic pH may have resulted in a limited degree of particle reaction, as small particles require large silane additions due to their high surface area and basic pH conditions promote self-condensation reactions which may limit silane availability for reaction to particles.

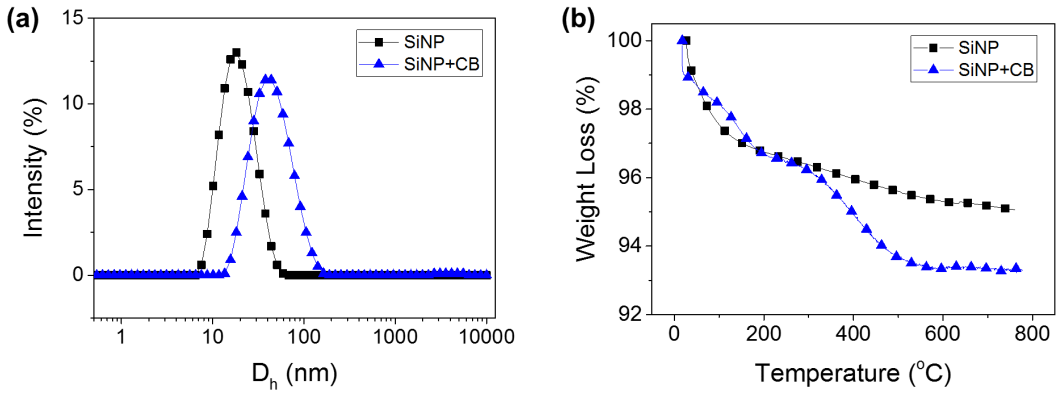

Figure 3.7: Hydrodynamic diameter of particles as measured by DLS (a) and TGA of bare and CB functionalised SiNPs (b).

Coatings of SiNP+CB were prepared from 4 wt% particle dispersions, where the dispersion pH was adjusted to 3 or 10 prior to coating deposition. Spin-coating solutions onto PEI coated QCM sensors produced thin, uniform coatings with average contact angles of 22° and 15° for coatings prepared at pH 3 and 10, respectively. The slight increase in CA for coatings prepared at pH 3 was again thought to arise from protonation of the carboxylate group and subsequent loss of zwitterionic character.

3.3.4 Protein Adsorption

Protein adsorption measurements were conducted using QCM-D to compare relative protein binding to the CB functionalised SiNP surfaces. Figure 3.8 presents the calculated mass of BSA bound to surface functionalised SiNP coatings prepared

by exposure to 1 and 10 mM solutions of CB at pH 3.5, 7.0, and 9.5. All CB modified surfaces presented significant reductions in BSA adsorption compared to the unmodified SiNP control surface (one-way ANOVA, $p < 0.05$). Furthermore, increasing functionalisation concentration from 1 to 10 mM brought about further reductions in BSA binding, particularly for pH 7.0 modified surfaces. The improved protein resistance observed under this functionalisation conditions (10 mM CB, pH 7.0) was thought to be the result of increased mass of self-assembled zwitterionic monomer on the SiNP coating surface. Comparatively, SiNP coatings functionalised with CB at pH 9.5 did not experience any dramatic improvement to protein resistance when functionalisation concentration was increased from 1 to 10 mM, as the mass of covalently bound CB was comparable under both concentration conditions (Figure 3.2c). While the protonation of CB under acidic conditions might be expected to reduce resistance to protein binding due to loss of zwitterionic character, the pH 3.5 functionalised SiNP surfaces still presented exceptional resistance to protein adsorption. It is proposed that the acid-catalysed polymerisation reactions that lead to increased mass binding at the SiNP surface also contributed to increased steric bulk at the coating interface, where compression of hydrated polymer chains brings about a steric repulsion effect, preventing the interaction and adsorption of proteins.[164, 166]

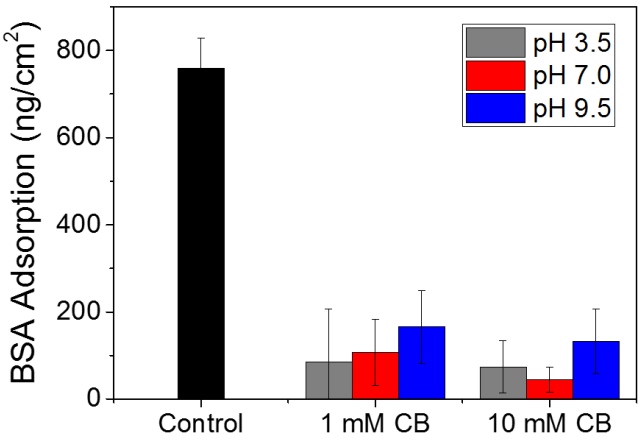

Figure 3.8: Mass of BSA adsorption onto CB functionalised SiNP coatings with varied concentration and pH. Mass calculated from modelling 3^{rd}, 5^{th}, and 7^{th} overtone f and D responses within the QCM-D. Error bars represent 95% CIs (n=3).

Similar protein adsorption measurements were conducted on CB modified SiNP coatings prepared via two-step surface functionalisation (AS+PL) and from solution modified silica nanoparticles (SiNP+CB) (Figure 3.9). In the case of the latter, 4 wt% dispersions of SiNP+CB were adjusted to pH 3 and pH 10 prior to their deposition

onto gold QCM sensors to compare the effect of dispersion pH on the protein resistant properties of the resultant coatings. Significant reductions in protein binding were observed across these three CB modified SiNP surfaces compared to the unmodified SiNP control surface (one-way ANOVA, $p < 0.05$). Most notably, increasing the pH of the SiNP+CB particle solution to pH 10 prior to coating preparation resulted in significantly improved resistance to protein binding compared to the pH 3 stabilised SiNP+CB coating. This result was attributed to the complete deprotonation of CB groups and enhanced zwitterionic character under alkaline conditions.

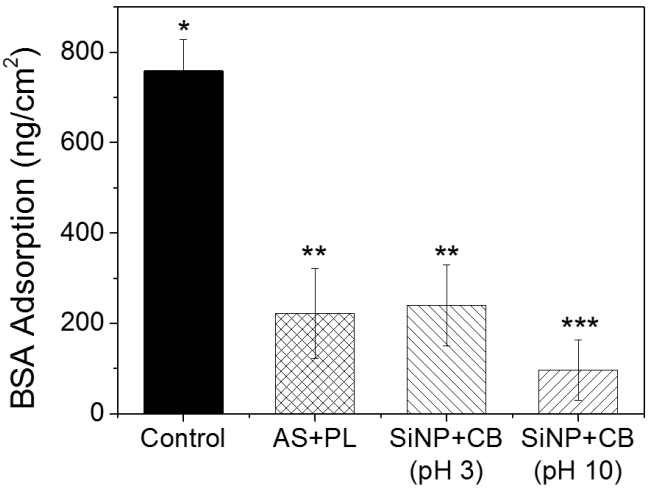

Figure 3.9: Mass of BSA adsorption onto two-step CB functionalised SiNP coatings (AS+PL) and coatings of solution modified particles (SiNP+CB) deposited at pH 3 and pH 10. Mass calculated from modelling 3^{rd}, 5^{th}, and 7^{th} overtone f and D responses within the QCM-D. Error bars represent 95% CIs (n=3).

3.4 Conclusions

This study has demonstrated multiple methods of preparing hydrophilic, zwitterion functionalised SiNP coatings. Attachment of CB to silica nanoparticle surfaces was monitored using QCM-D, where variation of zwitterion concentration and solution pH was found to influence the mass of covalent attachment and the mechanism of zwitterion organisation. A non-aqueous route of zwitterion functionalisation was also employed for the preparation of CB modified SiNPs via a two-step surface modification process. Finally, CB functionalised particles were prepared as aqueous dispersions for simple deposition as thin coatings. The slightly basic nature of the CB chemistry meant that the surface charge of modified SiNP coatings could be tuned with variation of pH and thus influence the protein resistant properties of the prepared surfaces.

All methods of preparing CB functionalised SiNP films resulted in hydrophilic surfaces that presented enhanced resistance to protein adsorption. Despite loss of zwitterionic character, surface modification under acidic conditions promoted polymeric growth of CB, resulting in enhanced steric bulk at the interface and good protein resistance. Increasing the concentration of the CB functionalisation solutions did result in increased CB attachment across the pH range studied but did not yield significant improvements to protein resistance. This finding contrasts with the results presented in Chapter 2, where the protein resistant properties of SB functionalised SiNP coatings were dependent upon the concentration of the functionalisation solution (i.e. functionalisation at higher concentrations improved protein resistance). Despite the much larger QCM-D f shifts observed for CB functionalisation of SiNP surfaces, SB functionalised coatings were able to provide superior protein resistance when prepared at the higher functionalisation concentration (10 mM). This comparison highlights the importance of monomer organisation at the coating interface, where a lower mass but highly organised self-assembled layer of zwitterionic SB demonstrated improved resistance to protein binding over a higher mass, oligomeric CB layer.

Having established that reaction of SiNP's with zwitterionic SB could produce more controlled monomer assembly and improved protein resistance than CB functionalised SiNP's, it was decided that further antifouling assessment of CB modified SiNP coatings would not be conducted. Additionally, several difficulties were encountered in the synthesis and handling of the CB species (i.e. harmful precursors and extreme hygroscopicity), contributing to the decision to not pursue further antifouling assessment with bacterial and fungal species. Finally, it was thought that the toxicity and moisture sensitivity of these materials would make them unsuitable for most industrial applications and thus further investigations of zwitterion functionalised silica nanoparticles were carried using the SB chemistry investigated in Chapter 2.

Chapter 4

Zwitterion Functionalised Silica Nanoparticle Coatings: The Effect of Particle Size

This Chapter has been adapted from the article "Zwitterion Functionalized Silica Nanoparticle Coatings: The Effect of Particle Size on Protein, Bacteria, and Fungal Spore Adhesion", *Langmuir*, 2018, doi:10.1021/acs.langmuir.8b01550. This article is part of the Zwitterionic Interfaces: Concepts and Emerging Applications special issue.

The exceptional fouling resistance of zwitterionic nanoparticle coatings, as described in Chapters 2 and 3, naturally led to further optimisation of silica nanoparticle coating properties. As surface roughness is known to mediate microbial adhesion, this Chapter explored modulating coating roughness through the deposition of differently sized silica nanoparticles, in combination with zwitterionic functionalisation for enhanced antifouling performance.

4.1 Introduction

As highlighted in Chapter 1, traditional approaches to preventing the biological fouling of surfaces have relied on coatings that contain or release biocides such as metal derivatives,[83, 107] poly(ammonium compounds)[127–129] and antibiotics.[67, 68] While generally effective, these types of coatings often suffer from reduced efficiencies over time, and the release of toxic compounds can have detrimental impacts to nontarget organisms and more generally, the environment.[48, 293] As a result, new strategies for reducing surface fouling have shifted away from incorporation of toxic biocides toward more environmentally benign antifouling coatings, that is, coatings that can minimise and prevent microbial interactions and adhesion.

Modulation of surface topography and optimisation of coating surface energy are among strategies that have been used to limit microbial adhesion and successfully reduce biological fouling.[135, 149] Low surface energy hydrophobic coatings often present water-repellent and self-cleaning properties, with a minimum bioadhesion achieved when surface energies fall in the range of 20–30 mJ/m^2, as described by Baier.[134] Furthermore, coating roughness is known to influence the adhesion strength of microorganisms with topography playing a role in the contactable area available for organisms to adhere. Coatings that present intricate, micro- and nanoscale topographical features of similar size to the fouling species of interest have been shown to limit interactions and reduce binding strength.[151, 152, 294] While coatings with highly structured topographical features have been demonstrated to effectively reduce adhesion of organisms, these coatings are rarely reproducible or robust enough to be produced on a large scale.

It is postulated that combining the antiadhesive properties of hydrophilic materials with control over nanotopographies within a coating, could enhance reduction in fouling across a broader range of fouling species. This Chapter is devoted to investigating the antifouling behaviour of coatings prepared from silica nanoparticles (SiNPs) of various sizes in combination with hydrophilic zwitterionic chemistries. The roughness and surface area of the SiNPs coatings were found to be easily tuned through variation in particle size, while the SiNPs themselves are naturally hydrophilic and provide a reactive surface for the tethering of hydrophilic chemistries. In Chapter 2, it was demonstrated that coatings of zwitterion modified 12 nm SiNPs presented excellent antifouling properties. Varying SiNP size was not only anticipated to change the coating morphology but also influence chemistry organisation and grafting density on the nanoparticle surface, as demonstrated in previous studies.[295–297] The optimal reaction conditions determined from previous chapters were employed to functionalise SiNPs ranging from 7 to 75 nm with zwitterionic sulfobetaine and coatings of SiNPs were prepared via a simple spin-coating process. The effect of particle size on the coatings' antifouling properties was investigated by comparing protein adsorption, bacterial adhesion, and fungal spore binding to coatings prepared from differently sized particles.

4.2 Experimental

4.2.1 Materials

Ludox® HS-40 colloidal silica (12 nm diameter), phosphate buffered saline (PBS, P5368), (*N,N*-dimethylaminopropyl)trimethoxysilane (539287), 1,3-propane sultone (P50706), poly(ethylenimine) solution (PEI, P3143), bovine serum albumin (BSA,

A3059), hydrophobin SC3 (68795), and acetone (270725) were purchased from Sigma-Aldrich. Bindzil® 30/360 (7 nm diameter), Levasil® CT13M (22 nm diameter), Levasil® CT8PL (30 nm diameter), and Levasil® 30/50 (75 nm diameter) colloidal silica dispersions were supplied by AkzoNobel. Acetone was dried with 3 Å molecular sieves and distilled before use. All other reagents purchased from commercial suppliers were used without further purification. Water used in experiments and to prepare aqueous solutions was purified using a Millipore water purification system with a minimum resistivity of 18.2 MΩ.cm at 25 ℃.

4.2.2 Synthesis of Zwitterionic SB

SB was synthesised following the method described in Section 2.2.2.

4.2.3 Reaction of SB to SiNPs

Reaction of SB to SiNPs of different diameters was performed following the procedure described by Estephan et al.[232] The appropriate amount of SB monomer for reaction to each of the different particle sizes was calculated based on the surface area reported by the manufacturer and 4.9 silanol groups per nm^2 of silica surface.[253] SB was dissolved in H_2O and the pH adjusted to 9.5 prior to dropwise addition to stirred nanoparticle solutions. Particle solutions were diluted to a final concentration of 10 wt%. Reaction mixtures were stirred for 2 h at RT and then then transferred to 12 K molecular weight cutoff dialysis membrane and dialysed against pure water.

4.2.4 Preparation of SiNP Coatings

SiNP coatings were prepared onto gold coated coverslips and onto A-T cut QCM sensors with a 10 mm diameter gold electrode and a fundamental resonance frequency of 5 MHz. Prior to coating, the gold surface of each sensor was cleaned with piranha solution (7:3 v/v mixture of H_2SO_4 (98%) and H_2O_2 (33%)) for 3 min, rinsed with deionised water and dried in a stream of nitrogen gas. Cleaned surfaces were then incubated in 0.5% poly(ethylenimine) (PEI) solution for 10 min at RT to form an adhesive layer. PEI was thoroughly rinsed from the surfaces with deionised water and surfaces were dried in a stream of nitrogen gas. SiNP solutions were prepared as 4 wt% dispersions in water for spin-coating. Coverslips and sensors were mounted into the spin-coater and particle films were prepared by depositing 20–50 μL of the 4 wt% dispersions onto their surface and spin-coating at 5000 rpm for 30 s. Coatings were cured for 1 h at 120 ℃ and thereafter thoroughly rinsed with deionised water and dried in a stream of nitrogen gas.

4.2.5 Characterisation

4.2.5.1 Dynamic Light Scattering/Zeta Potential

Z-Average particle size (hydrodynamic particle diameter) measured by dynamic light scattering (DLS) and zeta potential (ZP) measurements were performed on a Malvern Zetasizer Nano-ZS at 25 ℃ (colloidal silica refractive index: 1.40, absorption: 0.010, measurement angle: 173°). ZP measurements were performed on 0.5 wt% aqueous particle dispersions, pH adjusted with HCl and NaOH. DLS measurements were carried out on 0.5 wt% particle solutions dispersed in 10 mM NaCl.

4.2.5.2 Thermogravimetric Analysis

TGA (TA, Q500) was performed on freeze-dried nanoparticles. Briefly, dried particles were heated from RT to 800 ℃ at a heating rate of 10 ℃/min under a nitrogen atmosphere. The mass of polymer bound to the particle surface was calculated from mass losses observed above 150 ℃. The mass retained at 800 ℃ after polymer decomposition was considered to be the mass of bare particles and was used to calculate grafting density.

4.2.5.3 Contact Angle Goniometry

Contact angle measurements were acquired using a Dataphysics Contact Angle System (OCA 15EC) in conjunction with SCA20 software. The mean static contact angle made by a 2 μL sessile water droplet in contact with the particle coatings was measured. A minimum of three measurements were obtained for triplicate samples of each particle coatings.

4.2.5.4 Atomic Force Microscopy

The surface morphology of silica nanoparticle coatings were examined using a Parks System AFM, operating in tapping mode with a Mikromash NSC15 cantilever (spring constant ~37 N/m). Image scans of 2 μm × 2 μm and 5 μm × 5 μm were obtained at a scan rate of 1 Hz in air. Surface area and coating roughness were calculated using Gwyddion v.2.4.8. software.

4.2.5.5 Scanning Electron Microscopy

Images of the particle coatings were acquired using a field emission scanning electron microscope (SEM, JEOL JSM-7500FA) in secondary electron imaging mode. Images were obtained without further modification of the particle coating surface.

4.2.6 Antifouling Assessment

4.2.6.1 Protein Adsorption

Adsorption of protein onto the SiNP coatings was quantified using a Q-Sense E4 QCM-D (Q-Sense AB Västra, Frölunda, Sweden) coupled with an ISMATEC IPC High Precision Multichannel Dispenser (IDEX, Wertheim, Germany) in a flow-through setup. Coatings were prepared onto QCM sensors as described above. First, SiNP coated sensors were placed into standard Q-Sense flow modules (QFM 401) and equilibrated in PBS at a constant temperature of 22.00 ± 0.02 ℃ until the baseline signals stabilised. Bovine serum albumin (BSA) or hydrophobin solutions at concentrations of 1 mg/mL and 10 μg/mL, respectively, were introduced into the QCM chamber at a constant flow rate of 60 μL/min. After 30 min, PBS was reintroduced to rinse the coatings and remove any loosely bound proteins. The mass of adsorbed protein was calculated by applying the Voigt model using Q-Sense QTools analysis software v3.0.10.286 (Biolin Sci, AB). All experiments were run in triplicate. The following input parameters provided the best fit for the layer density (1150 kg/m^3), fluid density (1020 kg/m^3), layer viscosity ($10^{-6} \leq 10^{-2}$ kg/ms), layer shear modulus ($10^4 \leq 10^8$ Pa) and mass (1.15 $\leq$ 1.155 ng/cm^2). The 3^{rd}, 5^{th}, and 7^{th} overtones were used for modelling calculations.

4.2.6.2 Bacterial Adhesion Study

Bacterial solutions were prepared from a precultured JM109 strain of *Escherichia coli* and inoculated overnight in 10 mL of sterile LB (Luria-Bertani) medium at 37 ℃ in a Bioline incubator shaker 8500 (Edwards Instrument Co., Narellan, Australia). Inoculated culture (0.5 mL) was added to 10 mL of LB medium and optical density measurements carried out every 30 min using a Spectronic 200 (Thermo Scientific, Waltham, MA, U.S.A.) until the desired turbidity was achieved (OD_{600} 0.6–1.0). The number of colony forming units (CFU) in the bacterial suspension was determined by plating out dilutions of the suspension and was found to be 6.3 × 10^6 CFU/mL. Coverslips coated with SiNPs were first sterilised by briefly immersing them in EtOH (2 sec) and then placed into individual wells of sterile 12-well culture plates. Two mL of PBS with bacterial cells were added to each well, and culture plates were incubated at 37 ℃ for either 2 h or 24 h time periods. Coverslips were then removed from incubation, immersed in PBS with agitation (6×), rinsed with 2 mL PBS, and placed into fresh sterile 12-well culture plates. Bacteria were fixed onto coverslips and stained by applying 1 mL of 20 μg/mL Hoechst 33342 (Invetrogen - Life Technologies (Thermo Scientific)) in a 2.5 wt% glutaraldehyde solution. Stained bacteria were imaged using a Zeiss AxioImager A1M with an open HBO 100 mercury lamp and an

Axiocam MRm camera (Carl Zeiss, Oberkochen, Germany). Images were obtained at 10× magnification with bacterial counts determined using ImageJ® software (v.1.50b).

4.2.6.3 Fungal Spore Adhesion Study

Adhesion of *Epicoccum nigrum* (ATCC 42773) fungus to SiNP coatings was evaluated. *E. nigrum* spores were collected from a precultured agar plate (potato dextrose agar (BD 213400)) and dispersed in 7 mL of sterile water. The spore suspension was shaken vigorously and placed on an orbital shaker for 2 h. The suspension was then centrifuged for 5 min at 1500 rpm. The supernatant was removed, and spores were resuspended in 7 mL of sterile water. The spore suspension was then filtered through a 40 μm hollander weave mesh to ensure good spore separation and diluted ∼10-fold. Spin-coated nanoparticle coatings were placed into a sterile Greiner 12-well cell culture plate and covered with 1 mL sterile deionised water. An aliquot of spore suspension was then deposited onto coatings to give a concentration of 2×10^4 spores per cm^2 and samples were incubated at 30 ℃ for 24 h. Samples were removed from the incubator after 24 h and each coverslip was immersed in sterile water (3×) with gentle agitation and then was washed (3×) with sterile water. Spores were fixed with 2.5% (v/v) glutaraldehyde solution. Fixed spores were imaged at 5× magnification using a Zeiss Axiovert inverted microscope. Areas imaged were chosen randomly and spores counted using ImageJ® software (v.1.50b). A minimum of five images were obtained for each sample surface and each surface was sampled in triplicate with the total average reported.

4.2.7 Statistical Analysis

Results were analysed using one-way analysis of variance (ANOVA) with Tukey post hoc test. Probabilities of $p < 0.05$ were considered to be significantly different. All statistical analyses were performed using IBM SPSS Statistics 21 software.

4.3 Results and Discussion

4.3.1 Particle Functionalisation and Characterisation

For this work, five different SiNPs from commercial suppliers were selected, ranging from 7 to 75 nm in diameter. All particles were negatively charged, stabilised by a sodium or ammonium counterion, and supplied from the manufacturer in the pH range of 9.1–10.1 (Table 4.1). Although solutions containing particles in the range

of 7–22 nm were transparent, dispersions of 30 and 75 nm particles were opaque (Figure A.9).

Table 4.1: Summary of silica nanoparticle properties as specified by the manufacturer.

Commercial name	Concentration (wt%)	Particle size (nm)	Surface Area (m^2/g)	pH	Stabilising counterion
Bindzil 30/360	30	7	360	10.1	Na^+/NH_4^+
Ludox HS-40	40	12	220	9.8	Na^+/NH_4^+
Levasil CT13M	30	22	130	9.1	Na^+/NH_4^+
Levasil CT8PL	30	30	85	10.0	Na^+/NH_4^+
Levasil 30/50	30	75	35	9.5	Na^+/NH_4^+

SiNP dispersions were diluted to 10 wt% prior to reaction with zwitterionic SB. SB was dissolved in water and then pH adjusted to 9.5 to promote hydrolysis of the methoxy substituents. The addition of SB to the SiNP dispersions resulted in silanol condensation reactions and covalent binding of SB to the SiNP. No visual changes to the solutions upon reaction were observed. After the reaction, the unbound monomer was removed via dialysis. To ensure particles remained stable after the reaction procedure, the particle size was examined before and after functionalisation using DLS (Table 4.2). It was observed that the hydrodynamic diameter (D_h) of all particles were larger than the nominal particle size indicated by the manufacturer, as this technique also accounts for the hydration sphere of the solvated particles (Figure 4.1f). Polydispersity measurements revealed that the 22 and 75 nm particles were monodisperse and the 7, 12, and 30 nm particles had larger size distributions. Variation in particle size was particularly apparent for the 30 nm particles, as visualised by scanning electron microscopy of the 30 nm particle coating (Figure 4.1d).

Table 4.2: Hydrodynamic diameter and polydispersity index of particle solutions before and after modification with SB as measured by DLS.

	SiNP		SiNP+SB	
Nominal Size	**D_h (nm)**	**PDI**	**D_h (nm)**	**PDI**
7 nm	22.2 ± 0.2	0.124	22.2 ± 0.5	0.158
12 nm	21.8 ± 0.1	0.129	24.6 ± 0.3	0.119
22 nm	32.1 ± 0.3	0.025	32.2 ± 0.2	0.033
30 nm	81.6 ± 0.7	0.145	80.9 ± 1.6	0.137
75 nm	100.7 ± 0.7	0.019	101.3 ± 1.7	0.015

After functionalisation, very little to no change in particle size was observed. This

is likely due to the small size of the SB monomer (∼1.2 nm) and the particles already presenting a high degree of solvation prior to functionalisation. This result confirmed that no particle aggregation occurred during functionalisation and that particle dispersions were stable and well dispersed. The degree of particle functionalisation (grafting density) was quantified using TGA (Figure A.10). Mass losses above 150 ℃ were attributed to SB decomposition (mass losses at lower temperatures are likely from adsorbed water). Percentage mass losses were found to increase with decreasing particle size due to smaller particles presenting higher surface areas (Table 4.3). However, calculation of surface coverage, factoring in surface area and theoretical number of silanol groups available for reaction (8.14 μmol/m^2 or 4.90 molecules/nm^2),[253] revealed that the larger particles (in fact) presented the highest degree of particle functionalisation.

Table 4.3: Surface coverage of SB modification calculated from mass loss observed during thermogravimetric analysis.

			Surface Coverage	
Particle Size	**Surface Area (m^2/g)**	**Mass Loss (%)**	**μmol/m^2**	**molecules/nm^2**
7 nm	360	5.79	0.63	0.38
12 nm	220	5.69	0.99	0.60
22 nm	130	4.31	1.24	0.75
30 nm	85	3.31	1.45	0.87
75 nm	35	1.14	1.16	0.70

For all particle modifications, the quantity of SB added was equivalent to theoretical saturation of all available silanol sites on the particle surfaces. However, only 8–18% of sites were calculated to have been functionalised. This result is consistent with previous studies where maximum silanol functionalisations of ∼25% have been achieved.[232, 233] Despite the larger surface area presented by smaller SiNPs, the 7 and 12 nm particles experienced the lowest degree of functionalisation. As all functionalisation reactions were carried out at particle concentrations of 10 wt%, the relative amount of silane addition increased dramatically with decreasing particle size. This increase in silane concentration in combination with alkaline conditions which favour rapid hydrolysis and condensation reactions was thought to promote self-condensation reactions and oligomer formation, thus reducing the amount of silane available to react to the particle surface.[298] Additionally, the number of silanol groups per unit area of silica is proposed to decrease with decreasing particle size due to incomplete or retarded formation of silanol groups at the surface of smaller silica nanoparticles.[252] This could lead to an underestimation of the total possible degree of particle functionalisation for the smaller SiNPs.

The surface charge of SiNPs was characterised by measuring the zeta potential (ZP) of particle dispersions across the pH range of 3.0–11.0 (Figure A.11, A.12). Overall, particle dispersions presented negative ZP values due to the presence of deprotonated silanol groups. Decreasing pH had the effect of increasing the ZPs as a higher proportion of surface groups became protonated. The larger 30 and 75 nm particles presented slightly more negative overall ZPs. This result is consistent with previous reports where larger particles have demonstrated increased acidity due to a higher fraction of vicinal silanol groups and a higher proportion of ionised silanol groups.[299] Functionalisation of SiNPs with SB did not drastically alter the ZP profile across the pH range studied. Slightly higher ZPs were recorded with SB modification due to occupation of some silanol/siloxide sites, however the overall surface charge remained largely unchanged.

4.3.2 Coating Preparation and Characterisation

Particle coatings were prepared via a simple spin-coating process. Particle dispersions were diluted to 4 wt%, deposited onto PEI coated gold QCM sensors and gold-coated glass coverslips, and spun at 5000 rpm for a period of 30 s. SEM images revealed that spin-coating produced homogeneous particle coatings from a single deposition of particle dispersions for the 7, 12, and 22 nm particle sizes (Figure 4.1a-c). A second layer of spin-coated particles was required to ensure complete surface coverage of the larger 30 and 75 nm particles (Figure 4.1d-e).

Surface energy and roughness are two factors known to influence the wettability of surfaces. Additionally, these parameters can have a pronounced effect on the antifouling behaviour presented by an interface. For this reason, SiNP coating wettability was investigated by measuring surface water contact angles, and coating roughness was probed using AFM. We observed that control (unmodified) particle coatings all presented low static water contact angles ($< 15°$), indicating hydrophilic properties at the coating interface (Table 4.4). While substrates presenting similar surface chemistry, such as glass, require UV/O_3 or plasma cleaning to generate increased surface hydrophilicity,[300] these SiNP coatings presented exceptional hydrophilicity without exposure to any form of surface treatment. SiNP surface chemistry is expected to play a role here with particles presenting an abundance of protonated (Si-OH) and/or deprotonated (Si-O^-) silanol groups available to interact with water through hydrogen bonding or ionic solvation, respectively.[260] In addition to the surface chemistry presented by the SiNP coatings, it is also anticipated that the nanoscaled surface topography would further enhance surface hydrophilicity, as described by the Cassie-Baxter equation.[137]

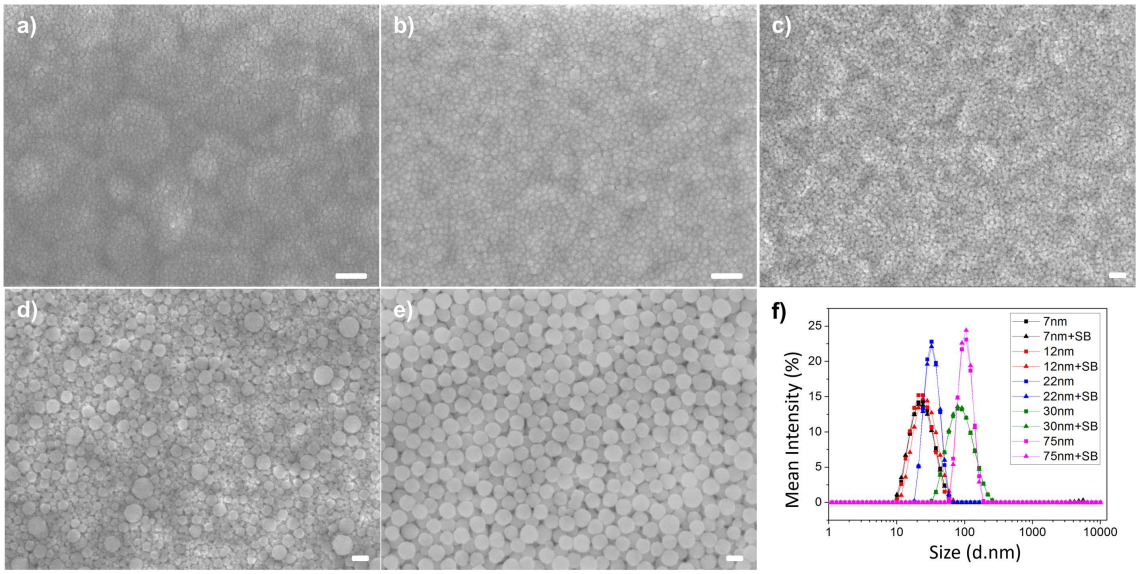

Figure 4.1: Scanning electron microscope images of SB modified SiNP coatings of particle size: 7 (a), 12 (b), 22 (c), 30 (d), and 75 nm (e) (scale bars are 100 nm), and hydrodynamic diameter of particles before and after modification using DLS (f).

Coatings prepared from zwitterion modified particles (SiNP+SB) presented a higher degree of hydrophilicity than their unmodified coating controls. For all SB modified SiNP coatings, contact angles were reduced to $< 8°$, indicating zwitterion chemical addition had a stronger influence on coating hydrophilicity than the SiNP size. This result was anticipated, as the strong hydration capacity of zwitterionic polymers is well documented,[207, 301] and the change in coating contact angles (on addition of SB) was small due to the inherent hydrophilicity of the SiNPs.

Table 4.4: Roughness (R_q) and surface area of SB modified SiNP coatings as calculated from 5 μm $\times$ 5 μm AFM scans. Contact angles of control (unmodified) and SB modified SiNP coatings ($\pm$ 95% CI).

	Surface Properties		Contact Angle (°)	
Particle Size	**R_q (nm)**	**Surface Area (μm^2)**	**SiNP**	**SiNP+SB**
7 nm	2.82 $\pm$ 0.56	25.09 $\pm$ 0.02	7.8 $\pm$ 2.9	7.6 $\pm$ 1.4
12 nm	3.18 $\pm$ 0.22	25.20 $\pm$ 0.03	9.0 $\pm$ 2.6	7.0 $\pm$ 1.3
22 nm	3.04 $\pm$ 0.31	25.20 $\pm$ 0.05	14.8 $\pm$ 3.5	6.5 $\pm$ 0.5
30 nm	19.34 $\pm$ 1.16	28.52 $\pm$ 0.72	10.0 $\pm$ 3.3	5.8 $\pm$ 2.1
75 nm	17.80 $\pm$ 1.11	28.58 $\pm$ 0.81	11.2 $\pm$ 1.1	7.5 $\pm$ 1.2

In addition to surface wettability, the effect of particle size on coating roughness was also of interest. AFM scans revealed that the SiNP coatings presented nanoscaled surface features and a size dependent variation in coating roughness (Table 4.4).

Image scans (5 μm $\times$ 5 μm) of 7, 12, and 22 nm particle coatings displayed very small increases in contactable surface area and nanometre root-mean-square surface roughness (R_q). A much larger increase in both surface area and R_q roughness were observed for the larger 30 and 75 nm particle coatings. The 30 nm SiNP coating was found to present the highest surface roughness due to this particle's larger size distribution, as observed from SEM imaging and DLS/PDI measurements (Figure 4.1d, f).

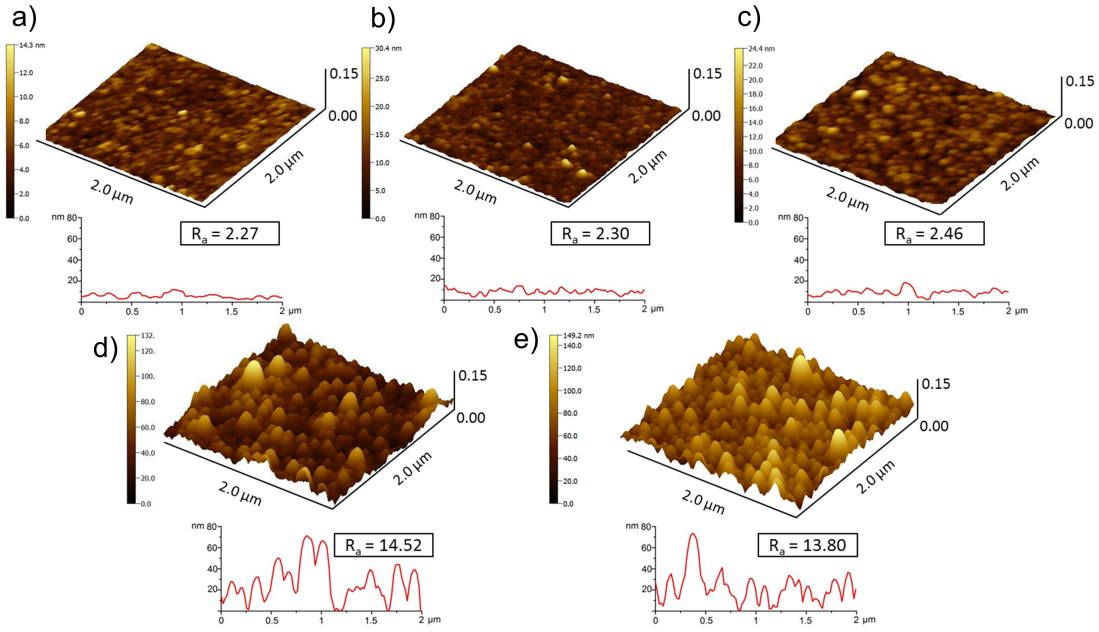

Figure 4.2: The 3D AFM scans (2 μm $\times$ 2 μm) and cross-sectional profile of SB modified SiNP coatings of particle diameter: 7 (a), 12 (b), 22 (c), 30 (d), and 75 nm (e).

While R_q measurements provide an insight into overall coating roughness, they are not a good indicator of true surface topography as they do not account for variation in lateral roughness and profile skewness.[302] Differences in SiNP coating morphology are more easily observed in the three-dimensional (3D) AFM scans presented in Figure 4.2. The R_a values presented are again similar for the three smaller particle coating scans (2 μm $\times$ 2 μm), however, differences in the height and spacing of features are much more pronounced. Cross-sectional coating profiles further illuminate the dramatic change in dimension of surface features with increasing particle size. Although the topographic features generated from the deposition of SiNPs are random, the overall scale and arrangement of surface features appears fairly consistent for each particle size. This highlights the ease with which we can very simply prepare and tune the nanoscaled surface topography presented at an interface.

4.3.3 Antifouling Assessment

Despite immense interest in the field of scaled topographies for fouling prevention, relatively few studies have explored engineered topography on the nanoscale. Most work presented in the literature has focused on the generation of surface topographies with similar dimensions to the fouling species of interest, as this has been demonstrated to drastically influence adhesion.[152, 222, 303] However, while organisms such as bacteria have dimensions in the micrometre size range, their surface appendages and adhesive structures are in the nanometre range.[304] This highlights the need for control of surface topography at both the nano- and microscale for effective prevention of biological fouling.

Recent advances in the generation of nanoscale surface features using lithographic or chemical patterning techniques (see Anselme et al. for review)[302] have allowed for the fabrication of intricately patterned substrates with high degrees of spatial resolution. However, there is often a trade-off between the expense, resolution, and time taken to prepare surfaces depending on the choice of patterning technique. In this work, the preparation of coatings through the deposition of differently sized SiNPs has allowed for the simple fabrication of nanoscaled interfacial patterning. We have examined the effect of nanoscaled features on adsorption and adhesion of fouling species with dimensions ranging over several orders of magnitude.

4.3.3.1 Protein Adsorption

Protein adsorption is a key process in the formation of biofilms as bacteria and cellular interactions with a substrate are mediated by the presence of a surface conditioning film, comprised of adsorbed proteins, glycoproteins, and polysaccharides.[133, 302] Therefore, by understanding protein interactions with surfaces, we can further elucidate the effect of nanoscale surface topography on fouling processes. The binding of BSA and hydrophobin proteins to unmodified and SB modified SiNP coatings were investigated using QCM-D. BSA is a globular protein (66 kDa, $\sim$14 $\times$ 4 nm) commonly used as a model protein in fouling studies, and hydrophobin is a small globular amphiphilic protein (7.2 kDa, $\sim$3 nm) found on the outer surface of fungal spores and hyphae that assists adhesion to surfaces.[305, 306]

Examples of typical QCM-D frequency (f) and dissipation (D) responses for the 22 nm control and SB modified coatings on exposure to protein are shown in Figure 4.3. Similar responses were recorded for all other particle sizes. Control coatings experienced large negative f shifts on exposure to protein solutions at time zero, indicating adsorption to the coating surface. Binding of BSA was rapid, reaching a plateau within the 30 min exposure period. Only a small positive f shift was observed upon rinsing with PBS, indicating that majority of protein was irreversibly bound

to the coating surface. Binding of hydrophobin to the control coating was more gradual and resulted in a smaller overall f shift compared to BSA. Hydrophobins are known to self-assemble onto hydrophilic-hydrophobic interfaces by undergoing conformational changes that promote favourable surface interactions.[307] However, as both the protein containing solution and coating interface are hydrophilic, binding rates may have been slowed due to conformational rearrangement to present less of the hydrophobic domain. Alternatively, adsorption may occur in bilayers, lowering the interfacial energy gap.[306]

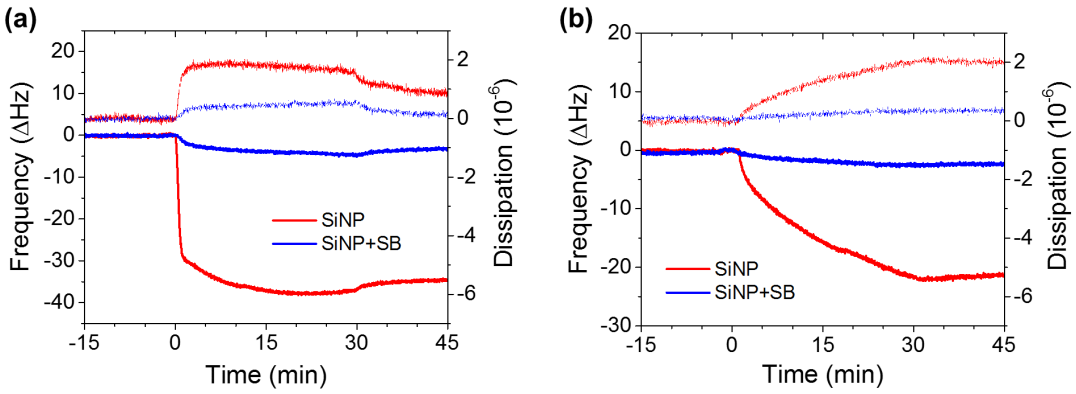

Figure 4.3: Example QCM-D f and D shifts of 22 nm control and SB Modified SiNP coatings on exposure to BSA (a) and hydrophobin (b) proteins (5^{th} overtone shown).

QCM-D f and D shifts were converted to mass of adsorbed protein by applying Voigt modelling (Figure 4.4). Mass adsorption per unit area was then normalised to coating surface area based on the AFM measurements presented above (ratio: adsorption × (calculated area/actual area)). Interestingly, no significant difference in binding of BSA protein was observed onto the unmodified control surfaces prepared from different-sized SiNPs, although there appeared to be a trend of increasing SiNP size resulting in decreased BSA adsorption (Figure 4.4a).

It has been reported previously that BSA will undergo conformational changes when interacting with substrate curvature. Roach et al. demonstrated that BSA undergoes drastic changes in conformation upon adsorption onto large silica spheres, with loss of secondary structure and an increase in random coil/extended chain structure.[308] Smaller particles with larger surface curvature support albumin in a more native-like structure, which could assist protein assembly and contribute to the slightly higher adsorptions reported here.

Adsorption of BSA was also measured onto a planar surface presenting the same surface chemistry as the SiNPs (SiO_2 QCM sensor). The roughness of this surface was measured by AFM (Figure A.13) and found to be less than any of the nanoparticle coatings (R_q = 2.50 nm). Additionally, BSA adsorption was slightly less on this

surface than for any of the SiNP control coatings (531 ng/cm^2) (Figure A.14). This indicates that the increased surface area and topographical features imparted by particle curvature may enhance protein uptake. Similar results have been presented in other studies, where nanostructured features on polyurethane and titanium have increased protein binding compared to smooth surfaces of the same material.[148, 309] SB modification was able to significantly reduce protein binding across the range of particle sizes studied, indicating that changes to surface chemistry and energy (water structuring) have a more significant impact on binding than the presence of nanoscaled topographical features (Figure 4.4a).

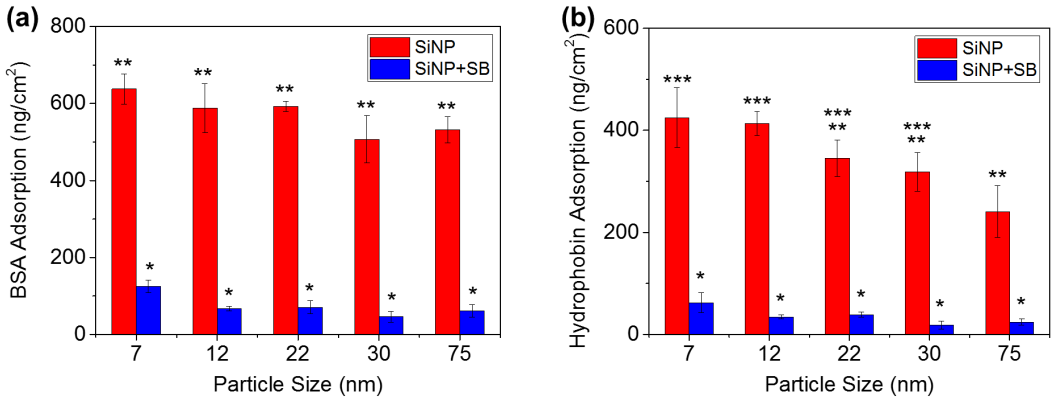

Figure 4.4: Mass of BSA (a) and hydrophobin (b) adsorbed onto SiNP coatings with and without SB modification. Mass of the adsorbed protein was calculated from modelling the 3^{rd}, 5^{th}, and 7^{th} overtone f and D responses within the QCM-D. Error bars represent SD of the mean (n=3). Asterisks (*) denote statistically similar subsets.

Adsorption of hydrophobin protein to SiNP coatings revealed a similar trend to that presented by BSA (Figure 4.4b). Hydrophobin adsorption decreased onto coatings as particle size increased, with significantly less protein found to adsorb onto the 75 nm control coatings compared to the 7 and 12 nm SiNP surfaces. The conformational flexibility of hydrophobin is well documented with hydrophobins known to undergo conformational changes to promote self-assembly onto surfaces.[310] Additionally, hydrophobins assemble into rodlets consisting of four molecule bilayer bundles with the spacing between rodlets (measured between the tops of two successive fibres) in the range of 8–13 nm.[311] It is unlikely that this spacing would be greatly perturbed by the small increase to surface roughness presented by the smaller SiNP coatings. However, the topographical features presented by the larger particles may disrupt the rodlet organisation at the coating interface and thus lower the overall protein uptake.

Despite hydrophobins ability to bind to both hydrophilic and hydrophobic surfaces through presentation of like (hydrophilic/hydrophobic) domains, modification of SiNPs with hydrophilic SB still resulted in dramatic reductions in hydrophobin

adsorption (Figure 4.4b). Again, the presentation of the zwitterionic molecules had a much more dramatic effect on protein adsorption than the size of the particle to which it was attached. There were no significant differences in hydrophobin adsorption between the SB modified SiNP coatings.

4.3.3.2 Bacterial Adhesion Study

The effect of nanoscale topography on cellular adhesion is a growing area of research, both in the interest of enhancing cell growth and proliferation and in the prevention of cellular attachment. The *E. coli* investigated in this study have dimensions in the range of $\sim 0.5 \times 2.0$ μm, however, the adhesion of *E. coli* to surfaces is mediated by filamentous organelles and adhesive secretions that are much smaller than the organism itself. Pili and fimbria are organelles anchored to the outer bacterial membrane, ranging from 2–6 nm flexible hairlike filaments to 6–8 nm stiff rodlike filaments.[312] These structures are accompanied by adhesins, specialised adhesive proteins that mediate attachment to abiotic surfaces.[313]

The presence of these adhesive mechanisms operating at different scales is likely to influence the interaction behaviour of the bacteria with the nanoparticle surfaces. For the short-term adhesion assay performed over 2 h (Figure 4.5a), significantly less bacteria adhered to coatings of the larger 30 and 75 nm control (unmodified) coatings than on to coatings prepared from 7 and 12 nm SiNP coatings. The 22 nm SiNP surfaces presenting an intermediate level of bacterial binding. This indicates that the surface topography presented by the different sized SiNPs influenced the adhesion of *E. coli* to the coated surfaces.

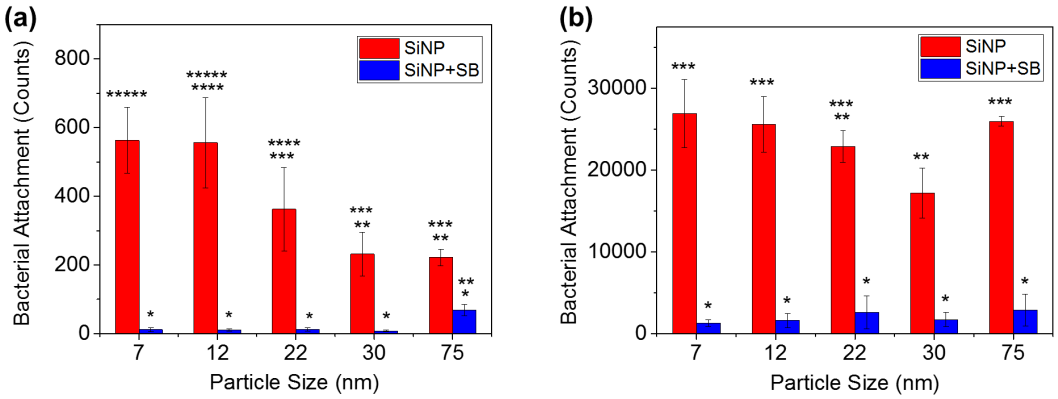

Figure 4.5: Bacterial attachment to SB modified SiNP coatings compared to control coatings after 2 h (a) and 24 h (b). Error bars represent SD of the mean (n=3). Asterisks (*) denote statistically similar subsets.

This result is in agreement with previous studies, where the presence of nanoscaled surface features produced a reduction in bacterial adhesion. Mitik-Divena et al. demonstrated that bacterial attachment onto nanorough glass was reduced compared

to chemically etched, nanosmoother glass surfaces.[314] Similarly, Rizzello et al. demonstrated that *E. coli* adhesion was reduced onto a nanorough gold substrate compared to a flat control surface.[315] It appears that not only the presence of nanoscaled features but their size heavily influences interactions. Analogous to the results presented here, Dalby et al. demonstrated differences in cellular response to nanometric islands prepared by polymer demixing.[316] For islands of 13, 35, and 95 nm in height, cell spreading, and proliferation was highest on 13 nm islands and lowest on 95 nm islands, with significant differences observed in cell morphologies depending on their interactions with the island features. Comparing the control SiNP surfaces to their respective SB modified coatings, all particle sizes experienced reductions in bacterial adhesion (Figure 4.5a). These reductions were found to be statistically significant ($p < 0.05$) for SB modified 7, 12, 22, and 30 nm SiNP coatings. The 75 nm SB modified particles still exhibited a reduction in bacterial adhesion but the result was not significantly less than the unmodified control coating (likely due to the lower adhesion presented by the control group).

Whereas significant differences in bacterial adhesion were observed among the control group for the 2 h study, less variation was presented after 24 h (Figure 4.5b). Unmodified 22 and 30 nm SiNPs experienced the smallest degree of bacterial fouling among the control group, whereas it appears the topographical effects exhibited by the 75 nm coatings were unable to produce a pronounced antiadhesion effect over the longer-term study. Bacteria are well-known to secrete extra cellular adhesives in response to their arrival and adhesion to a surface.[317] The deployment of these adhesives over time is likely to modify both the chemical and topographic characteristics of the surface, masking the native surface and providing a more favourable surface for the maintenance and growth of bacteria. This process likely contributes to the diminished fouling resistant properties of the unmodified SiNPs after 24 h observed here. In the case of SB modified SiNP coatings, particle zwitteration had the desired effect of drastically reducing adhesion of bacteria (Figure 4.5b). However, no significant difference was observed across the different particle sizes studied for all SB modified SiNPs.

4.3.3.3 Fungal Spore Adhesion

Fungi are opportunistic foulers that are well adapted for growth on surfaces.[29] Fungal contamination and colonisation can result in food spoilage and the biodeterioration of materials and may also present allergenic and pathogenic risks.[37] Fungal fouling is usually combatted through the application of harmful fungicides, while adhesion prevention approaches have not been widely studied. Only a low percentage of the total number of fungal spores that settle onto a habitable substrate will attach, therefore, coatings that could minimise spore adhesion would

be beneficial in lowering overall fungal growth and proliferation. The *E. nigrum* examined here is a prolific surface fouler, forming dense "mats" and reproducing through the generation of spores. Spores are approximately 10 μm in size and rely on a combination of surface texture and secreted adhesives (e.g., hydrophobins) to promote their attachment. Hydrophobin proteins assemble at the air-water interface, lowering water surface tension and facilitating attachment of the spore to surfaces. Our protein adsorption study indicated a slight reduction in binding with increasing particle size but significant reductions across all particle sizes when modified with SB. A similar trend was observed when comparing overall spore attachment (Figure 4.6).

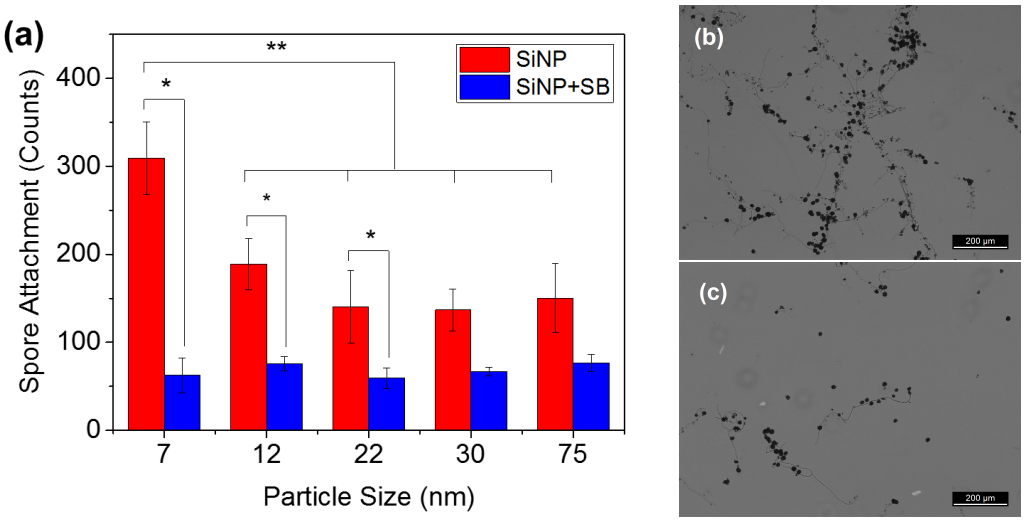

Figure 4.6: *E. nigrum* attachment to SiNP coatings after 24 h incubation (a). Error bars represent SD of the mean (n=3). Asterisks (*) denote statistically different subsets. Representative images of spore attachment onto 22 nm coatings without (b) and with (c) SB modification.

The 7 nm SiNP coating experienced the worst degree of fungal fouling, with significantly higher spore counts compared to any of the other unmodified control surfaces (p <0.05). SB modified 7 nm particle coatings brought about the largest reduction in spore adhesion (80%), whereas 12 and 22 nm modified particle coatings also showed significant reductions in spore attachment compared to their respective control surfaces. There was no statistically significant reduction in spore attachment for SB modified 30 and 75 nm coatings, however, these coatings still halved the number of spore counts compared to their respective controls. While these reductions were not as large as those seen for the protein and bacteria studies, hyphae growth was also reduced on the SB modified coatings (Figure 4.6c). This would lower the spore's overall adhesion strength and potentially allow for spores to be removed by shear forces or gentle mechanical cleaning.

It was anticipated that the antifouling assessment of SiNP coatings would reveal

differences in their ability to inhibit biological fouling due to differences in surface nanotopography and chemical functionalisation (grafting density and organisation). Unmodified SiNP coatings did present differences in their ability to prevent fouling as a result of surface topographic effects, with increasing particle size and coating roughness correlating with improved fouling resistance. In contrast, all functionalised particle coatings showed drastic improvements in fouling prevention regardless of particle size and coating topography. It may be noted that functionalised particles presented nonidentical surface coverage (Table 4.3) and yet there were no observable differences in antifouling performance. This was attributed to lower grafting densities on smaller particles presenting higher masses of bound SB due to increased surface area. In this way, there appears to be a trade-off between increased surface coverage and increased mass of SB incorporated into SiNP coatings. Despite these differences, all SB functionalised SiNP coatings were shown to protect surfaces from fouling, highlighting the versatility this system offers in terms of coating fabrication, where coatings could be tailored to suit particular applications through the choice of particle size.

4.4 Conclusions

The simple fabrication of hydrophilic SiNP coatings with tunable nanoscaled surface topography is reported. The roughness and topography of coatings could be easily adjusted through variation of particle size, while the nanoparticle surface chemistry lent itself to easy functionalisation with the zwitterionic, sulfobetaine moiety. This Chapter has demonstrated that nanoscaled topography influences interaction and adhesion of a range of fouling species with proportions spanning several orders of magnitude. Zwitterion functionalisation of SiNPs imparted a high degree of fouling resistance across all particle sizes and across the range of proteins and microbial organisms studied. In contrast, unmodified particle coatings presented size-dependent differences in their ability to resist fouling. In most instances the 22, 30, and 75 nm particle coatings offered superior resistance to fouling compared the smaller 7 and 12 nm SiNP surfaces.

This study identified that both surface chemistry and topography were responsible for determining the interactions and adhesion of fouling species. Functionalisation of SiNPs with zwitterionic SB increased SiNP coating hydrophilicity resulting in improved resistance to protein binding and bacterial adhesion. Additionally, small differences in protein binding were also observed with varied coating roughness. This result is consistent with a previous report, where smooth CH_3 (hydrophobic) and OH (hydrophilic) modified substrata promoted thick ($\sim$20 nm) and thin ($\sim$6 nm) layers of protein to form on these surfaces, respectively.[318] On the same surfaces presenting a roughened substrate, similar amounts of protein adsorbed; however, the organisation of protein molecules was affected. Similar findings were reported by Vertegel et al., where the interaction of lysozyme protein with silica nanoparticles were found to be strongly dependent on the nanoparticles size.[319] Strong protein-particle interactions between the lysozyme and large (100 nm) particles resulted in protein unfolding and loss of secondary structure. A similar phenomenon may have caused perturbation of BSA and hydrophobin protein structures when interacting with the surface of large particle coatings, resulting in an overall decrease in protein adsorption. This theory is supported by the findings of Roach et al., who demonstrated a deviation away from monolayer BSA adsorption onto hydrophobic and hydrophilic silica spheres due to loss of secondary structure when adsorbed onto spheres of increasing radii.[308]

Considering protein interactions alone may not provide an accurate assessment of the antifouling properties of surfaces presenting nanoscale topography. An interesting study by Rizzello et al. demonstrated that *E.coli* bacteria could colonise both flat and nanostructured metal substrates with comparable numbers of adherent cells but that bacteria growing on nanorough substrates did not express type-1 fimbriae adhesive organelles and thus had weak interactions with the underlying surface.[315]

This highlights the need to consider several factors when designing nano- and microstructured surfaces for fouling prevention, including the surface chemistry, substrate topography, and the organisms that will be interacting with it.

Overall, the exceptional fouling resistance exhibited by the functionalised particle coatings presented in this Chapter confirms the versatility of SiNP based antifouling coating systems and demonstrates flexibility in terms of coating formulation through variation in particle size, surface chemistry, and coating application.

Chapter 5

Modified Silica Nanoparticle Coatings: Dual Effects of Self-Assembled Quaternary Ammonium and Zwitterionic Silanes

This Chapter has investigated the reaction of a quaternary ammonium silane to silica nanoparticles coatings, on its own and in combination with zwitterionic sulfobetaine, with the intention of generating dual antimicrobial-antifouling surfaces. Interestingly, dual-functionalised coatings were not found to exhibit strong antimicrobial action but instead presented exceptional antifouling properties. Additionally, quaternary ammonium modified silica nanoparticle coatings demonstrated resistance to protein fouling when prepared under optimised reaction conditions. The underlying charge of the silica nanoparticle coating is proposed to play a significant role in the antifouling properties presented by the prepared surfaces and is examined in this Chapter.

5.1 Introduction

As discussed in Chapter 1, current approaches to combat surface fouling generally fall under one of two categories: (i) antimicrobial coatings, which kill microorganisms either through contact-killing or release based mechanisms, or (ii) antifouling coatings, which prevent microbial interactions and attachment. Antimicrobial surfaces or coatings that rely on the release of biocides have demonstrated exceptional fouling resistance across a range of applications,[67, 83, 96, 320] however, controlling the rate of biocide release remains a challenge and insufficient dosages can lead to the

development of biocide resistant organisms.[20, 102] Tethering biocidal chemistries directly to the underlying substrate offers advantages over release based surface coatings, with increased antimicrobial efficiencies and longevity reported.[122, 321, 322]

Quaternary ammonium compounds (QAC) are cationic disinfectants that are commonly added to cleaning products and commercial coatings to impart antimicrobial properties.[323] These properties arise from electrostatic interaction between the positively charged ammonium group and the negatively charged bacterial cell wall.[126] It is proposed that QAC chains may penetrate the cell membrane or induce cation exchange, thereby disrupting membrane integrity, causing cell lysis and leakage of interstitial fluids.[121, 127] However, dead microorganisms can accumulate on these surfaces, shielding active functional groups and facilitating further growth.

On the other hand, antifouling coating approaches have shown promise in preventing microbial attachment but do not present any active killing mechanisms. Surfaces functionalised with hydrophilic polymers, including polyethylene glycol (PEG) and zwitterions, effectively prevent protein adsorption and microbial interactions through a combination of steric repulsion and interfacial water structuring.[173, 204, 270, 277, 324–327] Ideally, surfaces could present both antimicrobial and antifouling properties; synergistically killing organisms that contact them and preventing their accumulation on the surface.

This Chapter presents an investigation into the combined antifouling-antimicrobial effect of silica nanoparticle (SiNP) coatings functionalised with quaternary ammonium silane (QAS) and zwitterionic sulfobetaine siloxane (SB). SiNPs could be easily deposited as thin films, providing reactive surface chemistries for self-assembly of silanes. First, the reaction of QAS to SiNP coatings was optimised under different solution concentrations and pH, then adsorption of BSA protein to these surfaces was compared. Second, dual-functionalised surfaces were prepared by sequentially exposing SiNP coatings to solutions of QAS and SB, varying solution concentration and order of addition. Surface functionalisation and protein adsorption were monitored using QCM-D and adhesion of bacteria to surfaces and evidence of bactericidal properties were compared amongst the prepared coatings.

5.2 Experimental

5.2.1 Materials

Ludox® HS-40 colloidal silica (12 nm diameter), phosphate buffered saline (PBS, P5368), (*N,N*-dimethylaminopropyl)trimethoxysilane (539287), 1,3-propane sultone (P50706), bovine serum albumin (BSA, A3059), poly(ethylenimine) solu-

tion (PEI, P3143), and acetone (270725) were purchased from Sigma-Aldrich. *N*-trimethoxysilylpropyl-*N,N,N*-trimethylammonium chloride (50% in MeOH, SIT-8415.0) was purchased from Gelest. Acetone was dried with 3 Å molecular sieves and distilled before use. All other reagents purchased from commercial suppliers were used without further purification. Water used in experiments and to prepare aqueous solutions was purified using a Millipore water purification system with a minimum resistivity of 18.2 MΩ.cm at 25 ℃.

5.2.2 Synthesis of Zwitterionic SB

SB was synthesised following the method described in Section 2.2.2

5.2.3 Reaction of QAS to SiNPs

The appropriate amount of QAS monomer for reaction with SiNPs was calculated based on the surface area reported by the manufacturer and 4.9 silanol groups per nm^2 of silica surface.[253]. A 10 wt% dispersion of SiNPs was prepared and pH adjusted to 3 with dilute HCl. QAS (50% in MeOH) was added dropwise to the pH adjusted SiNP solution, with stirring. The reaction mixture was stirred for 6 h. Thereafter, the particle solution was placed into a 12 K molecular weight cutoff dialysis membrane and dialysed against pure water for 5 days. Particles were freeze-dried for further characterisation.

5.2.4 Preparation of SiNP Coatings

SiNP coatings were prepared onto A-T cut QCM sensors with a 10 mm diameter gold electrode and a fundamental resonance frequency of 5 MHz. Prior to coating, the gold surface of each crystal was cleaned with piranha solution (7:3 v/v mixture of H_2SO_4 (98%) and H_2O_2 (33%)) for 3 min, rinsed with deionised water and dried under a stream of nitrogen gas. Cleaned surfaces were then incubated in 0.5% poly(ethylenimine) (PEI) solution for 10 min at RT to form an adhesive layer. PEI was thoroughly rinsed from the surfaces with deionised water and surfaces were dried in a stream of nitrogen gas. SiNP solutions were prepared as 4 wt% dispersions in water for spin-coating. Sensors were mounted into the spin-coater and particle films were prepared by depositing 20 μL of the 4 wt% dispersions onto their surface and spin-coating at 5000 rpm for 30 s. Coatings were cured for 1 h at 120 ℃ and thereafter thoroughly rinsed with deionised water and dried in a stream of nitrogen gas.

5.2.5 Quartz Crystal Microbalance

Adsorption of QAS and SB onto SiNP coated gold QCM sensors, and protein adsorption experiments were carried out using Q-Sense E4 QCM-D (Q-Sense AB Västra, Frölunda, Sweden) coupled with an ISMATEC IPC High Precision Multichannel Dispenser (IDEX, Wertheim, Germany) in a flow-through setup. The use of the QCM-D allows for correlation between a change in the quartz crystals fundamental oscillation frequency and calculation of a mass absorbed to a surface. The mass of QAS, SB, and adsorbed protein was calculated by applying the Voigt model using Q-Sense QTools analysis software v3.0.10.286 (Biolin Sci, AB). All experiments were run in triplicate. The following input parameters provided the best fit for the layer density (1150 kg/m^3), fluid density (1020 kg/m^3), layer viscosity ($10^{-6} \leq 10^{-2}$ kg/ms), layer shear modulus ($10^4 \leq 10^8$ Pa) and mass (1.15 $\leq$ 1.155 ng/cm^2). The 3^{rd}, 5^{th}, and 7^{th} overtones were used for modelling calculations.

5.2.5.1 QAS and SB Binding

Aqueous solutions of QAS and SB monomer at concentrations of 0.5 mM, 1.0 mM, and 10 mM were prepared and pH adjusted immediately prior to functionalisation of SiNP coatings. SiNP coated sensors were placed into standard Q-Sense flow modules (QFM 401) and equilibrated in deionised water at a constant temperature of 22.00 $\pm$ 0.02 ℃ until baseline signals stabilised. QAS/SB solutions were introduced into the QCM chamber at a flow rate of 60 μL/min for 30 min. Coatings were then rinsed with neutral or pH adjusted aqueous solutions at the same flow rate for 15 min. For sequential surface functionalisations, a second solution of QAS/SB was introduced into the QCM chamber for 30 min and then surfaces were rinsed a second time. All experiments were run in triplicate.

5.2.5.2 Protein Adsorption

Adsorption of protein onto the QAS/SB functionalised SiNP coatings was quantified using QCM-D. SiNP coated sensors (functionalised as per Section 5.2.5.1) were placed into standard Q-Sense flow modules (QFM 401) and equilibrated in PBS at a constant temperature of 22.00 $\pm$ 0.02 ℃ until baseline signals stabilised. BSA dissolved in PBS at a concentration of 1 mg/mL was introduced into the QCM chamber at a constant flow rate of 60 μL/min. After 30 min, PBS was reintroduced to rinse the coatings and remove any loosely bound proteins. All experiments were run in triplicate.

5.2.6 Characterisation

5.2.6.1 Dynamic Light Scattering/Zeta Potential

Z-Average particle size (hydrodynamic particle diameter) measured by dynamic light scattering (DLS) and zeta potential (ZP) measurements were performed on a Malvern Zetasizer Nano-ZS at 25 ℃ (colloidal silica refractive index: 1.40, absorption: 0.010, measurement angle: 173°). ZP measurements were performed on 0.5 wt% aqueous particle dispersions, pH adjusted with HCl and NaOH. DLS measurements were carried out on 0.5 wt% particle solutions dispersed in 10 mM NaCl.

5.2.6.2 Thermogravimetric Analysis

The quantity of zwitterion bound to the particle surface was determined using thermogravimetric analysis (TA, Q500). Dried nanoparticles were heated from room temperature to 800 ℃ at a heating rate of 10 ℃/min under a nitrogen atmosphere. The mass of polymer bound to the particle surface was calculated from the weight loss measured between 150 and 800 ℃. The mass retained at 800 ℃ after polymer decomposition was assumed to be the mass of bare SiNPs.

5.2.6.3 Contact Angle Goniometry

Contact angle measurements were acquired using a Dataphysics Contact Angle System (OCA 15EC) in conjunction with SCA20 software. The mean static contact angle made by a 2 μL sessile water droplet in contact with the particle coatings was measured. A minimum of three measurements were obtained for triplicate samples of each particle coatings.

5.2.7 Bacterial Adhesion Study

Bacterial solutions were prepared from a precultured JM109 strain of *Escherichia coli* and inoculated overnight in 20 mL of sterile LB (Luria-Bertani) medium at 37 ℃ in a Bioline incubator shaker 8500 (Edwards Instrument Co., Narellan, Australia). Inoculated culture (0.5 mL) was added to 20 mL of LB medium and optical density measurements carried out every 30 min using a Spectronic 200 (Thermo Scientific, Waltham, MA) until the desired turbidity was achieved (OD_{600} 0.6–0.8). The number of colony forming units (CFUs) in the bacterial suspension was determined by plating out dilutions of the suspension and was found to be 1.03×10^7 CFU/mL.

Spin-coated SiNP films were prepared onto glass coverslips (22 mm diameter) following the same method described in Section 5.2.4 for the coating of QCM sensors. Surface functionalisation of SiNP coatings were conducted in a similar manner to

QCM-D reactions. Coatings were exposed to 2 mL of freshly prepared QAS and SB solutions for 30 min and then rinsed several times with deionised water. For dual-functionalisation's, rinsed surfaces were sequentially exposed to QAS and SB solutions, and rinsed again thoroughly with deionised water. Coated coverslips were placed into individual wells of sterile 12-well culture plates. PBS (2 mL) with bacterial cells were added to each well, and culture plates were incubated at 37 ℃ for 4 h. Coverslips were then removed from incubation, immersed in PBS with agitation (6×), rinsed with 2 mL PBS and placed into fresh sterile 12-well culture plates.

Bacteria were stained using a LIVE/DEAD® BacLight™ Viability Kit (Molecular Probes, Inc.), containing: SYTO™ 9 stain, to label all cells with green fluorescence, and propidium iodide, a red fluorescent stain that only penetrates cells with damaged membranes. Samples were imaged using confocal microscopy (Leica TSC SP5 II), at $\lambda_{ex} = 488$ nm and 543 nm to determine the degree of bacterial colonisation and evaluate the proportion of living and dead cells. Experiments were performed in triplicate with a minimum of 5 fluorescent images taken of each sample. Images were obtained at 8× magnification, with bacterial counts determined using ImageJ® software (v.1.51n).

5.2.8 Statistical Analysis

Results were analysed using one-way analysis of variance (ANOVA) with Tukey post hoc test. Probabilities of $p < 0.05$ were considered to be significantly different. All statistical analyses were performed using IBM SPSS Statistics 21 software.

5.3 Results and Discussion

5.3.1 Surface Functionalisation

The effect of QAS concentration and solution pH on the functionalisation of SiNP coatings was compared using QCM-D. SiNP coatings, prepared via spin coating of 4 wt% dispersions of particles onto gold QCM sensors, were equilibrated in the QCM with DI water. Solutions of 10 mM QAS were prepared and pH adjusted to 3.5, 7.0, and 9.5 immediately prior to reaction. Coatings were functionalised within the QCM-D by flowing through QAS solutions for a period of 30 min. Surfaces were then rinsed with DI water to remove any silane not covalently bound to the surface. Changes in the oscillation frequency (f) and dissipation (D) of the QCM sensor after QAS modification were converted to mass of adsorbed material by applying Voigt modelling (Figure 5.1). Mass of covalently bound silane was found to increase with increasing pH, consistent with previous reports that have demonstrated rapid

hydrolysis and condensation reactions of silanes under basic conditions.[259, 262] Additionally, the SiNP surface would present a higher proportion of deprotonated silanol groups (SiO^-) at pH 9.5 and could enhance electrostatic attraction of the positively charged quaternary ammonium group, leading to increased interaction and subsequent binding. While surfaces prepared across all pH conditions were hydrophilic, water contact angles were found to decrease slightly with increasing pH (Table A.4).

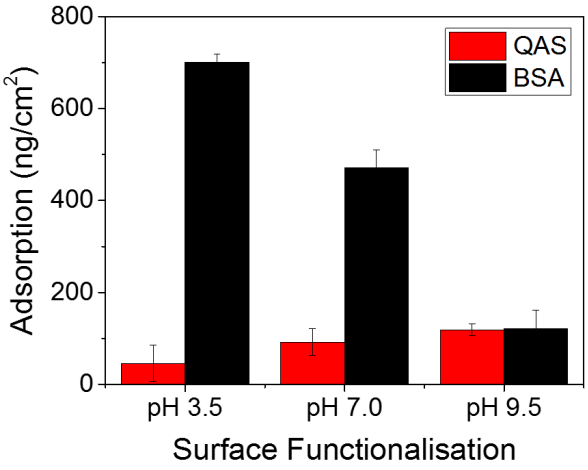

Figure 5.1: Mass of QAS bound to SiNP coatings when exposed at a concentration of 10 mM under different pH conditions and the resultant mass of BSA bound to the QAS functionalised surfaces. Mass was calculated from modelling the 3^{rd}, 5^{th}, and 7^{th} overtone f and D responses within the QCM-D. Error bars represent SD of the mean (n=3).

Protein (BSA) adsorption to QAS modified SiNP coatings was also monitored using QCM-D. Coatings were equilibrated in PBS before exposure to 1 mg/mL BSA solutions. Increased protein binding was observed with decreasing QAS functionalisation pH, where adsorption reached 701 ng/cm^2 for pH 3.5 modification and was reduced to 121 ng/cm^2 for pH 9.5 modification (Figure 5.1). While this decrease in protein adsorption correlated with increased QAS functionalisation, previous studies have not reported quaternary ammonium functionalisation to impart any degree of protein resistance. In fact, some reports indicate increased protein adsorption due to favourable electrostatic interactions with charged proteins.[189, 328] However, when quaternary ammonium moieties have been coupled with anionic (negative charge bearing) chemistries to generate pseudozwitterionic surfaces, resistance to protein adsorption is dramatically improved.[155, 329] With this in mind, it is likely that the surface charge of the underlying particles may also play a role in the coordination of water with the surface and affect the protein resistant properties of QAS modified surfaces depending on pH (Figure 5.2).

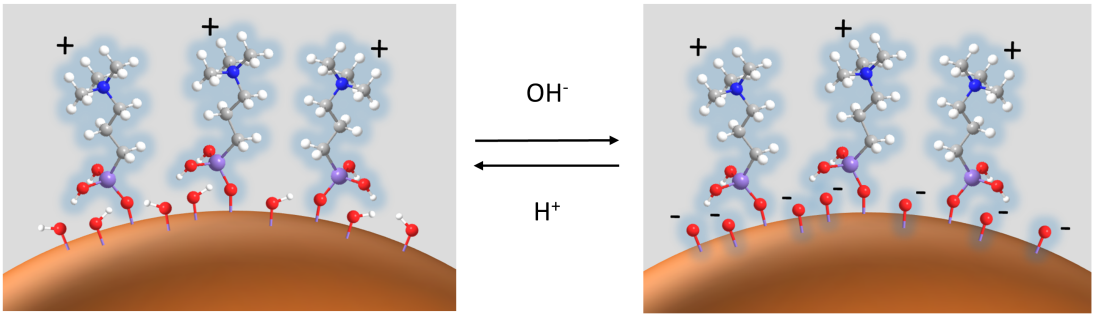

Figure 5.2: Schematic showing the pH dependent surface charge of the SiNP coating, where increased hydration capacity due to pseudozwitterionic character may be present at high pH conditions.

It is well known that surface hydration and water structuring are critical for imparting protein resistance to low-fouling hydrophilic materials.[214, 330] For this system, it is anticipated that SiNP coatings functionalised at pH 9.5 would have an increased electrostatic hydration capacity, owing to a larger number of deprotonated silanol groups on the SiNP surface (isoelectric point of silica is ∼2.5),[260] and thus may resemble a pseudozwitterionic interface. The distance between these charges is comparable to spacer lengths commonly presented by low-fouling zwitterionic systems and could explain the protein resistant properties exhibited by surfaces prepared at higher pH.[207, 331]

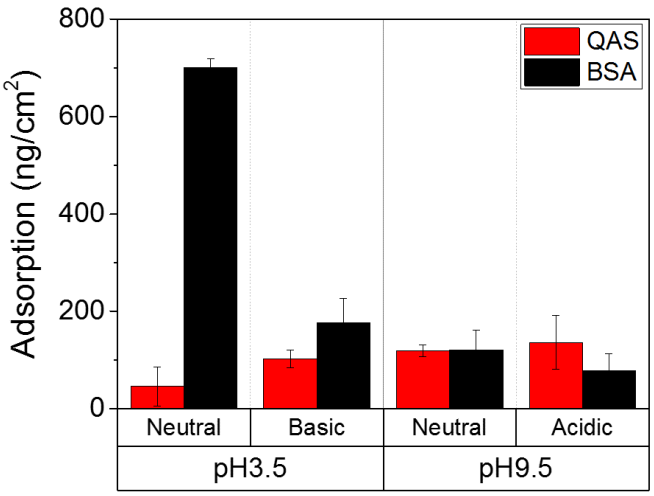

Figure 5.3: Comparison of QAS and BSA adsorption to SiNP coatings when pH 3.5 and pH 9.5 functionalised surfaces are rinsed with solutions of different pH (basic, neutral, or acidic) prior to exposure to protein as calculated from modelling the 3^{rd}, 5^{th}, and 7^{th} overtone f and D responses within the QCM-D. Error bars represent SD of the mean (n=3). *(note: neutral rinse data is the same as what is presented in Figure 5.1)

To test this hypothesis, SiNP coatings were functionalised as before with QAS

solutions adjusted to pH 3.5 and 9.5 and rinsed with DI water. This was followed by an additional rinse step with pH adjusted aqueous solutions of the opposite acidity/basicity to the functionalisation pH. The QAS and BSA mass adsorption for oppositely rinsed surfaces are presented in Figure 5.3.

Rinsing of the pH 9.5 modified coating with an acidic solution did not result in any change to the frequency observed at the sensor surface (Figure A.15) and thus the calculated mass of bound QAS was comparable to that of the neutral rinsed pH 9.5 modified coating. Protein binding was also similar for these two surfaces, indicating that the acidic rinse did not perturb the interfacial hydration and affect the coatings protein resistance. However, rinsing of the pH 3.5 modified surface with a basic solution resulted in a small decrease in f, indicating an overall increase in mass at the sensor surface (Figure A.16). QCM-D is a sensitive enough technique to respond in changes in surface hydrophilicity,[281] and as no additional silane was available to react, it was thought that the basic solution rinse may promote increased water association with the surface due to deprotonation of silanol groups and increased zwitterionic character. This would be expected to improve the protein resistance presented by the surface. Indeed, protein adsorption was significantly decreased by 75% compared to the pH 3.5 QAS modified surface rinsed with a neutral solution (one-way ANOVA, $p < 0.05$) and comparable to the protein adsorption observed on the pH 9.5 prepared surfaces.

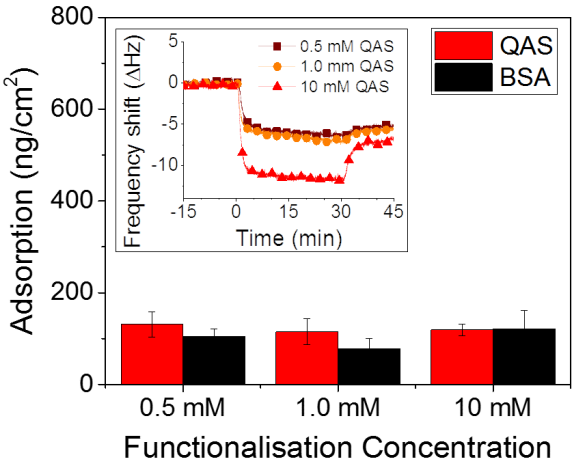

Figure 5.4: Mass of QAS bound to SiNP coatings under different solution concentrations (adjusted to pH 9.5) and the resultant mass of BSA bound to the QAS functionalised surfaces. Mass was calculated from modelling the 3^{rd}, 5^{th}, and 7^{th} overtone f and D responses within the QCM-D. Error bars represent SD of the mean (n=3). Inset: Raw f shifts observed on SiNP coating exposure to QAS solutions of different concentrations (5^{th} overtone shown). *(note: 10 mM data is the same as what is presented in Figure 5.1)

The superior performance of the pH 9.5 modified surfaces led us to examine

the effect of solution concentration during modification. Freshly prepared QAS solutions with concentrations of 0.5, 1.0, and 10 mM were pH adjusted to 9.5 and introduced into QCM chambers containing SiNP coated sensors. Raw QCM f responses revealed a larger negative shift for SiNPs on exposure to the higher concentration 10 mM QAS solution, however, rinsing after 30 min returned the f shift to a similar level to the lower concentration responses (Figure 5.4). Modelling of QCM responses revealed very little difference in QAS binding across the different functionalisation concentrations studied. It is postulated that the positive charge of the QAS would interact favourably with the negative charge presented by the SiNP surface under basic conditions, promoting association with the surface and leading to binding, even at low concentrations. All surfaces demonstrated comparable resistance to protein binding regardless of functionalisation concentration, likely due to the similar degree of QAS binding. Additionally, all surfaces presented comparable degrees of hydrophilicity with water contact angles of $< 16^{\circ}$ for all functionalisation concentrations (Table A.5).

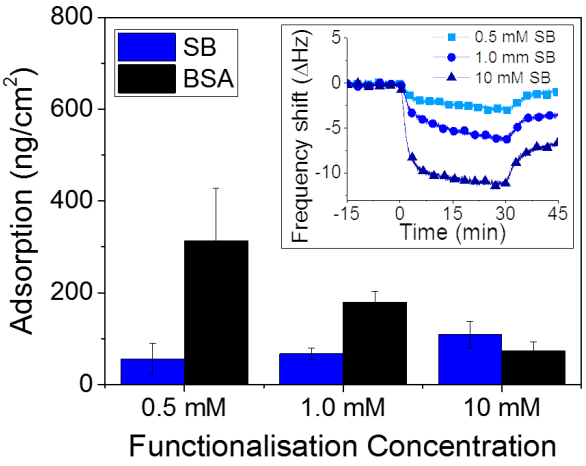

Figure 5.5: Mass of SB bound to SiNP coatings under different solution concentrations (adjusted to pH 9.5) and the resultant mass of BSA bound to the SB functionalised surfaces. Mass was calculated from modelling the 3^{rd}, 5^{th}, and 7^{th} overtone f and D responses within the QCM-D. Error bars represent SD of the mean (n=3). Inset: Raw f shifts observed on SiNP coating exposure to SB solutions of different concentrations (5^{th} overtone shown).

As the improved protein resistance presented by the pH 9.5 functionalised SiNP coatings was proposed to be the result of the generation of a pseudozwitterionic interface, it was of interest to compare protein fouling of QAS to a similar zwitterionic species. Silinated sulfobetaine (SB) shares the same silanol structure and quaternary ammonium group as QAS and the charge separation between cationic and anionic groups of SB are similar to the distance between the SiNP siloxide and quaternary ammonium groups presented by the pseudozwitterionic QAS-SiNP interface.

SiNP coatings were functionalised with SB under the same three solution concentrations as QAS (Figure 5.5). While the concentration dependence of SB binding to SiNP coatings at concentrations of 1.0 and 10 mM was previously reported in Chapter 2, this study was expanded to include the lower 0.5 mM concentration variable. Mass modelled from QCM-D shifts revealed only small increases in the mass of SB bound to SiNP coatings with increasing solution concentration, however, protein binding appeared highly dependent on the functionalisation concentration with adsorption decreasing from 313 to 73 ng/cm^2 as the functionalisation concentration was increased from 0.5 to 10 mM. In comparison, BSA adsorption to unfunctionalised SiNP coatings was 759 ng/cm^2, indicating that modification with either QAS or SB chemistries could effectively reduce protein binding to SiNP surfaces.

5.3.2 Functionalisation of Particle Dispersions

The surprising protein adsorption resistance imparted by SiNP coating modification with QAS led to an investigation of QAS functionalised SiNP dispersions. Particle modifications were attempted in H_2O/MeOH solvent mixtures (90:10, 80:20 & 50:50) as the QAS chemistry was supplied as a 50:50 mixture in MeOH. Similar to SB and CB particle functionalisations reported in previous chapters, QAS was added to stirred 10 wt% SiNP dispersions. Addition of QAS to particle dispersions in H_2O/MeOH mixtures (80:20 & 50:50) were carried out at room temperature without any adjustment to pH. However, the dispersions were found to turn slightly cloudy upon addition of QAS and would become more opaque with further reaction time and throughout the dialysis process. It was thought that this result arose from electrostatic attraction between the positively charged QAS and the negative charge of the SiNPs, causing irreversible particle aggregation.

A revised method was formulated to enhance particle stability during reaction by decreasing the particle surface charge. The pH of a 10 wt% particle dispersion was adjusted to ∼3, so as to reduce the number of deprotonated silanol surface groups and decrease the overall negative charge of the particles. Addition of QAS to the stirred particle dispersion did not result in any obvious change to solution opacity. Removal of unbound QAS by dialysis, did result in the particle dispersion turning slightly cloudy as the solution pH gradually increased to pH 7. However, increasing or decreasing the pH of the particle suspension was found to restore solution transparency, indicating reversible particle aggregation (Figure 5.6a). Functionalisation was confirmed by zeta potential analysis, were QAS modified particles showed a dramatic positive shift at low pH compared to unreacted particles (Figure 5.6b). Additionally, the isoelectric point of SiNP+QAS was ∼7, consistent with the cloudy dispersion behaviour observed at this pH.

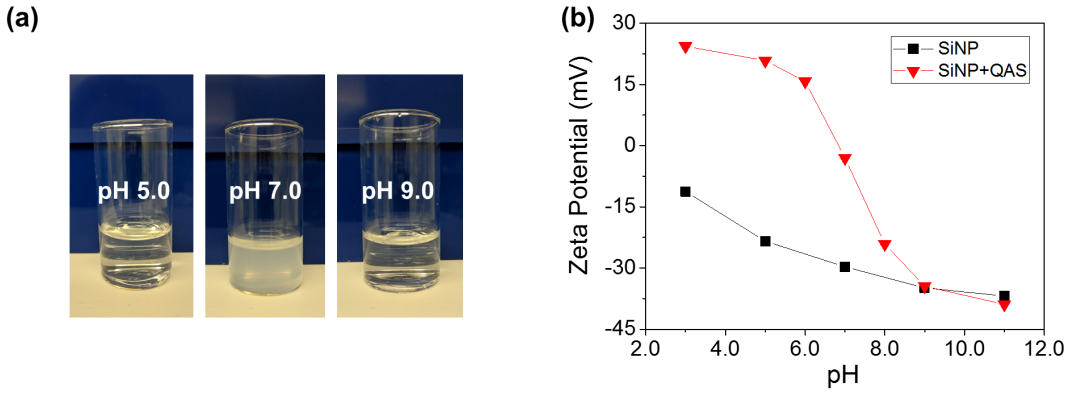

Figure 5.6: Images of QAS modified SiNPs at various pH, showing reversible aggregation at neutral pH (a) and zeta potential measurements of SiNP+QAS across pH 3.0 to 11.0 (b).

The size of particles before and after modification was compared using dynamic light scattering. The QAS modified particles showed only a slight increase in particle diameter after modification, consistent with the small size of the QAS chemistry (Figure 5.7a). SiNP+QAS dispersions did also show a small peak at larger particle diameters, indicating a slight degree of particle aggregation. Although, this result was not unexpected due to the potential for particle destabilisation and aggregation when conducting functionalisation reactions under acidic conditions. Thermogravimetric analysis showed characteristic differences between functionalised and unreacted particles (Figure 5.7b). SiNPs suffered a larger loss of adsorbed water at temperatures < 150 ℃, then exhibited a very gradual decrease in mass up to 800 ℃. Comparatively, SiNP+QAS experienced a quicker stabilisation after a smaller loss of adsorbed water, then underwent organic decomposition of the QAS monomer. The degree of particle functionalisation was calculated to be 0.84 μmol/m^2. This grafting density is lower than the base-catalysed zwitterion functionalisations reported in Chapters 2 & 3, but consistent with acid-catalysed particle functionalisation.

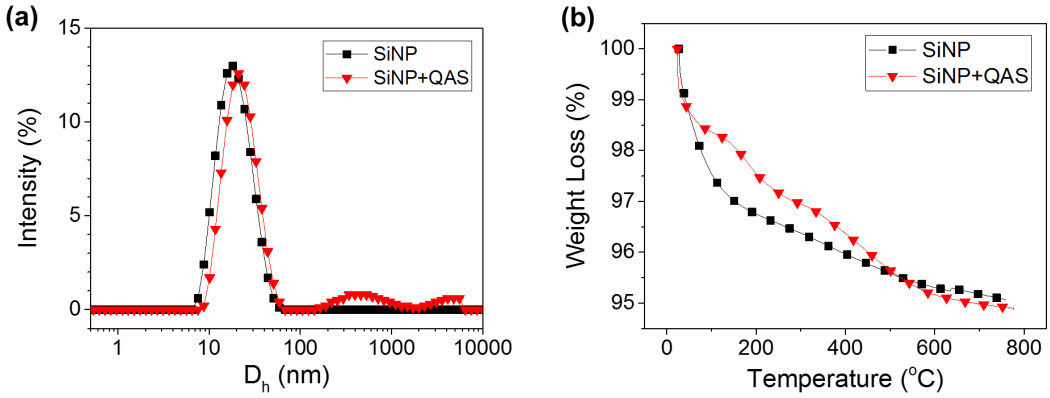

Figure 5.7: Hydrodynamic diameter of particles as measured by dynamic light scattering (a) and thermogravimetric analysis of bare and QAS functionalised SiNPs (b).

Coatings of QAS functionalised SiNPs were prepared from 4 wt% particle dispersions for protein adsorption measurements. Particle dispersions were adjusted to pH 9.5 prior to spin-coating to try and emulate surface modification conditions. Coatings were equilibrated in PBS under standard QCM conditions prior to the introduction of BSA (1 mg/mL in PBS). Exposure to protein solutions resulted in large f/D shifts (Figure A.17). The calculated mass of BSA adsorption to SiNP+QAS coatings averaged 680 ng/cm^2 for triplicate samples, only slightly less than for control SiNP surfaces (759 ng/cm^2), meaning QAS modification of SiNP dispersions was unable to significantly improve the fouling resistance of the particle coatings. This result indicates that the method of preparation of functionalised particles coatings, be it through surface modification or dispersion functionalisation, must play a large role in the organisation and presentation of the QAS chemistry and therefore impact on the fouling resistant properties of the particle coatings.

5.3.3 Dual-Functionalisation

Having demonstrated that both QAS and SB functionalised SiNP coatings present protein resistant properties, it was of interest to examine the combined reaction of QAS and SB to SiNPs to determine if the introduction of cationic QAS would disturb the fouling resistant properties of SB and/or provide a bactericidal property to the heterogenous surface. SiNP coatings were functionalised sequentially in the QCM with a brief water rinse (15 min) of the surfaces between reactions. The concentration and order of addition of QAS and SB solutions is denoted as A_xB_y, where A is the 1^{st} and B is the 2^{nd} solution exposed to the SiNP coatings, and x and y denote the concentrations of A and B in mM, respectively. The following eight combinations were prepared: $Q_{0.5}S_{0.5}$, Q_1S_1, Q_1S_{10}, $Q_{10}S_{10}$, $S_{0.5}Q_{0.5}$, S_1Q_1, S_1Q_{10}, and $S_{10}Q_{10}$.

Figure 5.8 shows representative QCM-D responses for Q_1S_1 and Q_1S_{10} SiNP coating functionalisations. Both surfaces exhibited similar responses on exposure to Q_1 solutions, however, differences were observed when comparing sequential binding of SB at concentrations of 1 and 10 mM. It appeared that very little SB was able to bind to the Q_1 functionalised SiNP surface when exposed at a concentration of 1 mM, with no net change in the frequency after the surface was rinsed (Figure 5.8a). A similar response was recorded for the $Q_{0.5}S_{0.5}$ system, with no further binding of SB observed (Figure A.18). Comparatively, exposing the Q_1 modified surface to the higher concentration 10 mM SB solution resulted in a further frequency decrease (Figure 5.8b), indicating successful SB binding and the presentation of dual chemistries at the coating interface. Consistent with the earlier concentration study, increasing the QAS concentration did not result in a significant increase in binding and thus the $Q_{10}S_{10}$ functionalisation (Figure A.19) presented a very similar response

to the Q_1S_{10} system.

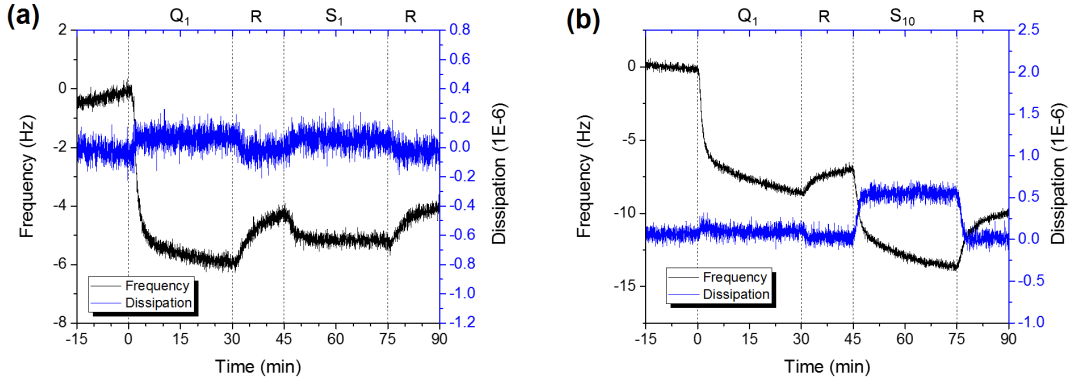

Figure 5.8: Example QCM-D f and D shifts for Q_1S_1 (a) and Q_1S_{10} (b) SiNP coating functionalisations (5^{th} overtone shown). R denotes rinsing periods.

After sequential modification, the prepared surfaces were exposed to BSA (1 mg/mL) protein solutions to gauge differences in resistance to protein binding. Mass adsorptions calculated from raw f/D responses on exposure to QAS, SB, and BSA are presented in Figure 5.9. Protein adsorption was greatly reduced on all functionalised surfaces (< 150 ng/cm^2) compared to unmodified SiNP coatings (759 ng/cm^2). Similar BSA adsorptions were observed for $Q_{0.5}S_{0.5}$ & Q_1S_1, and Q_1S_{10} & $Q_{10}S_{10}$ functionalised surfaces, consistent with their similar f/D binding profiles. It appeared that SB binding to the QAS modified surfaces and subsequent reductions to protein binding were only observed when the concentration of SB solution was increased to 10 mM.

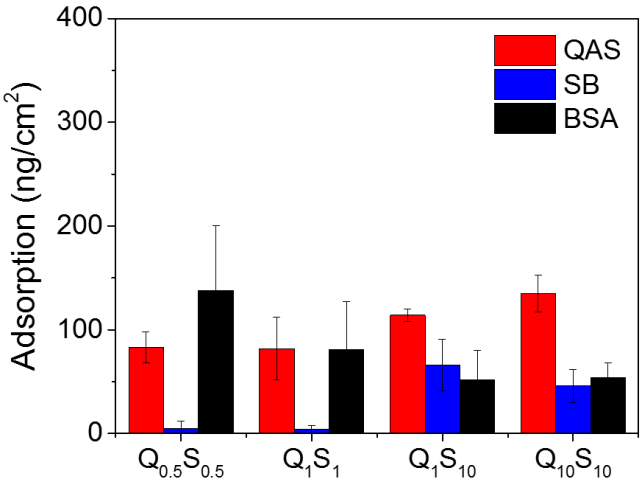

Figure 5.9: Mass modelled from the 3^{rd}, 5^{th}, and 7^{th} overtone shifts for dual-functionalisation of SiNP coatings with QAS (1^{st}) and SB (2^{nd}), and resultant protein adsorption. Error bars represent SD of the mean (n=3).

The reverse order of functionalisation was also investigated, where SB was reacted

to SiNP coatings first, followed by reaction of QAS. Figure 5.10 shows representative QCM responses for S_1Q_1 and S_1Q_{10} SiNP coating functionalisations. Interestingly, QAS was able to bind to the SiNP coatings after modification with SB, even when exposed at low concentrations (Figure A.20). This further emphasises the affinity of QAS to interact with and bind to the SiNP coating, even when partially functionalised by zwitterionic SB. Consistent with previous results, SB modification was promoted with increasing concentration, leaving fewer unreacted sites available for functionalisation by QAS (Figure A.21).

The mass of SB (1^{st}) and QAS (2^{nd}) adsorbed to SiNP surfaces and their resultant adsorption of BSA protein are presented in Figure 5.11. Again, protein adsorption was low across all dual-functionalised surfaces relative to unfunctionalised SiNP controls. Compared to the SB concentration study presented in Figure 5.5, where BSA adsorption onto 0.5 mM functionalised surfaces was 313 ng/cm^2, sequential functionaliation with 0.5 mM QAS was able to reduce BSA adsorption to 122 ng/cm^2 for the $S_{0.5}Q_{0.5}$ system. This result emphasises the affinity of the QAS to bind to the SiNP surface despite being partially functionalised and demonstrates the capacity for dual-functionalised surfaces to present increased levels of fouling resistance. Further increases in SB binding with increasing functionalisation concentration led to improved protein resistance, with the lowest protein adsorption observed on the $S_{10}Q_{10}$ system.

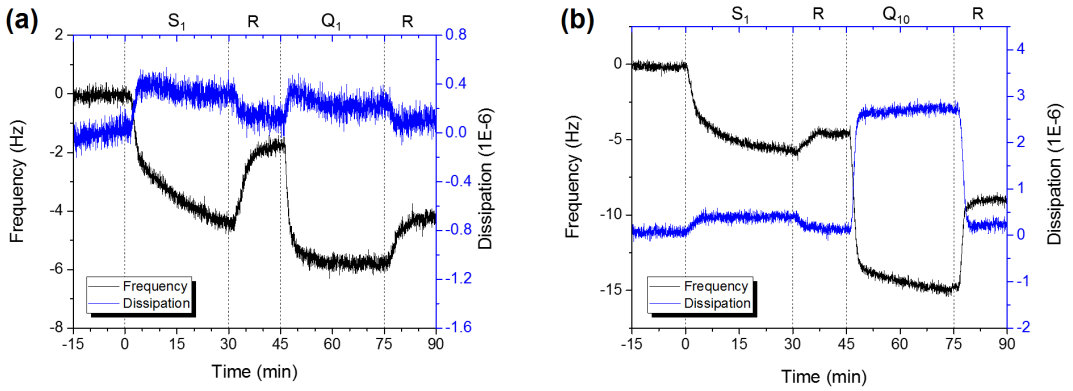

Figure 5.10: Example QCM-D f and D shifts for S_1Q_1 (a) and S_1Q_{10} (b) SiNP coating functionalisations (5^{th} overtone shown). R denotes rinsing periods.

The total relative mass (%) of SB and QAS bound to the SiNP coatings are presented in Table A.6. Evidently, functionalising surfaces first with QAS resulted in a higher proportion of surface binding, while modification with SB first offered a wider range of ratios between the two chemistries. Overall, this result highlights the ease with which dual-functionalised surfaces can be prepared and their protein resistant properties tuned through sequential exposure to SB and QAS chemistries.

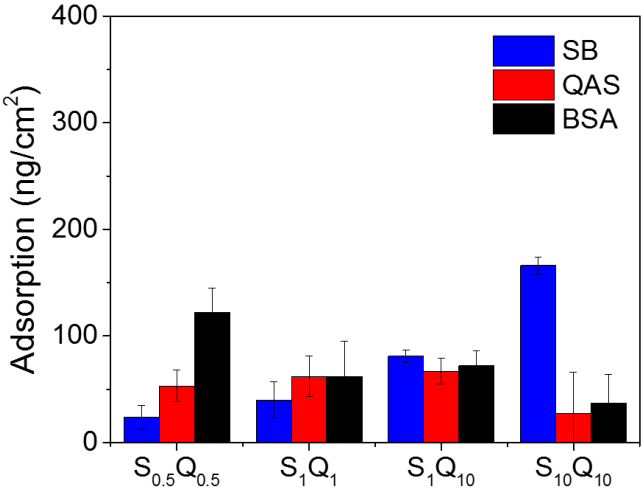

Figure 5.11: Mass modelled from the 3^{rd}, 5^{th}, and 7^{th} overtone shifts for dual-functionalisation of SiNP coatings with SB (1^{st}) and QAS (2^{nd}), and resultant protein adsorption. Error bars represent SD of the mean (n=3).

5.3.4 Bacterial Assays

Based on the results of QCM dual-functionalised SiNP coatings, several coatings were selected to assess their antibacterial properties. The following surface modifications and their approximate chemical ratios (QAS:SB) were chosen: Q_1S_1 (95:5), $Q_{10}S_{10}$ (75:25), S_1Q_1 (60:40), and $S_{10}Q_{10}$ (15:85). Comparison coatings of individually functionalised SB (S_{10}) and QAS (Q_{10}) surfaces were prepared under standard pH 9.5 conditions. Additionally, the pH dependent protein adsorption properties of QAS modified particle coatings led us to examine pH 3.5 modified QAS surfaces with neutral rinsing (Q_{10}*) and pH 9.5 rinsing (Q_{10}**). The contact angles of the prepared surfaces were measured and all were found to be appreciably hydrophilic with measured water contact angles $< 18°$ (Table A.7).

Coatings were exposed to *E. coli* for a period of 4 h, after which time surfaces were gently rinsed to remove any loosely adhered bacteria. To establish if the prepared surfaces presented antibacterial properties through cationic effect, the adhered bacteria were exposed to nucleic acid stains so that live and dead cells could be identified by fluorescence microscopy (Figure 5.12). Control (unmodified) SiNP coatings were found to have a moderate number of cells adhered to their surface with an equal ratio of live to dead cells (Figure 5.13). Surfaces functionalised with QAS (Q_{10}) saw small reductions in adhered bacteria with decreases of 22 and 50% for live and dead cells, respectively. In comparison, SB (S_{10}) functionalised surfaces generated slightly larger reductions in adhered bacteria compared to the control surface, with live and dead cell counts reduced by 80 and 60%, respectively. All surfaces presenting dual chemistries elicited dramatic reductions in the number of

adhered cells. Notably, the numbers of dead bacteria on all dual-functionalised surfaces were significantly less than the SiNP control coating (one-way ANOVA, $p < 0.05$).

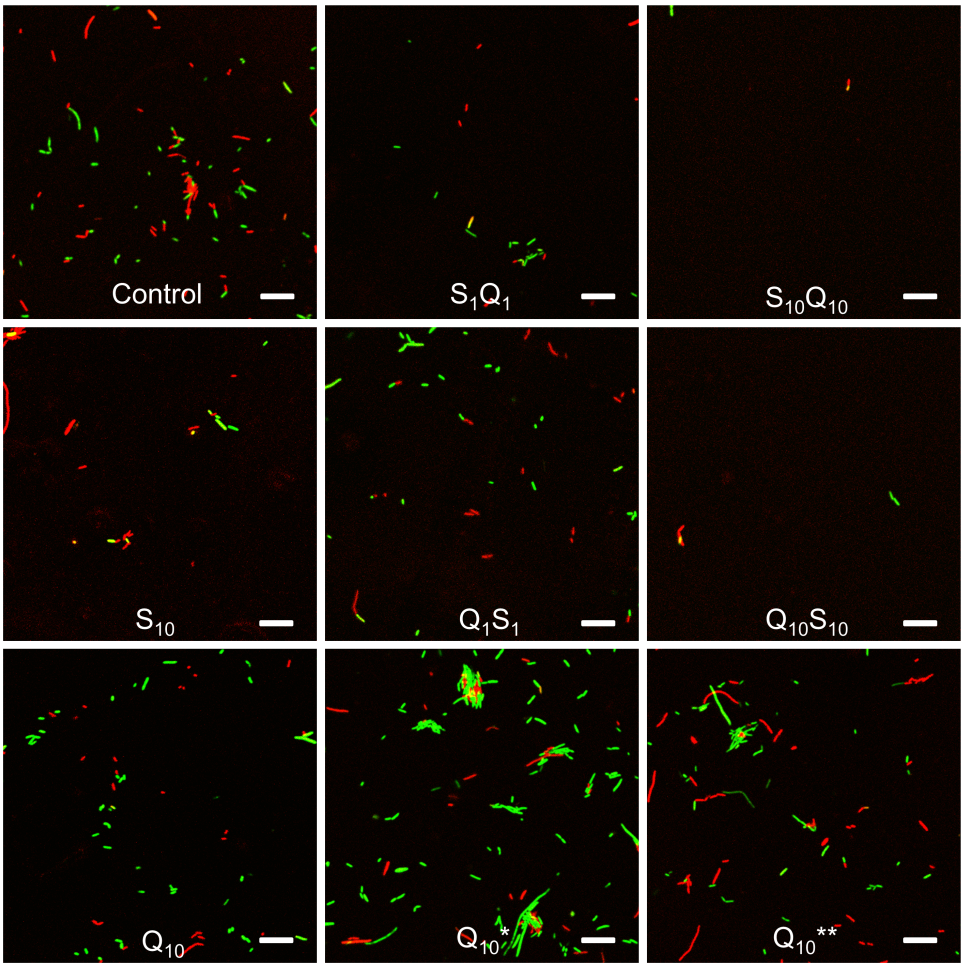

Figure 5.12: Representative fluorescence microscopy images of live (green) and dead (red) *E. coli* adhered to control (SiNP), dual-functionalised SB/QAS SiNP coatings, and individually functionalised SB and QAS SiNP coatings. Scale bars are 20 μm.

Surfaces modified at 10 mM solution concentrations provided superior resistance to adhesion than those surfaces modified at 1 mM due to increased surface functionalisation driven by higher solution concentrations. Of the 1 mM functionalised coatings, Q_1S_1 experienced a higher degree of bacterial attachment compared to S_1Q_1, mostly likely due to the lower proportion of SB chemistry present (as demonstrated by the QCM adsorption study). Regardless, all dual-functionalised surfaces produced comparable or improved resistance to bacterial adhesion compared to S_{10} and Q_{10} on their own. In particular, the dual-functionalised surfaces prepared at higher concentrations ($S_{10}Q_{10}$ and $Q_{10}S_{10}$) were exceptionally resistant to bacterial adhesion.

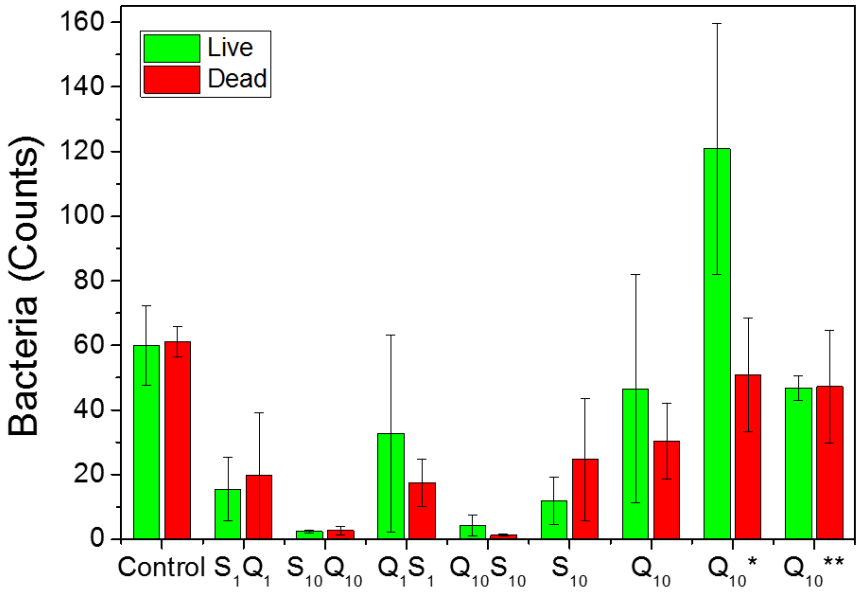

Figure 5.13: Cell counts of live and dead bacteria (*E. coli*) adhered to functionalised SiNP coatings. Error bars represent SD of the mean (n=3).

In the case of the pH 9.5 modified QAS surface (Q_{10}), a small reduction in both live and dead cells was observed compared to the SiNP control. This result was attributed to the zwitterionic character of the surface, which was earlier postulated to be responsible for this surfaces surprising resistance to protein adsorption. Functionalisation of the surface under pH 3.5 conditions (Q_{10}*) was anticipated to promote a bactericidal response at the coating interface due to reduced zwitterionic character (protonation of surface siloxide groups would result in an overall increase in cationic surface charge). Instead, an increase in the overall number of adhered bacteria was observed. It would appear that the increase in cationic surface charge also increased electrostatic interactions with the negatively charged bacterial cells but that surface charge density was not sufficient to elicit a dramatic bactericidal effect. Similar findings have been reported in a previous study, where surfaces grafted with cationic chemistries needed to exceed a charge-density threshold in order to promote bactericidal activity.[126] Consistent with protein adsorption experiments, QAS surfaces functionalised at pH 3.5 and rinsed at pH 9.5 (Q_{10}**) demonstrated a comparable level of bacterial adhesion to surfaces modified under pH 9.5 condition.

Based on both protein adsorption and bacterial adhesion results, it can be concluded that the underlying surface charge of the SiNP coating plays a vital role in antifouling activity. The adsorption of proteins to QAS modified coatings could be tuned through altering the surface charge of the particle layer to promote or suppress overall zwitterionic character. In a similar way, differences in bacterial adhesion were observed for samples modified under identical conditions (Q_{10}* & Q_{10}**) but

subjected to different rinsing treatments. What was surprising was the improved resistance to protein binding and bacterial adhesion that was presented by the dual-modified surfaces. Nanoparticle surfaces modified with zwitterionic SB alone were found to promote antifouling activity but when paired with QAS produced exceptional fouling resistance. Due to the fundamental limitation of self-assembled monolayers to functionalise all available silanol/siloxide groups on the SiNP surface, it would be anticipated that the charge at the SiNP coating interface would be made up of contributions from both the SB chemistry and unreacted negatively charged siloxide groups. These surface charges were thought to be balanced out by addition of the QAS chemistry to provide a more equal coupling of positive and negative charges (Figure 5.14). This result was consistent with a study reported by Guo et al. where zwitterionic (SBMA) and quaternary ammonium (METAC) chemistries copolymerised from silicon wafers where found to have improved resistance to protein adsorption and bacterial adhesion when the surface charge was tuned to zero.[226] In this way, the interfacial charge presented at the interface is made up of the sum of the individually charged components and thus helps to fulfill the criteria of hydrophilic antifouling materials.[188–191]

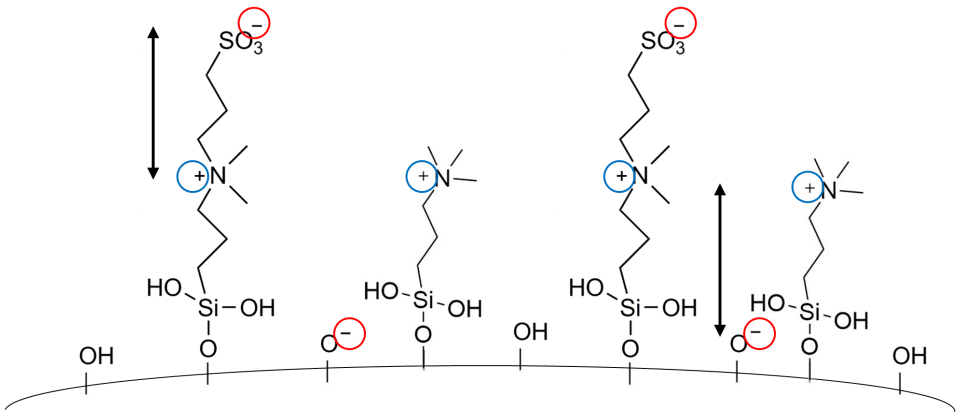

Figure 5.14: Schematic of a dual-functionalised SiNP surface illustrating contributions to surface charge from SB (+/-), QAS (+), and siloxide groups (-) at the coating interface, where charge separation between cationic and anionic groups is comparable between the zwitterionic and pseudozwitterionic systems.

5.4 Conclusions

This work sought to combine the antifouling properties of zwitterionic chemistries with the bactericidal properties presented by quaternary ammonium chemistries to provide a simple way of modifying surfaces through the application of silica nanoparticles. Instead, what was observed was the ability of the underlying surface charge to play a role in the overall fouling resistant properties of the modified surfaces. Here we have demonstrated that QAS functionalised surfaces may enhance or reduce protein adsorption and bacterial adhesion depending on the pH conditions of functionalisation and rinsing treatments. Reaction of QAS to SiNP dispersions did not offer the same control over particle properties and antifouling behaviour, indicating fundamental differences in chemistry organisation between surface and solution based particle modification. Pairing both QAS and zwitterionic SB to SiNP coatings could be conducted in a simple manner, with the ratios of chemistries controlled through functionalisation concentration and order of reaction to the surfaces. All combinations were found to reduce protein adsorption compared to unfunctionalised SiNP coatings, with higher ratios of SB generating the largest reductions in protein binding. Similarly, the largest reductions in bacterial adhesion were achieved by dual-functionalised SiNP coatings. The ease of coating preparation and the tunability of surface properties of functionalised SiNPs indicates the potential of these materials to be applied to surfaces for protection from biological fouling.

Chapter 6

Conclusions and Future Recommendations

The work presented in this thesis has detailed the development and optimisation of hydrophilic antifouling coatings using simple materials and scalable methods. Silica nanoparticles were employed as a platform material for the fabrication of antifouling coatings through their functionalisation with short chain hydrophilic chemistries. Coatings of particles could be easily prepared via a simple spin-coating technique, with coating roughness controlled through the deposition of silica nanoparticles of different size. The ability to tune coating roughness at the nanoscale could be utilised in targeted antifouling applications, where surface roughness can be tailored to minimise adhesion of target fouling species.

Simple zwitterionic and quaternary ammonium silane chemistries were able to be grafted to silica nanoparticles either before or after their deposition onto surfaces. Quartz crystal microgravimetry was employed as a tool to monitor and optimise reactions to nanoparticle coatings, and to further our understanding of protein interactions with the prepared surfaces. Functionalisation pH and silane concentration were found to control the degree of particle or surface functionalisation and play a role in chemistry organisation through the promotion of self-assembly or oligomeric type attachment mechanisms.

Coatings of zwitterion functionalised SiNPs, prepared from functionalised dispersions and surface modified films, were able to drastically improve resistance to protein adsorption, bacterial adhesion, and to some extent, fungal spore adhesion. These results indicate the potential for functionalised nanosilicas to be utilised as surface coatings for biofouling protection across a range of applications. Additionally, the nanoscaled topography introduced through the use of differently sized nanoparticles could provide another mechanism for targeted antifouling applications.

The preparation of SiNPs surfaces presenting both quaternary ammonium and zwit-

terionic chemistries did not generate the anticipated dual antimicrobial-antifouling effect, but instead provided evidence of underlying surface charge playing a role in antifouling activity. Quaternary ammonium modified SiNP coatings demonstrated surprising resistance to protein binding on their own and greatly enhanced resistance to bacterial adhesion when coupled with zwitterionic chemistries.

The promising antifouling properties of these materials, the simplicity of their preparation, and their high degree of processability could lead to their application in an industrial setting. Despite spin-coating being employed to prepare the coatings in this study, preliminary work has been conducted using spray-coating as an alternative technique to deposit SiNPs onto surfaces. Initial experiments using spray-coating as the method of coating application have generated uniform coatings with hydrophilic and antifouling properties.

In addition to the work presented in previous Chapters, several other studies were conducted during the completion of this thesis that have not been reported due to the preliminary nature of the findings. One such study investigated the protein resistant behaviours of amphiphilic SiNP coatings presenting a combination of hydrophobic and hydrophilic chemistries. It was anticipated that coatings presenting distinct hydrophilic/hydrophobic phases would disrupt the adhesion mechanism of biomacromolecules and reduce fouling. Surfaces were prepared by depositing coatings of commercially available SiNPs functionalised with a hydrophilic ligand (glycidoxypropyltrimethoxysilane) and back-filling the surface with a short chain fluorinated silane. Changes to the surface hydrophobicity and protein resistance of the coatings were highly dependent on the initial density of hydrophilic ligands prior to back-filling. Interestingly, increasing hydrophobic content did not improve the coatings antifouling performance and instead appeared to disrupt the inherent protein resistance of the underlying hydrophilic SiNP coating. Future work into the optimisation and characterisation of these amphiphilic systems would provide insight into the organisation and ratio of separated phases required to disrupt biomacromolecule adhesion mechanisms and impart antifouling properties.

The Chapters presented in this thesis have primarily concentrated on the development of simple and scalable low fouling hydrophilic coatings, however, there are many opportunities for future research to expand this body of work. Particularly, future efforts could be focused on the refinement of functionalisation techniques, determining optimal coating thickness, and optimising coating deposition to ensure minimal wastage and lower coating formulation costs. Given more time and access to equipment, it would have been beneficial to conduct more sophisticated characterisation of the functionalised SiNP coatings. Techniques such as x-ray photoelectron spectroscopy or time of flight secondary ion mass spectrometry could have been employed to confirm the mechanism of CB attachment proposed in Chapter 3 and

to confirm the chemical ratios of SB and QAS binding to the mass ratios obtained from QCM-D measurements presented in Chapter 5. Additionally, measurement of the surface zeta potential of functionalised coatings using electrokinetic analysis could have provided confirmation of the coating surface charge and contributed to the rationalisation of protein resistant behaviour.

Given the antifouling characteristics of these materials are proposed to arise from the hydrophilic properties presented at the coating interface, future work could be directed into investigating surface water structuring, utilising techniques such as frequency modulation atomic force microscopy which could provide further insight into the presence and extent of hydration layer water structuring at the interface. Furthermore, the interactions of microorganisms and their adhesion strength to the coatings could be quantified using force-curve measurements.

This thesis focused on the reaction of a limited number of chemistries to SiNPs to generate hydrophilic low fouling surface coatings. Further work could consider exploring a wider range of chemistries, investigating zwitterionic chemistries with different chain lengths, and combining different chemistries to achieve the desired surface properties. Assessment of antifouling properties could be expanded to include a wider range of proteins and adhesive organisms, with a focus on those likely to be encountered in specific coating applications. Test surfaces could also be exposed to multiple fouling species simultaneously to simulate more realistic environmental conditions. Having established the fouling resistance of these materials in the laboratory, it would be necessary to ensure that these chemistries and coatings are robust enough to withstand the environmental conditions that they may be subjected to when employed in real world applications.

To conclude, the work presented in this thesis has sought to further our understanding of hydrophilic zwitterionic, and quaternary ammonium modified silica nanoparticle coatings towards the development of platform antifouling materials. The outstanding antifouling performance demonstrated by these materials and their ease of fabrication make them a promising alternative to current commercial antifouling coating systems and could potentially lead to their utilisation as broad-spectrum antifouling coatings for widespread applications.

Bibliography

(1) S. Dürr and J. C. Thomason, *Biofouling*, Wiley, 2009.

(2) C. M. Magin, S. P. Cooper and A. B. Brennan, "Non-toxic antifouling strategies", *Mater. Today*, 2010, **13**, 36–44, DOI: 10.1016/S1369-7021(10)70058-4.

(3) B. Malhotra, A. Keshwani and H. Kharkwal, "Antimicrobial food packaging: potential and pitfalls", *Front. Microbiol.*, 2015, **6**, 1–9, DOI: 10.3389/fmicb.2015.00611.

(4) L. D. Chambers, K. R. Stokes, F. C. Walsh and R. J. K. Wood, "Modern Approaches to Marine Antifouling Coatings", *Surf. Coat. Technol.*, 2006, **201**, 3642–3652, DOI: 10.1016/j.surfcoat.2006.08.129.

(5) C. M. Grozea and G. C. Walker, *Approaches in designing non-toxic polymer surfaces to deter marine biofouling*, 2009, DOI: 10.1039/b910899h.

(6) W. J. Yang, K.-G. G. Neoh, E.-T. T. Kang, S. L.-M. M. Teo and D. Rittschof, "Polymer Brush coatings for Combating Marine Biofouling", *Prog. Polym. Sci.*, 2014, **39**, 1017–1042, DOI: 10.1016/j.progpolymsci.2014.02.002.

(7) J. A. Callow and M. E. Callow, "Trends in the Development of Environmentally Friendly Fouling-Resistant Marine Coatings", *Nat. Commun.*, 2011, **2**, 1–10, DOI: 10.1038/ncomms1251.

(8) M. P. Schultz, J. A. Bendick, E. R. Holm and W. M. Hertel, "Economic impact of biofouling on a naval surface ship", *Biofouling*, 2011, **27**, 87–98, DOI: 10.1080/08927014.2010.542809.

(9) D. M. Yebra, S. Kiil and K. Dam-Johansen, "Antifouling Technology - Past, Present and Future Steps Towards Efficient and Environmentally Friendly Antifouling Coatings", *Prog. Org. Coat.*, 2004, **50**, 75–104, DOI: 10.1016/j.porgcoat.2003.06.001.

(10) M. Lejars, A. A. Margaillan and C. Bressy, "Fouling Release Coatings: A Nontoxic Alternative to Biocidal Antifouling Coatings", *Chem. Rev.*, 2012, **112**, 4347–4390, DOI: 10.1021/cr200350v.

(11) A. Jain and N. B. Bhosle, "Biochemical composition of the marine conditioning film: Implications for bacterial adhesion", *Biofouling*, 2009, **25**, 13–19, DOI: 10.1080/08927010802411969.

(12) C. M. Kirschner and A. B. Brennan, "Bio-Inspired Antifouling Strategies", *Annu. Rev. Mater. Res.*, 2012, **42**, 211–229, DOI: 10.1146/annurev-matsci-070511-155012.

(13) E. Almeida, T. C. Diamantino and O. de Sousa, "Marine Paints: The Particular Case of Antifouling Paints", *Prog. Org. Coat.*, 2007, **59**, 2–20, DOI: 10.1016/j.porgcoat.2007.01.017.

(14) P. Stoodley, K. Sauer, D. G. Davies and J. W. Costerton, "Biofilms as Complex Differentiated Communities", *Annu. Rev. Microbiol.*, 2002, **56**, 187–209, DOI: 10.1146/annurev.micro.56.012302.160705.

(15) L. Hall-Stoodley, J. W. Costerton and P. Stoodley, "Bacterial biofilms: From the natural environment to infectious diseases", *Nat. Rev. Microbiol.*, 2004, **2**, 95–108, DOI: 10.1038/nrmicro821.

(16) J. Hoque, P. Akkapeddi, V. Yadav, G. B. Manjunath, D. S. Uppu, M. M. Konai, V. Yarlagadda, K. Sanyal and J. Haldar, "Broad Spectrum Antibacterial and Antifungal Polymeric Paint Materials: Synthesis, Structure-Activity Relationship, and Membrane-Active Mode of Action", *ACS Appl. Mater. Inter*, 2015, **7**, 1804–1815, DOI: 10.1021/am507482y.

(17) R. M. Klevens, J. R. Edwards, C. L. Richards, T. C. Horan, R. P. Gaynes, D. A. Pollock and D. M. Cardo, "Estimating Health Care-Associated Infections and Deaths in U.S. Hospitals, 2002", *Public Health Rep.*, 2007, **122**, 160–166, DOI: 10.1177/003335490712200205.

(18) K. Vasilev, J. Cook and H. J. Griesser, "Antibacterial surfaces for biomedical devices", *Expert Rev. Med. Devices*, 2009, **6**, 553–567, DOI: 10.1586/erd.09.36.

(19) N. Hadjesfandiari, K. Yu, Y. Mei and J. N. Kizhakkedathu, "Polymer Brush-Based Approaches for the Development of Infection-Resistant Surfaces", *J. Mater. Chem. B*, 2014, **2**, 4968–4978, DOI: 10.1039/c4tb00550c.

(20) D. Campoccia, L. Montanaro and C. R. Arciola, "The significance of infection related to orthopedic devices and issues of antibiotic resistance", *Biomaterials*, 2006, **27**, 2331–2339, DOI: 10.1016/j.biomaterials.2005.11.044.

(21) I. Kwiecień, G. Adamus, A. Bartkowiak and M. Kowalczuk, "Synthesis and structural characterization at the molecular level of oligo(3-hydroxybutyrate) conjugates with antimicrobial agents designed for food packaging materials", *Des. Monomers Polym.*, 2014, **17**, 311–321, DOI: 10.1080/15685551.2013.840505.

(22) P. Appendini and J. H. Hotchkiss, "Review of antimicrobial food packaging", *Innov. Food Sci. Emerg. Technol.*, 2002, **3**, 113–126, DOI: 10.1016/S1466-8564(02)00012-7.

(23) E. P. Ivanova and R. J. Crawford, *Antibacterial Surfaces*, Springer International Publishing, 2015.

(24) C. von Eiff, G. Peters and C. Heilmann, "Pathogenesis of infections due to coagulase-negative staphylococci", *Lancet Infect. Dis.*, 2002, **2**, 677–685, DOI: 10.1016/S1473-3099(02)00438-3.

(25) M. Salwiczek, Y. Qu, J. Gardiner, R. A. Strugnell, T. Lithgow, K. M. McLean and H. Thissen, "Emerging rules for effective antimicrobial coatings", *Trends Biotechnol.*, 2014, **32**, 82–90, DOI: 10.1016/j.tibtech.2013.09.008.

(26) I. Behlau and M. S. Gilmore, "Microbial biofilms in ophthalmology and infectious disease", *Arch. Ophthalmol.*, 2008, **126**, 1572–1581, DOI: 10.1001/archopht.126.11.1572.

(27) M. B. Miller and B. L. Bassler, "Quorum Sensing in Bacteria", *Annu. Rev. Microbiol.*, 2001, **55**, 165–99, DOI: 10.1146/annurev.micro.55.1.165.

(28) R. M. Donlan, "Biofilm Formation: A Clinically Relevant Microbiological Process", *Clin. Infect. Dis.*, 2001, **33**, 1387–1392, DOI: 10.1086/322972.

(29) M. W. Harding, L. L. Marques, R. J. Howard and M. E. Olson, "Can Filamentous Fungi Form Biofilms?", *Trends Microbiol.*, 2009, **17**, 475–480, DOI: 10.1016/j.tim.2009.08.007.

(30) K. Glinel, P. Thebault, V. Humblot, C. M. Pradier and T. Jouenne, "Antibacterial surfaces developed from bio-inspired approaches", *Acta Biomater.*, 2012, **8**, 1670–1684, DOI: 10.1016/j.actbio.2012.01.011.

(31) H. R. Ravikumar, S. S. Rao and C. S. Karigar, "Biodegradation of paints: A current status", *Indian J. Sci. Technol.*, 2012, **5**, 1977–1987, DOI: 10.17485/IJST/2012/V5I1/30969.

(32) V. Wiktor, F. De Leo, C. Urzì, R. Guyonnet, P. Grosseau and E. Garcia-Diaz, "Accelerated laboratory test to study fungal biodeterioration of cementitious matrix", *Int. Biodeterior. Biodegrad.*, 2009, **63**, 1061–1065, DOI: 10.1016/j.ibiod.2009.09.004.

(33) K. L. Garg, K. K. Jain and A. K. Mishra, "Role of fungi in the deterioration of wall paintings", *Sci. Total Environ.*, 1995, **167**, 255–271, DOI: 10.1016/0048-9697(95)04587-Q.

(34) C. Gaylarde, A. Otlewska, S. Celikkol-Aydin, J. Skóra, M. Sulyok, K. Pielech-przybylska, J. Gillatt, I. Beech and B. Gutarowska, "Interactions between fungi of standard paint test method BS3900", *Int. Biodeterior. Biodegrad.*, 2015, **104**, 411–418, DOI: 10.1016/j.ibiod.2015.07.010.

(35) A. T. Fazio, L. Papinutti, B. A. Gómez, S. D. Parera, A. Rodríguez Romero, G. Siracusano and M. S. Maier, "Fungal deterioration of a Jesuit South American polychrome wood sculpture", *Int. Biodeterior. Biodegrad. Biodegrad.*, 2010, **64**, 694–701, DOI: 10.1016/j.ibiod.2010.04.012.

(36) D. Lognoli, G. Lamenti, L. Pantani, D. Tirelli and L. Tomaselli, EUROPTO Conference on Remote Sensing for Earth Science Applications, 1999, pp. 339–346.

(37) K. Sterflinger, "Fungi: Their Role in Deterioration of Cultural Heritage", *Fungal Biol. Rev.*, 2010, **24**, 47–55, DOI: 10.1016/j.fbr.2010.03.003.

(38) G. M. Gadd and T. D. Dyer, "Bioprotection of the built environment and cultural heritage", *Microb. Biotechnol.*, 2017, **10**, 1152–1156, DOI: 10.1111/1751-7915.12750.

(39) G. M. Gadd, "Geomicrobiology of the built environment", *Nat. Microbiol.*, 2017, **2**, 16275, DOI: 10.1038/nmicrobiol.2016.275.

(40) M. A. Shirakawa, A. P. Werle, C. C. Gaylarde, K. Loh and V. M. John, "Fungal and phototroph growth on fiber cement roofs and its influence on solar reflectance in a tropical climate", *Int. Biodeterior. Biodegrad.*, 2014, **95**, 332–337, DOI: 10.1016/j.ibiod.2013.12.003.

(41) R. Levinson and H. Akbari, "Potential benefits of cool roofs on commercial buildings: conserving energy, saving money, and reducing emission of greenhouse gases and air pollutants", *Energy Effic.*, 2009, **3**, 53–109, DOI: 10.1007/s12053-008-9038-2.

(42) S. L. Tucker and N. J. Talbot, "Surface attachment and pre-penetration stage development by plant pathogenic fungi", *Annu. Rev. Phytopathol.*, 2001, **39**, 385–417, DOI: 10.1146/annurev.phyto.39.1.385.

(43) L. Epstein and R. L. Nicholson, "Adhesion of spores and hyphae to plant surfaces", *Plant Relationships*, 1997, 11–25, DOI: 10.1007/978-3-662-10370-8_2.

(44) L. Heaton, B. Obara, V. Grau, N. Jones, T. Nakagaki, L. Boddy and M. D. Fricker, "Analysis of fungal networks", *Fungal Biol. Rev.*, 2012, **26**, 12–29, DOI: 10.1016/j.fbr.2012.02.001.

(45) S. D. Harris, "Branching of fungal hyphae: regulation, mechanisms and comparison with other branching systems", *Mycologia*, 2008, **100**, 823–832, DOI: 10.3852/08-177.

(46) United States Naval Institute, *Marine Fouling and its Prevention*, tech. rep. 580, 1952.

(47) A. G. Nurioglu and A. C. C. Esteves, "Non-toxic, non-biocide-release antifouling coatings based on molecular structure design for marine applications", *J. Mater. Chem. B*, 2015, **3**, 6547–6570, DOI: 10.1039/c5tb00232j.

(48) I. Banerjee, R. C. Pangule and R. S. Kane, "Antifouling Coatings: Recent Developments in the Design of Surfaces that Prevent Fouling by Proteins, Bacteria, and Marine Organisms", *Adv. Mater.*, 2011, **23**, 690–718, DOI: 10.1002/adma.201001215.

(49) I. Omae, "Organotin antifouling paints and their alternatives", *Appl. Organomet. Chem.*, 2003, **17**, 81–105, DOI: 10.1002/aoc.396.

(50) J. Oehlmann, P. Fioroni, E. Stroben and B. Markert, "Tributyltin (TBT) effects on Ocinebrina aciculata (Gastropoda: Muricidae): imposex development, sterilization, sex change and population decline", *Sci. Total Environ.*, 1996, **188**, 205–223, DOI: 10.1016/0048-9697(96)05173-X.

(51) M. H. Salazar and S. M. Salazar, "Assessing site-specific effects of TBT contamination with mussel growth rates", *Mar. Environ. Res.*, 1991, **32**, 131–150, DOI: 10.1016/0141-1136(91)90038-A.

(52) J. E. Thain, *Toxicity of TBT to Bivalves: Effects on Reproduction, Growth and Survival.* Tech. rep., 1986, pp. 1306–1313, DOI: 10.1109/OCEANS.1986.1160370.

(53) M. A. Champ, "Economic and environmental impacts on ports and harbors from the convention to ban harmful marine anti-fouling systems", *Mar. Pollut. Bull.*, 2003, **46**, 935–940, DOI: 10.1016/S0025-326X(03)00106-1.

(54) N. Voulvoulis, M. D. Scrimshaw and J. N. Lester, "Alternative antifouling biocides", *Appl. Organomet. Chem.*, 1999, **13**, 135–143, DOI: 10.1002/(SICI)1099-0739(199903)13:3<135::AID-AOC831>3.0.CO;2-G.

(55) I. Fitridge, T. Dempster, J. Guenther, R. de Nys and R. D. Nys, "The Impact and Control of Biofouling in Marine Aquaculture: A Review", *Biofouling*, 2012, **28**, 649–669, DOI: 10.1080/08927014.2012.700478.

(56) P. Buskens, M. Wouters, C. Rentrop and Z. Vroon, "A brief review of environmentally benign antifouling and foul-release coatings for marine applications", *J. Coatings Technol. Res.*, 2013, **10**, 29–36, DOI: 10.1007/s11998-012-9456-0.

(57) I. K. Konstantinou and T. A. Albanis, "Worldwide occurrence and effects of antifouling paint booster biocides in the aquatic environment: a review", *Environ. Int.*, 2004, **30**, 235–248, DOI: http://dx.doi.org/10.1016/S0160-4120(03)00176-4.

(58) K. V. Thomas, M. McHugh and M. Waldock, "Antifouling paint booster biocides in UK coastal waters: inputs, occurrence and environmental fate", *Sci. Total Environ.*, 2002, **293**, 117–127, DOI: 10.1016/S0048-9697(01)01153-6.

(59) S. M. Evans, a. C. Birchenough and M. S. Brancato, "The TBT Ban: Out of the Frying Pan into the Fire?", *Mar. Pollut. Bull.*, 2000, **40**, 204–211, DOI: 10.1016/S0025-326X(99)00248-9.

(60) M. Danaher, H. De Ruyck, S. R. H. Crooks, G. Dowling, M. O'Keeffe and M. O'Keeffe, "Review of methodology for the determination of benzimidazole residues in biological matrices", *J. Chromatogr. B*, 2007, **845**, 1–37, DOI: 10.1016/j.jchromb.2006.07.046.

(61) C. Cacho, E. Turiel and C. Pérez-Conde, "Molecularly imprinted polymers: An analytical tool for the determination of benzimidazole compounds in water samples", *Talanta*, 2009, **78**, 1029–1035, DOI: 10.1016/j.talanta.2009.01.007.

(62) M. Lezcano, W. Al-Soufi, M. Novo, E. Rodríguez-Núñez and J. Vázquez Tato, "Complexation of several benzimidazole-type fungicides with α- and β-cyclodextrins", *J. Agric. Food Chem.*, 2002, **50**, 108–112, DOI: 10.1021/jf010927y.

(63) B. Tang, X. Wang, H. Liang, B. Jia and Z. Chen, "Study on the supramolecular interaction of thiabendazole and β-cyclodextrin by spectrophotometry and its analytical application", *J. Agric. Food Chem.*, 2005, **53**, 8452–8459, DOI: 10.1021/jf051683a.

(64) A. Bernardos, T. Marina, P. Zacek, E. Perez-Esteve, R. Martinez-Manez, M. Lhotka, L. Kourimska, J. Pulkrabek and P. Kloucek, "Antifungal effect of essential oil components against Aspergillus niger when loaded into silica mesoporous supports", *J. Sci. Food Agric.*, 2015, **95**, 2824–2831, DOI: 10.1002/jsfa.7022.

(65) A. Janatova, A. Bernardos, J. Smid, A. Frankova, M. Lhotka, L. Kourimská, J. Pulkrabek and P. Kloucek, "Long-term antifungal activity of volatile essential oil components released from mesoporous silica materials", *Ind. Crops Prod.*, 2015, **67**, 216–220, DOI: 10.1016/j.indcrop.2015.01.019.

(66) D. Campoccia, L. Montanaro and C. R. Arciola, "A Review of the Biomaterials Technologies for Infection-Resistant Surfaces", *Biomaterials*, 2013, **34**, 8533–8554, DOI: 10.1016/j.biomaterials.2013.07.089.

(67) W. Kohnen, C. Kolbenschlag, S. Teske-Keiser and B. Jansen, "Development of a Long-lasting Ventricular Catheter Impregnated with a Combination of Antibiotics", *Biomaterials*, 2003, **24**, 4865–4869, DOI: 10.1016/S0142-9612(03)00379-X.

(68) N. Aumsuwan, S. Heinhorst and M. W. Urban, "Antibacterial Surfaces on Expanded Polytetrafluoroethylene; Penicillin Attachment", *Biomacromolecules*, 2007, **8**, 713–718, DOI: 10.1021/bm061050k.

(69) N. Aumsuwan, S. Heinhorst and M. W. Urban, "The effectiveness of antibiotic activity of penicillin attached to expanded poly (tetrafluoroethylene)(ePTFE) surfaces: a quantitative assessment", *Biomacromolecules*, 2007, **8**, 3525–3530, DOI: 10.1021/bm700803e.

(70) N. Aumsuwan, R. C. Danyus, S. Heinhorst and M. W. Urban, "Attachment of Ampicillin to Expanded Poly (tetrafluoroethylene): Surface Reactions Leading to Inhibition of Microbial Growth", *Biomacromolecules*, 2008, **9**, 1712–1718.

(71) H. F. Chuang, R. C. Smith and P. T. Hammond, "Polyelectrolyte Multilayers for Tunable Release of Antibiotics", *Biomacromolecules*, 2008, **9**, 1660–1668, DOI: 10.1021/bm800185h.

(72) F. Wu, G. Meng, J. He, Y. Wu, F. Wu and Z. Gu, "Antibiotic-Loaded Chitosan Hydrogel with Superior Dual Functions: Antibacterial Efficacy and Osteoblastic Cell Responses", *ACS Appl. Mater. Interfaces*, 2014, **6**, 10005–10013, DOI: 10.1021/am502537k.

(73) T.-F. C. Mah and G. A. O'Toole, "Mechanisms of biofilm resistance to antimicrobial agents", *Trends Microbiol.*, 2001, **9**, 34–39, DOI: 10.1016/S0966-842X(00)01913-2.

(74) J. A. Lemire, J. J. Harrison and R. J. Turner, "Antimicrobial Activity of Metals: Mechanisms, Molecular targets and Applications", *Nat. Rev. Microbiol.*, 2013, **11**, 371–384, DOI: 10.1038/nrmicro3028.

(75) J. J. Harrison, H. Ceri, C. A. Stremick and R. J. Turner, "Biofilm susceptibility to metal toxicity", *Environ. Microbiol.*, 2004, **6**, 1220–1227, DOI: 10.1111/j.1462-2920.2004.00656.x.

(76) G. Borkow and J. Gabbay, "Copper, an ancient remedy returning to fight microbial, fungal and viral infections", *Curr. Chem. Biol.*, 2009, **3**, 272–278, DOI: 10.2174/187231309789054887.

(77) G. Grass, C. Rensing and M. Solioz, "Metallic copper as an antimicrobial surface", *Appl. Environ. Microbiol.*, 2011, **77**, 1541–1547, DOI: 10.1128/AEM.02766-10.

(78) P. H. Beswick, G. H. Hall, A. J. Hook, K. Little, D. C. McBrien and K. A. Lott, "Copper toxicity: evidence for the conversion of cupric to cuprous copper in vivo under anaerobic conditions", *Chem.-Biol. Interact.*, 1976, **14**, 347–356, DOI: 10.1016/0009-2797(76)90103-4.

(79) S. Mathews, R. Kumar and M. Solioz, "Copper Reduction and Contact Killing of Bacteria by Iron Surfaces", *Appl. Environ. Microbiol.*, 2015, **81**, 6399–6403, DOI: 10.1128/AEM.01725-15.

(80) B. Halliwell and J. M. C. Gutteridge, "Oxygen toxicity, oxygen radicals, transition metals and disease", *Biochem. J.*, 1984, **219**, 1–14, DOI: 10.1042/bj2190001.

(81) P. R. Chetana, B. S. Srinatha, M. N. Somashekar and R. S. Policegoudra, "Synthesis, spectroscopic characterisation, thermal analysis, DNA interaction and antibacterial activity of copper(I) complexes with N, N'- disubstituted thiourea", *J. Mol. Struct.*, 2016, **1106**, 352–365, DOI: 10.1016/j.molstruc.2015.10.010.

(82) S. L. Warnes, S. M. Green, H. T. Michels and C. W. Keevil, "Biocidal efficacy of copper alloys against pathogenic enterococci involves degradation of genomic and plasmid DNAs", *Appl. Environ. Microbiol.*, 2010, **76**, 5390–5401, DOI: 10.1128/AEM.03050-09.

(83) C. E. Santo, E. W. Lam, C. G. Elowsky, D. Quaranta, D. W. Domaille, C. J. Chang and G. Grass, "Bacterial Killing by Dry Metallic Copper Surfaces", *Appl. Environ. Microbiol.*, 2011, **77**, 794–802, DOI: 10.1128/AEM.01599-10.

(84) C. E. Santo, D. Quaranta, G. Grass, C. Esp, D. Quaranta and G. Grass, "Antimicrobial metallic copper surfaces kill Staphylococcus haemolyticus via membrane damage", *Microbiol. Open*, 2012, **1**, 46–52, DOI: 10.1002/mbo3.2.

(85) Y. L. Ma, B. Yang, T. Guo and L. Xie, "Antibacterial mechanism of Cu2+-ZnO/cetylpyridinium-montmorillonite in vitro", *Appl. Clay Sci.*, 2010, **50**, 348–353, DOI: 10.1016/j.clay.2010.08.025.

(86) M. Rai, A. Yadav and A. Gade, "Silver nanoparticles as a new generation of antimicrobials", *Biotechnol. Adv.*, 2009, **27**, 76–83, DOI: 10.1016/j.biotechadv.2008.09.002.

(87) T. V. Duncan, "Applications of nanotechnology in food packaging and food safety: Barrier materials, antimicrobials and sensors", *J. Colloid Interface Sci.*, 2011, **363**, 1–24, DOI: 10.1016/j.jcis.2011.07.017.

(88) N. Cioffi, L. Torsi, N. Ditaranto, G. Tantillo, L. Ghibelli, L. Sabbatini, T. Bleve-Zacheo, M. D'Alessio, P. G. Zambonin and E. Traversa, "Copper Nanoparticle/Polymer Composites with Antifungal and Bacteriostatic Properties", *Chem. Mater.*, 2005, **17**, 5255–5262, DOI: 10.1021/cm0505244.

(89) E. P. Ivanova, J. Hasan, V. K. Truong, J. Y. Wang, M. Raveggi, C. Fluke and R. J. Crawford, "The influence of nanoscopically thin silver films on bacterial viability and attachment", *Appl. Microbiol. Biotechnol.*, 2011, **91**, 1149–1157, DOI: 10.1007/s00253-011-3195-5.

(90) J. L. Clement and P. S. Jarrett, "Antibacterial Silver", *Met.-Based Drugs*, 1994, **1**, 467–482, DOI: 10.1155/MBD.1994.467.

(91) O. Gordon, T. V. Slenters, P. S. Brunetto, A. E. Villaruz, D. E. Sturdevant, M. Otto, R. Landmann and K. M. Fromm, "Silver coordination polymers for prevention of implant infection: thiol interaction, impact on respiratory chain enzymes, and hydroxyl radical induction", *Antimicrob. Agents Chemother.*, 2010, **54**, 4208–4218, DOI: 10.1128%2FAAC.01830-09.

(92) Q. L. Feng, J. Wu, G. Q. Chen, F. Z. Cui, T. N. Kim and J. O. Kim, "A mechanistic study of the antibacterial effect of silver ions on Escherichia coli and Staphylococcus aureus", *J. Biomed. Mater. Res.*, 2000, **52**, 662–668, DOI: 10.1002/1097-4636(20001215)52:43.0.CO;2-3.

(93) J. R. Morones, J. L. Elechiguerra, A. Camacho, K. Holt, J. B. Kouri, J. T. Ramirez and M. J. Yacaman, "The bactericidal effect of silver nanoparticles", *Nanotechnology*, 2005, **16**, 2346–2353, DOI: 10.1088/0957-4484/16/10/059.

(94) Rahisuddin, S. A. Al-Thabaiti, Z. Khan, N. Manzoor, R. Shaeel, A. A.-t. Zaheer and K. Nikhat, "Biosynthesis of silver nanoparticles and its antibacterial and antifungal activities towards Gram-positive, Gram-negative bacterial strains and different species of Candida fungus", *Bioprocess Biosyst. Eng.*, 2015, **38**, 1773–1781, DOI: 10.1007/s00449-015-1418-3.

(95) I. Sondi and B. Salopek-Sondi, "Silver nanoparticles as antimicrobial agent: a case study on E. coli as a model for Gram-negative bacteria", *J. Colloid Interface Sci.*, 2004, **275**, 177–182, DOI: 10.1016/j.jcis.2004.02.012.

(96) C. Damm and H. Münstedt, "Kinetic aspects of the silver ion release from antimicrobial polyamide/silver nanocomposites", *Appl. Phys. A*, 2008, **91**, 479–486, DOI: 10.1007/s00339-008-4434-1.

(97) Z.-m. Xiu, Q.-b. Zhang, H. L. Puppala, V. L. Colvin and P. J. J. Alvarez, "Negligible particle-specific antibacterial activity of silver nanoparticles", *Nano Lett.*, 2012, **12**, 4271–4275, DOI: 10.1021/nl301934w.

(98) K. Loza, J. Diendorf, C. Sengstock, L. Ruiz-Gonzalez, J. M. Gonzalez-Calbet, M. Vallet-Regi, M. Köller and M. Epple, "The dissolution and biological effects of silver nanoparticles in biological media", *J. Mater. Chem. B*, 2014, **2**, 1634, DOI: 10.1039/c3tb21569e.

(99) F. Furno, K. S. Morley, B. Wong, B. L. Sharp, P. L. Arnold, S. M. Howdle, R. Bayston, P. D. Brown, P. D. Winship and H. J. Reid, "Silver nanoparticles and polymeric medical devices: a new approach to prevention of infection?", *J. Antimicrob. Chemother.*, 2004, **54**, 1019–1024, DOI: 10.1093/jac/dkh478.

(100) N. Alissawi, V. Zaporojtchenko, T. Strunskus, T. Hrkac, I. Kocabas, B. Erkartal, V. S. K. Chakravadhanula, L. Kienle, G. Grundmeier and D. Garbe-Schönberg, "Tuning of the ion release properties of silver nanoparticles buried under a hydrophobic polymer barrier", *J. Nanoparticle Res.*, 2012, **14**, 1–12, DOI: 10.1007/s11051-012-0928-z.

(101) M. Banach, "Building Materials with Antifungal Efficacy Enriched with Silver Nanoparticles", *Chem. Sci. J.*, 2014, **5**, 1–5, DOI: 10.4172/2150-3494.1000085.

(102) S. Silver, L. T. Phung and G. Silver, "Silver as biocides in burn and wound dressings and bacterial resistance to silver compounds", *J. Ind. Microbiol. Biotechnol.*, 2006, **33**, 627–634, DOI: 10.1007/s10295-006-0139-7.

(103) I. Chopra, "The increasing use of silver-based products as antimicrobial agents: a useful development or a cause for concern?", *J. Antimicrob. Chemother.*, 2007, **59**, 587–590, DOI: 10.1093/jac/dkm006.

(104) P. Kanhed, S. Birla, S. Gaikwad, A. Gade, A. B. Seabra, O. Rubilar, N. Duran and M. Rai, "In vitro antifungal efficacy of copper nanoparticles against selected crop pathogenic fungi", *Mater. Lett.*, 2014, **115**, 13–17, DOI: 10.1016/j.matlet.2013.10.011.

(105) N. Cioffi, L. Torsi, N. Ditaranto, L. Sabbatini, P. G. Zambonin, G. Tantillo, L. Ghibelli, M. D'Alessio, T. Bleve-Zacheo, E. Traversa, M. D'Alessio, T. Bleve-Zacheo and E. Traversa, "Antifungal activity of polymer-based copper nanocomposite coatings", *Appl. Phys. Lett.*, 2004, **85**, 2417, DOI: 10.1063/1.1794381.

(106) L. Sintubin, B. De Gusseme, P. Van Der Meeren, B. F. G. Pycke, W. Verstraete and N. Boon, "The antibacterial activity of biogenic silver and its mode of action", *Appl. Microbiol. Biotechnol.*, 2011, **91**, 153–162, DOI: 10.1007/s00253-011-3225-3.

(107) N. Bellotti, R. Romagnoli, C. Quintero, C. Domínguez-Wong, F. Ruiz and C. Deyá, "Nanoparticles as Antifungal Additives for Indoor Water Borne Paints", *Prog. Org. Coat.*, 2015, **86**, 33–40, DOI: 10.1016/j.porgcoat.2015.03.006.

(108) H. L. Huang, C. C. Lin and K. Hsu, "Comparison of resistance improvement to fungal growth on green and conventional building materials by nano-metal impregnation", *Build. Environ.*, 2015, **93**, 119–127, DOI: 10.1016/j.buildenv.2015.06.016.

(109) H. A. Foster, I. B. Ditta, S. Varghese and A. Steele, "Photocatalytic disinfection using titanium dioxide: spectrum and mechanism of antimicrobial activity", *Appl. Microbiol. Biotechnol.*, 2011, **90**, 1847–1868, DOI: 10.1007/s00253-011-3213-7.

(110) F. Hossain, O. J. Perales-perez, S. Hwang and F. Román, "Antimicrobial nanomaterials as water disinfectant: Applications, limitations and future perspectives", *Sci. Total Environ.*, 2014, **466-467**, 1047–1059, DOI: 10.1016/j.scitotenv.2013.08.009.

(111) S. Kim, K. Ghafoor, J. Lee, M. Feng, J. Hong, D. U. Lee and J. Park, "Bacterial inactivation in water, DNA strand breaking, and membrane damage induced by ultraviolet-assisted titanium dioxide photocatalysis", *Water Res.*, 2013, **47**, 4403–4411, DOI: 10.1016/j.watres.2013.05.009.

(112) M. Cho, H. Chung, W. Choi and J. Yoon, "Linear correlation between inactivation of E. coli and OH radical concentration in TiO2 photocatalytic disinfection", *Water Res.*, 2004, **38**, 1069–1077, DOI: 10.1016/j.watres.2003.10.029.

(113) D. Gerrity, H. Ryu, J. Crittenden and M. Abbaszadegan, "Photocatalytic inactivation of viruses using titanium dioxide nanoparticles and low-pressure UV light", *J. Environ. Sci. Heal. Part A*, 2008, **43**, 1261–1270, DOI: 10.1080/10934520802177813.

(114) O. Seven, B. Dindar, S. Aydemir, D. Metin, M. A. Ozinel and S. Icli, "Solar photocalytic disinfection of a group of bacteria and fungi aqueous suspensions with TiO2, ZnO and sahara desert dust", *J. Photochem. Photobiol. A Chem.*, 2004, **165**, 103–107, DOI: 10.1016/j.jphotochem.2004.03.005.

(115) F. Chen, X. Yang and Q. Wu, "Antifungal capability of TiO2 coated film on moist wood", *Build. Environ.*, 2009, **44**, 1088–1093, DOI: 10.1016/j.buildenv.2008.07.018.

(116) S. B. Vucetic, O. Rudic, S. L. Markov, O. J. Bera, A. M. Vidakovic, A. S. Skapin and J. G. Ranogajec, "Antifungal efficiency assessment of the TiO2 coating on facade paints", *Environ. Sci. Pollut. Res.*, 2014, **21**, 11228–11237, DOI: 10.1007/s11356-014-3066-6.

(117) C. Chawengkijwanich and Y. Hayata, "Development of TiO2 powder-coated food packaging film and its ability to inactivate Escherichia coli in vitro and in actual tests", *Int. J. Food Microbiol.*, 2008, **123**, 288–292, DOI: 10.1016/j.ijfoodmicro.2007.12.017.

(118) K. Dai, D. Li, L. Lu, Q. Liu, C. Liang, J. Lv and G. Zhu, "Plasmonic TiO2/AgBr/Ag ternary composite nanosphere with heterojunction structure for advanced visible light photocatalyst", *Appl. Surf. Sci.*, 2014, **314**, 864–871, DOI: 10.1016/j.apsusc.2014.06.183.

(119) P. K. Jain, X. Huang, I. H. El-Sayed and M. A. El-Sayed, "Noble Metals on the Nanoscale: Optical and Photothermal Properties and Some Applications in Imaging, Sensing, Biology, and Medicine", *Acc. Chem. Res.*, 2008, **41**, 1578–1586, DOI: 10.1002/chin.200914223.

(120) J. Ma, Z. Xiong, T. David Waite, W. J. Ng and X. S. Zhao, "Enhanced inactivation of bacteria with silver-modified mesoporous TiO2 under weak ultraviolet irradiation", *Microporous Mesoporous Mater.*, 2011, **144**, 97–104, DOI: 10.1016/j.micromeso.2011.03.040.

(121) J. A. Lichter, K. J. Van Vliet and M. F. Rubner, "Design of Antibacterial Surfaces and Interfaces: Polyelectrolyte Multilayers as a Multifunctional Platform", *Macromolecules*, 2009, **42**, 8573–8586, DOI: 10.1021/ma901356s.

(122) J. Meng, X. Zhang, L. Ni, Z. Tang, Y. Zhang, Y. Zhang and W. Zhang, "Antibacterial cellulose membrane via one-step covalent immobilization of ammonium/amine groups", *Desalination*, 2015, **359**, 156–166, DOI: 10.1016/j.desal.2014.12.032.

(123) M. Charnley, M. Textor and C. Acikgoz, "Designed polymer structures with antifouling-antimicrobial properties", *React. Funct. Polym.*, 2011, **71**, 329–334, DOI: 10.1016/j.reactfunctpolym.2010.10.013.

(124) J. Hasan, R. J. Crawford and E. P. Ivanova, "Antibacterial surfaces: the quest for a new generation of biomaterials", *Trends Biotechnol.*, 2013, **31**, 295–304, DOI: 10.1016/j.tibtech.2013.01.017.

(125) J. C. Tiller, C.-J. Liao, K. Lewis and A. M. Klibanov, "Designing surfaces that kill bacteria on contact", *Proc. Natl. Acad. Sci.*, 2001, **98**, 5981–5985.

(126) R. Kügler, O. Bouloussa and F. Rondelez, "Evidence of a charge-density threshold for optimum efficiency of biocidal cationic surfaces", *Microbiology*, 2005, **151**, 1341–1348, DOI: 10.1099/mic.0.27526-0.

(127) H. Murata, R. R. Koepsel, K. Matyjaszewski and A. J. Russell, "Permanent, Non-leaching Antibacterial Surfaces 2: How High Density Cationic Surfaces Kill Bacterial Cells", *Biomaterials*, 2007, **28**, 4870–4879, DOI: 10.1016/j.biomaterials.2007.06.012.

(128) C. E. Codling, J. Y. Maillard and A. D. Russell, "Aspects of the Antimicrobial Mechanisms of Action of a Polyquaternium and an Amidoamine", *J. Antimicrob. Chemother.*, 2003, **51**, 1153–1158, DOI: 10.1093/jac/dkg228.

(129) B. Ahlström, M. Chelminska-Bertilsson, R. A. Thompson and L. Edebo, "Submicellar Complexes May Initiate the Fungicidal Effects of Cationic Amphiphilic Compounds on Candida albicans", *Antimicrob. Agents Chemother.*, 1997, **41**, 544–550, DOI: 10.1128/AAC.41.3.544.

(130) D. B. Vieira and A. M. Carmona-Ribeiro, "Cationic lipids and surfactants as antifungal agents: mode of action", *J. Antimicrob. Chemother.*, 2006, **58**, 760–767, DOI: 10.1093/jac/dkl312.

(131) Y. Park, M.-H. Kim, S.-C. Park, H. Cheong, M.-K. Jang, J.-W. Nah and K.-S. Hahm, "Investigation of the antifungal activity and mechanism of action of LMWS-chitosan", *J. Microbiol. Biotechnol.*, 2008, **18**, 1729–1734.

(132) B. M. El-Sadek and N. City, "Synthesis, Micellization and Hemolysis Evaluation of Biodegradable quaternary Ammonium Compounds", *Adv. Appl. Sci. Res.*, 2011, **2**, 363–372.

(133) T. Vladkova, "Surface Engineering for Non-Toxic Biofouling Control (Review)", *J. Univ. Chem. Technol. Metall.*, 2007, **42**, 239–256.

(134) R. E. Baier, "Surface Behaviour of Biomaterials: The Theta Surface for Biocompatibility", *J .Mater. Sci . Mater. Med.*, 2006, **17**, 1057–1062, DOI: 10.1007/s10856-006-0444-8.

(135) J. Genzer and K. Efimenko, "Recent Developments in Superhydrophobic Surfaces and their Relevance to Marine Fouling: A Review", *Biofouling*, 2006, **22**, 339–360, DOI: 10.1080/08927010600980223.

(136) R. N. Wenzel, "Resistance of solid surfaces to wetting by water", *Ind. Eng. Chem.*, 1936, **28**, 988–994, DOI: 10.1021/ie50320a024.

(137) A. B. D. Cassie and S. Baxter, "Wettability of Porous Surfaces", *Trans. Faraday Soc.*, 1944, **40**, 546–551, DOI: 10.1039/TF9444000546.

(138) R. F. Brady Jr, "Properties which influence marine fouling resistance in polymers containing silicon and fluorine", *Prog. Org. Coatings*, 1999, **35**, 31–35, DOI: 10.1016/S0300-9440(99)00005-3.

(139) C. Carl, A. J. Poole, B. a. Sexton, F. L. Glenn, M. J. Vucko, M. R. Williams, S. Whalan and R. de Nys, "Enhancing the settlement and attachment strength of pediveligers of Mytilus galloprovincialis by changing surface wettability and microtopography.", *Biofouling*, 2012, **28**, 175–86, DOI: 10.1080/08927014.2012.662676.

(140) C. J. Kavanagh, R. D. Quinn and G. W. Swain, "Observations of Barnacle Detachment from Silicones using High-Speed Video", *J. Adhes.*, 2005, **81**, 843–868, DOI: 10.1080/00218460500189331.

(141) P. J. Molino, S. Childs, M. R. Eason Hubbard, J. M. Carey, M. A. Burgman and R. Wetherbee, "Development of the primary bacterial microfouling layer on antifouling and fouling release coatings in temperate and tropical environments in Eastern Australia", *Biofouling*, 2009, **25**, 149–162, DOI: 10.1080/08927010802592917.

(142) P. J. Molino and R. Wetherbee, "The biology of biofouling diatoms and their role in the development of microbial slimes", *Biofouling*, 2008, **24**, 365–379, DOI: 10.1080/08927010802254583.

(143) R. Holland, T. M. Dugdale, R. Wetherbee, A. B. Brennan, J. A. Finlay, J. A. Callow and M. E. Callow, "Adhesion and motility of fouling diatoms on a silicone elastomer", *Biofouling*, 2004, **20**, 323–329, DOI: 10.1080/08927010400029031.

(144) G. Gomathi Sankar, S. Sathya, P. Sriyutha Murthy, A. Das, R. Pandiyan, V. P. Venugopalan and M. Doble, "Polydimethyl siloxane nanocomposites: Their antifouling efficacy in vitro and in marine conditions", *Int. Biodeterior. Biodegradation*, 2015, **104**, 307–314, DOI: 10.1016/j.ibiod.2015.05.022.

(145) M. Sun, C. Luo, L. Xu, H. Ji, Q. Ouyang, D. Yu and Y. Chen, "Artificial lotus leaf by nanocasting", *Langmuir*, 2005, **21**, 8978–8981, DOI: 10.1021/la050316q.

(146) W. Barthlott and C. Neinhuis, "Purity of the sacred lotus, or escape from contamination in biological surfaces", *Planta*, 1997, **202**, 1–8, DOI: 10.1007/s004250050096.

(147) Z. Yuan, H. Chen and J. Zhang, "Facile method to prepare lotus-leaf-like super-hydrophobic poly(vinyl chloride) film", *Appl. Surf. Sci.*, 2008, **254**, 1593–1598, DOI: 10.1016/j.apsusc.2007.07.140.

(148) J. Zheng, W. Song, H. Huang and H. Chen, "Protein adsorption and cell adhesion on polyurethane/Pluronic®surface with lotus leaf-like topography", *Colloids Surfaces B Biointerfaces*, 2010, **77**, 234–239, DOI: 10.1016/j.colsurfb.2010.01.032.

(149) A. J. Scardino, H. Zhang, D. J. Cookson, R. N. Lamb and R. de Nys, "The Role of Nano-Roughness in Antifouling", *Biofouling*, 2009, **25**, 757–767, DOI: 10.1080/08927010903165936.

(150) M. L. Carman, T. G. Estes, A. W. Feinberg, J. F. Schumacher, W. Wilkerson, L. H. Wilson, M. E. Callow, J. A. Callow and A. B. Brennan, "Engineered Antifouling Microtopographies - Correlating Wettability with Cell Attachment", *Biofouling*, 2006, **22**, 11–21, DOI: 10.1080/08927010500484854.

(151) X. Cao, M. E. Pettitt, F. Wode, M. P. Arpa Sancet, J. Fu, J. Ji, M. E. Callow, J. A. Callow, A. Rosenhahn and M. Grunze, "Interaction of Zoospores of the Green Alga Ulva with Bioinspired Micro- and Nanostructured Surfaces Prepared by Polyelectrolyte Layer-by-Layer Self-Assembly", *Adv. Funct. Mater.*, 2010, **20**, 1984–1993, DOI: 10.1002/adfm.201000242.

(152) J. F. Schumacher, N. Aldred, M. E. Callow, J. A. Finlay, J. A. Callow, A. S. Clare and A. B. Brennan, "Species-Specific Engineered Antifouling Topographies: Correlations between the Settlement of Algal Zoospores and Barnacle Cyprids", *Biofouling*, 2007, **23**, 307–317, DOI: 10.1080/08927010701393276.

(153) S. Chen, L. Li, C. Zhao and J. Zheng, "Surface Hydration: Principles and Applications toward Low-fouling/nonfouling Biomaterials", *Polym. J.*, 2010, **51**, 5283–5293, DOI: 10.1016/j.polymer.2010.08.022.

(154) J. Zheng, L. Li, H. K. Tsao, Y. J. Sheng, S. Chen and S. Jiang, "Strong repulsive forces between protein and oligo (ethylene glycol) self-assembled monolayers: a molecular simulation study", *Biophys. J.*, 2005, **89**, 158–166, DOI: 10.1529/biophysj.105.059428.

(155) M. T. Bernards, G. Cheng, Z. Zhang, S. Chen and S. Jiang, "Nonfouling polymer brushes via surface-initiated, two-component atom transfer radical polymerization", *Macromolecules*, 2008, **41**, 4216–4219, DOI: 10.1021/ma800185y.

(156) J. C. Hower, Y. He, M. T. Bernards and S. Jiang, "Understanding the nonfouling mechanism of surfaces through molecular simulations of sugar-based self-assembled monolayers", *J. Chem. Phys.*, 2006, **125**, 214704(1–7), DOI: 10.1063/1.2397681.

(157) T. Ekblad, Ph.D. Thesis, Linköpings Universitet, 2010.

(158) R. K. Smith, P. A. Lewis and P. S. Weiss, "Patterning self-assembled monolayers", *Prog. Surf. Sci.*, 2004, **75**, 1–68, DOI: 10.1016/j.progsurf.2003.12.001.

(159) B. Radhakrishnan, R. Ranjan and W. J. Brittain, "Surface initiated polymerizations from silica nanoparticles", *Soft Matter*, 2006, **2**, 386–396, DOI: 10.1039/b516508c.

(160) D. Li, Q. Zheng, Y. Wang and H. Chen, "Combining surface topography with polymer chemistry: exploring new interfacial biological phenomena", *Polym. Chem.*, 2014, **5**, 14–24, DOI: 10.1039/c3py00739a.

(161) J. S. Wang and K. Matyjaszewski, "Controlled/"Living" Radical Polymerization. Halogen Atom Transfer Radical Polymerization Promoted by a Cu(I)/Cu(II) Redox Process", *Macromolecules*, 1995, **28**, 7901–7910, DOI: 10.1021/ma00127a042.

(162) J. Ran, L. Wu, Z. Zhang and T. Xu, "Atom Transfer Radical Polymerization (ATRP): A Versatile and Forceful Tool for Functional Membranes", *Prog. Polym. Sci.*, 2014, **39**, 124–144, DOI: 10.1016/j.progpolymsci.2013.09.001.

(163) K. Matyjaszewski, "Transition Metal Catalysis in Controlled Radical Polymerization: Atom Transfer Radical Polymerization", *Chem. Eur. J.*, 1999, **5**, 3095–3102, DOI: 10.1002/(SICI)1521-3765(19991105)5:11%3C3095::AID-CHEM3095%3E3.0.CO;2-#.

(164) K. L. Prime and G. M. Whitesides, "Adsorption of Proteins onto Surfaces Containing End-Attached Oligo(ethylene oxide): A Model System Using Self-Assembled Monolayers", *J. Am. Chem. Soc.*, 1993, **115**, 10714–10721, DOI: 10.1021/ja00076a032.

(165) M. Malmsten, K. Emoto and J. M. Van Alstine, "Effect of chain density on inhibition of protein adsorption by poly (ethylene glycol) based coatings", *J. Colloid Interface Sci.*, 1998, **202**, 507–517, DOI: 10.1006/jcis.1998.5513.

(166) S. I. Jeon, J. H. Lee, J. D. Andrade and P. G. De Gennes, "Protein-surface interactions in the presence of polyethylene oxide. I. Simplified theory", *J. Colloid Interface Sci.*, 1991, **142**, 149–158, DOI: 10.1016/0021-9797(91)90043-8.

(167) I. Szleifer, "Protein Adsorption on Surfaces with Grafted Polymers: A Theoretical Approach", *Biophys. J.*, 1997, **72**, 595–612, DOI: 10.1016/S0006-3495(97)78698-3.

(168) S. Jo and K. Park, "Surface modification using silanated poly(ethylene glycol)s", *Biomaterials*, 2000, **21**, 605–616, DOI: 10.1016/S0142-9612(99)00224-0.

(169) B. Zhu, T. Eurell, R. Gunawan and D. Leckband, "Chain-length dependence of the protein and cell resistance of oligo(ethylene glycol)-terminated self-assembled monolayers on gold", *J. Biomed. Mater. Res.*, 2001, **56**, 406–416, DOI: https://doi.org/10.1002/1097-4636(20010905)56:3%3C406::AID-JBM1110%3E3.0.CO;2-R.

(170) J. Zheng, L. Li, S. Chen and S. Jiang, "Molecular Simulation Study of Water Interactions with Oligo (Ethylene Glycol)-Terminated Alkanethiol Self-Assembled Monolayers", *Langmuir*, 2004, **20**, 8931–8938, DOI: 10.1021/la036345n.

(171) Y. He, Y. Chang, J. C. Hower, J. Zheng, S. Chen and S. Jiang, "Origin of repulsive force and structure/dynamics of interfacial water in OEG-protein interactions: a molecular simulation study", *Phys. Chem. Chem. Phys.*, 2008, **10**, 5539–5544, DOI: 10.1039/b807129b.

(172) S. Sheikh, C. Blaszykowski, R. Nolan, D. Thompson and M. Thompson, "On the Hydration of Subnanometric Antifouling Organosilane Adlayers: A Molecular Dynamics Simulation", *J. Colloid Interface Sci.*, 2015, **437**, 197–204, DOI: 10.1016/j.jcis.2014.09.025.

(173) S. Sheikh, D. Y. Yang, C. Blaszykowski and M. Thompson, "Single ether group in a glycol-based ultra-thin layer prevents surface fouling from undiluted serum", *Chem. Commun.*, 2012, **48**, 1305–1307, DOI: 10.1039/c2cc15692j.

(174) C. Avci, S. Sheikh, C. Blaszykowski and M. Thompson, "Critical role of surface hydration on the dynamics of serum adsorption studied with monoethylene glycol adlayers on gold", *Chem. Commun.*, 2013, **49**, 466–468, DOI: 10.1039/c2cc37477c.

(175) C. Yoshikawa, J. Qiu, C. F. Huang, Y. Shimizu, J. Suzuki and E. van den Bosch, "Non-biofouling property of well-defined concentrated polymer brushes", *Colloids Surf., B*, 2015, **127**, 213–220, DOI: 10.1016/j.colsurfb.2015.01.026.

(176) J. Ladd, Z. Zhang, S. Chen, J. C. Hower and S. Jiang, "Zwitterionic Polymers Exhibiting High Resistance to Nonspecific Protein Adsorption from Human Serum and Plasma", *Biomacromolecules*, 2008, **9**, 1357–1361, DOI: 10.1021/bm701301s.

(177) Z. Zhang, M. Zhang, S. Chen, T. A. Horbett, B. D. Ratner and S. Jiang, "Blood Compatibility of Surfaces with Superlow Protein Adsorption", *Biomaterials*, 2008, **29**, 4285–4291, DOI: 10.1016/j.biomaterials.2008.07.039.

(178) Y. Chang, C.-Y. Ko, Y.-J. Shih, D. Quémener, A. Deratani, T.-C. Wei, D.-M. Wang and J.-Y. Lai, "Surface grafting control of PEGylated poly(vinylidene fluoride) antifouling membrane via surface-initiated radical graft copolymerization", *J. Memb. Sci.*, 2009, **345**, 160–169, DOI: 10.1016/j.memsci.2009.08.039.

(179) H. Xu, F. Yan, E. E. Monson and R. Kopelman, "Room-temperature preparation and characterization of poly (ethylene glycol)-coated silica nanoparticles for biomedical applications", *J. Biomed. Mater. Res. Part A*, 2003, **66**, 870–879, DOI: 10.1002/jbm.a.10057.

(180) S. M. S. Björkegren, L. Nordstierna, A. Törncrona, M. E. Persson, A. E. C. Palmqvist, S. Maria, S. M. S. Björkegren, L. Nordstierna, A. Törncrona, M. E. Persson and A. E. C. Palmqvist, "Surface activity and flocculation behavior of polyethylene glycol-functionalized silica nanoparticles", *J. Colloid Interface Sci.*, 2015, **452**, 215–223, DOI: 10.1016/j.jcis.2015.04.043.

(181) Q. He, J. Zhang, J. Shi, Z. Zhu, L. Zhang, W. Bu, L. Guo and Y. Chen, "The effect of PEGylation of mesoporous silica nanoparticles on nonspecific binding of serum proteins and cellular responses", *Biomaterials*, 2010, **31**, 1085–1092, DOI: 10.1016/j.biomaterials.2009.10.046.

(182) P. F. Holmes, E. P. Currie, J. C. Thies, H. C. Van Der Mei, H. J. Busscher and W. Norde, "Surface-Modified Nanoparticles as a New, Versatile, and Mechanically Robust Nonadhesive Coating: Suppression of Protein Adsorption and Bacterial Adhesion", *J. Biomed. Mater. Res., Part A*, 2009, **91**, 824–833, DOI: 10.1002/jbm.a.32285.

(183) P. Lin, C. W. Lin, R. Mansour and F. Gu, "Improving Biocompatibility by Surface Modification Techniques on Implantable Bioelectronics", *Biosens. Bioelectron.*, 2013, **47**, 451–460, DOI: 10.1016/j.bios.2013.01.071.

(184) W. Zhao, Q. Ye, H. Hu, X. Wang and F. Zhou, "Grafting Zwitterionic Polymer Brushes via Electrochemical Surface-Initiated Atomic-Transfer Radical Polymerization for Anti-Fouling Applications", *J. Mater. Chem. B*, 2014, **2**, 5352–5357, DOI: 10.1039/c4tb00816b.

(185) S. Jiang and Z. Cao, "Ultralow-Fouling, Functionalizable, and Hydrolyzable Zwitterionic Materials and their Derivatives for Biological Applications", *Adv. Mater.*, 2010, **22**, 920–932, DOI: 10.1002/adma.200901407.

(186) S. Chen, J. Zheng, L. Li and S. Jiang, "Strong Resistance of Phosphorylcholine Self-assembled Monolayers to Protein Adsorption: Insights into Nonfouling Properties of Zwitterionic Materials", *J. Am. Chem. Soc.*, 2005, **127**, 14473–14478, DOI: 10.1021/ja054169u.

(187) L. Mi and S. Jiang, "Integrated Antimicrobial and Nonfouling Zwitterionic Polymers", *Angew. Chemie Int. Ed.*, 2014, **53**, 1746–1754, DOI: 10.1002/anie.201304060.

(188) R. G. Chapman, E. Ostuni, S. Takayama, R. E. Holmlin, L. Yan and G. M. Whitesides, "Surveying for surfaces that resist the adsorption of proteins", *J. Am. Chem. Soc.*, 2000, **122**, 8303–8304, DOI: 10.1021/ja000774f.

(189) R. E. Holmlin, X. Chen, R. G. Chapman, S. Takayama and G. M. Whitesides, "Zwitterionic SAMs that Resist Nonspecific Adsorption of Protein from Aqueous Buffer", *Langmuir*, 2001, **17**, 2841–2850, DOI: 10.1021/la0015258.

(190) E. Ostuni, R. G. Chapman, M. N. Liang, G. Meluleni, G. Pier, D. E. Ingber and G. M. Whitesides, "Self-Assembled Monolayers That Resist the Adsorption of Proteins and the Adhesion of Bacterial and Mammalian Cells", *Langmuir*, 2001, **17**, 6336–6343, DOI: 10.1021/la010552a.

(191) E. Ostuni, R. G. Chapman, R. E. Holmlin, S. Takayama and G. M. Whitesides, "A survey of structure-property relationships of surfaces that resist the adsorption of protein", *Langmuir*, 2001, **17**, 5605–5620, DOI: 10.1021/la010384m.

(192) R. F. A. Zwaal and A. J. Schroit, "Pathophysiologic implications of membrane phospholipid asymmetry in blood cells", *Blood*, 1997, **89**, 1121–1132.

(193) K. Ishihara, H. Oshida, Y. Endo, T. Ueda, A. Watanabe and N. Nakabayashi, "Hemocompatibility of human whole blood on polymers with a phospholipid polar group and its mechanism", *J. Biomed. Mater. Res.*, 1992, **26**, 1543–1552, DOI: 10.1002/jbm.820261202.

(194) Y. Chang Chung, Y. Hong Chiu, Y. Wei Wu and Y. Tai Tao, "Self-assembled biomimetic monolayers using phospholipid-containing disulfides", *Biomaterials*, 2005, **26**, 2313–2324, DOI: 10.1016/j.biomaterials.2004.06.043.

(195) L. Wu, Z. Guo, S. Meng, W. Zhong, Q. Du and L. L. Chou, "Synthesis of a zwitterionic silane and its application in the surface modification of silicon-based material surfaces for improved hemocompatibility", *ACS Appl. Mater. Interfaces*, 2010, **2**, 2781–2788, DOI: 10.1021/am1004249.

(196) W. Feng, S. Zhu, K. Ishihara and J. L. Brash, "Adsorption of fibrinogen and lysozyme on silicon grafted with poly (2-methacryloyloxyethyl phosphorylcholine) via surface-initiated atom transfer radical polymerization", *Langmuir*, 2005, **21**, 5980–5987, DOI: 10.1021/la050277i.

(197) Y. He, J. Hower, S. Chen, M. T. Bernards, Y. Chang and S. Jiang, "Molecular Simulation Studies of Protein Interactions with Zwitterionic Phosphorylcholine Self-assembled Monolayers in the Presence of Water", *Langmuir*, 2008, **24**, 10358–10364, DOI: 10.1021/la8013046.

(198) D. E. Heath and S. L. Cooper, "Design and Characterization of Sulfobetaine-containing Terpolymer Biomaterials", *Acta Biomater.*, 2012, **8**, 2899–2910, DOI: 10.1016/j.actbio.2012.03.052.

(199) X. Zhao, W. Chen, Y. Su, W. Zhu, J. Peng, Z. Jiang, L. Kong, Y. Li and J. Liu, "Hierarchically engineered membrane surfaces with superior antifouling and self-cleaning properties", *J. Memb. Sci.*, 2013, **441**, 93–101, DOI: 10.1016/j.memsci.2013.04.012.

(200) M.-C. Sin, S.-H. Chen and Y. Chang, "Hemocompatibility of Zwitterionic Interfaces and Membranes", *Polym. J.*, 2014, **46**, 436–443, DOI: 10.1038/pj.2014.46.

(201) C.-J. Huang and Y.-C. Chang, "In Situ Surface Tailoring with Zwitterionic Carboxybetaine Moieties on Self-Assembled Thin Film for Antifouling Biointerfaces", *Materials (Basel).*, 2014, **7**, 130–142, DOI: 10.3390/ma7010130.

(202) S. Chen, S. Chen, S. Jiang, Y. Mo, J. Tang and Z. Ge, "Synthesis and Characterization of Siloxane Sulfobetaine Antimicrobial Agents", *Surf. Sci.*, 2011, **605**, L25–L28, DOI: 10.1016/j.susc.2011.03.013.

(203) P. Wang, J. Meng, M. Xu, T. Yuan, N. Yang, T. Sun, Y. Zhang, X. Feng and B. Cheng, "A Simple but Efficient Zwitterionization Method towards Cellulose Membrane with Superior Antifouling Property and Biocompatibility", *J. Memb. Sci.*, 2015, **492**, 547–558, DOI: 10.1016/j.memsci.2015.06.024.

(204) S. B. Yeh, C. S. Chen, W. Y. Chen and C. J. Huang, "Modification of silicone elastomer with zwitterionic silane for durable antifouling properties", *Langmuir*, 2014, **30**, 11386–11393, DOI: 10.1021/la502486e.

(205) Q. Shao and S. Jiang, "Molecular Understanding and Design of Zwitterionic Materials", *Adv. Mater.*, 2015, **27**, 15–26, DOI: 10.1002/adma.201404059.

(206) Q. Shao, Y. He, A. D. White and S. Jiang, "Difference in Hydration between Carboxybetaine and Sulfobetaine", *J. Phys. Chem. B*, 2010, **114**, 16625–16631, DOI: 10.1021/jp107272n.

(207) Q. Shao and S. Jiang, "Influence of Charged Groups on the Properties of Zwitterionic Moieties: A Molecular Simulation Study", *J. Phys. Chem. B*, 2014, **118**, 7630–7637, DOI: 10.1021/jp5027114.

(208) J. G. Weers, J. F. Rathman, F. U. Axe, C. A. Crichlow, L. D. Foland, D. R. Scheuing, R. J. Wiersema and A. G. Zielske, "Effect of the intramolecular charge separation distance on the solution properties of betaines and sulfobetaines", *Langmuir*, 1991, **7**, 854–867, DOI: 10.1021/la00053a008.

(209) H. Vaisocherová, Z. Zhang, W. Yang, Z. Cao, G. Cheng, A. D. Taylor, M. Piliarik, J. Homola and S. Jiang, "Functionalizable Surface Platform with Reduced Nonspecific Protein Adsorption from Full Blood Plasma-Material Selection and Protein Immobilization Optimization", *Biosens. Bioelectron.*, 2009, **24**, 1924–1930, DOI: 10.1016/j.bios.2008.09.035.

(210) G. Cheng, Z. Zhang, S. Chen, J. D. Bryers and S. Jiang, "Inhibition of Bacterial Adhesion and Biofilm Formation on Zwitterionic Surfaces", *Biomaterials*, 2007, **28**, 4192–4199, DOI: 10.1016/j.biomaterials.2007.05.041.

(211) Z. Zhang, T. Chao, S. Chen and S. Jiang, "Superlow fouling sulfobetaine and carboxybetaine polymers on glass slides", *Langmuir*, 2006, **22**, 10072–10077, DOI: 10.1021/la062175d.

(212) G. Cheng, G. Li, H. Xue, S. Chen, J. D. Bryers and S. Jiang, "Zwitterionic Carboxybetaine Polymer Surfaces and their Resistance to Long-term Biofilm Formation", *Biomaterials*, 2009, **30**, 5234–5240, DOI: 10.1016/j.biomaterials.2009.05.058.

(213) C. Leng, H. C. Hung, S. Sun, D. Wang, Y. Li, S. Jiang and Z. Chen, "Probing the Surface Hydration of Nonfouling Zwitterionic and PEG Materials in Contact with Proteins", *ACS Appl. Mater. Interfaces*, 2015, **7**, 16881–16888, DOI: 10.1021/acsami.5b05627.

(214) C. Leng, H. C. Hung, O. A. Sieggreen, Y. Li, S. Jiang and Z. Chen, "Probing the Surface Hydration of Nonfouling Zwitterionic and Poly(ethylene glycol) Materials with Isotopic Dilution Spectroscopy", *J. Phys. Chem. C*, 2015, **119**, 8775–8780, DOI: 10.1021/acs.jpcc.5b01649.

(215) P. F. Ren, H. C. Yang, H. Q. Liang, X. L. Xu, L. S. Wan and Z. K. Xu, "Highly Stable, Protein-Resistant Surfaces via the Layer-by-Layer Assembly of Poly(sulfobetaine methacrylate) and Tannic Acid", *Langmuir*, 2015, **31**, 5851–5858, DOI: 10.1021/acs.langmuir.5b00920.

(216) K. Fujii, H. N. Matsumoto, Y. Koyama, Y. Iwasaki, K. Ishihara and K. Takakuda, "Prevention of Biofilm Formation with a Coating of 2-Methacryloyloxyethyl Phosphorylcholine Polymer", *J. Vet. Med. Sci.*, 2008, **70**, 167–173, DOI: 10.1292/jvms.70.167.

(217) M. C. Sin, Y. M. Sun and Y. Chang, "Zwitterionic-based stainless steel with well-defined polysulfobetaine brushes for general bioadhesive control", *ACS Appl. Mater. Interfaces*, 2014, **6**, 861–873, DOI: 10.1021/am4041256.

(218) R. B. Bodkhe, S. J. Stafslien, J. Daniels, N. Cilz, A. J. Muelhberg, S. E. Thompson, M. E. Callow, J. A. Callow and D. C. Webster, "Zwitterionic siloxane-polyurethane fouling-release coatings", *Prog. Org. Coatings*, 2015, **78**, 369–380, DOI: 10.1016/j.porgcoat.2014.07.011.

(219) S. Anthony Yesudass, S. Mohanty, S. K. Nayak and C. C. Rath, "Zwitterionic–polyurethane coatings for non-specific marine bacterial inhibition: A nontoxic approach for marine application", *Eur. Polym. J.*, 2017, **96**, 304–315, DOI: 10.1016/j.eurpolymj.2017.09.019.

(220) R. J. Pieper, A. Ekin, D. C. Webster, F. Cassé, J. A. Callow and M. E. Callow, "Combinatorial approach to study the effect of acrylic polyol composition on the properties of crosslinked siloxane-polyurethane fouling-release coatings", *J. Coatings Technol. Res.*, 2007, **4**, 453–461, DOI: 10.1007/s11998-007-9032-1.

(221) Y. Zhang, H. Hu, X. Pei, Y. Liu, Q. Ye and F. Zhou, "Polymer brushes on structural surfaces: a novel synergistic strategy for perfectly resisting algae settlement", *Biomater. Sci.*, 2017, **5**, 2493–2500, DOI: 10.1039/C7BM00842B.

(222) A. J. Scardino, E. Harvey and R. De Nys, "Testing Attachment Point Theory: Diatom Attachment on Microtextured Polyimide Biomimics", *Biofouling*, 2006, **22**, 55–60, DOI: 10.1080/08927010500506094.

(223) P.-S. Liu, Q. Chen, X. Liu, B. Yuan, S. S. Wu, J. Shen and S. C. Lin, "Grafting of zwitterion from cellulose membranes via ATRP for improving blood compatibility", *Biomacromolecules*, 2009, **10**, 2809–2816, DOI: 10.1021/bm9006503.

(224) P.-S. Liu, Q. Chen, S.-S. Wu, J. Shen and S.-C. Lin, "Surface modification of cellulose membranes with zwitterionic polymers for resistance to protein adsorption and platelet adhesion", *J. Memb. Sci.*, 2010, **350**, 387–394, DOI: 10.1016/j.memsci.2010.01.015.

(225) M. Wang, J. Yuan, X. Huang, X. Cai, L. Li and J. Shen, "Grafting of carboxybetaine brush onto cellulose membranes via surface-initiated ARGET-ATRP for improving blood compatibility", *Colloids Surf., B*, 2013, **103**, 52–58, DOI: 10.1016/j.colsurfb.2012.10.025.

(226) S. Guo, D. Jańczewski, X. Zhu, R. Quintana, T. He and K. G. Neoh, "Surface charge control for zwitterionic polymer brushes: Tailoring surface properties to antifouling applications", *J. Colloid Interface Sci.*, 2015, **452**, 43–53, DOI: 10.1016/j.jcis.2015.04.013.

(227) Z. Cao and S. Jiang, "Super-Hydrophilic Zwitterionic Poly(carboxybetaine) and Amphiphilic non-ionic Poly(ethylene glycol) for Stealth Nanoparticles", *Nano Today*, 2012, **7**, 404–413, DOI: 10.1016/j.nantod.2012.08.001.

(228) W. Yang, L. Zhang, S. Wang, A. D. White and S. Jiang, "Functionalizable and ultra stable nanoparticles coated with zwitterionic poly(carboxybetaine) in undiluted blood serum", *Biomaterials*, 2009, **30**, 5617–5621, DOI: 10.1016/j.biomaterials.2009.06.036.

(229) W. Yang, J.-R. Ella-Menye, S. Liu, T. Bai, D. Wang, Q. Yu, Y. Li and S. Jiang, "Cross-linked carboxybetaine SAMs enable nanoparticles with remarkable stability in complex media", *Langmuir*, 2014, **30**, 2522–2529, DOI: 10.1021/la404941m.

(230) G. Jia, Z. Cao, H. Xue, Y. Xu and S. Jiang, "Novel Zwitterionic-Polymer-Coated Silica Nanoparticles", *Langmuir*, 2009, **25**, 3196–3199, DOI: 10.1021/la803737c.

(231) Z. G. Estephan, P. S. Schlenoff and J. B. Schlenoff, "Zwitteration as an alternative to PEGylation", *Langmuir*, 2011, **27**, 6794–6800, DOI: 10.1021/la200227b.

(232) Z. G. Estephan, J. A. Jaber and J. B. Schlenoff, "Zwitterion-Stabilized Silica Nanoparticles: Toward Nonstick Nano", *Langmuir*, 2010, **26**, 16884–16889, DOI: 10.1021/la103095d.

(233) F. Hu, K. Chen, H. Xu and H. Gu, "Functional Short-chain Zwitterion Coated Silica Nanoparticles with Antifouling Property in Protein Solutions", *Colloids Surf., B*, 2015, **126**, 251–256, DOI: 10.1016/j.colsurfb.2014.12.036.

(234) Y. Matsuda, M. Kobayashi, M. Annaka, K. Ishihara and A. Takahara, "Dimensions of a Free Linear Polymer and Polymer Immobilized on Silica Nanoparticles of a Zwitterionic Polymer in Aqueous Solutions with Various Ionic Strengths", *Langmuir*, 2008, **24**, 8772–8778, DOI: 10.1021/la8005647.

(235) H. Suzuki, M. Murou, H. Kitano, K. Ohno and Y. Saruwatari, "Silica particles coated with zwitterionic polymer brush: formation of colloidal crystals and anti-biofouling properties in aqueous medium", *Colloids Surf., B*, 2011, **84**, 111–116, DOI: 10.1016/j.colsurfb.2010.12.023.

(236) P. Król and P. Chmielarz, "Recent advances in ATRP methods in relation to the synthesis of copolymer coating materials", *Prog. Org. Coat.*, 2014, **77**, 913–948, DOI: 10.1016/j.porgcoat.2014.01.027.

(237) Z. Zhang, G. Cheng, L. R. Carr, H. Vaisocherova, S. Chen and S. Jiang, "The hydrolysis of cationic polycarboxybetaine esters to zwitterionic polycarboxybetaines with controlled properties", *Biomaterials*, 2008, **29**, 4719–4725, DOI: 10.1016/j.biomaterials.2008.08.030.

(238) G. Cheng, H. Xue, Z. Zhang, S. Chen and S. Jiang, "A switchable biocompatible polymer surface with self-sterilizing and nonfouling capabilities", *Angew. Chemie Int. Ed.*, 2008, **47**, 8831–8834, DOI: 10.1002/anie.200803570.

(239) Z. Cao, L. Mi, J. Mendiola, J. R. Ella-Menye, L. Zhang, H. Xue and S. Jiang, "Reversibly switching the function of a surface between attacking and defending against bacteria", *Angew. Chemie Int. Ed.*, 2012, **51**, 2602–2605, DOI: 10.1002/anie.201106466.

(240) B. Cao, Q. Tang, L. Li, J. Humble, H. Wu, L. Liu and G. Cheng, "Switchable antimicrobial and antifouling hydrogels with enhanced mechanical properties", *Adv. Healthc. Mater.*, 2013, **2**, 1096–1102, DOI: 10.1002/adhm.201200359.

(241) P. Shivapooja, Q. Yu, B. Orihuela, R. Mays, D. Rittschof, J. Genzer, G. P. Lo, G. P. López and G. P. Lo, "Modification of Silicone Elastomer Surfaces with Zwitterionic Polymers: Short-Term Fouling Resistance and Triggered Biofouling Release", *ACS Appl. Mater. Interfaces*, 2015, **7**, 25586–25591, DOI: 10.1021/acsami.5b09199.

(242) I. I. Slowing, J. L. Vivero-Escoto, C. W. Wu and V. S. Y. Lin, "Mesoporous silica nanoparticles as controlled release drug delivery and gene transfection carriers", *Adv. Drug Deliv. Rev.*, 2008, **60**, 1278–1288, DOI: 10.1016/j.addr.2008.03.012.

(243) Y. Wang, Q. Zhao, N. Han, L. Bai, J. Li, J. Liu, E. Che, L. Hu, Q. Zhang, T. Jiang and S. Wang, "Mesoporous silica nanoparticles in drug delivery and biomedical applications", *Nanomedicine Nanotechnology, Biol. Med.*, 2015, **11**, 313–327, DOI: 10.1016/j.nano.2014.09.014.

(244) E. Scrinzi, S. Rossi, P. Kamarchik and F. Deflorian, "Evaluation of Durability of Nano-Silica containing Clear Coats for Automotive Applications", *Prog. Org. Coat.*, 2011, **71**, 384–390, DOI: 10.1016/j.porgcoat.2011.04.009.

(245) T. Mizutani, K. Arai, M. Miyamoto and Y. Kimura, "Application of Silica-Containing Nano-Composite Emulsion to Wall Paint: A New Environmentally Safe Paint of High Performance", *Prog. Org. Coat.*, 2006, **55**, 276–283, DOI: 10.1016/j.porgcoat.2005.12.001.

(246) I. M. Rio-Echevarria, F. Selvestrel, D. Segat, G. Guarino, R. Tavano, V. Causin, E. Reddi, E. Papini and F. Mancin, "Highly PEGylated silica nanoparticles: "ready to use" stealth functional nanocarriers", *J. Mater. Chem.*, 2010, **20**, 2780–2787, DOI: 10.1039/b921735e.

(247) I. A. Rahman and V. Padavettan, "Synthesis of Silica Nanoparticles by Sol-Gel: Size-Dependent Properties, Surface Modification, and Applications in Silica-Polymer Nanocomposites—A Review", *J. Nanomater.*, 2012, **2012**, 1–15, DOI: 10.1155/2012/132424.

(248) W. Stober and A. Fink, "Controlled Growth of Monodispersed Silica Spheres in the Micron Size Range", *J. Colloid Interface Sci.*, 1968, **26**, 62–69, DOI: 10.1016/0021-9797(68)90272-5.

(249) D. J. Belton, O. Deschaume and C. C. Perry, "An overview of the fundamentals of the chemistry of silica with relevance to biosilicification and technological advances", *FEBS J.*, 2012, **279**, 1710–1720, DOI: 10.1111/j.1742-4658.2012.08531.x.

(250) D. Rother, T. Sen, D. East and I. J. Bruce, "Silicon, silica and its surface patterning/activation with alkoxy-and amino-silanes for nanomedical applications", *Nanomedicine*, 2011, **6**, 281–300, DOI: 10.2217/nnm.10.159.

(251) G. A. Parks, "The Isoelectric Points of Solid Oxides, Solid Hydroxides, and Aqueous Hydroxo Complex Systems", *Chem. Rev.*, 1965, **65**, 177–198, DOI: 10.1021/cr60234a002.

(252) I. A. Rahman, P. Vejayakumaran, C. S. Sipaut, J. Ismail and C. K. Chee, "Size-dependent Physicochemical and Optical Properties of Silica Nanoparticles", *Mater. Chem. Phys.*, 2009, **114**, 328–332, DOI: 10.1016/j.matchemphys.2008.09.068.

(253) L. T. Zhuravlev, "Concentration of Hydroxyl Groups on the Surface of Amorphous Silicas", *Langmuir*, 1987, **3**, 316–318, DOI: 10.1021/la00075a004.

(254) L. T. Zhuravlev, "The surface chemistry of amorphous silica. Zhuravlev model", *Colloids Surf., A*, 2000, **173**, 1–38, DOI: 10.1016/S0927-7757(00)00556-2.

(255) H. Kamiya, M. Mitsui, H. Takano and S. Miyazawa, "Influence of particle diameter on surface silanol structure, hydration forces, and aggregation behavior of alkoxide-derived silica particles", *J. Am. Ceram. Soc.*, 2000, **83**, 287–293, DOI: 10.1111/j.1151-2916.2000.tb01187.x.

(256) E. Vansant, P. V. D. Voort and K. Vrancken, *Characterization and Chemical Modification of the Silica Surface*, Elsevier Science, 1995.

(257) B. Arkles, J. R. Steinmetz, J. Zazyczny and P. Mehta, "Factors Contributing to the Stability of Alkoxysilanes in Aqueous Solution", *J. Adhes. Sci. Technol.*, 1992, **6**, 193–206, DOI: 10.1163/156856192X00133.

(258) E. R. Pohl and O. F. D, *Molecular Chracterization of Composite Interfaces*, ed. Springer, PlenumPress: New York, 1985, pp. 157–170.

(259) F. D. Osterholtz and E. R. Pohl, "Kinetics of the hydrolysis and condensation of organofunctional alkoxysilanes: a review", *J. Adhes. Sci. Technol.*, 1992, **6**, 127–149, DOI: 10.1163/156856192X00106.

(260) C. J. Brinker, "Hydrolysis and Condensation of Silicates: Effects on Structure", *J. Non-Cryst. Solids*, 1988, **100**, 31–50, DOI: 10.1016/0022-3093(88)90005-1.

(261) K. J. McNeil, J. A. DiCaprio, D. A. Walsh and R. F. Pratt, "Kinetics and Mechanism of Hydrolysis of a Silicate Triester, Tris(2-Methoxyethoxy)Phenylsilane", *J. Am. Chem. Soc.*, 1980, **102**, 1859–1865, DOI: 10.1021/ja00526a015.

(262) M.-C. C. Brochier Salon, P.-A. A. Bayle, M. Abdelmouleh, S. Boufi and M. N. Belgacem, "Kinetics of Hydrolysis and Self Condensation Reactions of Silanes by NMR Spectroscopy", *Colloids Surf., A*, 2008, **312**, 83–91, DOI: 10.1016/j.colsurfa.2007.06.028.

(263) M.-C. Brochier Salon and M. N. Belgacem, "Competition between hydrolysis and condensation reactions of trialkoxysilanes, as a function of the amount of water and the nature of the organic group", *Colloids Surf., A*, 2010, **366**, 147–154, DOI: 10.1016/j.colsurfa.2010.06.002.

(264) M. C. Brochier Salon and M. N. Belgacem, "Hydrolysis-condensation kinetics of different silane coupling agents", *Phosphorus, Sulfur Silicon Relat. Elem.*, 2011, **186**, 240–254, DOI: 10.1080/10426507.2010.494644.

(265) J. Sagiv, "Organized Monolayers by Adsorption. 1. Formation and Structure of Oleophobic Mixed Monolayers on Solid Surfaces", *J. Am. Chem. Soc.*, 1980, **102**, 92–98, DOI: 10.1021/ja00521a016.

(266) S. R. Wasserman, Y. T. Tao and G. M. Whitesides, "Structure and reactivity of alkylsiloxane monolayers formed by reaction of alkyltrichlorosilanes on silicon substrates", *Langmuir*, 1989, **5**, 1074–1087, DOI: 10.1021/la00088a035.

(267) R. Banga, J. Yarwood, A. M. Morgan, B. Evans and J. Kells, "FTIR and AFM Studies of the Kinetics and Self-Assembly of Alkyltrichlorosilanes and (Perfluoroalkyl)trichlorosilanes onto Glass and Silicon", *Langmuir*, 1995, **11**, 4393–4399, DOI: 10.1021/la00011a036.

(268) K. Bierbaum, M. Grunze, A. A. Baski, L. F. Chi, W. Schrepp and H. Fuchs, "Growth of Self-Assembled n-Alkyltrichlorosilane Films on Si(100) Investigated by Atomic Force Microscopy", *Langmuir*, 1995, **11**, 2143–2150, DOI: 10.1021/la00006a049.

(269) A. Ulman, "Formation and Structure of Self-Assembled Monolayers", *Chem. Rev.*, 1996, **96**, 1533–1554, DOI: 10.1021/cr9502357.

(270) C. R. Emmenegger, E. Brynda, T. Riedel, Z. Sedlakova, M. Houska and A. B. Alles, "Interaction of Blood Plasma with Antifouling Surfaces", *Langmuir*, 2009, **25**, 6328–6333, DOI: 10.1021/la900083s.

(271) A. M. Alswieleh, N. Cheng, I. Canton, B. Ustbas, X. Xue, V. Ladmiral, S. Xia, R. E. Ducker, O. El Zubir, M. L. Cartron, C. N. Hunter, G. J. Leggett and S. P. Armes, "Zwitterionic Poly(amino acid methacrylate) Brushes", *J. Am. Chem. Soc.*, 2014, **136**, 9404–9413, DOI: 10.1021/ja503400r.

(272) L. Li, R. E. Marchant, A. Dubnisheva, S. Roy and W. H. Fissell, "Anti-Biofouling Sulfobetaine Polymer Thin Films on Silicon and Silicon Nanopore Membranes", *J. Biomater. Sci., Polym. Ed.*, 2011, **22**, 91–106, DOI: 10.1163/092050609X12578498982998.

(273) Z. Zhang, J. A. Finlay, L. Wang, Y. Gao, J. A. Callow, M. E. Callow and S. Jiang, "Polysulfobetaine-Grafted Surfaces as Environmentally Benign Ultralow Fouling Marine Coatings", *Langmuir*, 2009, **25**, 13516–13521, DOI: 10.1021/la901957k.

(274) L. Portilla and M. Halik, "Smoothly Tunable Surface Properties of Aluminum Oxide Core-Shell Nanoparticles by a Mixed-Ligand Approach", *ACS Appl. Mater. Interfaces*, 2014, **6**, 5977–5982, DOI: 10.1021/am501155r.

(275) B. Thierry, L. Zimmer, S. McNiven, K. Finnie, C. Barbé and H. J. Griesser, "Electrostatic Self-Assembly of PEG Copolymers onto Porous Silica Nanoparticles", *Langmuir*, 2008, **24**, 8143–8150, DOI: 10.1021/la8007206.

(276) J. T. Sun, Z. Q. Yu, C. Y. Hong and C. Y. Pan, "Biocompatible Zwitterionic Sulfobetaine Copolymer-Coated Mesoporous Silica Nanoparticles for Temperature-Responsive Drug Release", *Macromol. Rapid Commun.*, 2012, **33**, 811–818, DOI: 10.1002/marc.201100876.

(277) K. T. Huang, S. B. Yeh and C. J. Huang, "Surface Modification for Superhydrophilicity and Underwater Superoleophobicity: Applications in Antifog, Underwater Self-Cleaning, and Oil-Water Separation", *ACS Appl. Mater. Interfaces*, 2015, **7**, 21021–21029, DOI: 10.1021/acsami.5b07362.

(278) Z.-b. Li, Y.-h. Xiang, X.-j. Zhou, J.-j. Nie, M. Peng and B.-y. Du, "Thermosensitive poly(DEGMMA-co-MEA) microgels: Synthesis, characterization and interfacial interaction with adsorbed protein layer", *Chin. J. Polym. Sci.*, 2015, **33**, 1516–1526, DOI: 10.1007/s10118-015-1694-z.

(279) J. Li, Z. Zhang, X. Zhou, T. Chen, J. Nie and B. Du, "PNIPAmx–PPO36–NIPAmx thermo-sensitive triblock copolymers: chain conformation and adsorption behavior on a hydrophobic gold surface", *Phys. Chem. Chem. Phys.*, 2016, **18**, 519–528, DOI: 10.1039/C5CP06079F.

(280) M. Litt and T. Matsuda, "Siloxane Zwitterions: Synthesis and Surface Properties of Crosslinked Polymers", *J. Appl. Polym. Sci.*, 1975, **19**, 1221–1225, DOI: 10.1002/app.1975.070190502.

(281) K. A. Marx, "Quartz Crystal Microbalance: A Useful Tool for Studying Thin Polymer Films and Complex Biomolecular Systems at the Solution-Surface Interface", *Biomacromolecules*, 2003, **4**, 1099–1120, DOI: 10.1021/bm020116i.

(282) G. Socrates, "Infrared Characteristic Group Frequencies, Tables and Charts", 1995.

(283) Y. Song, Y. Sun, X. Zhang, J. Zhou and L. Zhang, "Homogeneous Quaternization of Cellulose in NaOH/Urea Aqueous Solutions as Gene Carriers", *Biomacromolecules*, 2008, **9**, 2259–2264, DOI: 10.1021/bm800429a.

(284) R. K. Iler, *The Chemistry of Silica: Solubility, Polymerization, Colloid and Surface Properties and Biochemistry of Silica*, Wiley, 1979.

(285) L. Chu, M. W. Daniels and L. F. Francis, "Use of (Glycidoxypropyl)trimethoxysilane as a Binder in Colloidal Silica Coatings", *Chem. Mater.*, 1997, **9**, 2577–2582, DOI: 10.1021/cm9702880.

(286) L. Wu, J. Jasinski and S. Krishnan, "Carboxybetaine, Sulfobetaine, and Cationic Block Copolymer Coatings: A Comparison of the Surface Properties and Antibiofouling Behavior", *J. Appl. Polym. Sci.*, 2012, **124**, 2154–2170, DOI: 10.1002/app.35233.

(287) M. Stupar, M. L. Grbić, A. Džamić, N. Unković, M. Ristić, A. Jelikić and J. Vukojević, "Antifungal Activity of Selected Essential Oils and Biocide Benzalkonium Chloride against the Fungi Isolated from Cultural Heritage Objects", *South African J. Bot.*, 2014, **93**, 118–124, DOI: 10.1016/j.sajb.2014.03.016.

(288) H. A. Wösten, F. H. Schuren and J. G. Wessels, "Interfacial Self-Assembly of a Hydrophobin into an Amphipathic Protein Membrane Mediates Fungal Attachment to Hydrophobic Surfaces", *EMBO J.*, 1994, **13**, 5848–5854, DOI: 10.1002/j.1460-2075.1994.tb06929.x.

(289) H. Du and X. Qian, "The hydration properties of carboxybetaine zwitterion brushes", *J. Comput. Chem.*, 2016, **37**, 877–885, DOI: 10.1002/jcc.24234.

(290) T. L. Gresham, J. E. Jansen, F. W. Shaver, R. A. Bankert and F. T. Fiedorek, "β-Propiolactone. XI. Reactions with Ammonia and Amines", *J. Am. Chem. Soc.*, 1951, **73**, 3168–3171, DOI: 10.1021/ja01151a050.

(291) D. Liaw, C. Huang, W. Lee, J. Borbély and E. Kang, "Synthesis and Characteristics of the Poly(carboxybetaine)s and the Corresponding Cationic Polymers", *J. Polym. Sci. Part A Polym. Chem.*, 1997, **35**, 3527–3536, DOI: 10.1002/(SICI)1099-0518(19971130)35:16<3527::AID-POLA19>3.0.CO;2-H.

(292) S. W. Schmidt, T. Christ, C. Glockner, M. K. Beyer and H. Clausen-Schaumann, "Simple Coupling Chemistry Linking Carboxyl-Containing Organic Molecules to Silicon Oxide Surfaces under Acidic Conditions", *Langmuir*, 2010, **26**, 15333–15338, DOI: 10.1021/la102435f.

(293) R. D. C. Oliveira, R. E. Santelli, R. de Carvalho Oliveira and R. E. Santelli, "Occurrence and Chemical Speciation Analysis of Organotin Compounds in the Environment: A Review", *Talanta*, 2010, **82**, 9–24, DOI: 10.1016/j.talanta.2010.04.046.

(294) M. V. M. Graham, A. P. A. Mosier, T. R. T. Kiehl, A. E. A. Kaloyeros and N. N. C. Cady, "Development of Antifouling Surfaces to Reduce Bacterial Attachment", *Soft Matter*, 2013, **9**, 6235–6244, DOI: 10.1039/c3sm50584g.

(295) R. L. Jones, N. C. Pearsall and J. D. Batteas, "Disorder in Alkylsilane Monolayers Assembled on Surfaces with Nanoscopic Curvature", *J. Phys. Chem. C*, 2009, **113**, 4507–4514, DOI: 10.1021/jp8081358.

(296) M. Barisik, S. Atalay, A. Beskok and S. Qian, "Size Dependent Surface Charge Properties of Silica Nanoparticles", *J. Phys. Chem. C*, 2014, **118**, 1836–1842, DOI: 10.1021/jp410536n.

(297) H. D. Hill, J. E. Millstone, M. J. Banholzer and C. A. Mirkin, "The Role Radius of Curvature Plays in Thiolated Oligonucleotide Loading on Gold Nanoparticles", *ACS Nano*, 2009, **3**, 418–424, DOI: 10.1021/nn800726e.

(298) P. Greenwood and B. Gevert, "Aqueous Silane Modified Silica Sols: Theory and Preparation", *Pigm. Resin Technol.*, 2011, **40**, 275–284, DOI: 10.1108/03699421111176171.

(299) S. V. Patwardhan, F. S. Emami, R. J. Berry, S. E. Jones, R. R. Naik, O. Deschaume, H. Heinz and C. C. Perry, "Chemistry of Aqueous Silica Nanoparticle Surfaces and the Mechanism of Selective Peptide Adsorption", *J. Am. Chem. Soc.*, 2012, **134**, 6244–6256, DOI: 10.1021/ja211307u.

(300) M. Niwano, M. Suemitsu, Y. Ishibashi, Y. Takeda, N. Miyamoto and K. Honma, "Ultraviolet Ozone Oxidation of Si Surface Studied by Photoemission and Surface Infrared Spectroscopy", *J. Vac. Sci. Technol., A*, 2000, **10**, 3171–3175, DOI: 10.1116/1.577838.

(301) C.-J. Wu, C.-J. Huang, S. Jiang, Y.-J. Sheng and H.-K. Tsao, "Superhydrophilicity and Spontaneous Spreading on Zwitterionic Surfaces: Carboxybetaine and Sulfobetaine", *RSC Adv.*, 2016, **6**, 24827–24834, DOI: 10.1039/C6RA01825D.

(302) K. Anselme, P. Davidson, A. M. Popa, M. Giazzon, M. Liley and L. Ploux, "The Interaction of Cells and Bacteria with Surfaces Structured at the Nanometre Scale", *Acta Biomater.*, 2010, **6**, 3824–3846, DOI: 10.1016/j.actbio.2010.04.001.

(303) A. J. Scardino, J. Guenther and R. de Nys, "Attachment Point Theory Revisited: The Fouling Response to a Microtextured Matrix", *Biofouling*, 2008, **24**, 45–53, DOI: 10.1080/08927010701784391.

(304) M. Graham and N. Cady, "Nano and Microscale Topographies for the Prevention of Bacterial Surface Fouling", *Coatings*, 2014, **4**, 37–59, DOI: 10.3390/coatings4010037.

(305) P. Roach, D. Farrar and C. C. Perry, "Interpretation of Protein Adsorption: Surface-induced Conformational Changes", *J. Am. Chem. Soc.*, 2005, **127**, 8168–8173, DOI: 10.1021/ja042898o.

(306) M. B. Linder, G. R. Szilvay, T. Nakari-Setala and M. E. Penttila, "Hydrophobins: The Protein-amphiphiles of Filamentous Fungi", *FEMS Microbiol. Rev.*, 2005, **29**, 877–896, DOI: 10.1016/j.femsre.2005.01.004.

(307) H. A. B. Wösten, "Hydrophobins: Multipurpose Proteins", *Annu. Rev. Microbiol.*, 2001, **55**, 625–646, DOI: 10.1146/annurev.micro.55.1.625.

(308) P. Roach, D. Farrar and C. C. Perry, "Surface Tailoring for Controlled Protein Adsorption: Effect of Topography at the Nanometer Scale and Chemistry", *J. Am. Chem. Soc.*, 2006, **128**, 3939–3945, DOI: 10.1021/ja056278e.

(309) S. D. Puckett, E. Taylor, T. Raimondo and T. J. Webster, "The Relationship between the Nanostructure of Titanium Surfaces and Bacterial Attachment", *Biomaterials*, 2010, **31**, 706–713, DOI: 10.1016/j.biomaterials.2009.09.081.

(310) M. B. Linder, "Hydrophobins: Proteins that Self Assemble at Interfaces", *Curr. Opin. Colloid Interface Sci.*, 2009, **14**, 356–363, DOI: 10.1016/j.cocis.2009.04.001.

(311) A. Zykwinska, M. Pihet, S. Radji, J. P. Bouchara and S. Cuenot, "Self-assembly of proteins into a three-dimensional multilayer system: Investigation of the surface of the human fungal pathogen Aspergillus fumigatus", *Biochim. Biophys. Acta*, 2014, **1844**, 1137–1144, DOI: 10.1016/j.bbapap.2014.03.001.

(312) E. Hahn, P. Wild, U. Hermanns, P. Sebbel, R. Glockshuber, M. Häner, N. Taschner, P. Burkhard, U. Aebi and S. A. Müller, "Exploring the 3D Molecular Architecture of Escherichia coli Type 1 Pili", *J. Mol. Biol.*, 2002, **323**, 845–857, DOI: 10.1016/S0022-2836(02)01005-7.

(313) L. A. Pratt and R. Kolter, "Genetic Analysis of Escherichia coli Biofilm Formation: Roles of Flagella, Motility, Chemotaxis and Type I Pili", *Mol. Microbiol.*, 2001, **65**, 43–59, DOI: 10.1046/j.1365-2958.1998.01061.x.

(314) N. Mitik-Dineva, J. Wang, V. K. Truong, P. R. Stoddart, F. Malherbe, R. J. Crawford and E. P. Ivanova, "Differences in Colonisation of Five Marine Bacteria on Two Types of Glass Surfaces", *Biofouling*, 2009, **25**, 621–631, DOI: 10.1080/08927010903012773.

(315) L. Rizzello, A. Galeone, G. Vecchio, V. Brunetti, S. Sabella and P. P. Pompa, "Molecular Response of Escherichia Coli Adhering onto Nanoscale Topography", *Nanoscale Res. Lett.*, 2012, **7**, 575, DOI: 10.1186/1556-276X-7-575.

(316) M. Dalby, M. Riehle, H. Johnstone, S. Affrossman and A. Curtis, "Polymer-Demixed Nanotopography: Control of Fibroblast Spreading and Proliferation", *Tissue Eng.*, 2002, **8**, 1099–1108, DOI: 10.1089/107632702320934191.

(317) S. Tsuneda, H. Aikawa, H. Hayashi, A. Yuasa and A. Hirata, "Extracellular Polymeric Substances Responsible for Bacterial Adhesion onto Solid Surface", *FEMS Microbiol. Lett.*, 2003, **223**, 287–292, DOI: 10.1016/S0378-1097(03)00399-9.

(318) A. Denis, P. Hanarp, D. S. Sutherland, J. Gold, C. Mustin, P. G. Rouxhet and Y. F. Dufre, "Protein Adsorption on Model Surfaces with Controlled Nanotopography and Chemistry", *Langmuir*, 2002, **18**, 819–828, DOI: 10.1021/la011011o.

(319) A. A. Vertegel, R. W. Siegel and J. S. Dordick, "Silica nanoparticle size influences the structure and enzymatic activity of adsorbed lysozyme", *Langmuir*, 2004, **20**, 6800–6807, DOI: 10.1021/la0497200.

(320) K. Cooksey, "Effectiveness of antimicrobial food packaging materials", *Food Addit. Contam.*, 2005, **22**, 980–987, DOI: 10.1080/02652030500246164.

(321) J. Lin, S. Qiu, K. Lewis and A. M. Klibanov, "Bactericidal Properties of Flat Surfaces and Nanoparticles Derivatized with Alkylated Polyethylenimines", *Biotechnol. Prog.*, 2002, **18**, 1082–1086, DOI: 10.1021/bp025597w.

(322) D. D. Iarikov, M. Kargar, A. Sahari, L. Russel, K. T. Gause, B. Behkam and W. A. Ducker, "Antimicrobial surfaces using covalently bound polyallylamine", *Biomacromolecules*, 2014, **15**, 169–176, DOI: 10.1021/bm401440h.

(323) G. Mcdonnell and A. D. Russell, "Antiseptics and disinfectants: Activity, action, and resistance", *Clin. Microbiol. Rev.*, 1999, **12**, 147–179, DOI: 10.1128/CMR.12.1.147.

(324) J. Blümmel, N. Perschmann, D. Aydin, J. Drinjakovic, T. Surrey, M. Lopez-Garcia, H. Kessler and J. P. Spatz, "Protein repellent properties of covalently attached PEG coatings on nanostructured SiO2-based interfaces", *Biomaterials*, 2007, **28**, 4739–4747, DOI: 10.1016/j.biomaterials.2007.07.038.

(325) B. R. Knowles, P. Wagner, S. Maclaughlin, M. J. Higgins and P. J. Molino, "Silica Nanoparticles Functionalized with Zwitterionic Sulfobetaine Siloxane for Application as a Versatile Antifouling Coating System", *ACS Appl. Mater. Interfaces*, 2017, **9**, 18584–18594, DOI: 10.1021/acsami.7b04840.

(326) B. R. Knowles, D. Yang, P. Wagner, S. Maclaughlin, M. J. Higgins and P. J. Molino, "Zwitterion Functionalized Silica Nanoparticle Coatings: The Effect of Particle Size on Protein, Bacteria, and Fungal Spore Adhesion", *Langmuir*, 2018, DOI: 10.1021/acs.langmuir.8b01550.

(327) P. J. Molino, D. Yang, M. Penna, K. Miyazawa, B. R. Knowles, S. Maclaughlin, T. Fukuma, I. Yarovsky and M. J. Higgins, "Hydration Layer Structure of Biofouling-Resistant Nanoparticles", *ACS Nano*, 2018, DOI: 10.1021/acsnano.8b06856.

(328) S. Tada, C. Inaba, K. Mizukami, S. Fujishita, M. Gemmei-Ide, H. Kitano, A. Mochizuki, M. Tanaka and T. Matsunaga, "Anti-biofouling properties of polymers with a carboxybetaine moiety", *Macromol Biosci*, 2009, **9**, 63–70, DOI: 10.1002/mabi.200800150.

(329) Y. Chang, S. H. Shu, Y. J. Shih, C. W. Chu, R. C. Ruaan and W. Y. Chen, "Hemocompatible mixed-charge copolymer brushes of pseudozwitterionic surfaces resistant to nonspecific plasma protein fouling", *Langmuir*, 2010, **26**, 3522–3530, DOI: 10.1021/la903172j.

(330) D. Nagasawa, T. Azuma, H. Noguchi, K. Uosaki and M. Takai, "Role of Interfacial Water in Protein Adsorption onto Polymer Brushes as Studied by SFG Spectroscopy and QCM", *J. Phys. Chem. C*, 2015, **119**, 17193–17201, DOI: 10.1021/acs.jpcc.5b04186.

(331) Q. Shao and S. Jiang, "Effect of Carbon Spacer Length on Zwitterionic Carboxybetaines", *J. Phys. Chem. B*, 2013, **117**, 1357–1366, DOI: 10.1021/jp3094534.

Appendix A

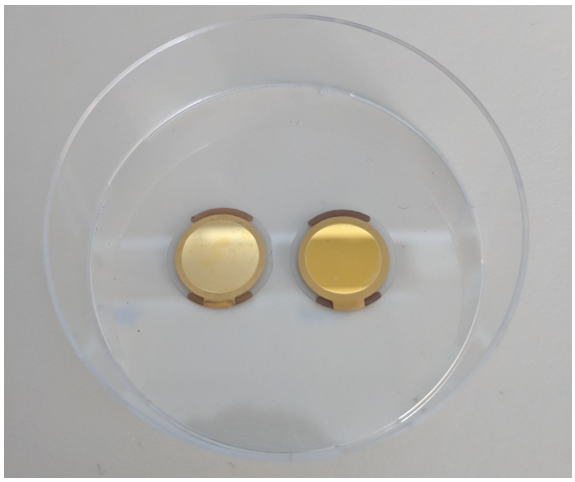

Figure A.1: Image of an uncoated gold QCM sensor (left) and a SiNP coated gold QCM sensor (right) prepared via spin coating.

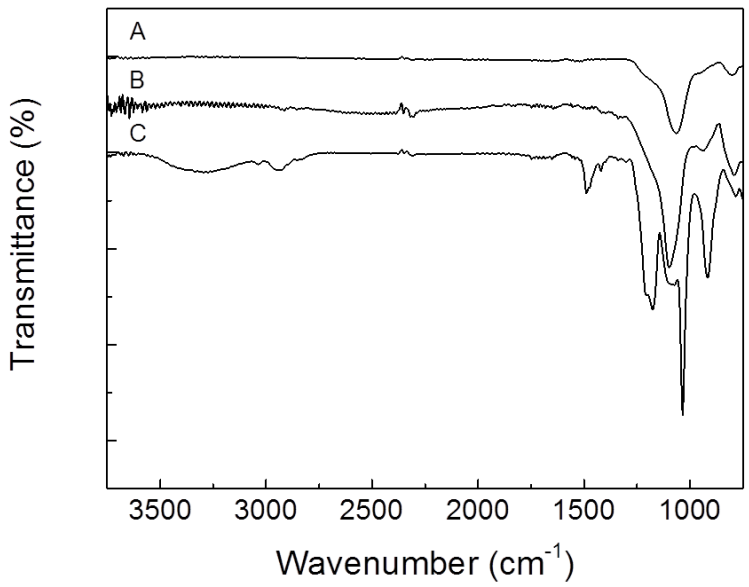

Figure A.2: FTIR transmission spectra of unfunctionalised SiNP (A), SiNP+SB (B), and SB (C).

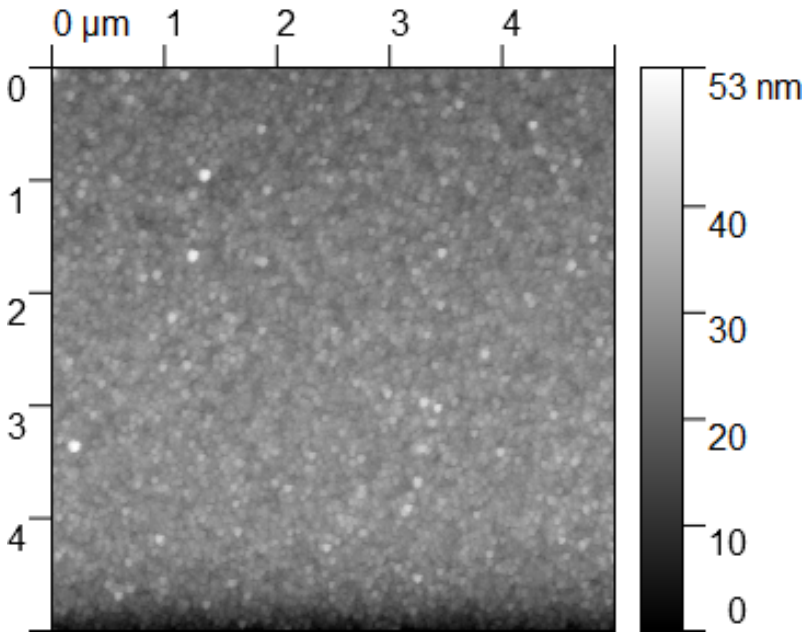

Figure A.3: AFM scan (5 μm x 5 μm) of a SiNP+SB (pH 9.5) particle coating.

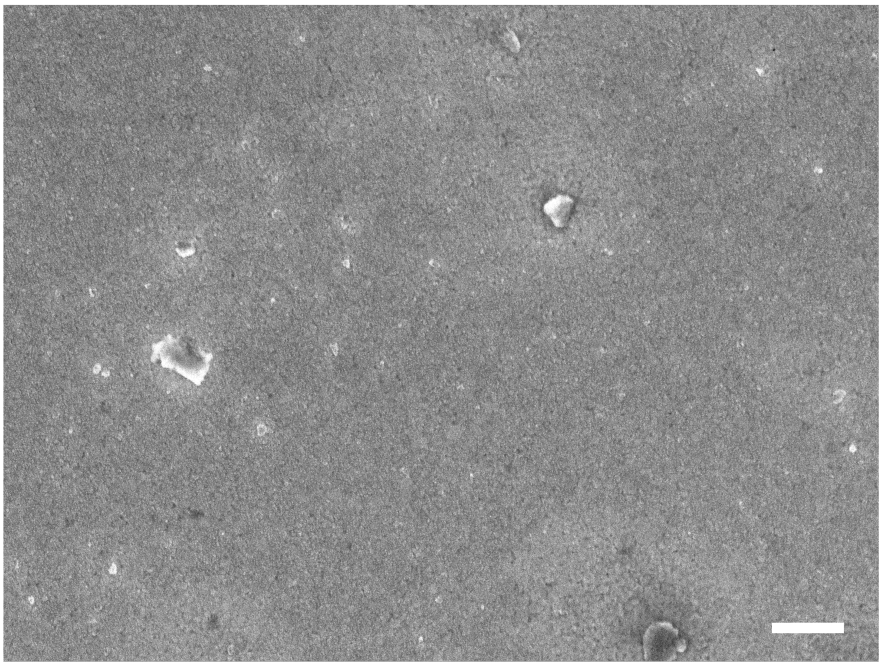

Figure A.4: SEM image of SiNP+SB (pH 3.5) coating showing the presence of aggregates. Scale bar is 1 μm.

Table A.1: Sessile water contact angles made on coatings prepared from 4 wt% SiNP dispersions. Unfunctionalised SiNP coatings present contact angles of 9.5 ± 0.3°.

	Contact Angle (°)		
Coating	**pH 3.5**	**pH 7.0**	**pH 9.5**
SiNP - 1 mM SB	6.1 ± 0.4	5.6 ± 0.5	5.4 ± 0.4
SiNP - 10 mM SB	5.9 ± 0.5	5.6 ± 0.7	5.9 ± 0.4
SiNP+SB	3.6 ± 0.3	4.8 ± 0.7	5.3 ± 0.2

Table A.2: Hydrodynamic diameter (D_h) and polydispersity index (PDI) of SiNPs after functionalisation with SB at various pH conditions.

	Z-Ave (d.nm)	**PDI**
SiNP Control	18.29	0.20
SiNP+SB (pH 3.5)	147.93	0.51
SiNP+SB (pH 7.0)	24.93	0.46
SiNP+SB (pH 9.5)	30.10	0.49

Table A.3: Degree of surface functionalisation as determined by TGA analysis.

	Mass loss (%)	**μmol/m^2**	**silanol/nm^2**
SiNP+SB (pH 3.5)	4.54	0.78	0.47
SiNP+SB (pH 7.0)	6.92	1.22	0.73
SiNP+SB (pH 9.5)	6.11	1.06	0.64

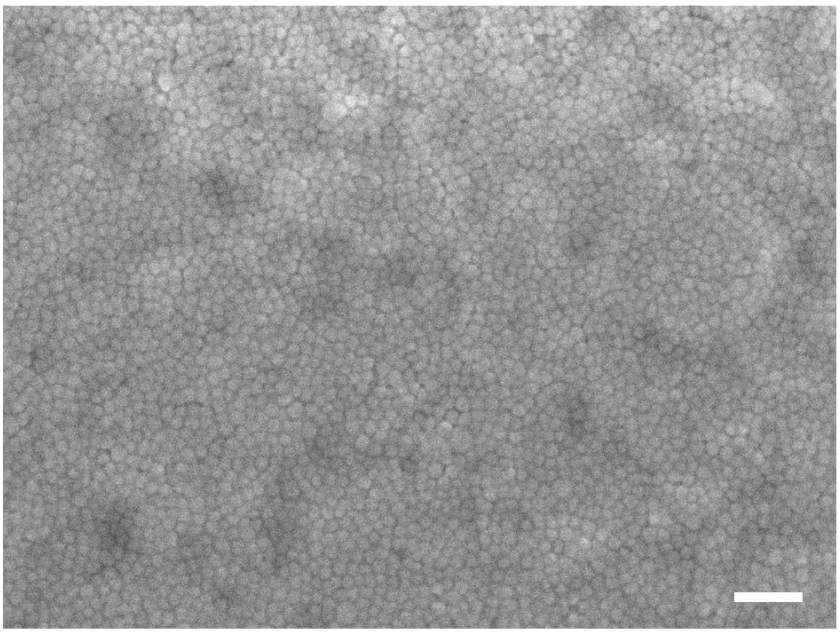

Figure A.5: SEM image of a spin-coated SiNP film functionalised at pH 9.5 with 10 mM CB. Scale bar is 100 nm.

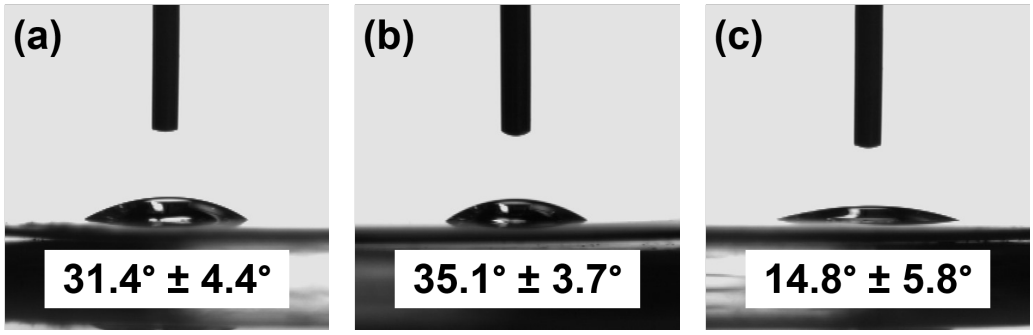

Figure A.6: Representative images of water contact angles made with the surface of SiNP coatings functionalised with 10 mM CB at pH 3.5 (a), 7.0 (b), and 9.5 (c). Insets: Average contact angles measured on the prepared surfaces (± SD).

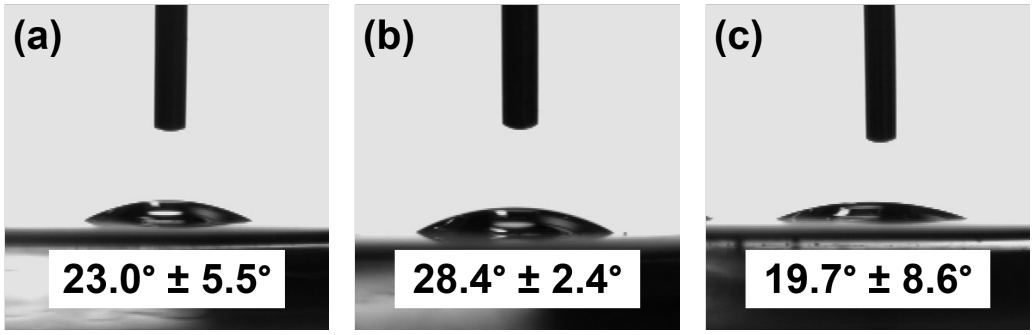

Figure A.7: Representative images of water contact angles made with the surface of SiNP coatings functionalised with 1 mM CB at pH 3.5 (a), 7.0 (b), and 9.5 (c). Insets: Average contact angles measured on the prepared surfaces (± SD).

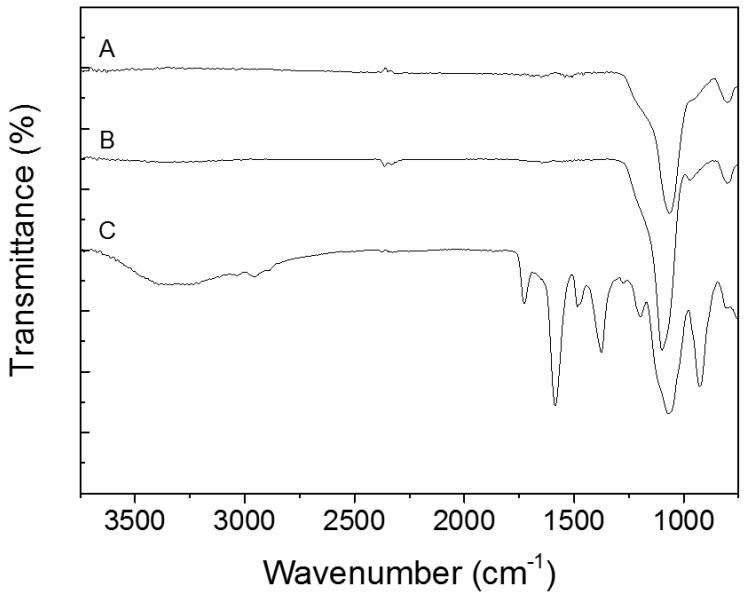

Figure A.8: FTIR transmission spectra of unfunctionalised SiNP (A), SiNP+CB (B), and CB (C).

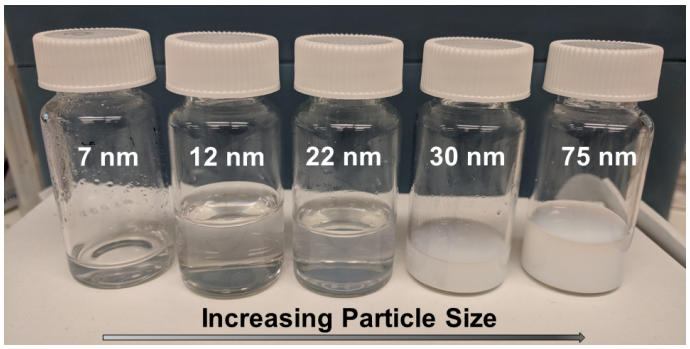

Figure A.9: Image of SiNP dispersions demonstrating the increase in solution opacity with increasing particle size.

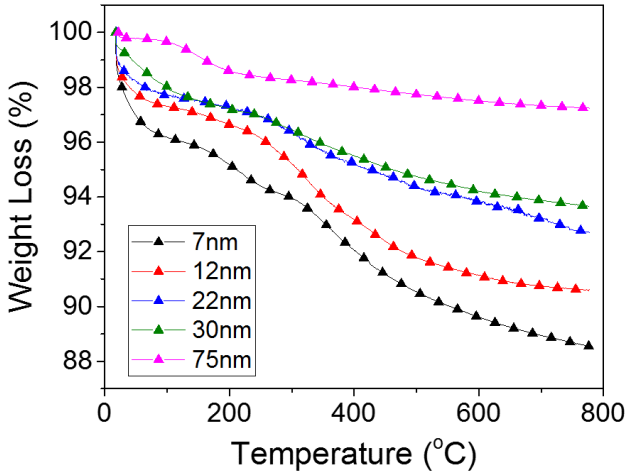

Figure A.10: Weight loss (%) of SB modified SiNPs of different sizes as measured by TGA.

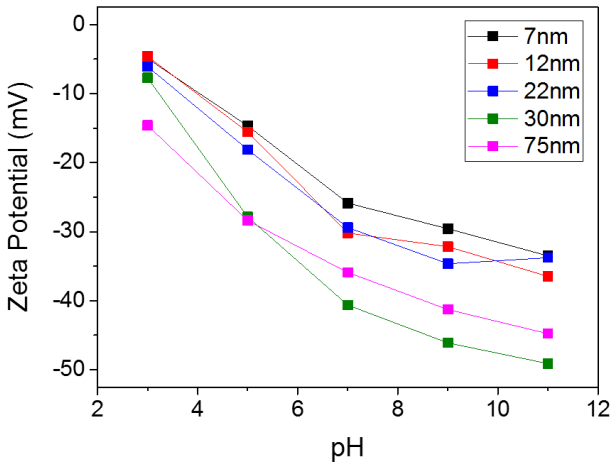

Figure A.11: ZP measurements performed on SiNP dispersions between pH 3.0 and 11.0.

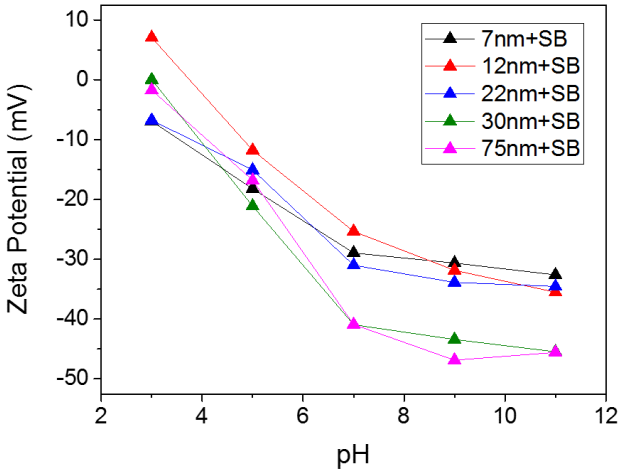

Figure A.12: ZP measurements performed on SiNP+SB dispersions between pH 3.0 and 11.0.

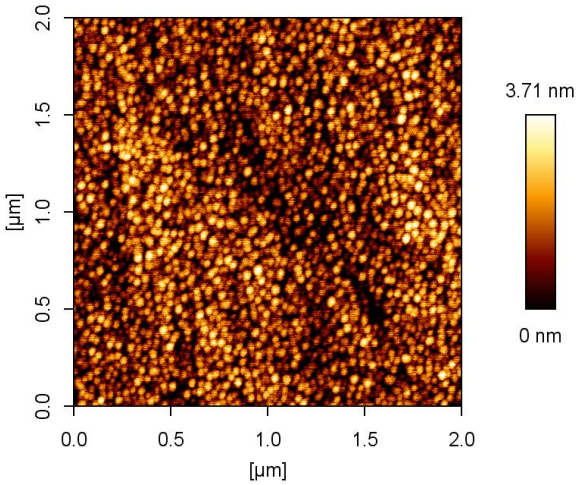

Figure A.13: Representative AFM scan (2 μm $\times$ 2 μm) of a SiO_2 QCM sensor.

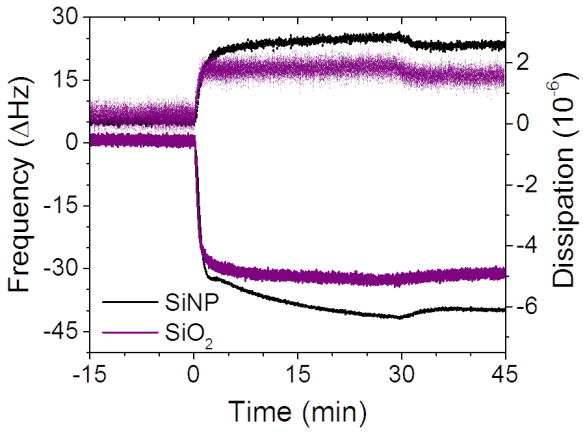

Figure A.14: Comparison QCM-D f/D shifts for BSA adsorption onto a SiO_2 QCM sensor and SiNP (12nm) coating.

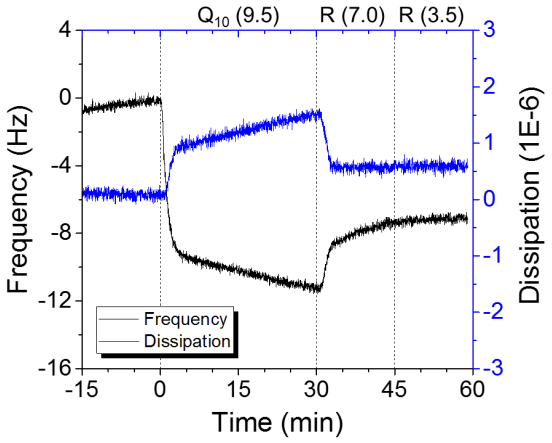

Figure A.15: Example QCM-D f and D responses for a SiNP coating functionalised with 10 mM QAS at pH 9.5, successionally rinsed with pH 7.0 and pH 3.5 aqueous solutions (5^{th} overtone shown).

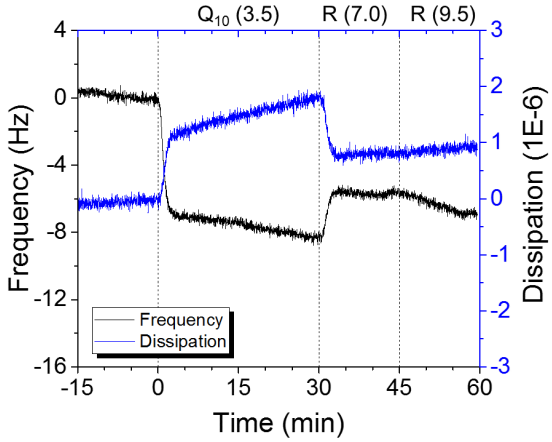

Figure A.16: Example QCM-D f and D responses for a SiNP coating functionalised with 10 mM QAS at pH 3.5, successionally rinsed with pH 7.0 and pH 9.5 aqueous solutions (5^{th} overtone shown).

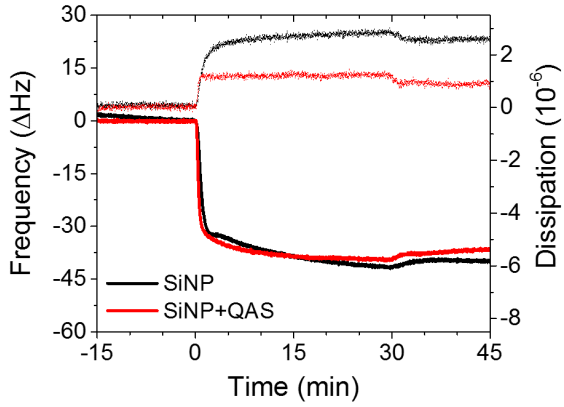

Figure A.17: Comparison QCM-D f and D shifts for BSA adsorption onto SiNP+QAS and SiNP coatings (5^{th} overtone shown).

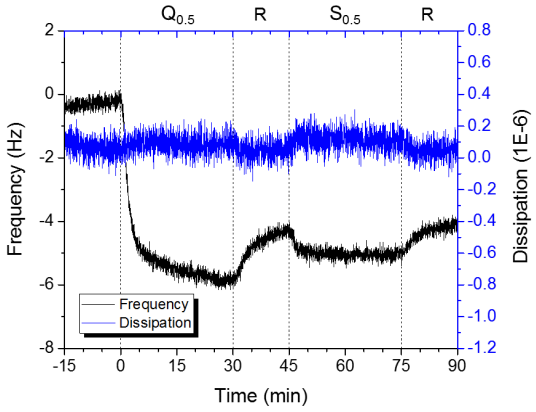

Figure A.18: Example QCM-D f and D shifts for $Q_{0.5}S_{0.5}$ SiNP coating functionalisation (5^{th} overtone shown). R denotes rinsing periods.

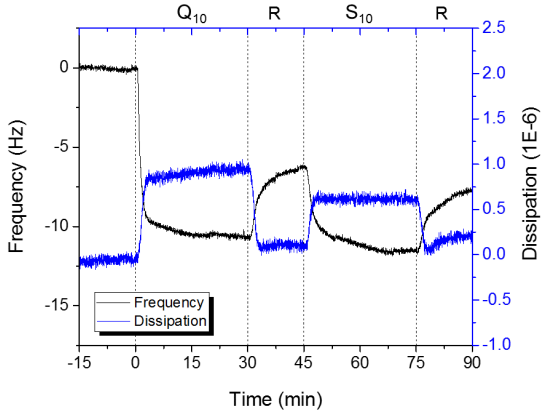

Figure A.19: Example QCM-D f and D shifts for $Q_{10}S_{10}$ SiNP coating functionalisation (5^{th} overtone shown). R denotes rinsing periods.

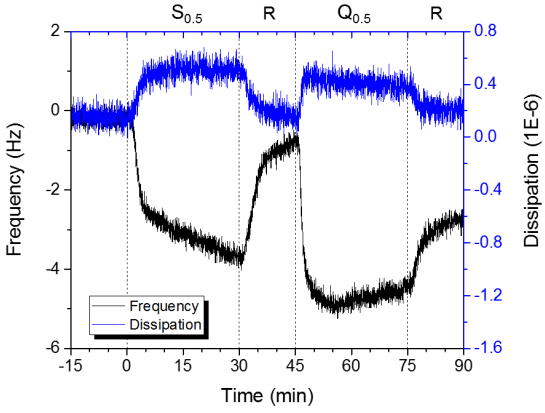

Figure A.20: Example QCM-D f and D shifts for $S_{0.5}Q_{0.5}$ SiNP coating functionalisation (5^{th} overtone shown). R denotes rinsing periods.

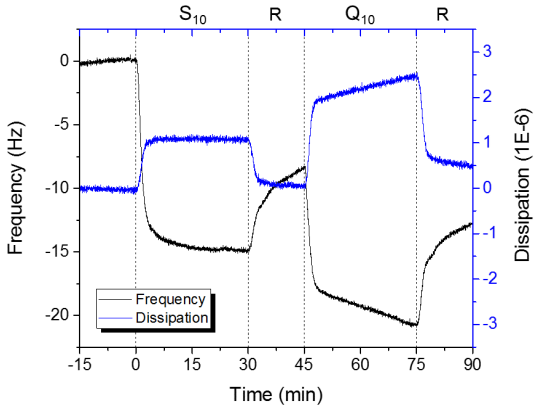

Figure A.21: Example QCM-D f and D shifts for $S_{10}Q_{10}$ SiNP coating functionalisation (5^{th} overtone shown). R denotes rinsing periods.

Table A.4: Average static water contact angles measured onto QAS modified SiNP coatings, functionalised with 10 mM QAS solutions under different pH conditions (± SD).

pH	Contact Angle (°)
3.5	16.4 ± 2.3
7.0	14.5 ± 3.4
9.5	12.0 ± 3.0

Table A.5: Average static water contact angles measured onto QAS modified SiNP coatings, functionalised at pH 9.5 under different concentration conditions (± SD).

Concentration	Contact Angle (°)
0.5 mM	12.1 ± 5.9
1.0 mM	14.1 ± 5.4
10 mM	15.3 ± 3.9

Table A.6: Ratio of QAS to SB on SiNP functionalised surfaces. Functionalisation conditions are denoted by (A_xB_y), where A is the 1^{st} and B is the 2^{nd} solution exposed to the SiNP coatings, and x and y denote the concentrations of A and B in mM, respectively.

	$Q_{0.5}S_{0.5}$	Q_1S_1	Q_1S_{10}	$Q_{10}S_{10}$	$S_{0.5}Q_{0.5}$	S_1Q_1	S_1Q_{10}	$S_{10}Q_{10}$
QAS	94%	95%	63%	75%	68%	61%	45%	14%
SB	6%	5%	37%	25%	32%	39%	55%	86%

Table A.7: Average static water contact angles measured onto dual-functionalised SiNP coatings prepared for bacterial adhesion assays. Functionalisation conditions are denoted by (A_xB_y), where A is the 1^{st} and B is the 2^{nd} solution exposed to the SiNP coatings, and x and y denote the concentrations of A and B in mM, respectively.

	Control	S_1Q_1	$S_{10}Q_{10}$	Q_1S_1	$Q_{10}S_{10}$	S_{10}	Q_{10}	$Q_{10}{}^*$	$Q_{10}{}^{**}$
CA (°)	15.4	17.0	17.9	15.9	13.0	10.9	17.8	14.6	14.4
SD	1.8	0.6	0.1	0.8	0.2	2.5	1.4	0.3	0.8